URETHANE/ACRYLIC HYBRID LATEXES FOR APPLICATION AS PSA

Elise Degrandi

THESE DE DOCTORAT de
L'UNIVERSITE PIERRE ET MARIE CURIE

Spécialité
Chimie et Physico-Chimie des Polymères
(ED 397)

Présentée par

Melle Elise DEGRANDI

Pour obtenir le grade de
DOCTEUR DE L'UNIVERSITE PIERRE ET MARIE CURIE

Sujet de la Thèse :

LATEX HYBRIDES URETHANE/ACRYLIQUE POUR APPLICATIONS ADHESIVES

Soutenue le 17 décembre 2009

Devant le jury composé de :

M. Laurent Bouteiller,	Directeur de Recherche, UPMC,	Président
Mme Catherine Gauthier,	Professeur, INSA de Lyon,	Rapporteur
M. Julian Oberdisse,	Chargé de Recherche, Université de Montpellier,	Rapporteur
M. José M. Asua,	Professeur, Université du Pays Basque	Examinateur
Mme Elodie Bourgeat-Lami,	Directeur de Recherche, ESCPE,	Examinateur
M. Christophe Derail	Professeur, Université de Pau,	Examinateur
M. Joseph L. Keddie	Professeur, Université de Surrey	Examinateur
M. Costantino Creton,	Directeur de Recherche, ESPCI	Directeur de thèse

Les chapitres ont été relus une nouvelle fois, les dernières corrections ont été apportées, il est temps maintenant de remercier les différents acteurs qui ont permis à ce travail d'aboutir.

Durant près de quatre ans, j'ai fait partie du laboratoire PPMD de l'ESPCI et je tiens à remercier François Lequeux et Christian Frétigny, directeurs successifs pendant cette période, pour leur accueil dans ce laboratoire.

Mes sincères remerciements vont à Catherine Gauthier et Julian Oberdisse qui ont accepté de rapporter ce travail. S'y ajoute un grand merci aux différents membres du jury : Elodie Bourgeat-Lami, Laurent Bouteiller, Christophe Derail, Joe Keddie et Txema Asua qui fut malheureusement bloqué par la neige le jour de la soutenance.

Pendant quatre années, mon travail a été supervisé par Costantino Creton et je tiens à le remercier vivement pour sa confiance dès le début du projet, pour ses explications toujours pédagogiques et pour sa grande disponibilité malgré ses nombreux déplacements. Je garde aussi un très bon souvenir des dégustations de vins organisées au sein de l'équipe, et des récits de voyage qui donnent encore plus envie de parcourir le monde.

Des voyages, il y en a eu beaucoup pendant cette thèse, notamment grâce au cadre du projet européen NAPOLEON. Stockholm, Cambridge, Saint-Sébastien sont quelques unes des villes que j'ai pu (re)découvrir avec plaisir. Je souhaite dire un grand merci à tous les membres de ce projet, rencontrés de manière plus ou moins régulièrement lors des réunions techniques et avec qui les échanges ont toujours été fructueux. En particulier, je remercie Aitziber Lopez, Txema Asua, Ravindra Udagama et Elodie Bourgeat-Lami pour les nombreuses discussions sur la chimie de ces systèmes. Ce fut chaque fois de nouveaux éclairements et de nouvelles pistes qui s'ouvraient.
Un grand merci aux membres de l'institut POLYMAT à Saint-Sébastien, pour leur accueil chaleureux dans leur laboratoire et lors des meetings semestriels. Merci aussi à Christopher Plummer et Riccardo Ruggerone pour les semaines passées à Lausanne et pour m'avoir consacré leur temps pour imager ces particules et ces films bien complexes.
Il me faut aussi remercier entre autre Elizabetta Canetta et Joe Keddie, Keltoum Ouzineb, Yves Holl, Laurent Chazeau et les différents doctorants du projet NAPOLEON pour les échanges aussi bien scientifiques qu'humains.

Les voyages furent nombreux mais c'est au PPMD que j'ai passé la plus grande partie de mon temps et je voudrais remercier les différentes personnes que j'y ai côtoyées.
Tous mes remerciements vont à Hélène Montès (pour le RDA mais surtout pour sa bonne humeur matinale), à Freddy Martin (un peu pour le MEB et aussi pour les bons petits plats le midi), à Sandrine Mariot (que je retrouve maintenant en post-doc), à Ludovic Olanier (pour les pièces mécaniques qu'il faut toujours faire au plus vite !), à Guylaine Ducouret et Agnès Pallier pour les manips de RMN et de rhéologie, à Yvette Tran pour le soutien moral en fin de thèse, à Gilles Garnaud pour le courrier du matin et à Armand Hakopian pour, entre autre, le sauvetage in extremis de mon ordinateur de retour de vacances.

Jean-Louis Halary et Alba Marcellan m'ont fait confiance et m'ont donné la possibilité d'enseigner à plusieurs reprises en tutorats ou en TP. Je leur en suis très reconnaissante car cela fut une expérience très riche qui a révélé une vraie vocation.

Un grand merci aussi à tous les non-permanents : Guillaume qui a toujours une réponse à mes nombreuses questions (scientifiques ou non), Elodie, Astrid et Juliette avec qui j'ai partagé les joies et les douleurs de la fin de thèse, François (bonne chance pour cette thèse qui commence), David (quand est-ce qu'on se retrouve à Fontainebleau ?), Aurélie, Eric, Jordan, Samy qui fut aussi « collègue de thèse », Griffith.

Certains sont partis avant moi mais je ne les oublie pas pour autant. Beaucoup sont devenus des amis au-delà du PPMD. Tous mes remerciements à Fanny et Clara, pour l'encadrement de mon stage et leur aide précieuse sur les manips de tack, à Karine pour son accueil dès mon arrivée au labo, à Angélina, Antonella, Diane, François, Alex, Arnaud, Nick, Lars (pour toutes les explications sur l'AFM). Merci aussi à Marie-Hélène, Thomas ou Régis pour la motivation au moment d'aller nager ou courir le midi.

Je voudrais saluer Perrine, Thomas et Nicolas, rencontrés aux Journées de l'Adhésion 2007, retrouvés pour organiser les Graines d'Adhésion 2008 à Bordeaux et avec qui j'ai partagé les différents moments de la thèse, des galères de la rédaction au soulagement d'après la soutenance, en passant par le stress avant les présentations en conférence internationale.

Lors des premières années de la thèse, j'ai aussi découvert le théâtre avec beaucoup de plaisir. Je tiens à dire merci à Mylène pour la manière avec laquelle elle aborde et transmet cet art, et à Alexandre, Hugo, Loreleï, Magali, Anne-Charlotte et tous les autres membres (avec un coucou supplémentaire à Pauline) pour deux belles années au sein de Tellem Chao.

Je salue aussi les « collègues de grimpe », de l'ASP6 à Roc 14 (Lila, Pascaline, Jean-François, Lucas et Vinh qui se sont aussi défoulés sur les voies coriaces du gymnase Alice Milliat ou sur les blocs de Bleau)

Il y a une vie avant la thèse et je dis un grand merci à tous les amis, utécéens et autres, qui m'ont soutenu pendant ces quatre ans sans toujours vraiment savoir ce que signifiait « être en thèse » : Bérengère, Alexandra, Anne-Gaëlle, Justine, Aurélie, Hélène, Paul-Antoine, Sylvain et Sylvain, Yannick, Fabien, Charles et Julien.

Je n'aurais pas pu aller aussi loin sans le soutien inconditionnel et ininterrompu de mes parents, de ma sœur Clémence et de ma tante. Merci à eux, infiniment.

Enfin, un grand, très grand merci à Simon qui a su, pendant près de trois ans de thèse, me donner confiance en moi et m'apporter son soutien sans faille dans toutes les situations.

A mon grand-père,

A Simon

TABLE OF CONTENTS

LIST OF ABBREVIATIONS

^{13}C NMR	Carbon Nuclear Magnetic Resonance
2-EHA	2-EthylHexyl Acrylate
3M	Minnesota Mining and Manufacturing Company
AA	Acrylic Acid
AFERA	European Association for the self adhesive tape industry
AFM	Atomic Force Microscopy
ASTM	American Society for Testing and Materials
BA	Butyl Acrylate
BPA	Bisphenol A
CMC	Critical Micellar Concentration
CTA	Chain Transfer Agent
$Đ_M$	Molar Mass Dispersity
DSC	Differential Scanning Calorimetry
FINAT	Fédération INternationale des fabricants et transformateurs d'Adhésif et Thermocollants
GPC	Gel Permeation Chromatography
HEMA	HydroxyEthyl Methacrylate
HMDI	Hexamethylene DiIsocyanate
IOA	IsoOcty Acrylate
IPDI	IsoPhoro DiIsocyanate
IPN	InterPenetrated Network
KPS	Potassium PerSulfate
LVDT	Linear Variable Displacement Transformer
M_c	Molar mass between Crosslinks
MDI	4,4 Diphenyl Methane DiIsocyanate
M_e	Molar mass between Entanglements
MFFT	Minimum Film Formation Temperature

MMA	Methyl MethAcrylate
M_n	Number Average Molar Mass
M_w	Weight Average Molar Mass
NAPOLEON	Nanostructured wAterborne POLymEr films with OutstaNding properties
N_d	Number of Droplets
N_p	Number of Particles
ODA	OctaDecylAcrylate
OMPU	Oil-Modified PolyUrethane
PE	PolyEthylene
PPG	Poly(Propylene Glycol)
PSA	Pressure Sensitive Adhesive
PSTC	Pressure Sensitive Tape Council
PU	PolyUrethane
SDS	Sodium Dodecyl Sulfate
SEC	Steric Exclusion Chromatograhpy
SEM	Scanning Electron Microscopy
SFS	Sodium Formaldehyde Sulfoxylate
SS	Stainless Steel
TBHP	Tertiary Butyl HydroPeroxide
TDI	Toluene DiIsocyanate
TEM	Transmission Electronic Microscopy
T_g	Glass transition Temperature
THF	TetraHydroFuran
TLMI	Tag & Label Manufacturers Institute
TM	Tapping Mode
VOC	Volatile Organic Compound

INTRODUCTION GENERALE

Les adhésifs sensibles à la pression, appelés de façon plus commune autocollants, font pleinement partie de notre quotidien. Ces films minces, qui peuvent coller après application d'une faible pression, se retrouvent sous forme de rubans adhésifs, d'étiquettes autocollantes, de pansements ou encore de Post It©. Ces matériaux ont été développés à la fin de la seconde guerre mondiale et ont connu rapidement un essor important. Les premières applications étaient liées au domaine médical, mais très vite l'industrie automobile a également exploité ces nouveaux matériaux. Quelques décennies après les premières applications, la compréhension des mécanismes permettant cette adhésion sous faible pression s'est développée, entraînant l'élaboration d'adhésifs de plus en plus complexes et performants.

Une façon de classer ces adhésifs sensibles à la pression, ou en anglais *pressure sensitive adhesives* (PSA[1], terme qui sera employé par la suite dans cette thèse), consiste à les regrouper par mode de préparation. En effet, il existe des PSA dit *hot-melt* (préparés à haute température sous forme de polymère fondu), des PSA préparés en présence de solvant (polymère en solution) et des PSA à base aqueuse (polymère dispersé dans l'eau). Depuis plusieurs années, cette dernière catégorie suscite un intérêt tout particulier. En effet, elle permet de limiter les apports énergétiques requis pour la mise en œuvre des PSA h*ot-melt* ainsi que l'émission de Composés Organiques Volatiles (COV) présents dans les polymères dispersés dans un solvant organique. En cela, les PSA à base aqueuse répondent bien aux exigences environnementales qui se développent actuellement.

D'une manière plus générale, le développement des technologies permettant la préparation de polymères en émulsion a connu un intérêt grandissant depuis plusieurs années et de nouveaux types de matériaux sont apparus. Ainsi en est-il des matériaux hybrides qui sont constitués de deux polymères immiscibles, permettant une synergie de propriétés de ces deux polymères. La préparation, la compréhension, et le développement de ces matériaux

[1] Les acronymes utilisés dans ce manuscrit sont listés en page 15

hybrides préparés en émulsion sont le cœur du projet européen NAPOLEON (pour NAnostructured waterborne POLymEr films with outstaNding properties) dans lequel s'intègre cette thèse. Il s'agit plus particulièrement dans ce projet d'utiliser une voie de synthèse en base aqueuse relativement récente, la polymérisation par miniémulsion, pour préparer des matériaux polymères hybrides. En effet, par cette voie de synthèse, l'amorçage et la polymérisation ont lieu directement dans de très petites (100 - 200 nm) gouttelettes de monomères. En utilisant un mode de dispersion efficace, il est alors possible d'incorporer une seconde phase, de nature polymérique (tels que des polycondensats) ou inorganique (telles que des plaquettes d'argile), dans la phase monomère avant la formation de ces gouttelettes. Après polymérisation, on obtient ainsi des particules de polymère en suspension dans l'eau (plus généralement appelé latex) de nature hybride. Le séchage de ces latex permet d'obtenir des films minces (20 – 500 μm), auxquels les deux phases présentes dans les particules apportent des propriétés complémentaires. Dans le cadre du projet NAPOLEON, plusieurs applications ont été envisagées : comme revêtements (type peinture, vernis …), comme adhésifs sensibles à la pression et comme produits cosmétiques. Dans ce travail, nous nous intéressons aux utilisations en tant que PSA, et plus particulièrement dans le cas d'un système hybride à base acrylique auquel est incorporé du polyuréthane.

Si ces systèmes uréthane/acrylique ont été fortement étudiés en tant que revêtement depuis le milieu des années 1990, il existe en revanche encore peu de travaux sur les formulations adhésives. Or le polyuréthane peut avoir un réel impact positif sur les adhésifs acryliques : il peut apporter une résistance aux solvants, une meilleure filmification ou encore permettre le maintien de l'adhésion des acryliques à plus haute température. L'acrylique, qui est un type d'adhésif largement utilisé de nos jours dans les PSA, assure quant à lui un bon contrôle de l'adhésion et une diminution des coûts.

Le projet NAPOLEON regroupe douze centres de recherche et neuf entreprises présents dans plusieurs pays européens. Les compétences se repartissent dans des domaines allant de la synthèse de polymère en émulsion à l'étude de propriétés macroscopiques des latex et des polymères en passant par la formation des films ou l'étude de la bio-compatibilité. Nous nous sommes intéressés pour notre part aux propriétés mécaniques et adhésives de ces films de latex hybrides.

Parmi les différents partenaires du projet, nous avons collaboré plus directement avec deux laboratoires de chimie qui se sont focalisés sur la synthèse des polymères dans les particules. Le premier est le LCPP (Laboratoire de Chimie et Procédés de Polymérisation) à Lyon, où Ravindra Udagama, étudiant en thèse, a réalisé la synthèse de systèmes hybrides par un procédé batch, sous la direction de Elodie Bourgeat-Lami et Timothy Mc Kenna. Des systèmes plus proches des conditions de synthèse industrielles ont été préparés par Aitziber Lopez, doctorante de l'institut POLYMAT de l'Université du Pays Basque situé à Donostia-San Sebastian (Espagne), supervisée par le professeur Txema Asua. Les propriétés de ces matériaux et leur préparation à l'échelle industrielle ont été testées par Keltoum Ouzineb et

Olivier Dupont de l'entreprise Cytec Surfaces Specialties, basée à Bruxelles. Enfin, nous avons également collaboré avec le professeur Christopher Plummer de l'Ecole Polytechnique Fédérale de Lausanne (Suisse) pour l'étude de la morphologie des particules et des films par des techniques avancées de microscopie (en particulier AFM et TEM), ainsi qu'avec Elizabetta Canetta, post-doc au département de physique de l'Université de Surrey (Angleterre) dans l'équipe du professeur Joseph Keddie, qui a utilisé des techniques d'AFM notamment pour déterminer la morphologie des particules ainsi que les propriétés de films adhésifs.

Ce travail a comporté deux aspects fortement liés. Nous avons d'une part travaillé en étroite collaboration avec les équipes chargées de la synthèse de ces latex avec comme objectif la mise en évidence des conditions de synthèse permettant d'optimiser les propriétés adhésives. Ce travail préliminaire a été mené au début de la thèse et ne sera que peu discuté dans ce manuscrit. L'étude de la morphologie de ces systèmes optimisés (tant à l'échelle de la particule qu'à celle du film) et la compréhension des propriétés macroscopiques en fonction de l'architecture du réseau polymère uréthane/acrylique ont été au centre de ce travail.

Les techniques de microscopie électronique en transmission (TEM) et de microscopie à force atomique (AFM) ont été utilisées pour déterminer la morphologie des particules et des films. L'étude des propriétés macroscopiques s'est basée sur différents tests mécaniques usuels tels que la rhéologie et la traction. Cela nous a permis de caractériser les propriétés viscoélastiques linéaires et non-linéaires de ces systèmes. Une analyse poussée de ces données nous a permis d'identifier les paramètres architecturaux responsables des propriétés viscoélastiques. En particulier, l'exploitation des tests de traction (développée par Fanny Deplace dans sa thèse portant sur des films préparés à partir de latex cœur-écorce (Deplace 2008)) a été menée de façon approfondie, notamment par la réalisation de tests à plusieurs vitesses nominales de traction. Les conclusions issues de cette analyse ont été renforcées par l'utilisation de tests de probe-tack. Finalement, nous avons réalisé de manière systématique des mesures de taux de gel et de gonflement à l'équilibre de la partie gel du polymère pour d'améliorer encore la compréhension de l'architecture du réseau.

Le premier chapitre fait le point sur les connaissances théoriques nécessaires à la compréhension de ce travail. Les éléments fondamentaux ainsi que l'état de l'art et les avancées récentes sur les différents aspects de la thèse y sont présentés.
Dans les chapitres 2 et 3, nous présentons respectivement les méthodes de synthèse employées et les techniques expérimentales mises en œuvre. Il faut noter que le chapitre 2 ne reprend que les éléments de synthèse essentiels à la compréhension des systèmes. Plus de détails peuvent être trouvés dans les manuscrits de thèse de Ravindra Udagama (Udagama R. 2009) ou de Aitziber Lopez ((Lopez 2009)).
Les chapitres 4, 5 et 6 présentent les principaux résultats obtenus durant cette thèse. Dans le chapitre 4, une analyse de la morphologie est présentée, pour les particules et les films. On y discute en particulier l'importance du greffage du polyuréthane au réseau acrylique et

l'impact de la quantité de polyuréthane sur la morphologie. Le chapitre 5 présente une étude des propriétés de systèmes hybrides bien contrôlés et détermine le rôle joué par les paramètres de synthèse que sont la quantité de polyuréthane et la densité de greffage sur l'architecture du réseau. Dans le chapitre 6, nous essayons d'extrapoler les analyses du chapitre 5 à des systèmes qui se révèlent plus complexes car préparés dans des conditions plus proches des conditions industrielles.
Le dernier chapitre présente les résultats d'expérimentations menées en fin de thèse, portant sur la résistance au fluage de ces matériaux adhésifs. L'objectif est de déterminer un test moins long que ceux employés actuellement dans l'industrie afin d'obtenir des critères pertinents pour prédire la résistance au cisaillement des adhésifs. Les résultats et les premières interprétations sont donnés.
Enfin, une conclusion résume les apports de ce travail et les perspectives éventuelles.

Concernant la rédaction de ce manuscrit, deux remarques doivent être faites. Cette thèse étant le résultat d'une forte collaboration entre laboratoires européens, il nous a semblé important de rendre accessible ce manuscrit aux différents acteurs de cette collaboration. Le manuscrit a donc été rédigé en anglais, exception faite de cette introduction, de la conclusion et d'un résumé long. D'autre part, nous avons choisi de présenter les trois premiers chapitres de résultats sous forme d'articles qui seront soumis à publication à l'issue de cette thèse. Cela implique quelques répétitions notamment concernant la préparation des échantillons et les techniques utilisées. Celles-ci sont indiquées au lecteur par des passages en italique. Cependant, nous avons fait en sorte de conserver une homogénéité dans la numérotation de ces articles, aussi bien pour le plan que pour les figures, tables et équations.
Nous espérons que ces éléments quelque peu inhabituels ne perturberont pas trop et permettront, malgré tout, une lecture fluide et compréhensible de ce manuscrit.

- Deplace, F., PPMD, *University Paris VI*, **2008**
- Lopez, A., POLYMAT, *University of the Basque Country*, **2009**
- Udagama R., Laboratoire de Chimie, Catalyse, Polymères et Procédés, *University Claude Bernard - Lyon I*, **2009**

1. Theoretical Background

1.1 Pressure Sensitive Adhesives

Adhesives are defined as substances capable of holding two surfaces together in a strong and permanent manner. They find many applications in industry and can be divided in several classes. Pressure Sensitive Adhesives (PSAs) are one of these classes. They are characterized by instantaneous adhesion after application of a light pressure.

Being one of the high growth sectors among adhesives in the industry nowadays, PSA are the subject of many research studies targeted at understanding the relationship between their molecular structure, obtained from a synthesis process, and their mechanical properties, in particular in the emerging field of waterborne pressure sensitive adhesives.

1.1.1 What is a pressure sensitive adhesive (PSA)?

Pressure Sensitive Adhesives (PSA) are what we generally call self-adhesives. They are a specific class of adhesives that must stick, permanently or not, on a given substrate after application of a light pressure during a short time and without any chemical reaction, and that must not leave residues on the surface after debonding. Tapes, labels or protective films are good examples of PSA. Post-it Notes© are typical non-permanent PSA that can be easily debonded from their substrate. In the following work, we focus more specifically on permanent PSA.

Compared to the age-old technology of adhesion (5000 years old carvings containing glue have been discovered in Thebes (Jovanovic and Dubé, 2004)),PSA represent a recent technology. They were first developed for medical and first aids applications in the middle of the nineteenth century and industrial applications for automobile appeared at the beginning of the 1920s. As an example, in 1926, the Minnesota Minning and Manufacturing Company (3M) attempted to develop a masking tape for the automotive aftermarket and choose to use crimped paper as the backing. This started the development of saturated paper tapes which became the most important tape category. 3M Company is nowadays one the most important company in the trade of PSA (Satas, 1989).

PSA distinguish themselves from other types of adhesive because they adhere to the substrate without any substantial state modification. Whereas other classes of adhesives bond surfaces together thanks to a transition from the liquid state to the solid state, PSA are soft viscoelastic solids that can stick only through a fine control of the mechanical properties. The only interface forces active in a PSA bond are low-energy forces like Van der Waals (Creton, 2003).To fulfill this application, the material chosen as a PSA must have both behavior of a liquid to wet the contact with only a light pressure even on rough surfaces and the behavior of a solid to be cohesive enough to resist shear and to debond adhesively without residues on the substrate.

PSA are characterized by their properties in tack, peel and resistance to shear (see section 1.5 for a description of these tests). In order to obtain the best compromise between these

properties, viscoelastic materials are used and, above all, a fine control of the polymer network is required (Creton, 2003).
A limited number of materials can be used for PSA applications to suit well these requirements:

- Rubber-based PSA which are a blend of natural rubber and miscible tackifying resin with a low molecular weight.
- Styrenic block copolymers, that is a blend of triblocks (Styrene-Isoprene-Styrene, SIS) and diblocks (SI) or star-blocks mixed with a low molar mass high T_g tackifying resin (Roos and Creton, 2005). This class of PSA needs to be heavily formulated to optimize processing and function as a PSA.
- Acrylic-based PSA, a class of PSA permitting a wide range of formulation and optimization due to the wide composition possibilities of the monomers. The crosslinking step is necessary to avoid the PSA flowing (Lindner, Lestriez *et al.*, 2006; Satas, 1989).
- Silicone adhesives also exist for applications at extreme temperatures, for reversible low adhesion or for medical applications, but their cost is high.

Acrylic adhesives are composed of random copolymers. The main monomer is typically a long side-chain one giving a homopolymer with a low T_g (typically butyl acrylate BA, 2 ethyl hexyl acrylate 2EHA or isooctyl acrylate IOA). A short side-chain is added to adjust the T_g of the final copolymer (typically methyl methacrylate, MMA). Acrylic or methacrylic acid completes the formulation with the aim to improve adhesion.
One of the main advantages of acrylic PSAs is that they can be prepared in solution as well as in emulsion. Aqueous acrylic polymers are then in the class of latexes, that is to say polymer dispersions stabilized in water. Aqueous processes are favored by environmental concerns but also because they allow the production of latexes with very high molecular weights without a large increase of the viscosity. From an industrial point of view, this is very interesting because the low viscosity latexes obtained can be cast on substrates much faster than high viscosity solutions (Jovanovic and Dubé, 2004). For these reasons, waterborne acrylic adhesives present a great interest in the field of PSA nowadays.

1.1.2 Waterborne acrylic PSA

In solution as well as in emulsion, the random acrylic copolymers are obtained by free radical polymerization. During this polymerization process, chain transfer reactions can occur. Inter-molecular chain transfer reactions result in the branching between different chains. Acrylate monomers are prone to this chain transfer to the polymer and typically in the bulk part of the polymer chains are chemically crosslinked, that is to say connected by covalent bonds. The fraction of the crosslinked chains is called the gel fraction and plays an important role on the properties of the final polymer bulk inside the latex particles.
The chain transfer reactions are favored by high molar mass chains. Preparation of high molar mass polymers is then limited in solution because viscosity strongly increases with

branching and crosslinking. In emulsion process, the viscosity of the latex only depends on particle size and particle size distribution (Heyes and Sigurgeirsson, 2004). High molar mass and high gel fraction can be obtained more easily.

The development of waterborne acrylic adhesive started in the 1970s and these materials represent nowadays a large part of the production of acrylic adhesives (Jovanovic and Dubé, 2004). The waterborne processes are now well controlled but the properties of the final films are still inferior to that of hot-melt or solvent-borne PSA (Jovanovic and Dubé, 2004). The main two reasons are first the complex control of the acrylic network at high conversions in emulsion polymerization, and secondly the difficulty mastery of the formation of the interfaces between particles generated by the drying process.
Research on waterborne acrylic adhesives is mainly developed in two areas: the improvement in the understanding on the drying and coalescence process and its relation with the final mechanical properties of the dry film (Lin and Meier, 1995; Joanicot, Wong *et al.*, 1996; Lin and Meier, 1996; Routh and Russel, 2001) and the development of synthetic tools to improve the PSA properties inside the particle and the morphology of the film. It is for example possible to modify the particles morphology to control the design of the polymer network which in turns controls the adhesive properties. The production of core-shell particles (Mayer, Pith *et al.*, 1995; Dos Santos, Fabre *et al.*, 2000; Aymonier, Ledercq *et al.*, 2003; Dos Santos and Leibler, 2003; Deplace, Carelli *et al.*, 2009), of particles with a controlled composition profile (Laureau C., Vicente M. *et al.*, 2000; Chauvet, Asua *et al.*, 2005) or particle size distribution (do Amaral, Roos *et al.*, 2005) have for example resulted in adhesive films with improved mechanical and adhesive properties.
The emerging field of miniemulsion polymerization opens the possibility to generate hybrid particles, i.e. latex particles containing two or more different polymers (Guyot, Landfester *et al.*, 2007). The films obtained from such particles present a synergism between the properties of the different component. New materials with out-standing properties are thus developed. This miniemulsion process has been used to produce the hybrid materials studied in this thesis and is discussed in the next section.

1.2 Synthesis of waterborne polymers

Most of time, waterborne polymers are produced by conventional emulsion polymerization. This process is briefly described in the next section. However, this type of aqueous process presents some limitations, which are also exposed. Improvements are brought by the miniemulsion synthesis, which has been used in this work and is then presented.

1.2.1 Emulsion polymerization

Conventional emulsion polymerization (the shorter term "emulsion polymerization" is preferred in the following) is based on free-radical polymerization. It is generally carried out in stirred tank reactors working in batch, semi-continuous or continuous modes.
Smith and Ewart, and Hawkins, in the 1940s (Smith and Ewart, 1948; Blackley, 1975) developed the first theory of emulsion polymerization and described it as a three-stage process. Although it does not apply in all cases, it is commonly recognized as a useful picture to describe emulsion polymerization.
It is based on three different entities: micelles, monomer droplets and polymer particles, as shown in **Figure 1-1**.

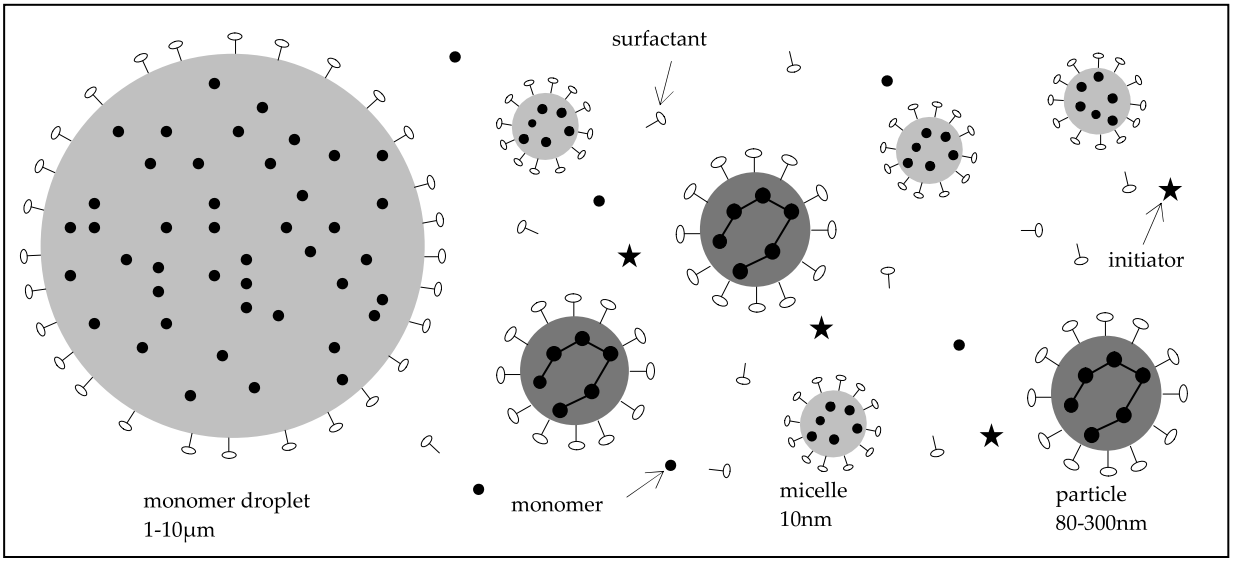

Figure 1-1: Different entities present during emulsion polymerization

At the beginning of emulsion polymerization organic and aqueous phases are mixed together in the reactor. The organic phase contains the monomer (or monomers mixture) whereas the aqueous phase is made of deionized water and emulsifier. An amount of emulsifier large enough to overcome the Critical Micellar Concentration (CMC) is added and formation of monomer droplets stabilized by emulsifier is possible. The excess of emulsifier forms micelles swollen by monomer. Monomer droplets have an average size of 1-10 µm but micelles are much smaller (around 10 nm). Thus, the surface area covered by the micelles is

much larger than the area covered by the monomer droplets. Emulsion polymerization begins with the addition of a water-soluble initiator.
The following table gives a simplified interpretation of the three stages defined by Smith and Ewart, and Hawkins. They are defined as particle nucleation, polymer particle growth and final stage.

Table 1:Different intervals of an emulsion polymerization (from (Jovanovic and Dubé, 2004))

Interval	Typical conversion range (%)	Micelles	Monomer droplets	Particle number	Particle size
1	0 - 10	Present	Present	Increases	Increases
2	10 - 40	Absent	Present	Constant	Increases
3	40 - 100	Absent	Absent	Constant	~ Constant

Particle nucleation refers to the initiation of polymerization and the apparition of the polymer chains. Due to the presence of monomers in monomer droplets, micelles and water, it can take place in these three loci. Once particles are nucleated, initiator can also enter particles and initiate polymer chains in this new locus. Homogeneous nucleation is the nucleation occurring directly in the aqueous medium, whereas heterogeneous nucleation corresponds to the nucleation of polymer particles in the droplets and micelles. Nevertheless, as the area covered by the micelles is much higher than the area covered by the droplets, the initiator enters preferentially in the micelles to generate polymer particles.
Once they have been nucleated, particles continue growing thanks to the monomer diffusion from the monomer droplet through water to the growing particles (interval 2). The end of this stage is characterized by a complete transformation of micelles into particles.
This last stage (interval 3) is characterized by a continuously decreasing monomer concentration. Indeed, the two first stages occur for low monomer conversion rate. All the remaining monomers polymerize during this stage. At the end, only polymer particles are present in the aqueous phase and a latex with a high solid content (around 50 - 65 %) and sub micron polymer particles (diameter around 80 - 300 nm) is obtained.

This three-step mechanism describes conventional emulsion polymerization in batch conditions. This process is characterized by a large increase of temperature due to almost instantaneously initiation of polymerization and requires then a permanent cooling to control temperature and avoid coagulation of the particles. This increase of temperature can limit the scale-up of batch emulsion for industrial processes.
One alternative is semi-continuous polymerization, where monomers, surfactants and initiators are fed continuously to an initial seed. Initiation reactions of the radical polymerization do not occur at the same time which limits the temperature increase. Further, the control of the monomer, initiator and surfactant feeds allow a better control of the copolymer composition profile (Laureau, Vicente *et al.*, 2000). Then polymer particles produced by semi-continuous process are more homogeneous.
This process also allows synthesizing particles under starved conditions. In that case, the feed rate of the monomer(s) is adjusted in order to be constantly under the reaction rate. That

means that the reaction environment is constant during the synthesis and, as a consequence, the monomer composition in the final copolymer is equal to the desired polymer composition. A better control of the polymer composition is permitted. It is useful to say that under starved conditions, polymer chain transfer reactions are more likely to occur, due to a high ratio polymer/monomer in the polymerization loci. In addition, it was demonstrated that because of a high polymer concentration during synthesis, the gel content is higher in starved semi-continuous process than in batch (Arzamendi and Asua, 1995).
The lower composition drift of the final polymer, the better adjustment of the gel content and architecture and finally the easy scale-up justify the choice of semi-continuous process compared to batch for commercial production of latexes.

Although conventional emulsion polymerization is well understood and widely used in industry, this process has shown its limitations. The most important one comes from its fundamental monomer feeding mechanism: monomer diffusion through water. Indeed, this seriously limits the possibilities to polymerize water insoluble monomers (Asua, 2002) and to use water-sensitive polymerization techniques (Landfester, 2001).
Moreover, the production of hybrid latex particles, containing at least two different polymers, is made more complicated by the difficulty to have homogeneous repartition of the different polymers in the particles.
Finally, until recently Controlled Free Radical Polymerization (CFRP) remained complex to implement in conventional emulsion due to initiation stage occurring in different loci (micelles, aqueous phase, particle already formed and monomer droplet). This drawback has been overcome at the beginning of the 2000's (in particular with the work of the team of Charleux (Qiu, Charleux *et al.*, 2001)), but has also motivated the development of miniemulsion polymerization (Asua, 2002).

1.2.2 Miniemulsion polymerization

One emerging alternative to conventional emulsion polymerization is miniemulsion polymerization. With this process, the incorporation of hydrophobic components or the hybridization of incompatible components becomes possible. For this reason, miniemulsion polymerization has been chosen for the synthesis of all the latexes studied here. Its mechanism is detailed here.
The basic principle of miniemulsion is to limit the initiation loci to the monomer droplets only. Each droplet becomes a single reactor and a one-to-one copy of monomer droplets is obtained (see Figure 1-2).

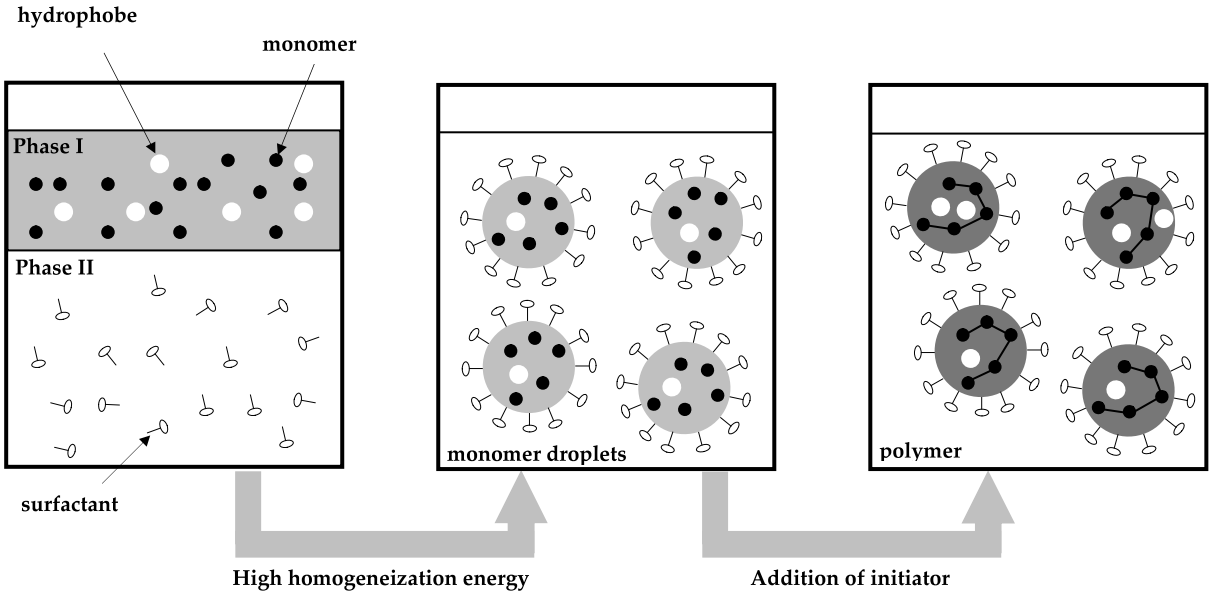

Figure 1-2: The principle of miniemulsion polymerization (after (Landfester, 2001))

To have initiators going preferentially into the droplets more than into the micelles, the surface area covered by the droplets must be higher than that of the micelles. A huge reduction of the size of the monomer droplets is necessary. Only high shear energy can decrease the droplet size enough to sub-micron size: Manton-Gaulin high pressure homogenizer (Lopez, Chemtob *et al.*, 2008), ultrasonication (Mason and Lorimer, 1988), rotor-stators (Ouzineb 2003) or static mixers (Farzi, Bourgeat-Lami *et al.*, 2008) are different tools to dramatically reduce the droplet sizes. This stage is generally called miniemulsification.

To stabilize this dispersion of droplets from Ostwald ripening (degradation of the dispersion by molecular diffusion) or from coalescence between droplets, additions of a monomer-soluble water-insoluble component (usually called hydrophobe or costabilizer) and of surfactants specific to the composition are required.

Stabilization of the monomer droplets and efficiency of the one-to-one copy mechanism are generally checked through the ratio of the number of particles N_p over the number of droplets N_d. A value of N_p/N_d equal to one is the objective but some deviations can be observed. A ratio higher than one indicates that secondary nucleation of particles took place in water, due to homogeneous nucleation. On the contrary, if N_p/N_d is lower than one, some droplets may have coalesced before polymerization.

As polymerization occurs directly in the nanoreactors (the sub-micron droplets), homogeneous incorporation of a hydrophobic component or of a prepolymer is possible. Indeed, it is possible to first dissolve or disperse a hydrophobic or incompatible phase in the monomer or monomers solution, then miniemulsify the whole phase and finally perform the polymerization in the two-phase droplets. Moreover, other types of reactions can take place directly in the particles like addition polymerization, condensation, anionic polymerization (Landfester, 2001).

The incorporation of hydrophobic resins such as alkyds for example becomes possible by miniemulsion polymerization (Wu, Schork *et al.*, 1999). Numerous possibilities are also offered to encapsulate inorganic particles like clays, TiO_2 or silica. The different possibilities of hybridization have been reviewed by Landfester and Asua at the beginning of the 2000s (Landfester, 2001; Asua, 2002).
The specific incorporation of polyurethane polymer chains in acrylic polymer network by miniemulsion polymerization is the core of this work and will be discussed later on.

1.3 From the particles to the film

1.3.1 Film-formation mechanisms and challenges

One of the advantages of emulsion polymerization is the possibility to have high solid content dispersion of high molar mass polymer with the viscosity of the final latex remaining low. Without limits due to the viscosity, latexes can be cast at important rates on a substrate to be dried. However, the drying process of these latexes, starting from particles dispersed in water to go to a solid film is not obvious and is particularly important for high T_g coatings. The film-formation process has been studied in considerable details, as seen in a review by Keddie on this subject (Keddie, 1997). It is generally described as a three-stage process (see Figure 1-3). During the first stage, water evaporation takes place and particles form a close-packed structure. The latexes are dried at a temperature higher than the T_g of the polymer constituting the particles, called minimum film formation temperature (MFFT). At this specific temperature, particles are soft enough to deform and fill the space between them; this is the second step. A temperature higher than MFFT is also required for the last stage, which is crucial for the cohesion inside the film. There, mobile polymer chains diffuse between particles interfaces so that particles can coalesce.

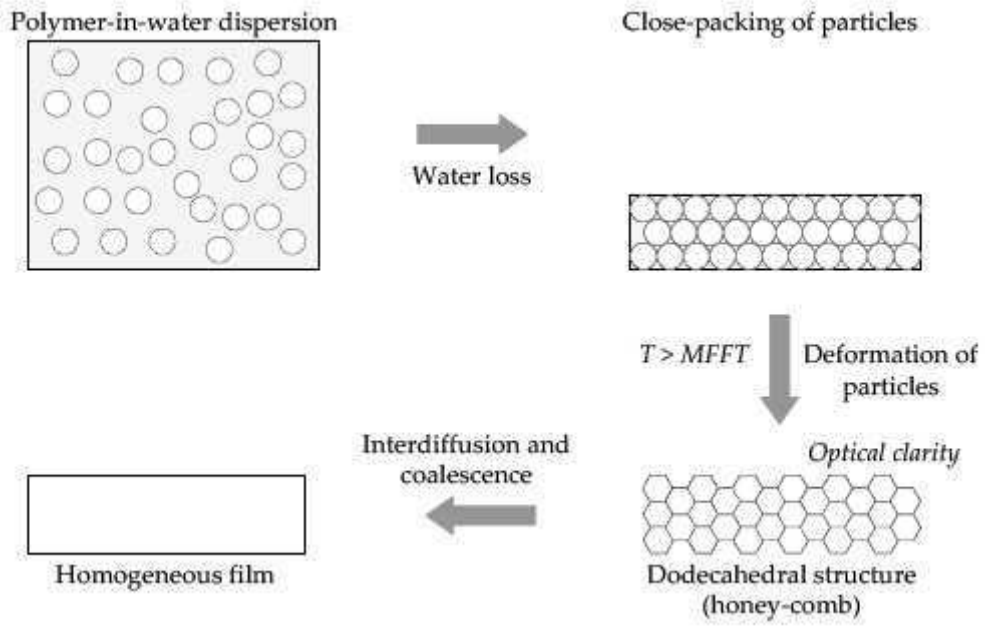

Figure 1-3: Successive mechanisms of latex film formation

Depending on how complete this interdiffusion is, the memory of the particle interfaces is retained or not in the final structure of the film. The mobility and length of the chains and the degree of crosslinking inside each particle have a huge effect on this interdiffusion stage. Figure 1-4 presents two extreme situations. When particles are lightly crosslinked with high

molar mass chains, the interfaces completely disappear and the particle structure does not remain in the film (Figure 1-4(a)). When low molar mass chains are highly crosslinked, almost no particle coalescence happens and the interfaces remain very weak (Figure 1-4(b)).

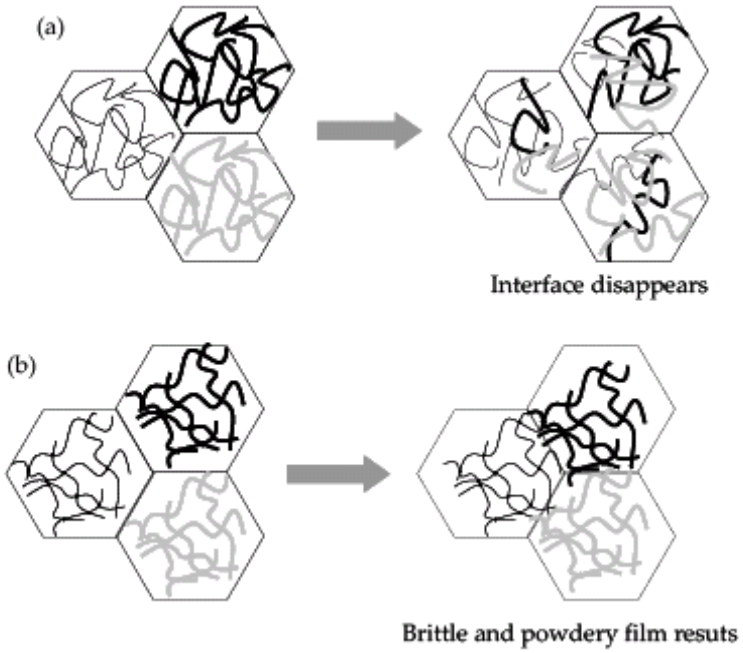

Figure 1-4: (a): interdiffusion, mixing of polymer chains and disappearance of interface for free chains; (b): limited interdiffusion between crosslinked particles

Ideally, the film formed by this coalescence process is expected to be transparent, crack free and with enough cohesion. This depends on the polymer characteristic and impacts on the macroscopic properties. We will see that the quality of the interdiffusion between particles affects mostly the large-strain properties of the film.
The different elements required to understand the structure of the polymer film are now presented.

1.3.2 Gel content and swelling of crosslinked networks

1.3.2.a Characteristic molar masses

A soluble polymer chain is characterized by its number average molar mass M_n and by its weight average molar mass M_w. The second one is more influenced by the contribution of high molar mass chains (Halary and Laupretre, 2006) and it will be preferentially analyzed in this work. Both are measured by size exclusion chromatography (SEC) formerly called gel permeation chromatography (GPC), but only for soluble molecules and not for crosslinked fraction of the polymer.

The molar-mass dispersity $Đ_M$, defined as M_w/M_n, is also an important value describing how narrow the molar mass distribution is (Stepto, 2009). Ideally equal to one for a uniform polymer, it is generally greater than one for real polymers.
In a polymer bulk, two other important molar masses must be considered. M_e is the average molar mass between entanglements. Based on the reptation model developed by de Gennes and Doi and Edwards and developed later by Noolandi (Doi and Edwards, 1986) the molar mass between entanglements, M_e, can be determined from the packing length which depends on monomer size, chain flexibility and temperature (Rubinstein and Colby, 2003; Halary and Laupretre, 2006). In essence the smaller is the monomer and the less flexible is the chain, the lower is M_e. Thus, for a given polymer at a given temperature M_e is fixed and values for homopolymers are tabulated in polymer handbooks. Polyacrylates such as poly(2-ethyl-hexyl acrylate) combine a very large monomer volume and a flexible chain, giving very high values of M_e.
In the situation where polymer chains are crosslinked, it is also necessary to know the average molar mass between crosslinks M_c. This molar mass depends on molecular and synthesis parameters and determines the density of elastically active chains in the polymer network. In the case of free radical polymerization, which is the polymerization process involved in this work, crosslinking points are formed by intermolecular chain transfer reactions. This mechanism can occur at one or both ends of a polymer chain. When only one end is crosslinked to another one, it forms a branching or dangling chain. Bonding chains on the contrary designate polymer chains crosslinked at their two extremities. The gel fraction corresponds to the total amount of crosslinked and branched polymer chains whereas the sol fraction is made of the free chains.

1.3.2.b Swelling of polymer networks

Extraction experiments are used to separate the gel fraction from the soluble one. These experiments can be performed in a specific set-up, called a Soxhlet, by a dynamic method. The polymer is put in a cartridge installed inside the Soxhlet. The solvent is heated in a balloon and the reflux passes into the cartridge, extracting the soluble chains. It is a reliable method to completely extract the soluble part. However, it requires the specific Soxhlet set-up and the extraction is long (at least 24h). The uncrosslinked chains are found in the solvent (which can be used for SEC measurements) and the gel fraction is in the cartridge. Weight measurements of the polymer bulk before and after extraction (and drying of the remaining solvent) give the gel fraction, according to equation 1-1.

$$\text{Gel content} = \frac{W_3 - W_1}{W_2 - W_1} \times 100 \qquad \textbf{Eq. 1-1}$$

with:
W_1: weight of the cartridge
W_2: weight of the polymer bulk before extraction
W_3: weight of the polymer bulk after extraction and solvent evaporation

A static method consists in placing the polymer bulk in a test tube or a bottle full of solvent and letting the solvent dissolves the soluble chains. It is easier to set up and, even if it takes longer to fully extract the soluble part (at least one week), several experiments can be done at the same time. The same gravimetric measurements give the gel/sol ratio and results are found to be consistent with the dynamic method, even if higher values are generally obtained. In all cases, the choice of an appropriate solvent is needed.

The gel fraction, composed by crosslinked polymer chains, is swollen by the solvent. The weight swelling ratio Φ (so-called swelling ratio later on) is the ratio between the weight of the swollen gel fraction and the weight of the dried one and can also be obtained from the extraction experiments (see equation 1-2).

$$\text{Swelling ratio } \Phi = \frac{W_4}{W_3} \qquad \textbf{Eq. 1-2}$$

where:
W_3 is the same as defined previously and
W_4 is the weight of the polymer bulk after extraction before solvent evaporation

In a completely swollen gel, polymer chains between crosslinks are stretched relative to their equilibrium unswollen configuration and it is thus possible to estimate the average molar mass between crosslinks with the Flory-Rehner equation: (Flory and Rehner, 1943)

$$\frac{RT}{G'} = M_c = -\left[\rho_2 V_1 \upsilon_2^{1/3}\right] / \left[\ln(1-\upsilon_2) + \upsilon_2 + \chi_{12}\upsilon_2^2/2\right] \qquad \textbf{Eq. 1-3}$$

giving that:

$$\upsilon_2 = \frac{1}{\Phi_2} \qquad \textbf{Eq. 1-4}$$

where the indice 1 refers to the solvant and the indice 2 to the polymer.
With:
G' : dynamic elastic modulus
M_c : molar mass between crosslinks
ρ_2 : density of the polymer
χ_{12} : Flory interaction parameter between solvent and polymer
V_1 : molar volume of the solvent
Φ_2 : swelling ratio of the polymer at equilibrium

For poorly crosslinked networks such as those found in PSA, which are composed of individual microgels (for each particle), it is not very meaningful to extract an average value of M_c. However the swelling ratio in a good solvent remains a good quantitative measure of the average level of crosslinking.

In a crosslinked polymer network, not only the gel content but also the gel architecture (Chauvet, Asua *et al.*, 2005) or the spatial distribution of the gel microdomains and their connectivity (do Amaral, Roos *et al.*, 2005) have an influence on the macroscopic properties. Swelling measurements are thus interesting to combine with the gel fraction measurements to bring information on this architecture.

The introduction of the different molecular weights and of the notion of gel and sol are very important as they are used to tune the adhesive properties of the adhesive layer. A brief review on their effect on mechanical properties is presented and ways of improvement of PSAs are then presented.

1.3.3 Important parameters of waterborne acrylic-based PSA

An optimized PSA requires a balance of properties of peel adhesion, tackiness and shear resistance. Peel strength and tack can be obtained if the material dissipates energy during the debonding process. This is the case for a highly viscous liquid. Shear resistance on the other side is obtained with a minimized creep at long times, which is optimum for solids. An optimal balance has to be found between these two opposite behaviors. In the family of acrylic polymers widely used for PSAs, striking this balance means choosing the right monomer composition and the right molar mass distribution and level of crosslinking. The influence of these three parameters has been studied for a long time and is partially reported here.

Monomer composition

To be able to bond the surface with only a light pressure, PSAs must be soft enough to wet the surface in a short time i.e. at high strain rates. The most important adjustment to have a material in the range of very soft polymer is on the glass transition temperature. Zosel in particular argued that a maximum of adhesion can be expected between 50 °C and 70 °C above the T_g of the copolymer the PSA is made of (Zosel, 1985). Thus, for a use at room temperature, copolymers must have a T_g close to -50 to -30 °C. This low T_g can be obtained with an appropriate monomer composition. However, when adjusting the monomer composition, one also has to take into account the changes in M_e due to the different monomers and their propensity for chain transfer reactions. For example, it is known that an increase in M_e gives a higher deformability and typically improves peel and tack. On the other hand, more transfer reactions to the polymer also changes the level of crosslinking in the polymer network.
In the usual acrylic compositions for adhesives, the main monomer has a very low T_g. Butyl acrylate (BA) and 2-ethyl hexyl acrylate (2EHA) are the most common monomers used in a PSA composition. Their weight proportions are around 80-90 %.
A high T_g monomer (typically, styrene but more often methyl methacrylate) is then added to finely adjust T_g. Also important in the monomer composition is the role of acrylic acid (AA).

The increase in the adhesion due to AA has been reported in the litterature (Chan, H.K. and Howard, G.J., 1978; Aubrey, D.W. and Sherriff, M., 1980; Gower, M.D. and Shanks, R.A., 2006). It is explained by the formation of hydrogen bonds at the adhesive-surface interface thanks to the acid functions of AA. However, AA can also increase the gel content and the long relaxation times, effect which typically reduces the level of dissipation and enhances the shear resistance. Once again, a precise adjustment of the AA proportions is required (Aubrey and Sherriff, 1980; Chan and Howard, 1978; Gower and Shanks, 2006).

Molar mass distribution

Increasing the resistance to shear requires a high level of cohesion in the polymer bulk. An increase in M_w goes in that direction, whereas a low M_w favors relaxation and dissipation in the network which in turn increases peel adhesion.
The molar mass and molar mass distribution are mainly controlled by the propensity of the monomers to have chain transfer reactions. The amount of chain transfer agent (CTA) can also be used to control the M_w. The role of a CTA is to neutralize the free radical in the polymer chain during radical polymerization. This limits the chain transfer reactions. Thus higher molecular weights with lower gel content are obtained. The impact is a decrease in the cohesion of the PSA, leading to a decrease in the shear resistance.

Level of crosslinking

To optimize shear resistance and cohesion inside the sample, it is necessary to get a relatively high amount of gel fraction (typically around 50%). This increases the elastic modulus and prevents flow. However, a too high gel content (coupled with high molecular weight) strongly decreases the dissipation properties and thus, peel strength and tackiness.
Furthermore, as explained in 1.3.1, in the particular case of waterborne PSA, when the gel content is too high, polymer chain mobility decreases and interdiffusion between particles occurs on a shorter distance. Interfaces are thus weaker, which does not favor high deformability. An optimized amount of CTA can be used to adjust the level of crosslinking to the required application. Generally, for PSA at room temperature, optimized properties are found for a gel content between 50-60% (Creton, 2003).

1.3.4 Tools to improve waterborne PSA's

Waterborne acrylic polymer network prepared by radical polymerization are relatively homogeneous. The optimization of adhesive properties is not easy to obtain and requires a fine adjustment of the network. Indeed, if one wants to improve resistance to shear, it is necessary to modify the network in a way that will decrease the peel and tack properties, and reciprocally.

Nevertheless, some strategies have been developed in the recent years to overcome this limitation and prepare materials with increasing properties as PSAs.

One of the main possibilities is to prepare latex particles with specific morphologies that will be retained in the final film during the drying. For example, Aymonier (Aymonier, Ledercq *et al.*, 2003) or Mallegol (Mallegol, Dupont *et al.*, 2001) have demonstrated that acrylic core-shell particles retain their initial structures in the final film. This type of film architecture can form a percolating network that improves large strain properties and hence increase adhesive properties.

Another work based on core-shell particles has been done in our lab by Deplace and coworkers (Deplace, 2008; Deplace, Rabjohns *et al.*, 2009). They prepared soft-soft core-shell particles with a shell that can crosslink during the drying of the latex by addition of a specific agent just before casting the latexes. This crosslinking occurs inside and between shells and is a way to obtain stronger interfaces between particles. A final percolating network is obtained. The soft core increases the dissipation in the materials, whereas the percolating network improves the large strain elongation properties. They showed that even a thin shell can have strong effects on mechanical properties. They particularly focused on improvement of adhesion on low adhesive surfaces but one can think about the same strategies for higher adhesive surfaces.

Another type of strategies has been developed to improve adhesion of waterborne PSA on low adhesive surfaces. Recently a team from Spain (Agirre, Nase *et al.*, 2008) prepared acrylic particles in which they add a wetting agent directly inside the dispersion. The presence of hydrophobic components inside the latex particles had a positive effect on the adhesion on low energy surfaces (e.g. polypropylene).

With the aim to prepare new type of materials with outstanding properties, acrylic latexes were prepared with the addition of carbon nanotubes (CNT) in the particle dispersion: CNT functionalized with poly (vinyl-alcohol) are made hydrophilic and can be dispersed in water in a way that they interact with acrylic particles of butyl acrylate (BA) (Wang, T., Lei *et al.*, 2006). The effect is that adhesion energy is improved thanks to the CNT but the electrical properties also are increased.

These non exhaustive examples show that improvement of acrylic latexes for adhesive applications are brought by specific architecture or hybridization of particles. However, not so many researches on hybrid particles for adhesive applications have been made for the moment. This is explained by the fact that the requirements on microstructure and molecular architecture are not yet well defined to improve mechanical properties (Deplace, Rabjohns *et al.*, 2009). However, this is an emerging field and new products start to appear, mainly based on hybrid polymer particles.

The state of the art on polyurethane/acrylic hybrid particles will be presented in the next section but one can already say that it represents an interesting field to optimize properties of adhesives. Indeed the hybridization of these two polymers can be a way to maintain a satisfying level of adhesion with the acrylic and to improve film formation, water or chemical resistance, or temperature resistance with the polyurethane.

1.4 Polyurethane chemistry

1.4.1 Generalities on the polyurethane

Polyurethanes (PU) are obtained by the reaction of an isocyanate with a hydroxyl group which gives a urethane group, –RNHCOOR'–. The wide diversity of the final polyurethane family comes from the possible combination of many different isocyanates with numerous different polyols. Furthermore commercial PU systems frequently contain urea and allophanate groups. The first development as a usable product has been made by Otto Bayer (1902-1984) in 1937 (German Patent 728.981 (1937) I.G. Farben). The first goal of the work on polyurethanes was to synthesize synthetic fibers to supply nylon. As for many polymeric products, World War II saw the development of the polyurethane technology and its applications were extended as substitute of nylon and natural rubber not only as a fiber but also for coatings applications. But the main development of polyurethanes is due, as often in chemistry, to an involuntary mistake. The accidental addition of water during the basic reaction produced polyurethane foam. From this point, in 1954 began the production and commercialization of flexible polyurethane foams. Nowadays, polyurethane foams remain a wide field of application (*e. g.* structural or isolating foam) but applications also exist as paints, print papers or adhesives (Berthier). In the specific field of Pressure Sensitive Adhesives, PU are mainly used as low tack, low peel protective liners (Satas, 1989).

1.4.2 Elements of polyurethane chemistry

Polyurethanes are versatile polymers based on a urethane group –RNHCOOR'– (also named carbamate) obtained by the reaction between an isocyanate and an hydroxyl by polyaddition. The general reaction is the following:

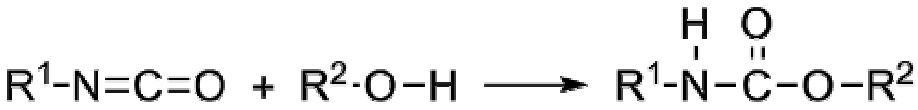

Figure 1-5: Generalized polyurethane reaction

Polyurethane polymers are formed through step-growth polymerization by reacting a monomer containing at least two isocyanate functional groups with another monomer containing at least two hydroxyl groups. The presence of a catalyst is required to accelerate the reaction. The final polyurethane is a block-copolymer with polyols as soft-segments and isocyanate as hard-segments. The various numbers of isocyanates and polyols open a wide field of possible polyurethanes. The use fo multifunctional building blocks can easily lead to crosslinked networks as well.

Polyols:

Polyols are low molar mass polymers based on a primary hydroxyl group –OH. Diols and triols are the most common compounds. Their low-molar mass polymer represents the soft segment of the polyurethane polymer. The main part of the soft chain is typically either a polyether (which cannot crystallize) or a polyester (which can crystallize). A variety of properties can be obtained by changing the ratio of short and long polyols.

Isocyanates:

They are reactive compounds characterized by the presence of a –N=C=O group. The most common aromatic isocyanates are the TDI (toluene diisocyanate) and the MDI (diphenyl methane diisocyanate). Aliphatic ones also exist such as hexamethylene diisocyanate (HDI) or isophorone diisocyante (IPDI). Examples of these molecules are presented in Figure 1-6. Due to the low mobility of the -NCO groups and their complex structure, isocyanates together with short diols represent the hard-segments.

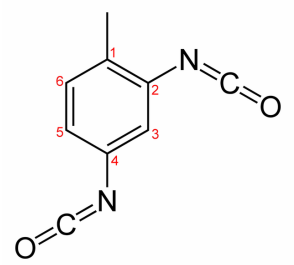

Toluene diisocyanate TDI

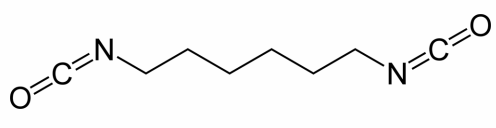

Hexamethylene diisocyanate
HMDI

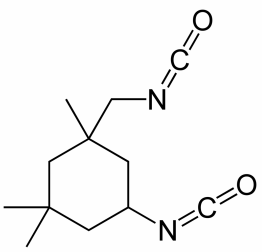

Isophorone Diisocyanate IPDI

Figure 1-6: Structures of aromatic and alliphatic diisocyantes

The isocyanate function is highly reactive with active hydrogens present in the –OH or –NH groups. Although reaction with an alcohol is wished for the formation of polyurethane, reactions with other components containing active hydrogens are possible: water, amine, or carboxylic acid, based on the reaction principle detailed below:

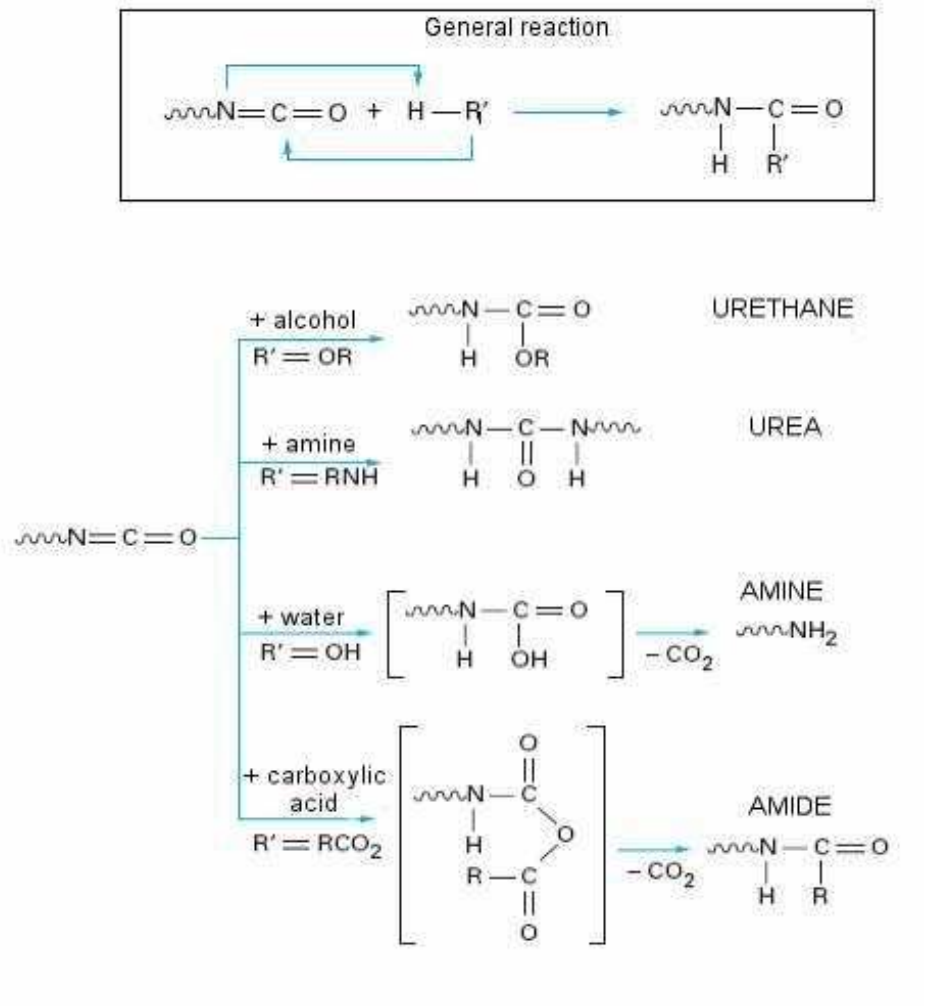

Figure 1-7: Possible reactions of isocyanate group (after (Berthier))

The stoechiometric ratio of hard segments (isocyanate) to soft segments (polyols) strongly affect the properties of the final product such as viscosity or M_e (Florez, Munoz *et al.*, 2005; Florez, Munoz *et al.*, 2006). The ratio of isocyanate to hydroxyl groups (NCO/OH) also represents a crucial parameter in the formation of the final product (Berthier). Indeed, an excess of NCO during polymerization will lead to the formation of a reactive polyurethane, that is to say final polyurethane still containing isocyanate groups. In this type of polyurethane, the reactions described below can still occur as long as –NCO groups remain. The polyurethane used in this work is a reactive one, which gives possibilities of hybridization with other types of polymers, among those acrylate polymers, by reaction with an acrylic monomer containing a hydroxyl group (e.g. HEMA, hydroxyl ethyl methacrylate). The chain extension process also becomes possible thanks to small hydrophobic diol molecules, such as Bisphenol A (BPA). Both reactions are crucial in the PU incorporation inside the particles and are detailed in Figure 1-8 and Figure 1-9.

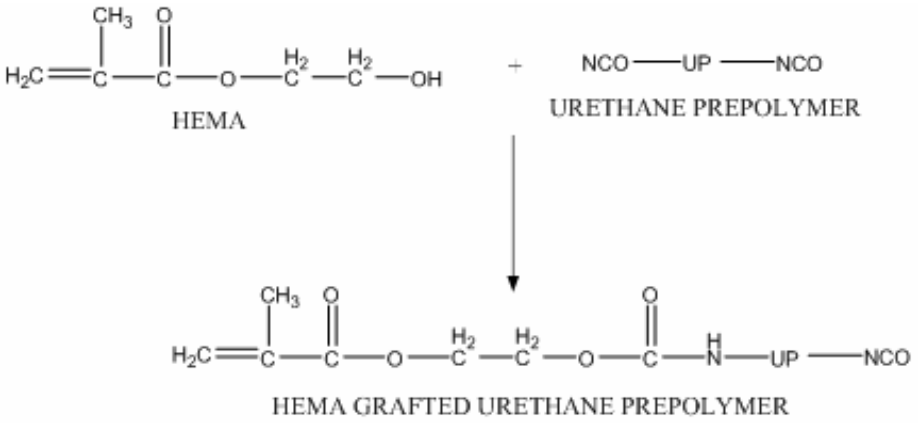

Figure 1-8: Grafting reaction between PU and HEMA (Udagama, 2009)

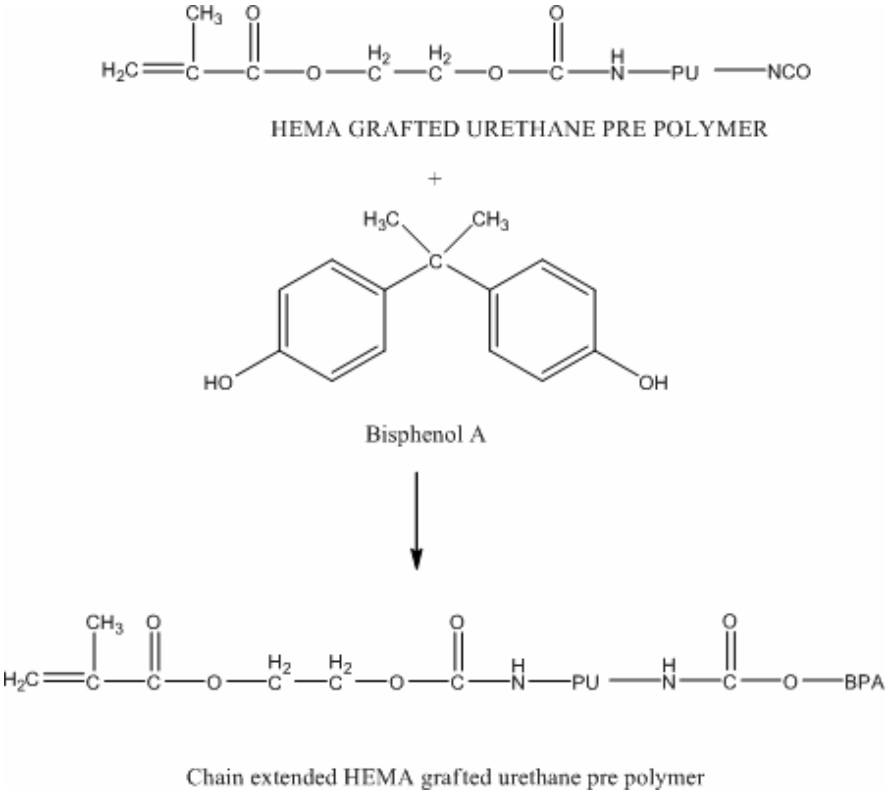

Figure 1-9: Chain extension of grafted PU by Bisphenol A (Udagama, 2009)

1.4.3 Waterborne PU and PU/acrylic hybrids

High chemical and solvent resistance, good film-formation or toughness are the main advantages of polyurethane. Nevertheless, a high cost and its solvent-borne nature can appear as drawbacks for some applications (Gooch, Dong *et al.*, 2000; Kukanja D., Golob J. *et al.*, 2000; Li, Daniel *et al.*, 2005; Wang C., Chu F. *et al.*, 2005). To optimize the cost/performance balance, PU are often used in hybrid systems with polyesters, alkyds or acrylics (Kukanja,

Golob *et al.*, 2000; Li, M., Daniel *et al.*, 2005). Acrylic/urethane ones are the most widespread hybrids nowadays. Acrylic brings the outdoor and alkali resistance, the fast drying, the pigmentability and the low cost; urethane enhances toughness, flexibility and film-forming performances. These hybrid systems have been developed for a long time: in 1981 for example, low peel adhesives have been prepared by polymerizing a low molar mass acrylic containing hydroxyl groups with an isocyanate terminated prepolymer (US Patent 4,306,996) (Schenk, 1981; Satas, 1989)

However, the development of waterborne polymers also impacted on polyurethane and aqueous dispersions are nowadays an important part of polyurethane uses, even if the high cost remains. As acrylic polymers are the most widespread in the field of waterborne polymers, they are naturally used to form urethane/acrylic hybrid emulsions and several studies have been carried out on these systems since the end of the 1990s. It is worth noting that high molar mass PU and acrylic polymers are mutually immiscible. That impacts on the films obtained from such latexes where phase separation can take place. Therefore, efforts have to be made to improve the combination of polyurethane and acrylics.
Hegedus and Kloiber (Hegedus and Kloiber, 1996) published in 1996 a study on aqueous acrylic-urethane dispersions. The two polymers were produced at the same time and formed interpenetrating networks (IPN), increasing the miscibility of both components.
Then, Kukanja and coworkers (Kukanja, Golob *et al.*, 2000) developed a hybrid process. They polymerized acrylic monomers in emulsion in the presence of a PU aqueous dispersion. No chemical reaction occurs in this specific system but PU particles can be swollen by acrylic polymers so that both type of chains are either entangled or partially grafted. The authors found that this process improved both mechanical and chemical properties of the films compared to simple physical blends of two polymer emulsions.
Another option to improve compatibility of both components has been investigating by Hirose *et al*. They prepared core-shell hybrid latexes through an emulsion process. Acrylic/Urethane (A/U), Urethane/Acrylic (U/A) and Acrylic/Urethane-*graft*-Acrylic (A/U-g-A) particles were prepared with different acrylic/urethane ratios. They prepared successfully Acrylic/Urethane in a first study (Hirose, Kadowaki *et al.*, 1997). The core-shell structure was clearly observed by transmission electronic microscopy (TEM). The analysis of the film showed that the surface was polyurethane-rich and that a crosslinking took place within and between particles. In a second paper (Hirose, Zhou *et al.*, 2000), they prepared core-shell structure with acrylic in the shell by phase inversion method from amphiphilic acrylic-urethane graft copolymers. Once again, the hydrophilic component in the shell orientates preferentially at the surface layer of the final films.
Gooch *et al.* were the first to study the option to obtain such systems by miniemulsion polymerization (Gooch, Dong *et al.*, 2000). Using oil-modified polyurethane (OMPU) as the hydrophobe, they performed miniemulsion polymerization of a (MMA, BA, AA) monomer mix. Impact of the ratio between OMPU and acrylate on the chemical and mechanical properties was analyzed and they showed in particular that the presence of double bonds remaining in the OMPU facilitated the grafting (at least partial) of PU on the acrylic.

A very interesting study has been carried out by Wang *et al.* since 2003 (Wang, Chu *et al.*, 2003; Wang, Chu *et al.*, 2006; Wang C., Chu F. *et al.*, 2005; Wang C., Chu F. *et al.*, 2005; Wang, Chu *et al.*, 2009). They also used miniemulsion polymerization to produce urethane/acrylic hybrid properties. A polyurethane obtained from isophorone diisocyanate (IPDI) and polypropylene glycol (PPG) was used as a hydrophobe and miniemulsified in a monomer mixture of MMA and BA. They performed a complete study from chemical properties of the latexes to the mechanical properties of the dried films and confirmed a better homogeneity of these particles compared to physical blends. Studying the impact of the PU fraction, they showed in particular that an optimum exists for mechanical properties. In a paper focused on mechanical properties of such systems(Wang, C. , Chu, Graillat, Guyot and Gauthier, 2005), they showed that it is possible to graft the PU chains to the acrylic chains by modifying the PU chain ends with a methacrylic group. This grafting produces PU chains bonded to the acrylic network with two crosslinking points. The films obtained from these particles are slightly stiffer compared to the ones with non-grafted PU.

Finally, the work of Li, El-Aasser *and co* (Li, M., Daniel *et al.*, 2005) introduces the fundamentals of the PU preparation used in the present study. Also based on a miniemulsion process, they prepared polyurethane/poly(n-butyl methacrylate) hybrid latex particles of a very small diameter (~50nm). The PU chains were grafted to the acrylic network, still through a hydroxyl-ended acrylate (hydroxyl ethyl methacrylate HEMA here). They were also chain-extended with the help of a hydrophobic chain extender inside the particles. This chain extender is a small molecule with hydroxyl groups at both ends with the ability to react with two PU chains. Although they performed a full study of latex properties, no mechanical properties of such hybrids were tested.

Morphologies of such hybrids have also been investigated, mostly from a thermodynamic point of view. Some previous works demonstrated the importance of different crucial molecular parameters on the morphologies of hybrid latex particles: the interfacial tension between the two immiscible liquids (Torza and Mason, 1970), the viscosity inside the polymerization locus (in emulsion, micelles or particles mainly) related the mobility of the chains (Dimonie, Elaasser *et al.*, 1988) or the free energy balance (Sundberg, Casassa *et al.*, 1990).

The recent work of a Taiwanese group (Li, C.-Y., Chiu *et al.*, 2007) used thermodynamic considerations to predict the morphologies of PU/PMMA hybrid particles obtained from miniemulsion. They varied the type of initiator, the amount of chain extender and the ratio NCO/OH during preparation of the PU. They showed in particular that for systems close to the ones presented here, homogeneous hybrid particles should be obtained.

Specific techniques like atomic force microscopy (AFM), scanning electron microscopy (SEM) or transmission electron microscopy (TEM) have been used to study the morphology from an experimental point of view. However, most of time imaging techniques were used to compare hybrid systems with blends. It appeared that hybrid particles have a more homogeneous morphology. Furthermore, Wang and coworkers (Wang, C., Chu, Graillat, Guyot, Gauthier *et al.*, 2005; Wang, C., Chu *et al.*, 2006) showed that the higher the grafting of polyurethane , the more homogeneous the particles are.

The hybridization of polyurethane and acrylics in aqueous dispersion has been widely reported for a decade now. Nevertheless, despite the numerous studies on such systems, almost no system with very soft hybrid particles suitable for adhesive applications has been investigated.

1.5 Adhesive and mechanical characterizations of PSAs

PSAs are very soft viscoelastic materials characterized by a fraction of insoluble part around 50 % and by an elastic modulus at 1 Hz usually lower than 0.1MPa (Creton, 2003). The specific characterization techniques used to analyze these materials fall into three categories:

- characterization of the morphology
- characterization of the deformation properties in small and large strain
- characterization of the adhesive properties

We briefly summarize here the standard tools used to describe PSAs.

1.5.1 Characterization of the morphology

1.5.1.a AFM technique

The observation of latex particles and latex film-formation has seen remarkable progress with the development of atomic force microscopy (AFM). For example, the different steps of the film-formation process have been understood with this technique ((Keddie, 1997). Also the migration of solvents stabilizing the latex particles has been studied by AFM. However, the fact that very soft particles have a T_g low below room temperature have limited, at first, the observation of waterborne films to coatings (i.e. with T_g close to or higher than room temperature) and waterborne acrylic PSA had not been imaged before the work of Mallégol and coworkers in 2001 (Mallegol, Dupont *et al.*, 2001).

PSAs require indeed contradictory conditions for optimized imaging. The most appropriate mode is the intermittent or tappin mode (TM) where the AFM tip is oscillated by a piezzocrystal near the canitlever resonnace frequency is brought into contact with the sample surface when it reaches the lower point of its oscillation. This limits the damages of the soft surface. To minimize the surface deformation of very soft surfaces made of PSA particles, a light tapping is required. But, as particles are also tacky, they requires an energetic tapping to debond from the surface during each cycle (Mallegol, Dupont *et al.*, 2001). Hence, a good equilibrium must be found between the different parameters of the tapping mode (the spring constant of the cantilver k, the cantilever initial amplitude A_0 and the ratio between the tip-surface distance and the initial amplitude, called the set point r_{sp}).

The AFM technique has been used by Brown *et al* (Brown, Coogan *et al.*, 2005). to study the morphology of urethane/acrylic waterborne particles. They prepared acrylic particles by emulsion polymerization with PU dispersion as a seed and observed the final particles. The tapping mode was used and they could determine structured particles with hard and soft regions. However, their particles were hard particles for applications as coatings.

If AFM can be used to characterize hybrid particles morphology, electronic microscopy (and in particular transmission electronic microscopy, TEM) is most often preferred.

1.5.1.b TEM observations

Transmission electronic microscopy is often used to study the PU/acrylic hybrid particles. In spite of the existing contrast in electronic density between polyurethane chains and acrylic chains, one phase of the sample is generally stained (acrylic or PU phase equivalently). TEM was used in particular by Hirose *et al* to observe single particle morphology (staining with osmium tetroxide) and determine the mechanism of particle formation (Hirose, Kadowaki *et al.*, 1997; Hirose, Zhou *et al.*, 2000). In the important work of Wang and coworkers on urethane/acrylic hybrid particles, for coating applications the morphology was determined by staining styrene units especially added to the acrylic phase with uranyl acetate. TEM imaging was used to detect any heterogeneity at the particle scale between particles between particles prepared by emulsion and miniemulsion. When prepared by miniemulsion polymerization, particles were homogeneous whereas seeded emulsion polymerization resulted in phase-separated morphologies. The observation of the films obtained from the seeded emulsions showed that the specific morphology may be retained after drying (Wang, C., Chu *et al.*, 2006).

It is also common to stain polyurethane with phosphotungstic acid (PTA) before imaging particles morphology (Li, M., Daniel *et al.*, 2005; Chai, Jin *et al.*, 2008). An interesting theoretical work on particle morphology has been proposed by Li *et al* (Li, C.-Y., Chiu *et al.*, 2007). Based on thermodynamic calculations, they proposed different morphologies for PU/PMMA hybrid particles depending on the ratio between isocyanate NCO and hydroxyl OH groups, the type of initiator and the PU chain extender. TEM is as a great tool to compare their calculation to images of particles prepared in their specific conditions. The images they obtained were in good agreement with the morphologies predicted by calculation.

However, if TEM is widely used for urethane/acryilic hybrid particle observations, only few studies focused on morphology of films obtained from the drying of these particles (Wang, C., Chu, Graillat, Guyot, Gauthier *et al.*, 2005; Wang, C., Chu *et al.*, 2006).

Moreover, for adhesive applications, as films are well above T_g at room temperature, the use of a cryo-ultramicrotome is required to be able to section rigid thin layer of material for the TEM observations.

1.5.2 Characterization of adhesive properties

A PSA is characterized by an optimal balance of properties of peel, shear and tack. Peel is correlated to the force required to remove the PSA from its substrate. The shear resistance is referred to the minimization of creep in shear, whereas tack is defined as the capacity to stick instantaneously to a substrate with a light pressure.

In the industry, several organizations (ASTM, PSTC, TLMI, AFERA, FINAT) have implemented a normalization for these tests. They are briefly exposed in a first section. However, the in-depth understanding of the mechanisms occurring during debonding is limited with this type of empirical tests. To overcome this limitation, the probe-tack test has

been developed (Zosel, 1989) and improved (Lakrout, Sergot *et al.*, 1999; Josse, Sergot *et al.*, 2004). This test properly analyzed can bring crucial information to identify accurately adhesive properties and mechanisms.

1.5.2.a Industrial characterization

Examples of the classical industrial tests used to evaluate PSA properties are presented in Figure 1-10.

The peel adhesion quantifies the strength required to remove (adhesively or cohesively) the PSA from a standard test plate surface, over the width of the tape, at a given velocity (Figure 1-10 a and b). It is expressed in N/m. The peeling rate, the substrate or the time between bonding and debonding (i.e. contact time) can be varied. The angle between the adhesive strip and the substrate can be 90° or 180°. The peeling properties are strongly influenced by the viscoelasticity: peel strength is dependent on the dissipative properties and on the deformability of the sample. However, a level of cohesion in the PSA is required to ensure a debonding at the interface PSA/substrate, i.e. an adhesive debonding (Derail, C., Allal, A. *et al.*, 1997; Derail, C., Allal, A. *et al.*, 1999; Marin, G. and Derail, C., 2006). For permanent PSA as well as for non-permanent, the peel strength must be well controlled. The adhesive debonding is required to avoid residus on the substrate after the debonding.

Different tack methods exist such as the loop tack test (a loop of adhesive is brought into contact with a substrate and removed (Figure 1-10-d)), the rolling ball (a stainless-steel ball rolls on an inclined ramp and come in contact with the adhesive strip). All these tests provide quick results regarding to the adhesive properties and are easy to implement. Nevertheless, they bring limited information on the details of the debonding mechanisms. The probe-tack test, developed at the end of the 1980s has filled this gap.

Generally speaking, tack refers to the ability of the PSA to stick instantly and with a light pressure on a substrate. To have a good tack, adhesive layers must be able to deform easily in the time scale allowed for bond formation. In this way it can conform to the topological irregularities of the substrate. The tack properties can be controlled by a good optimization of the rheological properties. An important viscous part ensures the tackiness during contact. Moreover, since good tack involves the breaking of the bond, tack is enhanced by a low short time modulus and greater ultimate elongation at break and very viscoelastic behavior.

The resistance to shear, more commonly called shear in the context of PSA, characterizes the time before an adhesive bond, submitted to a normalized shear force, fails, adhesively or cohesively (Figure 1-10-c). The PSAs msut resist shear over a long period of time (e.g. FINAT method requires a shear resistance of at least 10 000 min) and a minimized creep in the material favors this resistance. To have a satisfying shear resistance a certain level of cohesion must be present in the material at low frequency so that it can resist flow. Thus, a good shear resistance can be reached when the material has an acceptable elastic modulus at small and intermediate strains and does not exhibit liquid-like behavior but is, on the contrary, characterized by a strain hardening at high strains. It has been shown that long

term creep can be greatly reduced and thus resistance to shear can be greatly enhanced by crosslinking (Creton, 2003; Deplace, Carelli *et al.*, 2009).

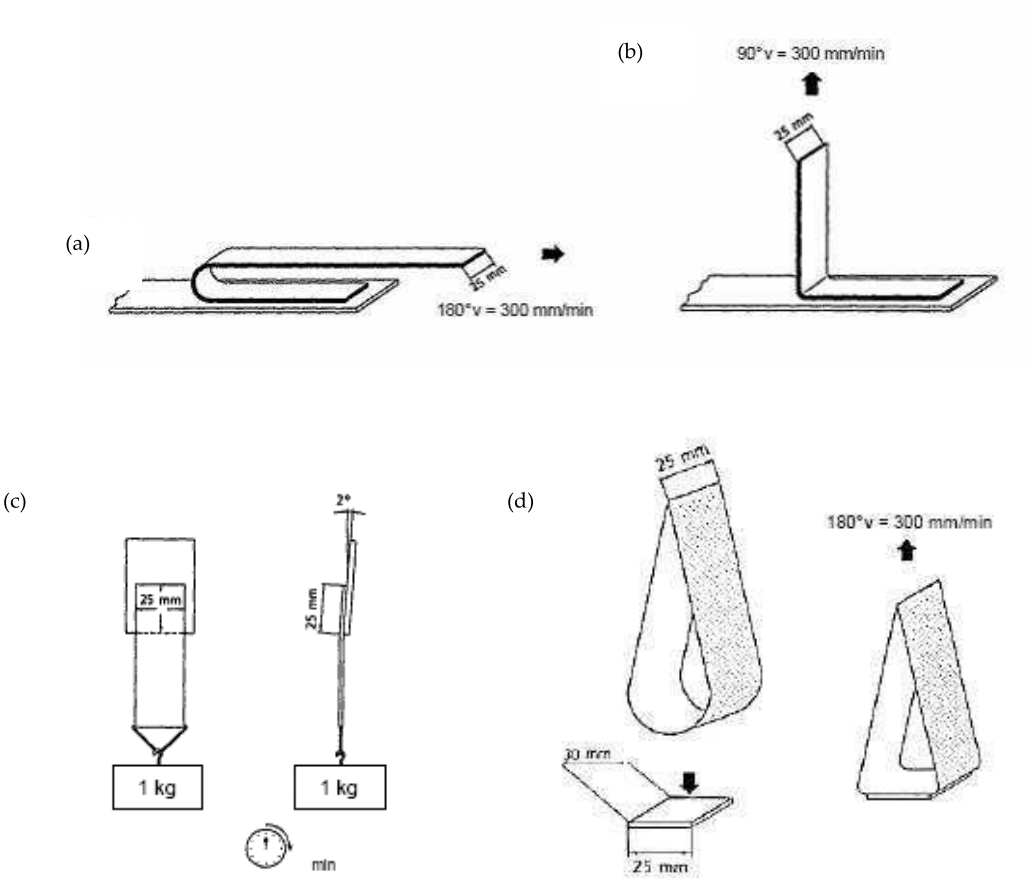

Figure 1-10: Standard tests; (a): 180-degree peel test; (b): 90-degree peel test; (c): shear test; (d) loop-tack test

1.5.2.b Probe-tack test

Despite advantages of easy set up and quick analysis of the results, the standard industrial tests presented above provide limited information on the debonding mechanisms. Moreover, it is neither possible to control independently the experimental parameters (contact time and pressure, debonding velocity) (Creton and Fabre, 2002) nor to describe these mechanisms as a function of time (Lakrout, Sergot *et al.*, 1999). Furthermore, they are pretty dependent on test geometries (Creton and Fabre, 2002). An instrumented probe-tack test was developed for the first time by Zosel (Zosel, 1989) at the end of 1980s and improved by further studies done in particular in our laboratory with the development of a real time visualization setup (Lakrout, Sergot *et al.*, 1999; Creton and Fabre, 2002; Josse, Sergot *et al.*, 2004). These improvements and especially the in-situ visualization have brought very important information on the deformation behavior of thin adhesive films. The highlights obtained from this probe-tack test have been recently reviewed by Shull and Creton (Shull and Creton, 2004).

In a typical probe-tack test, a flat-ended probe comes in contact with an adhesive film cast on rigid substrate. After contact (with controlled pressure and time), the probe is pulled off from the film. The debonding can be so-called "adhesive" (with interfacial detachment of the adhesive layer from the probe) or "cohesive" with a failure within the adhesive layer, as exposed in Figure 1-11. An optimized PSA (permanent or non permanent) has to debond adhesively to leave clean substrates.

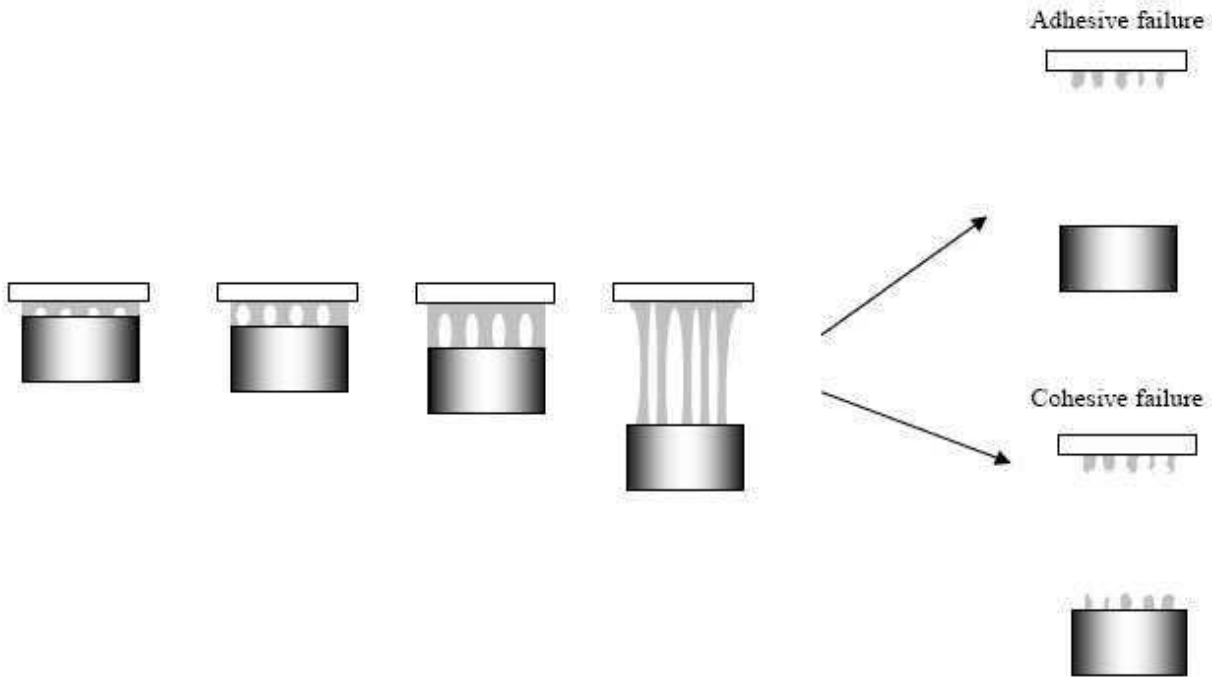

Figure 1-11: Sequences of a probe-tack test with two possible debonding scenarii

The force *F* required to debond the probe and the displacement of the probe *d*(t) are recorded during the test. From these data, stress *vs.* strain tack curves $\sigma_N = f(\varepsilon)$[1] can be obtained (see Figure 1-12).

The specific shape of the curve corresponding to an optimized PSA (Figure 1-12) and the associated mechanisms have been intensively studied (Creton and Fabre, 2002; Creton C. and L., 1996; Lakrout, Sergot *et al.*, 1999) and will not be detailed here. Nevertheless, some general comments on the interpretation of the stress-strain curves are necessary to understand this thesis work.

The sharp peak at low strain corresponds to the first stages of debonding, i.e. the nucleation and growth of cavities in the confined adhesive layer when the probe is pulled. The maximum of the curve, σ_{max}, is related to the elasticity and cohesion of the samples: the stiffer the adhesive layer is, the higher is the stress required to nucleate cavities. The plateau observed after the peak characterizes the fibrillation mode. At this stage, the contact area is filled of cavities and the walls of these cavities are stretched. A fibrillar structure is observed. The stress corresponding to the beginning of fibrillation, σ_f, depends on the sample elasticity at large strains (Roos and Creton, 2005) whereas the moment where this stress drops back to

[1] In tack test, the strain is usually written ε, even if large strain can be reached

zero, $\varepsilon_{max,}$ (debonding of the fibrils from the substrate) is a complex function of the level of dissipation and of the elasticity at very large strains (strain hardening).

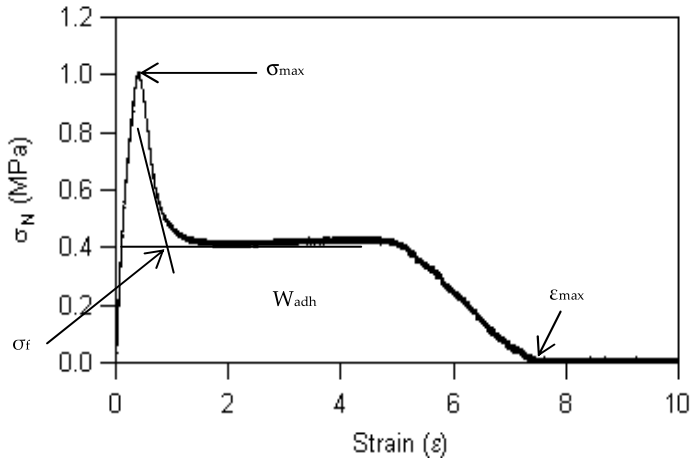

Figure 1-12: Curve obtained with a probe-tack test for a typical PSA

The adhesion energy W_{adh} is defined as the area under the curve multiplied by the initial thickness of the layer h_0:

$$W_{adh} = h_0 \int_0^{\varepsilon_{max}} \sigma_N d\varepsilon \qquad \textbf{Eq. 1-5}$$

It is a simple quantitative tool to compare PSA having the same debonding mode. For permanent PSA, the adhesion energy W_{adh} must be as high as possible, as long as an adhesive failure occurs.

This type of debonding mode is strongly dependent on the viscoelastic properties of the samples and on a fine balance between viscous and elastic behaviours. When the balance is not properly achieved, different debonding modes can be observed. They also have been extensively studied (Creton C., Hooker J. *et al.*, 2001; Crosby, Shull *et al.*, 2000) and are presented in Figure 1-13.

Materials with a very high elastic modulus and low level of dissipation debond adhesively but with a lack of fibrillation and with low adhesion energy (Figure 1-13-a). The cavities are formed but coalesce when they came in contact and an interfacial propagation of cracks occurs. This debonding mode is required for non-permanent PSA, such as Post-It Notes© that must debond easily.

On the other side of the spectrum, when materials are very dissipative and almost not elastic, a cohesive failure takes place. Fibrils are formed but a lack of cohesion inside each fibril makes them break in their middle at very large strains. This mode, represented on Figure 1-13-c, is not desirable at all for a good PSA.

Intermediate fibrillation mode (Figure 1-13(b)) can sometimes present a hardening stage, characterized by an increase of the plateau stress, like on Figure 1-13(b2).

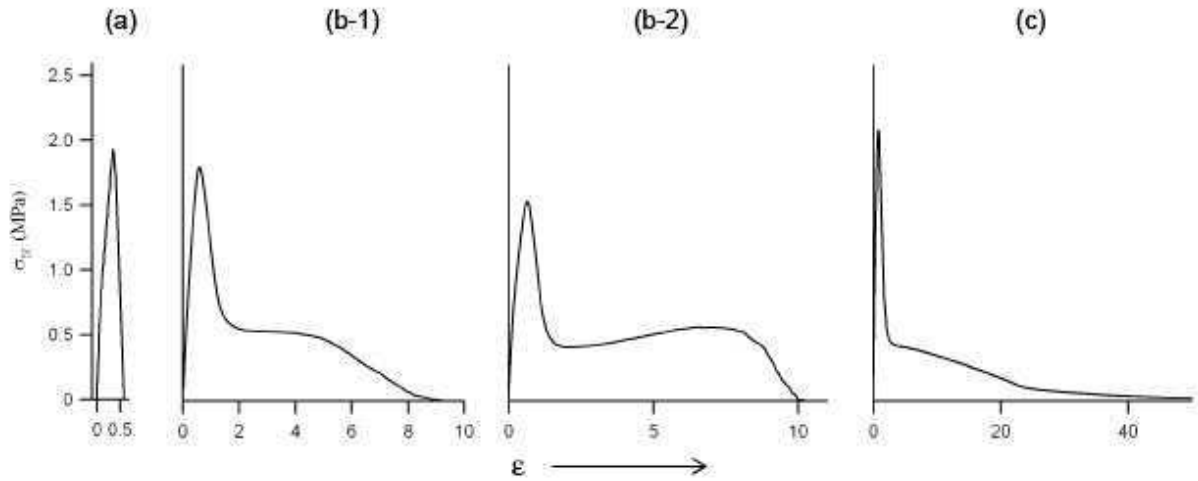

Figure 1-13: Different stress-strain tack curves; (a) : interfacial debonding ; (b) : fibrillation debonding with hardening in the case of b-2 ; (c) liquid-like behavior with cohesive debonding

1.5.3 Prediction of the debonding mode from linear small-strain viscoelasticity

With classical rheology measurements, values of storage modulus G', loss modulus G'' and phase angle tanδ are obtained. Some assumption can be made to predict the debonding mode from these quantities.

For example, the well-known Dahlquist criterion (Dahlquist, 1969) says that the elastic modulus G' at 1 Hz must be usually lower than 100-200kPa. This refers to the necessity of the material to be soft enough to wet the surface to fit the topological defects of the surface at high strain rates (i.e. short contact times). On the prediction of the debonding modes, nevertheless, one can go further using the rheological properties of the adhesives.

Indeed, the debonding mode depends directly on the growth of the cavities nucleated in the early stages of the probe-tack test. This growth can be correlated with the small-strain linear viscoelastic properties (Lakrout, Creton *et al.*, 2001; Lindner, Lestriez *et al.*, 2006).

The evolution of cavities is governed by the competition between two phenomena. On one hand, the cavities can propagate at the interface and this mainly depends on the critical energy-release rate G_c. This energy release rate G_c can be seen as the energy required by the system to make an interfacial crack move. On the other hand, the growth of the cavities in the bulk is controlled by the elastic modulus E and the energy necessary to deform the bulk of a sample of thickness b and elastic modulus E can be written as Eb.

The ratio G_c/Eb (with some simplification considering G_c/E) has then been determined as a satisfying criterion to predict the debonding mode (Crosby, Shull *et al.*, 2000; Creton, Hooker *et al.*, 2001; Webber, Shull *et al.*, 2003). Indeed, when the propagation of a crack costs high energy, bulk mechanisms are preferred for the cavity growth. On the other side, interfacial mechanisms are favored when the elastic deformation of layers requires high energy. Nevertheless, the exact determination of the G_c remains complex and work has been done to establish relationship between this values and the rheological properties of the materials.

First, it is useful to recall that $\mathcal{G}_c$ for viscoelastic materials can be written as

$$\mathcal{G}_c = \mathcal{G}_0(1+\varphi(a_T v)) \qquad \textbf{Eq. 1-6}$$

as established by Maugis and Barquins (Maugis and Barquins, 1978).

$\mathcal{G}_0$ is the limiting value of the energy release rate at low rates. $\varphi(a_T v)$ represents the viscoelastic dissipation in the system, that can be proportional to $\tan\delta = G''/G'$, according to Maugis and Barquins. One can then re-write $\mathcal{G}_c \sim \mathcal{G}_0\tan\delta$, and substitute it in $\mathcal{G}_c/Eb$. One finally gets:

$$\frac{\mathcal{G}_C}{Eb} \sim \frac{\mathcal{G}_0 \tan\delta}{G'b} \qquad \textbf{Eq. 1-7}$$

with
G': the dynamic elastic modulus
b: the initial thickness

This parameter depends only on the linear rheological properties of the adhesive and on the determination of $\mathcal{G}_0$, easy obtained by measuring the work of adhesion at very low rate (Carelli, Deplace *et al.*, 2007). Hence we have an effective parameter to determine the debonding process. The efficient prediction of the debonding mode from this parameters has been demonstrated by Deplace (Deplace, Carelli *et al.*, 2009) and a more complete experimental verification has been carried out by Nase (Nase, Lindner *et al.*, 2008).
The $\mathcal{G}_c/Eb$ ratio can be used as a good prediction of the propensity of the PSA to form fibrils during debonding. A critical value can be determined below which the crack propagation mode is preferred to the growth of cavities in the bulk and the fibrillation mode. This value varies with the substrate, as energy release rate $\mathcal{G}_0$ depends only on the surface energy.
However, when going to very high values of $\mathcal{G}_0\tan\delta/G'$, this criterion becomes irrelevant Indeed, when the elastic modulus becomes much lower than the Dahlquist criterion, the sample cannot sustain a resistance to shear high enough and will flow, which is not acceptable for a good PSA.
The non-linear large strain viscoelasticity which evaluate more finely long relaxation times and crosslinking can bring additional clues usable to optimize adhesive properties.

1.5.4 Prediction of the debonding mode from the non-linear large strain viscoelasticity

If linear small strain properties are useful to predict which debonding mode is favored between interfacial propagation of cracks and fibrillation process, no criteria has been well defined yet to predict whether eventual adhesive or cohesive failure will occur.
To understand the problem, one has to think that when fibrillation occurs, the walls of the cavities, forming the fibrils, are elongated to very large strains. The confined geometry of the beginning of the test, which favors shear stresses, is no longer valid at large strain and long time. The shape of the fibril structure depends on the competition between viscoelastic extension of the cavity walls and detachment of these fibrils from the probe (Verdier and Piau, 2003).
The non-linear elastic behavior has to be taken into account and tensile experiments represent then an appropriate tool to predict the adhesive layer behavior at large strain. The standard curve representing the nominal stress σ_N vs the strain λ[2] for a typical viscoelastic adhesive is shown on Figure 1-15. This curve is characterized by a linear increase of the stress corresponding to the linear elastic regime. This regime is influenced by the number of permanent and non-permanent crosslinking points in the material. The second phase of the curve shows a less pronounced increase (and sometimes even a decrease) of the stress in the domain of intermediate strains. It is generally called "softening" and is due to the relaxation process in the material. After this "softening" phase, the stress strongly increases again in the very large strain regime. This is characteristic of the "hardening" in the sample when the finite extensibility of the chains is reached. The final part of the curve corresponds to the drop of the stress after a maximum is reached, which is due to the failure of the sample after striction or flow in the material. It is generally not relevant of a specific behavior of the material and is not taken into account.

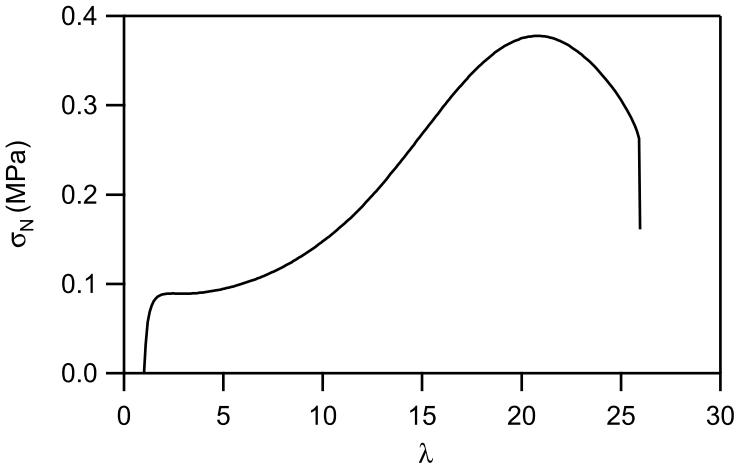

Figure 1-14 : Standard tensile curve $\sigma_N = f(\lambda)$ for a typical soft viscoelastic adhesive

[2] $\lambda = 1+\varepsilon$
In the large strain regime, this notation λ is generally preferred to ε, which refers to the the small strain

The terms of "softening" and "hardening" are defined from the comparison of the experimental behavior in tension of a soft rubber with the theoretical behavior as a neo-Hookean material made by Treloar (Treloar, 1975) and represented below.

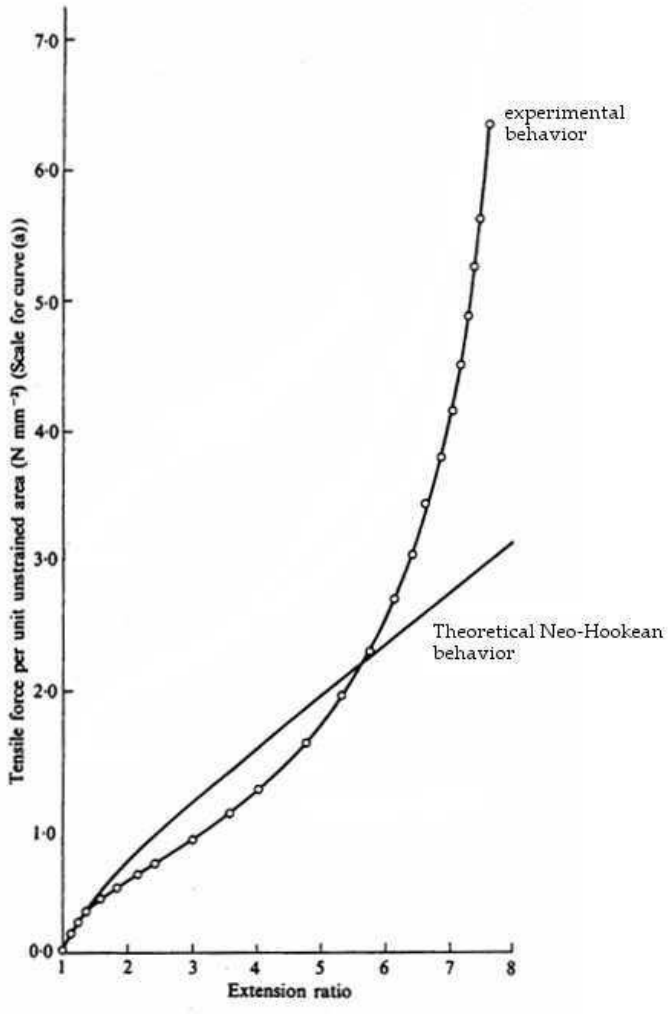

Figure 1-15: Theoretical neo-Hookean and experimental behaviors of a standard rubber (after Treloar)

Hence, at intermediate strain, the rubber requires less force than the theoretical neo-Hookean model to reach the same strain (there is softening), whereas at large strain, a larger force is required (there is hardening). The standard viscoelastic adhesive shows the shape of curve than the rubber, with more pronounced softening.

The softening stage is characteristic of a pronounced viscoelastic behavior. Indeed, softening comes from the relaxation of non-permanent crosslinks and of free chains. This relaxation generates dissipation of the energy accumulated during the fibrils extension. It is worth noting that this relaxation is due to the topological reorganization of the entanglements and to the viscoelastic flow of the free chains. Thus it is both strain and strain-rate dependent.
On the other hand, the hardening stage is related to the finite extensibility of the shorter elastic chains of the polymer network. At this point, chain elasticity is no longer Gaussian

(entropic) but as it becomes more and more extended, interatomic forces replace the rearrangement of the entanglements, as described in Langevin's molecular model (Treloar, 1975). This hardening stage is crucial to determine the type of debonding: from this point, less dissipation takes place and energy coming from the stretching is stored in the fibrils. When the stored energy is higher than the surfaces forces, the fibrils can detach adhesively from the probe (Glassmaker, Hui *et al.*, 2008).
On the contrary, in the case of under-crosslinked liquid-like samples, no hardening can be observed because polymers chains flow instead of harden when finite extension is reached. On the point of view of the tack experiment, this results in a failure of the fibrils in their middle, i.e. a cohesive debonding.

Although softening and hardening are characteristic of the material, it is not always easy to properly define them from a nominal stress σ_N *vs* strain λ curve. The Mooney representation is often preferred to analyze the non-linear behavior of PSAs and quantitatively compare samples. This representation is based on the Mooney or reduced stress σ_R, defined as:

$$\sigma_R = \frac{\sigma_N}{\left(\lambda - \frac{1}{\lambda^2}\right)} \qquad \textbf{Eq. 1-8}$$

It corresponds to the normalization of the reduced stress by the predicted behavior of a standard (or Neo-Hookean) rubber having the same modulus as the PSA and it is generally plotted versus $1/\lambda$, as seen on Figure 1-16.

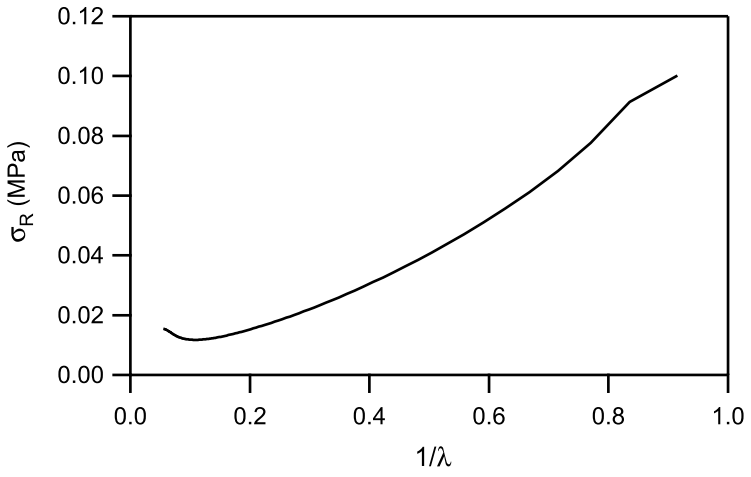

Figure 1-16: Mooney representation of the reduced or Mooney stress σ_R versus the inverse strain $1/\lambda$

The softening corresponds to the decreasing part of the curve, read from right to left, whereas the beginning of the hardening is characterized by the minimum of the curve. The existence of this well-defined minimum is thus a good prediction of an adhesive debonding of the fibrils (Deplace, Carelli *et al.*, 2009).
From this representation, two characteristic parameters of the non-linear behavior can be determined, characterizing respectively the softening and hardening, C_{soft} and C_{hard}. These

empirical parameters have been first defined by Deplace (Deplace, Carelli *et al.*, 2009) and as the same qualitative physical significance than the G_e and G_c parameters of the Rubinstein-Panyukov model for elastic networks (Rubinstein and Panyukov, 1997). Of course they do not replace a fit with a full non linear viscoelastic model but are much easier to determine for the purpose of comparing materials and their physical significance remains clear.

The C_{soft} characterizes the relaxation and orientation of the entanglements present in the materials. It has been defined as the slope of a line drawn between ($\sigma_R(0.8)$; $1/\lambda = 0.8$) and ($\sigma_R(min)$; $1/\lambda(min)$). The C_{soft} characterizes the non-permanent crosslinking in the network and the relaxation phase. After this softening phase, the minimum in reduced stress is characteristic of the beginning of the hardening, corresponding to the moment where the finite extensibility of the network chains can be felt. C_{hard} is defined as the reduced stress corresponding to this minimum. Figure 1-17 illustrates the determination of these two parameters which have the physical meaning of relaxing and non relaxing part of the initial modulus.

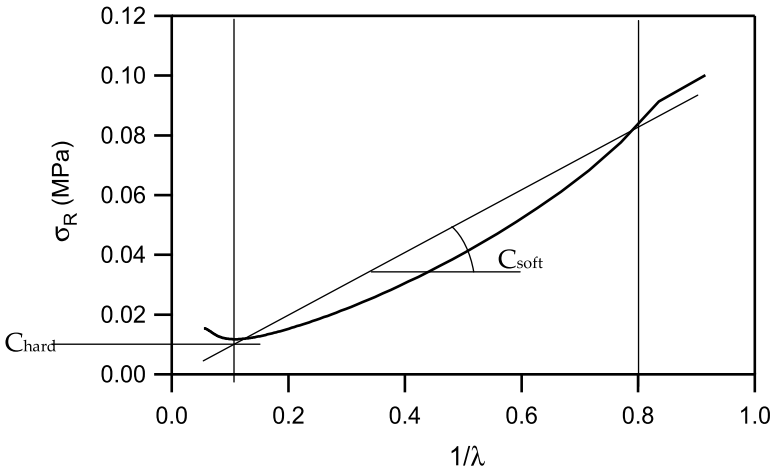

Figure 1-17: Determination of C_{soft} and C_{hard}

The C_{soft}/C_{hard} ratio corresponds to the viscoelastic relaxation of the sample relative to its permanent crosslink structure (Deplace, Carelli *et al.*, 2009). Then, one can note that a high C_{soft}/C_{hard} ratio characterizes a dissipative sample with many non-permanent crosslinks (that can relax) and less permanent crosslinks. It is then correlated with long fibrillation plateau in the tack test.

On the contrary, if the material contains more permanent crosslinks (typically covalent bonds), low values of C_{soft}/C_{hard} are obtained. In that case, the storage of elastic energy during elongation is favored and leads to a rapid debonding of the adhesive layer when this energy is released. Interfacial propagation of cracks is then favored.

When polymer networks are under-crosslinked, chains flow instead of harden when finite extensibility is reached. No macroscopic hardening can be observed on the Mooney representation but a decrease of the nominal stress is observed at failure. This point is used then to define the slope for the determination of C_{soft} but C_{hard} is then undefined. During the tack test, a cohesive debonding is observed (Deplace, Carelli *et al.*, 2009).

These parameters can be used to tune the adhesive properties of PSAs measured by a probe-tack test. To summarize what has been explained here:

- the ratio C_{soft}/C_{hard} has to be high enough (e.g. a value ~ 2-3 has been demonstrated has optimal for adhesion on stainless steel (Deplace, Carelli *et al.*, 2009)) to have a good balance between dissipation and elasticity
- C_{hard} has to be defined, that is to say hardening is required to ensure an adhesive debonding

Note that these two parameters cannot be simultaneously optimized for a homogeneous network (with elastic chains having the same length). That is where the precise design of the network can play an essential role.

1.5.5 Prediction of the resistance to shear from the creep behavior

The two previous sections demonstrated how tackiness of an adhesive can be predicted from linear small-strain viscoelasticity and from non-linear large-strain behavior. Over the recent years, efforts have also been made to establish correlations between peel and small-strain rheological properties of materials (Derail, Allal *et al.*, 1997; Derail, Allal *et al.*, 1999). Furthermore, it is known that correlation can be made between peel and tack mechanisms (Kaelble, 1965; Creton and Fabre, 2002). Finally, the short-time failure mechanisms appear to be now well understood.

Nevertheless, not only tack and peel but also resistance to shear must be optimized in a standard PSA. In particular, the holding time (the time before an adhesive fails from a substrate when a constant weight is applied) must be as high as possible for the permanent PSA above all. But the shear tests can be long (for example FINAT test method recommends a holding time of 10000 min to validate the shear resistance of a PSA) and this is a major argument to try to find criteria for shear resistance and correlations with viscoelastic properties of the materials.

Moreover, typical test to measure shear resistance are very simple (a weight is fixed to the adhesive layer and holding time is measured) and do not allow accurate measurement of the deformation and mechanisms in the adhesive layer. Some studies have been performed on PSA to overcome these limitations. Zosel, for example, developed in 1994 (Zosel, 1994) a specific static shear test with the aim to correlate the results with rheological properties of the adhesive layer. He established that for low-viscosity samples (η_0 in the range of $2.5\ 10^5$Pa.s), satisfying predictions of the holding time are obtained from the dynamic viscosity of the polymer. This work was continued by Vaynberg (Vaynberg, Berta *et al.*, 2001) who showed that a power law constitutive equation for the viscosity is more accurate to predict shear resistance of more viscous PSA (highly branched or crosslinked PSA).

More recently, Lindner and coworkers (Lindner, Maevis *et al.*, 2004) focused on failure mechanisms at long time range. They studied the behavior of confined adhesive layer placed in a geometry equivalent to the one of the probe-tack test. The adhesive is pulled and then

kept under load for a given time. Deformation was measured and a video set-up allowed the observation of the failure mechanism. They noticed that two specific mechanisms are in competition during this creep loading: the nucleation of cavities and the propagation of interfacial cracks. Interestingly, they did not noticed simple homogeneous creep only. However, adhesive layers were highly confined in that case.

Resistance to shear is correlated to long-time failure mechanism. To enhances this resistance, it is clear that minimized creep must occur in the PSA (Creton, 2003). This minimized creep can be obtained through an important cohesion inside the material. Specific studies focused on the long-time creep behavior (i.e. the evolution of strain with time), of an adhesive under constant load. In most cases, however, these studies applied to structural adhesives such as epoxy (Dean, 2007), fiber reinforced composites (Ashcroft, Hughes *et al.*, 2001) in single or double lap-shear geometry. Few works have been found based on a tensile geometry. One by Wang *et al* focused on the creep behavior of elastomers (Wang, H. C., Thompson *et al.*, 2001). They showed in particular that the Burgers model, a viscoelastic model combining springs and dashpots, was efficient to describe the creep behavior of such materials. The same type of work has been made by a German team (Gleiss and Brockmann, 1997) on pressure-sensitive tapes and they obtained satisfying description of the creep behavior with this simple model.

Nevertheless, the use of creep experiments in a tensile geometry to predict the shear resistance of PSA has not been reported yet.

1.6 References

- Agirre, A., Nase, J., Creton, C.,Asua, J. M.; *Adhesives for Low-Energy Surfaces*; 48th Microsymposium on Polymer Colloids - From Design to Biomedical and Industrial Applications; Prague, CZECH REPUBLIC; **2008**.
- Arzamendi, G.,Asua, J. M.; *Macromolecules*; **1995**; *28*; (22); 7479-7490.
- Ashcroft, I. A., Hughes, D. J., Shaw, S. J., Wahab, M. A.,Crocombe, A.; *Journal of Adhesion*; **2001**; *75*; (1); 61-+.
- Asua, J. M.; *Progress in Polymer Science*; **2002**; *27*; (7); 1283-1346.
- Aymonier, A., Ledercq, D., Tordjeman, P., Papon, E.,Villenave, J. J.; *Journal of Applied Polymer Science*; **2003**; *89*; (10); 2749-2756.
- Berthier, J.-C.; *Techniques de l'Ingénieur*.
- Blackley, D. C.; *Emulsion Polymerisation*; London, Applied Science Publishers LTD; **1975**.
- Brown, R. A., Coogan, R. G., Fortier, D. G., Reeve, M. S.,Rega, J. D.; *Progress in Organic Coatings*; **2005**; *52*; 73-84.
- Carelli, C., Deplace, F., Boissonnet, L.,Creton, C.; *Journal of Adhesion*; **2007**.
- Chai, S. L., Jin, M. M.,Tan, H. M.; *European Polymer Journal*; **2008**; *44*; 3306-3313.
- Chauvet, J., Asua, J. M.,Leiza, J. R.; *Polymer*; **2005**; *46*; 9555-9561.
- Creton, C.; *MRS Bulletin*; **2003**; *28*; (6); 434-439.
- Creton, C.,Fabre, P.; *The mechanics of adhesion*; Dillard, D. A. and Pocius, A. V.: Amsterdam, Elsevier; **2002**; *1;* 535-576.
- Creton, C., Hooker, J.,Shull, K.; *Langmuir*; **2001**; *17*; 4948-4954.
- Crosby, A. J., Shull, K. R., Lakrout, H.,Creton, C.; *Journal of Applied Physics*; **2000**; *88*; (5); 2956-2966.
- Dahlquist, C. A.; *Treatise on Adhesion and Adhesives*; Patrick, R. L., Dekker; **1969**; *2;* 219-260.
- Dean, G.; *International journal of adhesion and adhesives*; **2007**; *27*; (8); 636-646.
- Deplace, F.; *Adhésifs Nanostructurés en Voie Emulsion*; PPMD: Paris; **2008.**
- Deplace, F., Carelli, C., Mariot, S., Retsos, H., Chateauminois, A., Ouzineb, K.,Creton, C.; *Journal of Adhesion*; **2009**; *85*; 18-54.
- Deplace, F., Rabjohns, M. A., Yamaguchi, T., Foster, A. B., Carelli, C., Lei, C. H., Ouzineb , K., Keddie, J. L., P.A., L.,Creton, C.*Bottom-up design of a soft-soft nanocomposite from polymer colloid particles*.**2009**. 5; 1440-1447.
- Derail, C., Allal, A., Marin, G.,Tordjeman, P.; *Journal of Adhesion*; **1997**; *61*; (1-4); 123-157.
- Derail, C., Allal, A., Marin, G.,Tordjeman, P.; *Journal of Adhesion*; **1999**; *68*; (3-4); 203-228.
- Dimonie, V., Elaasser, M. S.,Vanderhoff, J.; *Polymer Material Science and Engineering*; **1988**; *58*; 821-832.
- do Amaral, M., Roos, A., Asua, J. M.,Creton, C.; *Journal of Colloid and Interface Science*; **2005**; *281*; (2); 325-338.
- Doi, M.,Edwards, S. F.; *The theory of polymer dynamics*, Oxford; **1986**.
- Dos Santos, F. D.,Leibler, L.; *Journal of Polymer Science Part B-Polymer Physics*; **2003**; *41*; (3); 224-234.
- Dos Santos, F. D., Fabre, P., Drujon, X., Meunier, G.,Leibler, L.; *Journal of Polymer Science Part B-Polymer Physics*; **2000**; *38*; (23); 2989-3000.
- Farzi, G., Bourgeat-Lami, E.,McKenna, T.; *Journal of Applied Polymer Science*; **2008**.
- Florez, S., Munoz, M. E.,Santamaria, A.; *Journal of Rheology*; **2005**; *49*; (1); 313-325.

- Florez, S., Munoz, M. E.,Santamaria, A.; *Macromolecules Materials Engineering*; **2006**; *291*; 1194-1200.
- Flory, P. J.,Rehner, J.; *Journal of Chemical Physics*; **1943**; *11*; (11); 521-526.
- Glassmaker, N. J., Hui, C. Y., Yamaguchi, T.,Creton, C.; *European Physical Journal E*; **2008**; *25*; (3); 253-266.
- Gleiss, P. L.,Brockmann, W.; *Journal of Adhesion*; **1997**; *63*; (4); 253-263.
- Gooch, J. W., Dong, H.,Schork, F. J.; *Journal of Applied Polymer Science*; **2000**; *76*; (1); 105-114.
- Guyot, A., Landfester, K., Schork, J. F.,Wang, C.; *Progress in Polymer Science*; **2007**; *32*; 1439-1461.
- Halary, J. L.,Laupretre, F.; *De la Macromolécule au Matériau Polymère;* Ed.^Eds. Series, Belin.**2006**.
- Hegedus, C. R.,Kloiber, K. A.; *Journal of Coatings Technology*; **1996**; *68*; (860); 39-&.
- Heyes, D. M.,Sigurgeirsson, H.; *Journal of Rheology*; **2004**; *48*; (1); 223-248.
- Hirose, M., Kadowaki, F.,Zhou, J. H.; *Progress in Organic Coatings*; **1997**; *31*; (1-2); 157-169.
- Hirose, M., Zhou, J. H.,Nagai, K.; *Progress in Organic Coatings*; **2000**; *38*; (1); 27-34.
- Joanicot, M., Wong, K.,Cabane, B.; *Macromolecules*; **1996**; *29*; 4976-4984.
- Josse, G., Sergot, P., Creton, C.,Dorget, M.; *Journal of Adhesion*; **2004**; *80*; (1-2); 87-118.
- Jovanovic, R.,Dubé, M. A.; *Journal of Macromoleculaar Science Part C: Polymer Reviews*; **2004**; *C44*; (1); 1-51.
- Kaelble, D. H.; *Transactions of the Society of Rheology*; **1965**; *9*; (2); 135-163.
- Keddie, J. L.; *Materials Science & Engineering R-Reports*; **1997**; *21*; (3); 101-170.
- Kukanja, D., Golob, J., Zupancic-Vlant, A.,Kranjc, M.; *Journal of Applied Polymer Science*; **2000**; *78*; 67-80.
- Lakrout, H., Sergot, P.,Creton, C.; *Journal of Adhesion*; **1999**; *69*; (3/4); 307-359.
- Lakrout, H., Creton, C., Ahn, D. C.,Shull, K. R.; *Macromolecules*; **2001**; *34*; (21); 7448-7458.
- Landfester, K.; *Macromolecular Rapid Communications*; **2001**; *22*; (12); 896-936.
- Laureau, C., Vicente, M., Barandiaran, M. J., Leiza, J. R.,Asua, J. M.; *J. of Applied Polymer Science*; **2000**; *81*; 1258-1265.
- Laureau C., Vicente M., Barandiaran M.J., Leiza J.R.,Asua J.M.; *J. of Applied Polymer Science*; **2000**; *81*; 1258-1265.
- Li, C.-Y., Chiu, W.-Y.,Don, T.-M.; *Journal of Polymer Science Part A: Polymer Chemistry*; **2007**; *45*; 3359-3369.
- Li, M., Daniel, E. S., Dimonie, Sudol, E. D.,El-Aasser, M. S.; *Macromolecules*; **2005**; *38*; 4183-4192.
- Lin, F.,Meier, D. J.; *Langmuir*; **1995**; *11*; (7); 2726-2733.
- Lin, F.,Meier, D. J.; *Langmuir*; **1996**; *12*; (11); 2774-2780.
- Lindner, A., Maevis, T., Brummer, R., Luhmann, B.,Creton, C.; *Langmuir*; **2004**; *20*; (21); 9156-9169.
- Lindner, A., Lestriez, B., Mariot, S., Creton, C., Maevis, T., Luhmann, B.,Brummer, R.; *Journal of Adhesion*; **2006**; *82*; (3); 267-310.
- Lopez, A., Chemtob, A., Milton, J. L., Manea, M., Paulis, M., Barandiaran, M. J., Theisinger, S., Landfester, K., Hergeth, W. D., Udagama, R., McKenna, T., Simal, F.,Asua, J. M.; *Industrial & Engineering Chemistry Research*; **2008**; *47*; (16); 6289-6297.
- Mallegol, J., Dupont, O.,Keddie, J. L.; *Langmuir*; **2001**; *17*; (22); 7022-7031.
- Mason, T.,Lorimer, J.; *Sonometry: theory, applications and uses of ultrasound in chemistry;* Ed.^Eds. Series; Chichester, Ellis Horwood.**1988**.

- Maugis, D.,Barquins, M.; *Journal of Physics D-Applied Physics*; **1978**; *11*; (14); 1989-2023.
- Mayer, A., Pith, T., Hu, G. H.,Lambla, M.; *Journal of Polymer Science Part B-Polymer Physics*; **1995**; *33*; (12); 1781-1791.
- Nase, J., Lindner, A.,Creton, C.; *Physical Review Letters*; **2008**; *101*; 074503.
- Ouzineb , K.; *Emulsion and miniemulsion polymerization*; Lyon; **2003.**
- Qiu, J., Charleux, B.,Matyjaszewski, K.; *Progress in Polymer Science*; **2001**; *26*; (10); 2083-2134.
- Roos, A.,Creton, C.; *Macromolecules*; **2005**; *38*; (18); 7807-7818.
- Routh, A.,Russel, W.; *Industrial Engineering Chemistry Research*; **2001**; *40*; 4302-4308.
- Rubinstein, M.,Panyukov, S.; *Macromolecules*; **1997**; *30*; (25); 8036-8044.
- Rubinstein, M.,Colby, R. H.; *Polymer Physics;* Ed.^Eds. Series; Oxford, Oxford University Press.**2003**.
- Satas, D.; *Handbook of pressure-sensitive-adhesives*; Satas, D.: New York, Van Nostrand Reinhold; **1989**; *1;* 396-456.
- Satas, D.; *Handbook of pressure-sensitive-adhesives*; Satas, D.: New York, Van Nostrand Reinhold; **1989**; *1;* 518-526.
- Schenk, W. N.; US, B.F. Goodrich Company.**1981**. 4,306,996.
- Shull, K. R.,Creton, C.; *Journal of Polymer Science Part B-Polymer Physics*; **2004**; *42*; (22); 4023-4043.
- Smith, W. V.,Ewart, R. H.; *Journal of Chemical Physics*; **1948**; *16*; (6); 592-599.
- Stepto, R. F. T.; *Pure and Applied Chemistry*; **2009**; *81*; (2); 351-353.
- Sundberg, D. C., Casassa, A. P., Pantazopoulos, J., Muscato, M. R., Kronberg, B.,Berg, J.; *Journal of Applied Polymer Science*; **1990**; *41*; (7-8); 1425-1442.
- Torza, S.,Mason, S.; *Journal of Colloid and Interface Science*; **1970**; *33*; 67-76.
- Treloar, L. R. G.; *The physics of rubber elasticity*: Oxford, Clarendon Press; **1975**; 210-310.
- Udagama, R.; *Synthesis of polymer-polymer hybrids by miniemulsion polymerization and characterization of hybrid latex*; Laboratoire de Chimie, Catalyse, Polymères et Procédés: Lyon; **2009.**
- Vaynberg, K. A., Berta, A. T.,Dunckley, P. M.; *Journal of Adhesion*; **2001**; *77*; (4); 275-284.
- Verdier, C.,Piau, J. M.; *Journal of Polymer Science Part B-Polymer Physics*; **2003**; *41*; (23); 3139-3149.
- Wang, C., Chu, F., Graillat, C., Guyot, A.,Gauthier, C.; *Polymers For Advanced TEchnologies*; **2005**; *16*; 139-145.
- Wang, C., Chu, F., Guyot, A., C., G.,F., B.; *Journal of Applied Polymer Science*; **2006**; *101*; 3927-3941.
- Wang, C., Chu, F., Graillat, C., Guyot, A., Gauthier, C.,Chapel, J. P.; *Polymer*; **2005**; *46*; 1113-1124.
- Wang, H. C., Thompson, D. G., Schoonover, J. R., Aubuchon, S. R.,Palmer, R. A.; *Macromolecules*; **2001**; *34*; (20); 7084-7090.
- Wang, T., Lei, C. H., Dalton, A. B., Creton, C., Lin, Y., Fernando, K. A. S., Sun, Y. P., Manea, M., Asua, J. M.,Keddie, J. L.; *Advanced Materials*; **2006**; *18*; 2730-2734.
- Webber, R. E., Shull, K. R., Roos, A.,Creton, C.; *Physical Review E*; **2003**; *68*; (2).
- Wu, X. Q., Schork, J.,Gooch, J. W.; *J. of polymer science A: Polymer chemistry*; **1999**; *37*; 4159-4168.
- Zosel, A.; *Colloid and Polymer Science*; **1985**; *263*; (7); 541-553.
- Zosel, A.; *Journal of Adhesion*; **1989**; *30*; (1-4); 135-149.
- Zosel, A.; *Journal of Adhesion*; **1994**; *44*; (1-2); 1-16.

2. PREPARATION OF THE LATEXES

2.1 Introduction

All urethane/acrylic hybrid samples presented here have been prepared by miniemulsion polymerization. Two separate research groups specialized in emulsion polymerization synthesized the latex and used slightly different processes which are detailed here.
The first type of syntheses was carried out by Ravindra Udagama, from the LCPP lab at the CPE School in Lyon (France), under the supervision of Elodie Bourgeat-Lami and Timothy Mc Kenna. For these latexes, they used a three-step process where the polyurethane is prepared before being incorporated in the monomer solution and the miniemulsification. A batch process was used for radical polymerization of the acrylic. It is defined as Route I.
The second type of syntheses is defined as Route II is a one-step process based on a semi-continuous polymerization. The choice made for this process was to be closer to the industrial conditions used for the preparation of latexes. The route II has been used in the lab POLYMAT from the University of the Basque Country in Donostia – San Sebastian (Spain). Aitziber Lopez prepared the samples, supervised by Txema Asua.
The details of the polymerization procedure are described in specific thesis (Lopez 2009; Udagama 2009) and we only briefly recall here the main synthesis parameters which are necessary to understand our results.

2.2 Samples prepared by Route I

2.2.1 Synthesis

In Route I, a batch process has been used to synthesize the samples. The main monomer was n-butylacrylate, which, as a homopolymer has a T_g of -43 °C (Brandrup and Immergut 1999) so that final samples are in the range of very soft viscoelastic materials (Mallegol, Dupont et al. 2001).
The basic acrylic monomer composition of the matrix in weight percent (wt%) is as follow:

- Butylacrylate (BA): 89.5
- Methyl methacrylate (MMA): 9.5
- Acrylic acid (AA): 1

Incorez 701, a NCO terminated polyurethane (PU) prepolymer provided by Industrial Copolymers Limited, was incorporated in the acrylic polymer particles. This incorporation was performed in three steps:

1) The PU prepolymer chains were dissolved in the organic monomer phase, which also contained the hydrophobe costabilizer (octadecyl acrylate ODA) and hydroxyl ethyl methacrylate (HEMA). The reaction of free isocyanate groups (NCO) of the PU with the

hydroxyl moiety (OH) of the HEMA results in the grafting of the PU chains to the HEMA by polyaddition following the reaction described in Figure 2-1.

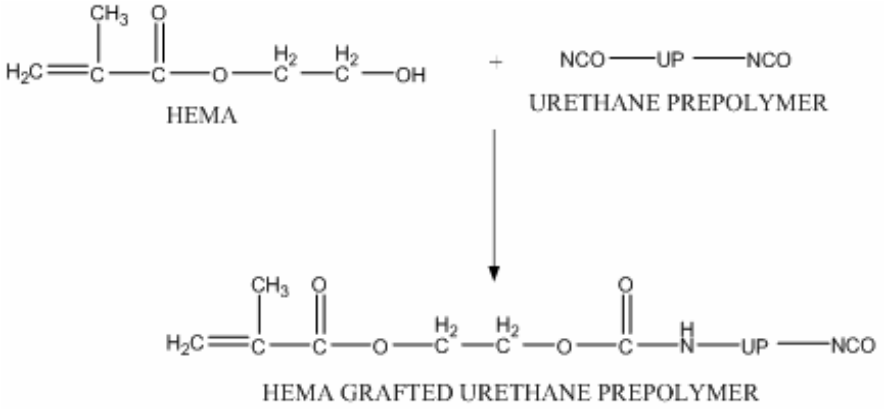

Figure 2-1: Polycondensation reaction between the end-functionalized urethane prepolymer and the hydroxyl function of the HEMA (Udagama 2009)

2) Bisphenol A (BPA) was added to the organic phase containing PU (including the PU that reacted with the HEMA). The Bisphenol A has a double hydroxyl moiety and can react with the remaining free NCO functions (see Figure 2-2). After step 1, a large number of free NCO functions remain in the solution and BPA played the role of chain extender of the PU prepolymer.

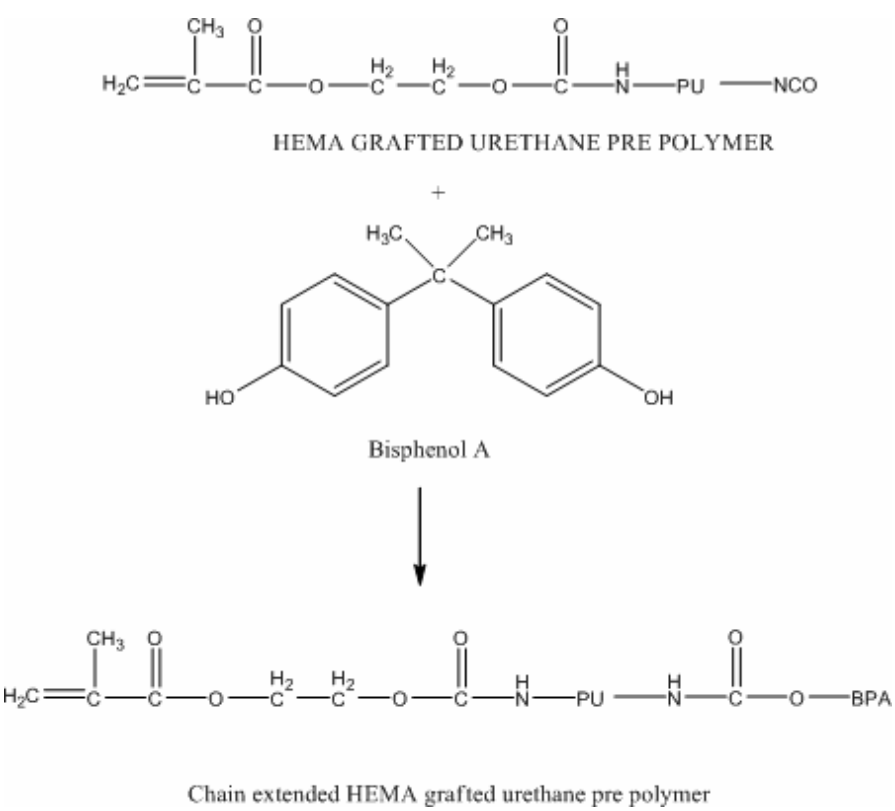

Figure 2-2: Polycondensation reaction between the isocyanate end group of the urethane prepolymer and the hydroxyl function of the Bisphenol A (Udagama 2009)

3) The organic phase containing the monomers and the HEMA-functionalized BPA-extended PU chains were added to the aqueous solution containing surfactant (Dowfax 2AI). Nanodroplets are formed by ultrasonication. The radical polymerization started with the addition of a redox initiator pair (Tertiary Butyl HydroPeroxide, TBHP, and Sodium Formaldehyde Sulfoxylate, SFS). Miniemulsion polymerization was carried out in batch.

To control the gel and sol fractions of the polymer in each particle, 1-dodecylmercaptan was used as Chain Transfer Agent (CTA) during the polymerization. A series of blank latexes containing no PU has been prepared by miniemulsion polymerization with weight fraction of CTA between 0 and 0.5 wt% relative to the total monomer content. In these matrices, neither HEMA nor BPA was added.

2.2.2 Compositional parameters

The two compositional parameters that were varied to control the incorporation of PU chains were the PU weight fraction and the HEMA/BPA molar ratio.
Different weight fractions of reactive PU prepolymer were incorporated in the acrylic organic phase before polymerization (step 1). The polyurethane weight ratio was calculated relative to the total monomer content to be between 5 wt% and 50 wt%.
The weight fraction of HEMA was varied to correspond to a given degree of grafting of the PU prepolymer. Between 5 % and 20 % of the NCO functions of the PU were reacted with HEMA. The extent of reaction of HEMA with the polyurethane prepolymer has been measured by inverse titration, and a maximum of 20% of the NCO functions can react with HEMA (Udagama 2009). BPA was added to neutralize the remaining NCO moieties and it is possible to calculate the molar ratio of OH functions coming from HEMA over OH functions coming from BPA, the so-called HEMA/BPA.
A limitation of the reaction between BPA and the free remaining NCO functions has been observed too. In Route I, Octadecylacrylate (ODA) is chosen as a hydrophobic component and is added to the particles to avoid Ostwald ripening (Landfester 2001). In presence of this hydrophobic costabilizer, flocculation of the particles was observed before the complete addition of the stoechiometric amount of Bisphenol A during the polymerization. The reason of this flocculation is related to the hydrophobic behavior of the particles when ODA is present in the particle core and is detailed by Udagama (Udagama 2009). Hence, only half of the calculated stoechiometric quantity of BPA can be added to the system to avoid flocculation. The first three series of latexes prepared by Route I have a ratio OH/NCO = 0.55. In the fourth series, ODA has been successfully taken out of the polymerization (without flocculation) and the stoechiometric amount of BPA can be added, so that OH/NCO=1. However, it is worth noting that even with a stoechiometric ratio OH/NCO=1, reaction between NCO and water is still probable.
Table 2-1 summarizes the different samples that have been prepared. The names of the samples are changed according to the synthesis route, the PU weight fraction, the ratio HEMA/BPA (or the CTA content for the first series of matrices) and the ratio OH/NCO. For

example, I_25PU(0.10)OH0.55 is a sample prepared in Route I, with 25 wt% of PU, a ratio HEMA/BPA equal to 0.10 and a ratio OH/NCO equal to 0.55.

Table 2-1: List of samples prepared by Route I

Sample	CTA[a]	% PU[b]	Grafting degree (%)	OH/NCO	HEMA/BPA[c]
I_0PU(0CTA)[d]	0	0			
I_0PU(0.5CTA)	0.5		/	/	/
I_0PU(0.2CTA)	0.2				
I_25PU(0.10)OH0.55	0.2	25	5	0.55	0.11
I_25PU(0.22)OH0.55			10		0.22
I_25PU(0.36)OH0.55			15		0.36
I_25PU(0.50)OH0.55			20		0.5
I_5PU(0.22)OH0.55	0.2	5	10		0.22
I_15PU(0.22)OH0.55		15			
I_35PU(0.22)OH0.55		35			
I_50PU(0.22)OH0.55		50			
I_25PU(0.11)OH1	0.3	25	10	1	0.11
I_25PU(0.25)OH1	0.2		20		0.25

a: wt%rel. to monomers
b: wt% rel. to monomers
c: molar ratio of the OH groups from HEMA over the OH group from BPA
d: No PU in these latexes; only the CTA fraction is indicated in the sample name

2.2.3 Calculation of the ratio HEMA/BPA in Route I

The ratio HEMA/BPA is defined as the molar ratio between OH functions coming from HEMA and OH functions coming from BPA:

$$\frac{HEMA}{BPA} = \frac{n(OH_{HEMA})}{n(OH_{BPA})} \qquad \textbf{Eq. 2-1}$$

In Route I, the degree of grafting GD is defined at the beginning of the synthesis and the weight fraction of HEMA is calculated according to this degree of grafting. The step 1 in the process allows a total reaction of the hydroxyl functions of HEMA with the isocyanate. We have:

$$n(OH_{HEMA}) = GD.n(NCO) \qquad \textbf{Eq. 2-2}$$

The Bisphenol A is added according to a previously defined ratio OH/NCO called θ and:

$$\theta.n(NCO) = n(OH_{HEMA}) + n(OH_{BPA}) \qquad \textbf{Eq. 2-3}$$

With equations 2-2 and 2-3 we have:

$$n(OH_{BPA}) = \theta.n(NCO) - GD.n(NCO) \qquad \textbf{Eq. 2-4}$$

And finally :

$$\frac{n(OH_{HEMA})}{n(OH_{BPA})} = \frac{HEMA}{BPA} = \frac{GD}{(\theta - GD)} \qquad \textbf{Eq. 2-5}$$

2.3 Samples prepared by Route II

2.3.1 Synthesis

Route II used conditions closer to industrial ones. In particular, the polymerization was performed in a semi-continuous process.
2-ethyl hexyl acrylate was used instead of butyl acrylate and the proportion of acrylic monomers was:

- 2 ethyl hexyl acrylate (2EHA): 97
- methyl methacrylate + hydroxy ethyl methacrylate (MMA + HEMA): 2
- methacrylic acid (MAA): 1

Droplets were stabilized by two surfactants: Dowfax 2A1 (2 % in weight by monomer wbm) and sodium dodecyl sulphate (SDS; 1% wbm). The hydrophobe stabilizing the particles and avoiding Oswald ripening was ODA (also called Stearyl Acrylate SA) (4% wbm) as in Route I. No chain transfer agent was added to the latexes.
The same reactive polyurethane Incorez 701 was used. A fixed amount of 10 % in weight relative to the total organic phase (wbo) of urethane prepolymer was added in all the recipes. The organic phase contained the acrylic monomers, the costabilizer ODA and the reactive urethane.

All organic components (monomers, PU prepolymer, grafting agent HEMA and chain extender BPA, and hydrophobic costabilizer ODA) were first mixed together. The organic phase is then mixed to the aqueous phase and miniemulsified in a Manton-Gaulin high pressure homogenizer (Lopez, Chemtob et al. 2008).
Polymerization occurred in the reactor with the addition of a thermal initiator, KPS (0.5% in weight by monomer, wbm). A seed of latex (20% of the total content) is produced by batch during one hour and the semi-continuous step is then started for 3 hours. A final cooking step lasted for 2 hours.

Incorporation of the PU chains in the acrylic copolymer backbone was made like in route I through the polycondensation of urethane with HEMA and/or BPA. They are added in the organic phase in controlled amounts. It is important to note that the weight fraction HEMA+MMA is fixed. Thus an increase in the fraction of HEMA results in a decrease in the fraction of MMA. The OH/NCO ratio was first kept equal to 1 and the molar ratio between grafting agent and chain extender (HEMA/BPA) was varied with values equal to 0.5/1/1.5/2.67. In a second stage, the OH/NCO ratio was varied to have an excess of hydroxyl (OH/NCO=2). This modification was made for three constant HEMA/BPA ratios (HEMA/BPA=0.21, 0.5. and 2.5). The ratio HEMA/BPA is calculated related to the HEMA weight fraction and to the OH/NCO ratio, based on the hypothesis that all HEMA moieties reacted with isocyanate. As

reaction of NCO with water was difficult to estimate, it was not taken into account although this reaction was highly probable. Calculation is detailed in the following section.

A blank latex (without PU) was prepared as reference sample. It contained neither PU nor BPA but HEMA was included in the acrylic part.
The Table 2-2 lists all the samples prepared in Route II with their main characteristic. The sample names are based on the same principle than in section 2.1.

Table 2-2: List of samples prepared with Route II

Sample	PU content[a]	HEMA/BPA[b]	Theoretical grafting degree[c]	OH/NCO
II_0PU(0)	0%	/	/	/
II_10PU(0.5)OH1	10%	0.5	35%	1
II_10PU(1)OH1		1	48%	
II_10PU(1.5)OH1		1.5	57%	
II_10PU(2.67)OH1		2.67	70%	
II_10PU(0)OH2		No grafting	0%	2
II_10PU(0.21)OH2		0.21	35%	
II_10PU(0.54)OH2		0.54	70%	
II_10PU(2.32)OH2		2.32	140%	

a: wt% rel. to monomers
b: molar ratio of the OH groups from HEMA over the OH group from BPA
c: based on the hypothesis that all HEMA react with free NCO

2.3.2 Calculation of the HEMA/BPA ratio and the degree of grafting

As explained previously, the ratio HEMA/BPA is:

$$\frac{HEMA}{BPA} = \frac{n(OH_{HEMA})}{n(OH_{BPA})} \quad \textbf{Eq. 2-6}$$

The weight of HEMA is calculated according to the monomer quantity:

$$m(HEMA) = \alpha.m(mon) \quad \textbf{Eq. 2-7}$$

with α the wt% of HEMA.

$$\text{Thus } n(OH_{HEMA}) = \alpha.\frac{m(mon)}{M(HEMA)} \quad \textbf{Eq. 2-8}$$

with M(HEMA) = 130 g.mol^{-1}

The ratio between OH and NCO (θ) is known and we have:

$$\theta.n(NCO) = n(OH_{HEMA}) + n(OH_{BPA}) \quad \textbf{Eq.2-9}$$

so that:

$$\frac{n(OH_{HEMA})}{n(OH_{BPA})} = \frac{n(OH_{HEMA})}{\theta n(NCO) - n(OH_{HEMA})} \quad \textbf{Eq.2-10}$$

The calculation of the molar quantity of NCO is now required. We have:

$$n(NCO) = \frac{m(PU)}{M_{eq}(NCO)} \quad \textbf{Eq. 2-11}$$

M_{eq} is the equivalent weight of isocyanate. It is the mass of polymer which corresponds to one mole of reactive NCO moiety. In the case of our polyurethane, we have

M_{eq}(NCO) = 1050 g.mol^{-1}

In the recipe, the polyurethane weight fraction is related to the total organic phase (wbo) so that:

$$m(PU) = \%PU(m(organic)) \quad \textbf{Eq. 2-12}$$

with:

$$m(organic) = m(monomers) + m(PU) + m(costabilizer) \quad \textbf{Eq. 2-13}$$

We can define φ the weight percentage of PU and express the PU weight:

$$m(PU) = \frac{\varphi}{1-\varphi}[m(mon) + m(co)] \quad \textbf{Eq. 2-14}$$

where

m(mon) is monomer weight and m(co) the costabilizer weight.

The costabilizer weight is related to the monomer content:

$$m(co) = \%co.m(mon) \quad \textbf{Eq. 2-15}$$

If we say β is the costabilizer weight %, we have:

$$m(PU) = \frac{\varphi}{1-\varphi}[(1+\beta).m(mon)] \quad \textbf{Eq.2-16}$$

The molar quantity of isocyanate is then:

$$n(NCO) = \frac{\varphi(1+\beta)}{1-\varphi}.\frac{m(mon)}{M_{eq}(PU)} \quad \textbf{Eq. 2-17}$$

Finally:

$$\frac{n(OH_{HEMA})}{n(OH_{BPA})} = \frac{\alpha(1-\varphi).M_{eq}(NCO)}{\theta.\varphi(1+\beta).M(HEMA) - \alpha(1-\varphi)M_{eq}(NCO)} \quad \textbf{Eq. 2-18}$$

more generally expressed as $\frac{HEMA}{BPA}$.

The degree of grafting is defined as the molar ratio between the isocyanate function and the hydroxyl function coming from HEMA:

$$GD = \frac{n(OH_{HEMA})}{n(NCO)} \times 100 \quad \textbf{Eq. 2-19}$$

From the previous calculation, the expression of the degree of grafting is as follow:

$$GD = \frac{\alpha(1-\varphi)}{\varphi(1+\beta)} \times \frac{M_{eq}(PU)}{M(HEMA)} \times 100 \quad \textbf{Eq. 2-20}$$

This is a theoretical degree of grafting based on the hypothesis that all HEMA reacts with isocyanate functions.

2.4 Theoretical network in the urethane/acrylic hybrid particles

Even if systems prepared in Routes I and II are quite different, one can try to define some common rules to understand the network architecture that will be useful in the following results chapters.

Conductometric titration of the NCO functions has been used to measure the molar mass of the initial PU prepolymer. The molar mass used in the different calculations is ~ 3000 $g.mol^{-1}$ (Udagama 2009). Moreover, infrared spectroscopy (ATR-IR) and ^{13}C nuclear magnetic resonance studies of the polymer have shown that no free isocyanate functions remain in the final polymer, which means that all NCO groups have reacted with HEMA, BPA or water eventually.

The PU prepolymer can react either on one or both ends with HEMA. In Route I systems, the reaction of two ends of the same prepolymer is less probable considering that only a maximum of 20% of NCO groups can react with HEMA (Udagama 2009) (in systems from Route II, no such limitation has been determined). More probably, one of the two NCO terminations can react with water or with BPA. If BPA has already reacted with another PU prepolymer, the PU chain is extended. Based on the different HEMA/BPA ratios, it seems reasonnable to think that all PU prepolymer have been extended at least once. Therefore, different types of PU chains are possible:

- BPA-extended chains which have reacted on both ends with HEMA form *bonded PU chains*. After acrylic copolymerization, these chains will be part of the gel fraction.
- BPA-extended chains which have reacted on only one end with HEMA are *dangling chains*. They are terminated either by a BPA or by an amine (obtained after reaction with water). These chains are connected to the acrylic backbone by only one side.
- BPA-extended chains which did not react with any HEMA form *free chains*. They are part of the soluble fraction inside the particles.

These three types of chains coexist in the particles and their proportions and lengths obviously change according to the fraction of PU, the OH/NCO ratio and the HEMA/BPA ratio.

To have an appropriate representation of the architecture of the hybrid network inside particles, one has to take into account two other parameters:

- The molar mass of the acrylic copolymer is much higher than that of the PU, even extended. Indeed, with steric exclusion chromatography (SEC), the acrylic molar mass has been found to be ~ 300 - 4000 $kg.mol^{-1}$ from a sample to another depending on the synthesis parameters. The PU prepolymer molar mass is ~ 3 000 $g.mol^{-1}$ and the final average PU molar mass depends on the extension by BPA but cannot achieve that of the acrylic.
- We assume that the PU chains are composed mostly of polyether (probably polypropylene glycol). A consequence is that PU is much more entangled than the

acrylic main chains. Molar mass between entanglements (M_e) for PU must be around 3000 - 5000 g.mol^{-1} (Brandrup and Immergut 1999; Florez, Munoz et al. 2006) while it is ~ 20 - 30 000 g.mol^{-1} for the main monomer, butyl acrylate (Tong and Jerome 2000; Moghbeli, Zamir et al. 2008).

The final PU chains are thus much shorter and much more entangled than those of the acrylic network. Taking in account the different possible connectivity of the PU chains, a schematic representation of the network is presented in Figure 2-3 (except that no reaction of NCO with water is shown).

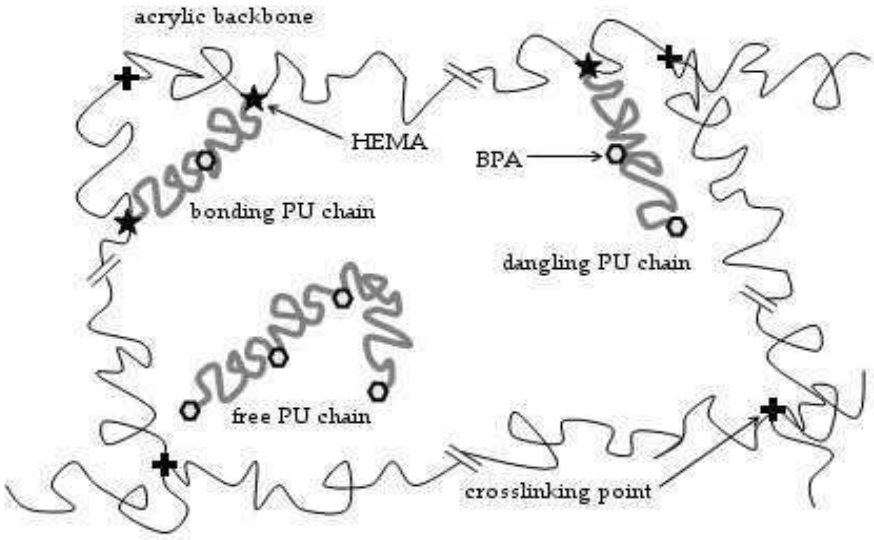

Figure 2-3: Theoretical urethane/acrylic hybrid network

2.5 Conclusion

The two synthesis routes have been detailed in this section. One can conclude that, even if the objective is the preparation of the same urethane/acrylic hybrid particles, the choices made for the two synthesis methods may lead to completely different particle structures.

The impact of the synthesis process will be discussed in the next chapters, but, to simplify the interpretation, results for systems from Route I and systems from Route II will be analyzed in two separate chapters.

2.6 References

- Brandrup, J.; Immergut, E., H., *Polymer Handbook,* New York, Wiley, **1999**.
- Florez, S.; Munoz, M. E.; Santamaria, A., *Macromolecules Materials Engineering*, **2006,** *291,* 1194-1200.
- Landfester, K., *Macromolecular Rapid Communications*, **2001,** *22*, (12), 896-936.
- Lopez, A., POLYMAT, Universit of the Basque Country, **2009**
- Lopez, A.; Chemtob, A.; Milton, J. L.; Manea, M.; Paulis, M.; Barandiaran, M. J.; Theisinger, S.; Landfester, K.; Hergeth, W. D.; Udagama, R.; McKenna, T.; Simal, F.; Asua, J. M., *Industrial & Engineering Chemistry Research*, **2008,** *47*, (16), 6289-6297.
- Mallegol, J.; Dupont, O.; Keddie, J. L., *Langmuir*, **2001,** *17*, (22), 7022-7031.
- Moghbeli, M. R.; Zamir, S. M.; Molaee, B., *Journal of Applied Polymer Science*, **2008,** *108*, (1), 606-613.
- Tong, J. D.; Jerome, R., *Polymer*, **2000,** *41*, (7), 2499-2510.
- Udagama, R., Laboratoire de Chimie, Catalyse, Polymères et Procédés, *University Claude Bernard -Lyon I*, **2009**

3. CHARACTERIZATION TECHNIQUES

3.1 Chemical characterization

3.1.1 Solid content

The solid content of the latexes was measured gravimetrically. It was maintained around 50 wt% for all latexes.

3.1.2 Droplet and particle sizes

Miniemulsion droplet and polymer particles average diameters were measured by dynamic light scattering (Zetasizer Nano Z, Malvern Instruments). The final particle size is between 95 and 200 nm. It depends on the synthesis route and the recipe of each latex. Values are presented and commented in chapter 4.

3.1.3 Glass transition temperature T_g

The glass transition temperature T_g was determined by differential scanning calorimetry (DSC; TA Instrument DSC 2920). Samples were first heated at 10 °C/min from room temperature to 200 °C and then cooled until -100 °C at 10 °C/min. Two ramps were performed for each sample and reproducibility was checked for selected samples. It was considered good.
The samples prepared in Route I (with BA as the main monomer) have an average T_g equal to -39.1°C ± 3.0°C and the samples prepared in Route II (with 2EHA as the main monomer) have an average T_g of -63.1°C ± 0.7°C. No influence of the PU has been detected and only one T_g is measured. The samples are in the range of the very soft polymers at room temperature.
It is worth noting that the T_g of the pure PU is estimated at around -48 °C. Therefore, the large distribution of the T_g of the copolymer and the closeness with T_g of the PU could mask out a possible phase separation. This will be discussed in the chapter 4.

3.1.4 Gel and swelling measurements

The gel content corresponds to the fraction of insoluble chains relative to the total amount of polymer. These insoluble chains are chemically crosslinked or strongly bonded to each other and form microgels in each particle. However since we are working with latexes, it is important to note that individual latex particles cannot be chemically bonded to each other without any additional crosslinking scheme ater coalescence. The macroscopic swelling capability is related to the density of crosslink points per unit volume in the microgels.
We measured these two parameters by static measurements. A small piece of solid film was cut and weighed (W_1). Then, it was immersed in THF for a week. After a week, the sample

completely swollen by the solvent was taken out and weighed again (W_2). It was then dried at 60 °C during 30 minutes to extract all the solvent and the dried part was weighed (W_3). The gel content was given by:

$$\%\text{gel} = \frac{W_3}{W_1} \times 100 \qquad \textbf{Eq. 3-1}$$

And the swelling ratio by:

$$\Phi = \frac{W_2}{W_3} \qquad \textbf{Eq. 3-2}$$

The gel and swelling measurements were performed several times for some selected samples. The error on the gel content was around 3% and on the swelling ratio, it was around 9 %. However, for gel contents lower than 25 – 30%, these experiments were not reliable. Indeed, it was not possible to take the sample out from the bottle properly because it broke in several parts. Errors were higher than 15% for the gel content and 50 % for the swelling ratio.

3.2 Characterization of the morphology

3.2.1 Preparation of the samples

Imaging of single particles by AFM and TEM requires a previous dilution of the latex. For the AFM imaging, latexes were diluted at a ratio 1:10000 and 4 microliters of the diluted latexes were deposited on a freshly cleaved mica sheet and dried at room temperature.
For TEM imaging, particles were previously negatively stained by phosphotungstic acid (PTA): 1.5 wt% of PTA was added to a solution of 1:80 diluted latex. The solution of diluted latex and PTA was sonicated for 30 minutes at 100 % of the maximum power of the sonifier. Then a small droplet of this solution was spin-coated onto a carbon covered 200 mesh copper grid at 1500 rpm for three minutes.
For the film observation, the latexes were cast in silicone moulds and placed in an oven at 40 °C for 4 hours until complete drying of the latexes. The resulting films (several hundred of µm in thickness) were sectioned with a cryo-ultramicrotome (Reichert-Jung Ultracut E/Diatome diamond knife) at approximately -90 °C. The sections, of approximately 100 nm in thickness, were picked up on carbon covered 400 mesh copper grids for observation.

3.2.2 AFM images

Lars Sonnenberg, post-doc researcher in our lab, made the AFM observations presented in this work. They were performed under ambient conditions of pressure, temperature and hygrometry. Cantilevers were provided by BudgetSensors (model Tap300) with a spring constant of 40 N/m and a resonance frequency calibrated at 300 kHz. AFM was used in intermittent contact mode throughout. The free oscillation amplitude A_0 varied from 48 nm to 74 nm. The set point r_{sp} was fixed at $0.9A_0$ and scanning speed was 1Hz. These conditions correspond to soft tapping mode with stiff cantilever. They were optimized for the observation of the soft adhesive particles at room temperature. The stiff cantilever is required to be able to debond from the adhesive surface, the free oscillation amplitude and the high set point correspond to soft taping needed to avoid damaging the surface by indentation of the tip (Mallegol, Dupont et al. 2001).
AFM phase images were used to evaluate the dissipative nature of the interactions between the AFM tip and the different parts of the specimen. Changes in dissipation were reflected by changes in the phase difference between the cantilever oscillation and the excitation signal. An artificial color code was used to translate these modifications on the final images. The red end of the spectrum corresponds to a weak phase shift, i.e. an elastic response, whereas blue end corresponds to more dissipative specimen-tip interactions.
The topology of the particle surface was evaluated with AFM height images. The differences in height resulted in differences of the reflected laser beam. In the false colored images presented here, the red colors correspond to higher areas whereas blue colors are for lower zones.

3.2.3 TEM images

These images were obtained at the EPFL, Lausanne (Switzerland) by Professor Christopher Plummer. A TEM Philips CM20 equipped with a LaB_6 filament operating at 200kV was used throughout. All images were obtained for samples at room temperature.
The contrast on the images is due to the differences in the electronic density of the domains. The PTA is believed to stain preferentially the PU domains (Li, Chiu et al. 2007) what results in PU domains which have a higher electronic cloud density and appears as darker areas on the TEM (Chai and Tan 2008). No distinction can be made between the different acrylic parts, as they have very similar electron transparency and degrade rapidly under the beam. The same distinction between PU and acrylic is expected when imaging PTA-stained films.
Unstained films have also been imaged. In that case, the contras appearing during irradiation of the films should arise from beam-induced mass-loss in the PU domains preferentially.

3.3 Mechanical characterization

3.3.1 Linear rheology

The linear viscoelastic properties of the adhesives where characterized with a rheometer RDAII with a parallel plate geometry. Frequency sweeps (5.10-2 Hz < F < 20 Hz) with imposed torsion strain γ between 5% and 10% were made on samples with a thickness around 500 µm. For each frequency, 10 torsion cycles were imposed to the sample and the average values of G', G'' and tanδ were recorded Tests were performed at room temperature.

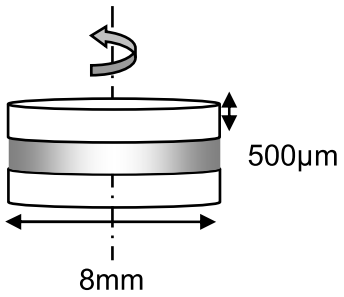

Figure-3-1 : Geometry of the rheology tests

.

To obtain thick films, latexes were cast in silicone moulds. A given volume V_{cast} was deposited in the moulds, calculated according to the targeted thickness and to the solid content of the latex, as described in the equation 3-3.

$$V_{cast} = \frac{L \times w \times h_{final}}{SC} \qquad \textbf{Eq.3-3}$$

with:
L and w: length and width of the silicon mould
h_{final}: targeted thickness
SC: solid content of the latex

The latexes were dried during a week, at room temperature, followed by 5 minutes in the oven at 110 °C. Samples were then protected by two sheets of release paper. The films obtained in these conditions have a thickness h of about 500 µm. Circular samples were cut with a 8mm diameter punch. Rheology experiments were performed within a week to ten days after the complete drying.

As experiments were long to perform, reproducibility was checked for selected samples and it was good. We assumed that it was good for all other samples.

3.3.2 Tensile experiments

We used a standard tensile INSTRON machine (model 5565) equipped with a videoextensometer (model SVE) allowing a precise measurement of the strain. The maximum displacement measured by the video extensometer is 200 mm, and the machine can measure displacements up to 600 mm. Strain can be measured both by the video extensometer and by the displacement of the crosshead. The machine uses a 10 N load cell with a resolution of 0.5 % from 1 % to 100 % of the full scale.
The tensile tests were performed on the same self-standing films than those used for rheology measurements. Some rectangular strips were cut from the film with a die-cutter. All of them were 5 mm wide (w_0) and the average thickness (e_0) is 500 μm. These values were controlled before each test.
The strips were marked in their middle by two white spots. With these marks, the videoextensometer can measure the initial length at the beginning of the test (l_{0e}) and during the first part of the test (l). After a certain displacement of the crosshead, the maximum capacity of the videoextensometer is reached and the displacement measurement switches to the crosshead. The initial length between the jaws (l_{0m}) is fixed at 15 mm ± 0.5 mm. The strain was then directly calculated by the software during the test.
The constant velocity of the crosshead was chosen either at 1.5 $mm.s^{-1}$ or at 15 $mm.s^{-1}$. As the initial length between jaws is 15 mm, these velocities correspond to nominal strain rate of 0.1 s^{-1} and 1 s^{-1}. Those two nominal strain rates were employed for all the tests. To avoid slippage of the samples, the jaws were closed with a dynamometric key with a controlled torque (from 15 $cN.m^{-1}$ to 25 $cN.m^{-1}$).
All tests were performed at room temperature. For each set of parameters (sample and velocity), three to five tests were performed to check the reproducibility. In all cases, reproducibility was considered good.

During the test, the force (F) and the displacement (l) were recorded. The nominal stress (σ_N) and the strain (λ) were calculated from these data and from the values of the initial width (w_0) initial thickness (e_0) and initial length measured by the videoextensometer (l_{0e}). When the measurement of the displacement switches from the videoextensometer to the crosshead, the initial length measured by the machine was taken in account to calculate λ. The reduced strain was calculated from σ_N and λ.
The classic representation of nominal stress σ_N versus strain λ (Figure 3-2) and the Mooney representation of the reduced stress σ_R versus $1/\lambda$ (Figure 3-3) were analysed. The final failure of the sample in tension can occur by brittle fracture or by homogeneous flow at very large strains. Since spurious effects such as slippage in the grips can also occur at these very large strains, only the meaningful part of the curves will be reported.

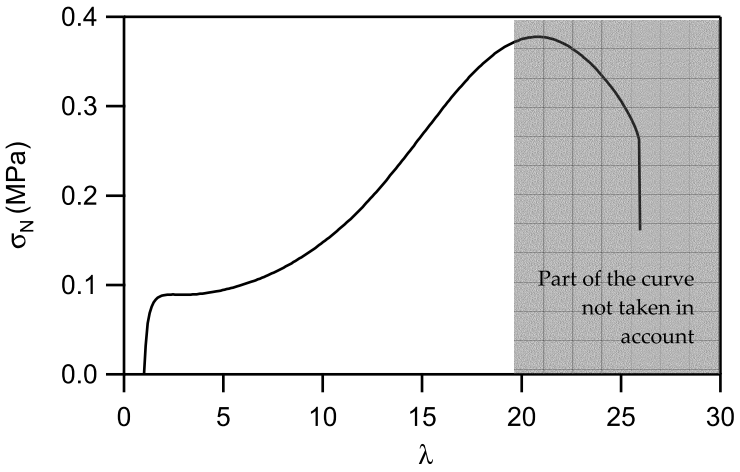

Figure 3-2: Standard representations used to analyse large strain data: Nominal stress σN vs strain λ

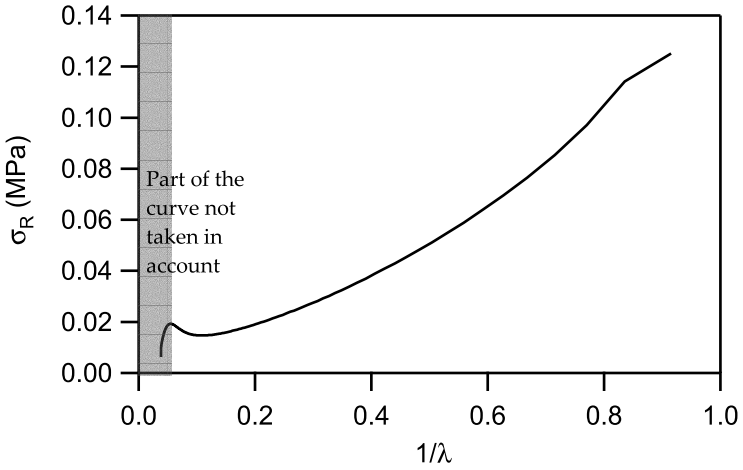

Figure 3-3: Mooney representation of the reduced or Mooney stress σR versus the inverse strain 1/λ

From the Mooney representation, which has to be read from right to left, characteristic parameters of the non-linear behavior can be determined, such as C_{soft} and C_{hard}. These parameters have already been defined and interpreted in chapter 1.
Figure 3-4 illustrates the practical determination of these two parameters which have the physical meaning of the relaxing and non relaxing part of the initial modulus.

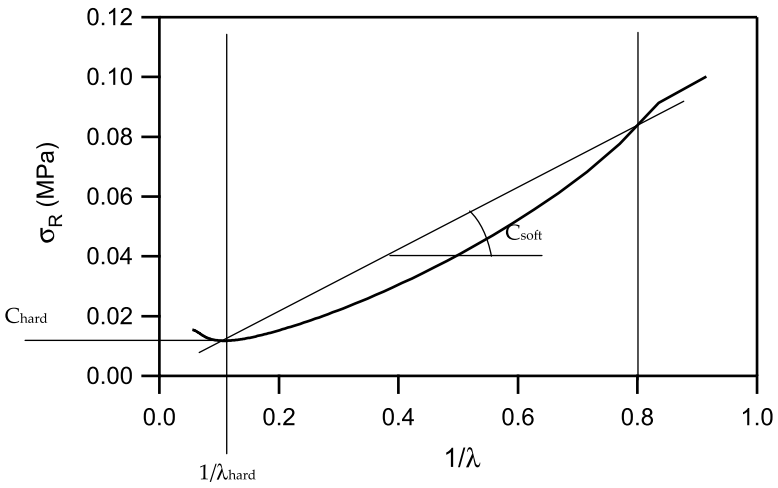

Figure 3-4: Determination of C_{soft}, C_{hard} and $1/\lambda_{hard}$

The ratio C_{soft}/C_{hard} characterizes the viscoelastic relaxation of the sample relative to its permanent crosslink structure. Another value can be obtained from the Mooney representation: the strain level corresponding to the minimum in reduced stress, called λ_{hard}. This value, which has not been used yet to analyze the network architecture, can bring important information about the finite extensibility of the chains.
When polymer networks are very lightly crosslinked, chains flow instead of hardening when the finite extensibility is reached. No macroscopic hardening can be observed on the Mooney representation but a decrease of the nominal stress is observed at failure. The corresponding strain and stress are defined as the minimum of the Mooney curve and are used to calculate the C_{soft} but C_{hard} is then undefined.

Analysis of the relaxation processes

The softening at intermediate strain is a consequence of a reversible strain-dependent non-linear elasticity and of a time-dependent relaxation process. To decorrelate both dependences, we compared two tests performed at different strain rates (see Figure 3-5).

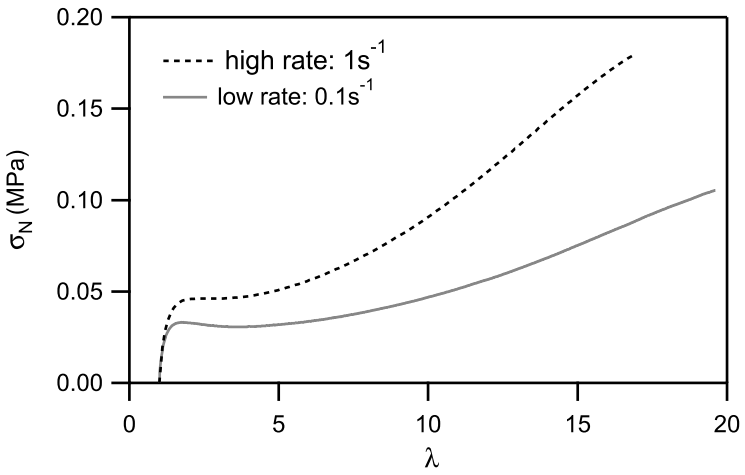

Figure 3-5: Tensile test of the same sample at two different initial strain rates

Hence, the non-linear elastic contribution should be the same but the extent of relaxation varies. A simple but instructive representation of the data is the ratio (for each λ) between the stress obtained for test carried out at a high nominal strain rate ($d\varepsilon/dt=1s^{-1}$) and the stress obtained for a test carried out at a low nominal strain rate ($d\varepsilon/dt=0.1s^{-1}$). The calculation of this ratio R(λ) decorrelates time-dependent relaxation and λ-dependent non-linear elasticity. Only the time-dependent relaxation between the two strain rates is represented as a function of λ. If the two processes are fully separated the ratio is constant whatever the λ (see Figure 3-6 (a)). On the other hand any variation of this ratio with λ reveals non-linear viscoelastic processes, i.e. the extent of relaxation depends on the strain (see Figure 3-6(b)). In any case, the absolute value of R(λ) is an indication of the level of viscoelasticiy in the sample.

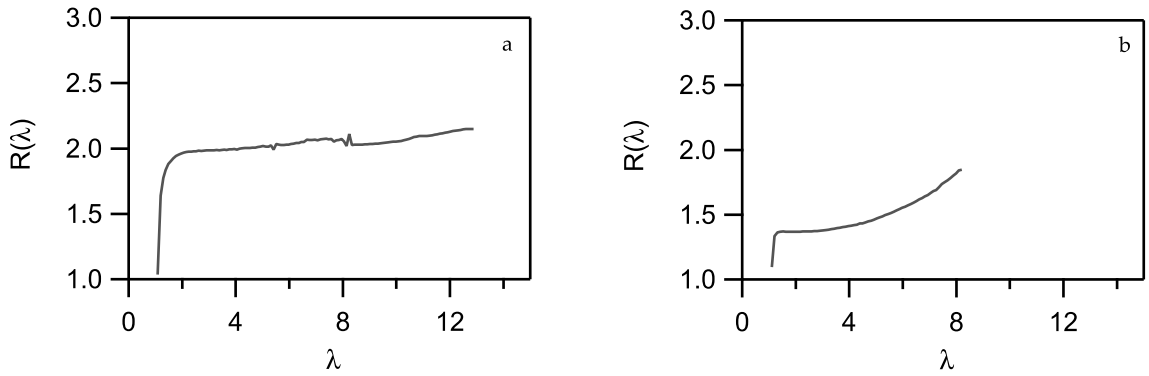

Figure 3-6 : Example of the evolution of R(λ) with λ; (a): constant ratio R(λ) whatever λ due to independent softening processes; (b): R(λ) increases with λ because of non-linear viscoelastic processes

a

3.3.3 Probe-tack tests

For all samples, we performed an analysis of the adhesive properties with the probe-tack test. In this well-known experiment (Zosel 1989; Lakrout, Sergot et al. 1999), a cylindrical stainless steel probe (diameter = 10 mm) came in contact with the adhesive layer and after a controlled contact (time and pressure), the probe was debonded at a constant velocity. In our set-up, a 45 ° mirror was installed behind the glass slide for the in-situ visualisation of the debonding mechanism and the measurement of the real contact area for each sample. A transparent substrate was then necessary. The geometry of this test is presented in the following schematic.

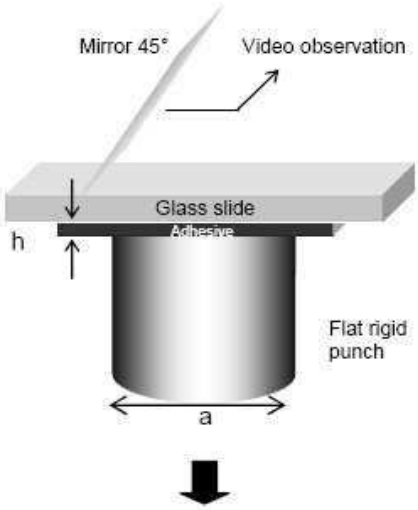

Figure 3-7 : Geometry of the probe-tack test

Using a cylindrical probe has the advantage to impose a spatially constant displacement in all parts of the contact area. However, as a consequence of this geometry, a fine control of the parallelism between the probe and the adhesive layer is required to have the largest contact area. The alignment of the glass slide with the probe was made through a tripod system, represented in Figure 3-8.

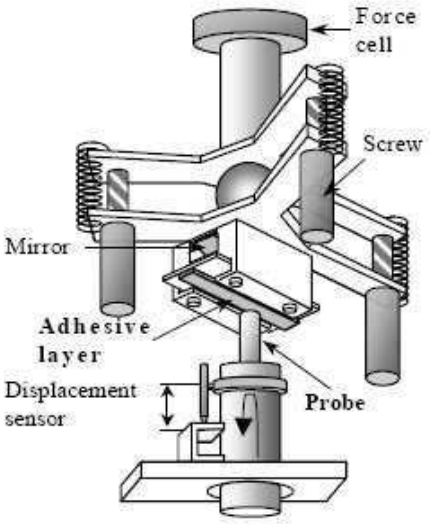

Figure 3-8 : Schematic of the probe-tack experimental set-up with the tripod system

The force was measured by a load cell (250 N, resolution 0.5 N). The displacement of the probe was measured with an LVDT extensometer (range 5 mm, resolution 0.5 µm). After data analysis, nominal stress versus strain curves $\sigma_N=f(\varepsilon)$ were obtained. The nominal strain σ_N corresponds to the measured force (F) divided by the initial contact area (A_{C0}):

$$\sigma_N = \frac{F}{A_{C0}} \qquad \textbf{Eq. 3-4}$$

The initial contact area was imaged at the beginning of the test and measured with the software ImageJ. An example of the initial contact area is given below:

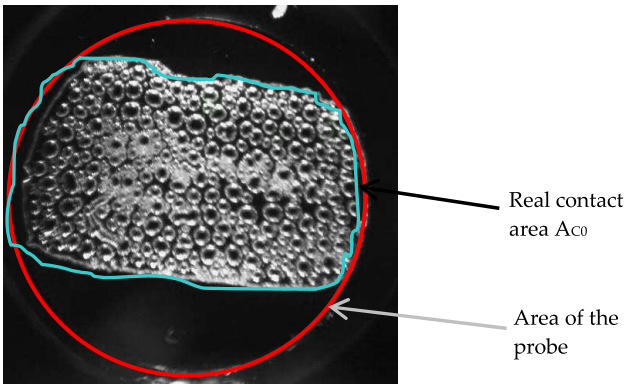

Figure 3-9 : Representation of the probe area (red circle) and of the real contact area A_{C0} (blue line)

The strain ε was calculated from the displacement of the probe divided by the initial thickness h_0.

$$\varepsilon = \frac{d(t)}{h_0} \qquad \textbf{Eq. 3-5}$$

An example of the curve obtained for a typical PSA is shown in Figure 3-10.

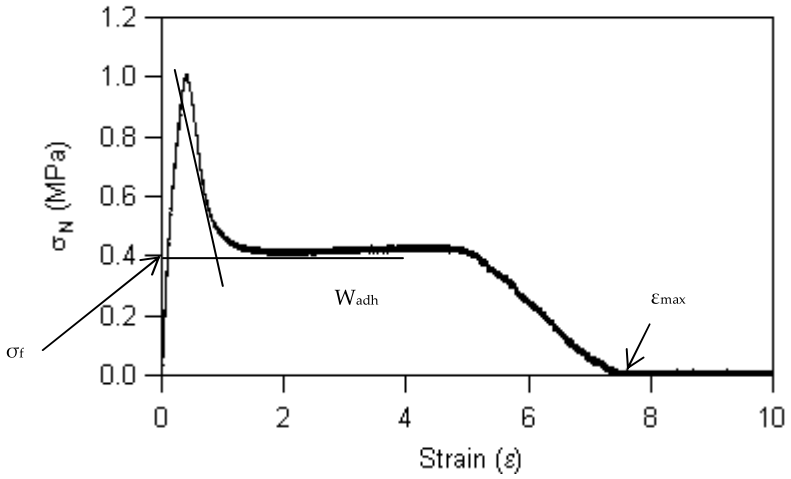

Figure 3-10 : Tack curve of the debonding of a typical PSA

The description of the possible debonding modes has been widely reported (Lakrout, Sergot et al. 1999; Crosby, Shull et al. 2000; Shull and Creton 2004) and will not be detailed here. However, it is useful to note that three parameters are mainly used to interpret the data (Lakrout, Sergot et al. 1999; Roos and Creton 2005). These parameters are indicated on Figure 3-10 and described as:

- σ_f: stress of the beginning of fibrillation. It is correlated to the elasticity of the sample.
- ε_{max}: strain for which adhesive completely debond from the probe. The dissipation and the strain hardening impact directly on this parameter.
- W_{adh}: adhesion energy, corresponding to the area under the curve multiplied by the initial thickness of the film, h_0.

Furthermore, the detailed shape of the curve can also be analyzed. Figure 3-10 represents the behavior of an optimized PSA with a long fibrillation plateau and a large maximum deformation. The absence of a fibrillation plateau with an ε_{max} lower than 1 is characteristic of an interfacial debonding with crack propagation at the probe-adhesive interface. This debonding mode corresponds to a low adhesion sample typically over crosslinked. On the contrary, a plateau stabilized around 0.1MPa with a decrease in stress at intermediate strain appears in the case of a cohesive debonding, where residues of the adhesive remain on the probe. Liquid-like samples with a low degree of crosslinking behaves that way.
We used standard values for the approach velocity (V_{app}), contact time (t_c), contact force (F_c) and debonding velocities (V_{deb}). The tests were made at room temperature. The Table 3-1 gives the values of the different parameters which we used.

Table 3-1 : Experimental parameters for the probe-tack tests

V_{app}	30 µm.s^{-1}
t_c	1 s
F_c	-70 N
V_{deb}	10-100 µm.s^{-1}

The adhesive layers were cast on microscope glass slides, required for observation of the contact area during the probe tack tests. We used two different techniques depending on the sample's viscosity.
When latexes are viscous enough ($\eta > 1.10^{-3}$ Pa.s), a doctor blade with a gap of 300µm was used to cast the latexes in a uniform thickness. For samples with viscosity close to 1.10^{-3} Pa.s, the doctor blade could not be used because the latex spreads below the walls of the applicator and there is no more control of the thickness. In this case, a given volume of latex was spread on the total area of the microscope glass-slide according to equation 3-3.

After casting the latex, the glass-slides were protected with a bell-jar for 48 hours to ensure a relatively slow drying rate and to avoid particle migration toward the edges of the films (Keddie 1997). After two days, the glass slides were put in the oven at 110°C for 1 minute, to finish water evaporation. All the films had a dry thickness around 120µm.
Tack tests were carried out within a maximum of two days following the film formation. To check out the reproducibility, three to five experiments were performed for one latex and one velocity. In all cases, reproducibility was good.

3.3.4 Characterization of the adhesives with industrial tests

The sample preparation and the specific conditions used for the industrial tests also need to be described. All industrial tests were performed at CYTEC Surface Specialties under the supervision of Dr. Olivier Dupont and Dr. Keltoum Ouzineb.
Latexes were first deposited on polyester sheets with a thickness of 23 µm and dried at 110°C for 3 minutes. Peel, loop tack and shear tests were then performed according to test methods established by the FINAT (2005). All tests were made under conditions imposed by FINAT, that is to say T = 23°C and RH = 50%.

Shear tests were performed on stainless steel. A 1 kg weight was applied to an adhesive area of 1 inch². The result is expressed in minutes. If cohesive failure occurs, CF is indicated with the result. The maximum time measured with this experiment was 10000 min. After that, the measurements were stopped.

Peel tests were performed at 180 ° on stainless steel 20 minutes and 24 hours after application of the adhesive layer on the substrate. Peel tests were also realized on polyethylene 24 hours after application. A 25 mm wide adhesive was applied on the substrate. The velocity was 300 mm/min. Results are given in N/25mm and eventual cohesive transfer (CT) is specified.

3.4 References

- *FINAT Technical Handbook*,**2005**.
- Chai, S. L.;Tan, H. M., *Journal of Applied Polymer Science*, **2008,** *107*,(6), 3499-3504.
- Crosby, A. J.;Shull, K. R.;Lakrout, H.;Creton, C., *Journal of Applied Physics*, **2000,** *88*,(5), 2956-2966.
- Keddie, J. L., *Materials Science & Engineering R-Reports*, **1997,** *21*,(3), 101-170.
- Lakrout, H.;Sergot, P.;Creton, C., *Journal of Adhesion*, **1999,** *69*,(3/4), 307-359.
- Li, C.-Y.;Chiu, W.-Y.;Don, T.-M., *Journal of Polymer Science Part A: Polymer Chemistry*, **2007,** *45*, 3359-3369.
- Mallegol, J.;Dupont, O.;Keddie, J. L., *Langmuir*, **2001,** *17*,(22), 7022-7031.
- Roos, A.;Creton, C., *Macromolecules*, **2005,** *38*,(18), 7807-7818.
- Shull, K. R.;Creton, C., *Journal of Polymer Science Part B-Polymer Physics*, **2004,** *42*,(22), 4023-4043.
- Zosel, A., *Journal of Adhesion*, **1989,** *30*,(1-4), 135-149.

4. PARTICLE AND FILM MORPHOLOGIES

4.1 Abstract

Hybrid urethane/acrylic latexes for Pressure Sensitive Adhesives (PSA) applications have been synthesized in an aqueous medium. The miniemulsion polymerization has been chosen to incorporate a urethane prepolymer into acrylic monomer droplets before free radical polymerization of the acrylic within the droplet. The mixing of both components in the final latex particles is a central question. The particle morphology has been analyzed by two techniques, Atomic Force Microscopy (AFM) and Transmission Electron Microscopy (TEM). For these soft tacky particles and films, TEM appears to be a technique easier to implement and interpret than AFM. The impact of the particle morphology on the film structure has then been studied with TEM.
It was found that grafting of the urethane chains to the acrylic backbone is required to avoid phase separation at the macroscopic scale. If the PU is not grafted, it forms separated domains of PU in the particle. These domains are retained in the film obtained upon drying of the latex. The film is then non-transparent, indicating a macroscopic phase separation, and its mechanical properties are poor for adhesive applications. When polyurethane is fully grafted, particles are more homogeneous resulting in a transparent and more uniform film at the microscopic and macroscopic scales. When there is only partial grafting, the PU comes at the borders of the particles, forming a shell which is thicker and more continuous as the PU weight fraction increases. Particles with high proportions of PU (50 wt%) are fully surrounded by this shell and the core-shell structure is retained in the final film As a consequence, interdiffusion between particles is hindered and the resulting particle-particle interfaces are weak.

4.2 Introduction

Films made from drying of waterborne emulsions are an important class of pressure sensitive adhesives (PSA), especially acrylic-based PSA (Creton 2003). This class of adhesives limits the use and evaporation of Volatile Organic Compounds (VOC) and is environmentally friendly. For these reasons, it has been widely developed in the past years. However, the final end-use properties of waterborne adhesives still remain inferior to those of hot melts or solution – based PSA in particular in terms of resistance to water whitening and resistance to shear (Jovanovic and Dubé 2004). These two limitations are related to some inherent shortcomings of emulsion polymerization. The synthesis by conventional emulsion requires diffusion of the monomer in the water phase, which limits the choice of possible monomers to those with a reasonable solubility in water. Then the film formation stage involves the coalescence of the particles in a film but does not typically involve crosslinking between particles. One way to expand the design options of the particles is to make hybrid latex particles, i. e. use two mutually immiscible polymers within the same particle. If the components are well chosen, the combination of both systems can lead to synergetic properties between the polymer networks. Miniemulsion is a synthesis technique where

polymerization occurs directly inside small droplets (50 – 300 nm). That means no diffusion of monomers through water is required. Hence this technique is very relevant when one of the hybrid components is hydrophobic (Landfester 2001; Asua 2002).

It is well known that in coating applications, polyurethane (PU) improves properties of waterborne acrylic latex such as resistance to solvent, film formation or toughness (Hirose, Kadowaki et al. 1997; Kukanja D., Golob J. et al. 2000; Li, Daniel et al. 2005). These systems have been widely studied since the end of the 1990 (Hegedus and Kloiber 1996; Hirose, Kadowaki et al. 1997; Gooch, Dong et al. 2000; Wang, Chu et al. 2003; Wang, Chu et al. 2006; Wang, Chu et al. 2009) and are now well understood. Miniemulsion polymerization has appeared to be a performing solution to prepare this type of PU/acrylic hybrid (Gooch, Dong et al. 2000; Wang, Chu et al. 2003; Li, Daniel et al. 2005; Wang, Chu et al. 2006). Since diffusion of components through water is not necessary, the hydrophobic PU prepolymer can be dissolved in the organic phase and then evenly distributed inside the droplets before polymerization. However the two polymers have a limited compatibility and a simple mixing of the PU in the acrylic phase could result in phase separation at the particle scale (Li, Daniel et al. 2005; Li, Chiu et al. 2007). A consequence of heterogeneous particle would be a perturbed drying and a final film with macroscopic phase separation (Routh and Russel 2001) and hence reduced mechanical properties. As explained by Li *et al.*, a covalent grafting of the polyurethane to the acrylic backbone can help to reduce this phase separation (Li, Daniel et al. 2005).

Some previous work on these type of hybrids were based on low T_g acrylic monomer recipes leading to T_g of the polymer film close to room temperature (with butyl methacrylate as the main component for example) that is to say soft particles (Li, Daniel et al. 2005). Nevertheless, these particles are not as soft as those used for PSA films. To the best of our knowledge, no research has yet been published focusing on urethane/acrylic for adhesive applications. Adhesive applications involve polymers with a very low elastic modulus (E < 100 kPa) , a T_g well below room temperature and a very low density of entanglements.

In that situation, one could expect improvements of the properties of the acrylic adhesive in terms of solvent resistance, an increase in stiffness due to high density of entanglements brought by the PU or a better retention of adhesion at high T because of the PU stability at high temperature.

Urethane/acrylic hybrid particles for coatings (*i.e.* with T_g above room temperature) can be imaged by atomic force microscopy (AFM). Brown and coworkers (Brown, Coogan et al. 2005) used AFM in intermittent contact mode (also called tapping mode) to observe films obtained from hybrid particles with hard acrylic and soft PU. They could distinguish hard acrylic nanodomains incorporated within a softer PU continuous phase. Transmission electron microscopy (TEM) has also been used to determine particle and film morphology. Acrylic or PU phases can be equivalently stained to improve contrast between both phases: ruthenium tetraoxide or osmium tetraoxide preferentially stain the acrylic phase (enriched with polystyrene) (Hirose, Zhou et al. 2000; Wang, Chu et al. 2003), whereas phosphotungstic acid (PTA) has been used to stain the PU phase (Li, Daniel et al. 2005; Chai, Jin et al. 2008).

It is worth noting that the softness and the tackiness of adhesive particles and films has limited their observation at the micro and nanoscopic scales. The determination of the appropriate conditions to image them with AFM is not trivial. PSA particles are at the same time soft (requiring light tapping to avoid excessive surface deformation) and tacky (requiring energetic tapping to debond from the surface during each cycle). Such systems have been observed successfully by AFM only a few years ago by Mallégol and coworkers (Mallegol, Dupont et al. 2001; Mallegol, Dupont et al. 2003). They found that the combination of a stiff cantilever with large amplitude and light tapping favors the observation of adhesive soft particle surfaces. TEM observations are also made difficult by the low intrinsic contrast afforded by the polymer systems and the particular sensitivity of acrylics to electron beam damage. For both techniques, the ability of particles to spread on the surface is another drawback and sample preparation must then be well adjusted.

The recent works of Udagama (Udagama 2009) and Lopez (Lopez 2009) have demonstrated the feasibility of the synthesis of urethane/acrylic hybrid particles for pressure sensitive adhesive applications. To be used as adhesive films, the particles must be very soft and the molecular architecture of the polymer carefully controlled with about 50/60% of gel fraction (Creton 2003). These requirements are met by a fine adjustment of the monomer composition and amount of chain transfer agent. Two series of samples were prepared, one based on 2-EthylHexylAcrylate (2EHA) and the other on butyl-acrylate (BA). Details of the synthesis conditions are presented in different papers by Lopez *et al.*for the first series (Lopez 2009) and by Udagama *et al.* for the second series (Udagama 2009). For each series a NCO-terminated PU was added in the droplets and the extent of grafting with the acrylic backbone was controlled with the incorporation of an OH functionalized comonomer, hydroxyethyl methacrylate (HEMA). The morphology of particles and films obtained upon the drying of these particles was investigated.

In the first results section of this paper, we present a comparison between systems with and without grafting of the PU. In the second set of results, the fraction of PU is changed, keeping a fixed grafting. The impact of the PU on the morphology can then be determined. For both cases, the morphology of coalesced films is observed by both TEM and AFM to elucidate how the structure of the particle remains during film formation.

4.3 Materials

All urethane/acrylic hybrid latexes presented here have been prepared by miniemulsion polymerization.

The first series was synthesized by Route II with a base composition of 2-ethylhexyl acrylate (2EHA; 97 wt%; T_g = -70.15 °C (Brandrup and Immergut 1999)), methyl-methacrylate (MMA; 0.7-2 wt%) and methacrylic acid (MA; 1 wt%). Route I was used for the second series, based on butyl-acrylate (BA; 89.5 wt%; T_g = -54.15 °C (Brandrup and Immergut 1999)), MMA (9.5 wt%) and acrylic acid (AA; 1 wt%). Both series contained variable amounts of industrial NCO-terminated polyurethane (PU) prepolymer (Incorez 701) provided by Industrial Copolymers Limited, hydroxyethyl methacrylate (grafting agent) and bisphenol-A (chain extender). Molecular analyses have demonstrated that this PU prepolymer is made of polypropylene glycol (PPG) for the soft segments and isophorone diisocyanate (IPDI) for the hard ones. Its molecular weight was checked by SEC and inversed titration of the isocyanate functions and was found to be ~ 3000 $g.mol^{-1}$.

The polyurethane chains were NCO-terminated at both ends and could therefore react with hydroxyl ethyl methacrylate (HEMA). The remaining free isocyanate functions were neutralized with Bisphenol A (BPA), a chain extender.

In the first series (Route II), a fixed amount of 10 wt% of PU relative to the organic phase (PU + acrylic monomers) was incorporated. The quantity of HEMA in the monomer composition was 0 wt%, 1.37 wt% or 2 wt%. For the formulations with 0 wt% and 2 wt% of HEMA, an excess of BPA was added and the molar ratio OH/NCO = 2. For the formulation with 1.37 wt%, no BPA was added. The theoretical degree of grafting of the PU chains, defined as the percentage of OH moles coming from HEMA related to the isocyanate moles are:

- For the formulation with no HEMA: 0 %
- When there is 1.37 wt% of HEMA: 70%
- For the formulation with 2 wt% of HEMA: 140. For this sample, one considers 100% grafting of the PU.

The Table 4-1 summarizes the main data about these three samples.

In the second series (Route I), different polyurethane weight fractions related to monomers were incorporated into the droplets during polymerization (5 wt%, 25 wt% and 50 wt%). The degree of grafting was fixed at 11 % which means that 11 % of the isocyanate groups reacted with HEMA to be connected to the acrylic backbone. This second series was synthesized in three stages, as described in chapter 2. The Table 4-1 gives the main characteristic of these samples as well.

Table 4-1 : Description of the different samples

Sample	PU[a]	Degree of grafting[b]	Particle size (nm)[c]
II_10PU(0)OH2	10%	No grafting	161
II_10PU(2.67)OH1[d]	↓	70%	161
II_10PU(TG)OH2[e]	↓	140%	161
I_5PU(0.22)OH0.55	5%	10%	94
I_25PU(0.22)OH0.55	25%	↓	121
I_50PU(0.22)OH0.55	50%	↓	132

a: wt% related to the monomer content
b: theoretical value based on the hypothesis of complete reaction with HEMA
c: particle size measured by DLS
d: no BPA is added in this formulation
e: TG is for total grafting

More details on chemistry of these systems can be found in works of Udagama (Udagama 2009) and Lopez (Lopez 2009).

4.4 Experimental part

4.4.1 DSC

The glass transition temperature was determined by dynamic scanning calorimetry (DSC; TA Instrument DSC 2920). Samples based on 2-EHA have a T_g of -63.1 °C ± 0.7 °C and samples based on BA have a T_g equal to -39.1 °C ± 3.0 °C.The impact of the PU on the global T_g is discussed later on.

4.4.2 Gel content

The gel content corresponds to the fraction of insoluble chains relative to the total amount of polymer. These insoluble chains are chemically crosslinked or strongly bonded to each other and form microgels in each particle. However since we are working with latexes, it is important to note that individual latex particles cannot be chemically bonded to each other.
We measured this gel content by static measurements. The latex was dried in a mould to obtain a self-standing film. A small piece of that film (~ 0.1 g) was cut and weighed (W_1). Then, it was immersed in THF for a week. After a week, the sample completely swollen by the solvent was taken out and weighed again (W_2). It was then dried at 60°C during 30 minutes to extract all the solvent and the dried part was weighed (W_3). The gel content was given by:

$$\%\text{gel} = \frac{W_3}{W_1} \times 100 \qquad \textit{Eq. 4-1}$$

4.4.3 Sample Preparation

Imaging of single particles by AFM and TEM requires a previous dilution of the latex. For the AFM imaging, latexes were diluted at a ratio 1:10000. 4 microliters of the diluted latexes were deposited on a freshly cleaved mica sheet and dried at room temperature.
For TEM imaging, particles were previously stained by phosphotungstic acid (PTA). 1,5 wt% of PTA was added to a solution of 1:80 diluted latex. The solution of diluted latex and PTA was sonicated for 30 minutes at 100 % of maximum power of the sonifier. Then a small droplet of this solution was spin-coated onto a carbon covered 200 mesh copper grid at 1500 rpm for three minutes.
For the film observation, the latexes were cast in silicone moulds and placed in an oven at 40° C for 4 hours until complete drying of the latexes. The resulting films (several hundred µm in thickness) were sectioned with a cryo-ultramicrotome (Reichert-Jung Ultracut E/Diatome diamond knife) at approximately -90 °C. The sections, of approximately 100 nm in thickness, were picked up on carbon covered 400 mesh copper grids for observation.

4.4.4 AFM

AFM observations were performed under ambient conditions of pressure, temperature and hygrometry. Cantilevers were provided by BudgetSensors (modelTap300) with a spring constant of 40 N/m and a resonance frequency calibrated at 300 kHz. The AFM was used in intermittent contact mode throughout. The free oscillation amplitude A_0 varied from 48nm to 74nm. The set point ratio r_{sp} was fixed at $0.9A_0$ and scanning speed was 1Hz. These conditions correspond to soft tapping mode with a stiff cantilever. They were optimized for the observation of the soft adhesive particles at room temperature. The stiff cantilever is required to be able to debond from the adhesive surface, the free oscillation amplitude and the high set point correspond to soft taping needed to avoid damaging the surface by indentation of the tip (Mallegol, Dupont et al. 2001).

AFM phase images are used to evaluate the dissipative nature of the interactions between the AFM tip and the different parts of the specimen. Changes in dissipation are reflected by changes in the phase difference between the cantilever oscillation and the excitation signal. An artificial color code is used to translate these modifications on the final images. The red end of the spectrum corresponds to a weak phase shift, i.e. an elastic response, whereas blue end corresponds to more dissipative specimen-tip interactions.

The topology of the particle surface is evaluated with AFM height images. The differences in height results in differences of the reflected laser beam. In the false colored images presented here, the red colors correspond to higher areas whereas blue colors are for lower zones.

4.4.5 TEM

A TEM Philips CM20 equipped with a LaB_6 filament operating at 200kV was used throughout. All images were obtained at room temperature.

The contrast on the images is due to the differences in the electronic density of the domains. The PTA is expected to stain preferentially the PU domains (Li, Chiu et al. 2007) resulting in PU domains which have a higher electronic cloud density and appear as darker areas on the TEM (Chai and Tan 2008). No distinction can be made between the different acrylic parts, as they have very similar electron transparencies and degrade rapidly under the beam. The same distinction between PU and acrylic is expected when imaging PTA-stained films.

Unstained films have also been imaged. In that case, the contrast should appear during irradiation of the films and should arise from beam-induced mass-loss in the PU domains.

4.5 Results and discussion

4.5.1 Particle analysis

The morphology of hybrid latex particles have been investigated with AFM and TEM. We first compare latexes with different grafting conditions of the polyurethane. In particular, particles with ungrafted PU and fully grafted PU are compared. In a second stage, the impact of the relative amount of incorporated PU on the particle morphology is discussed.

4.5.1.a Morphology of particles with different degrees of grafting

AFM images

Images of particles obtained in AFM tapping mode (amplitude A_0 = 48 nm) are shown in Figure 4-1. Height images are on the top, phase images are below. The particles with ungrafted PU (II_10PU(0)OH2) are presented on the left and those with grafted PU (II_10PU(TG)OH2) on the right.

On these images, individual round-shape particles well separated from each other can be observed. The height images show in both cases a thin corona (around 10 nm) on the border of the particles and a higher area withtin this particle (with thickness between 15 and 30 nm). The average diameter of the particles measured on these images is around 400 nm. This is a larger diameter compared to DLS measurements given in Table 4-1 (around 160 nm). The presence of thinner borders and the difference in apparent diameter indicate that particles from both latexes flatten on the substrate.

The phase images suggest that both the ungrafted (II_10PU(0)OH2) and grafted (II_10PU(TG)OH2) particles have a surface with a core-shell morphology. A thin, weakly dissipative layer is at the border (indicated by the warmer colors) and a more dissipative area in the center occupies the large majority of the surface of the particle. In these latexes 2-EHA, the main monomer (97 wt% of the acrylic content), is soft and dissipative. This monomer is more hydrophobic than the two other acrylic monomers (MMA and MAA here). Hence it is consistent with the images to think that 2EHA is inside and MMA and MAA form the shell. Despite the apparent surface core-shell morphology observed for latexes with two different grafting conditions, some differences appear between particles.

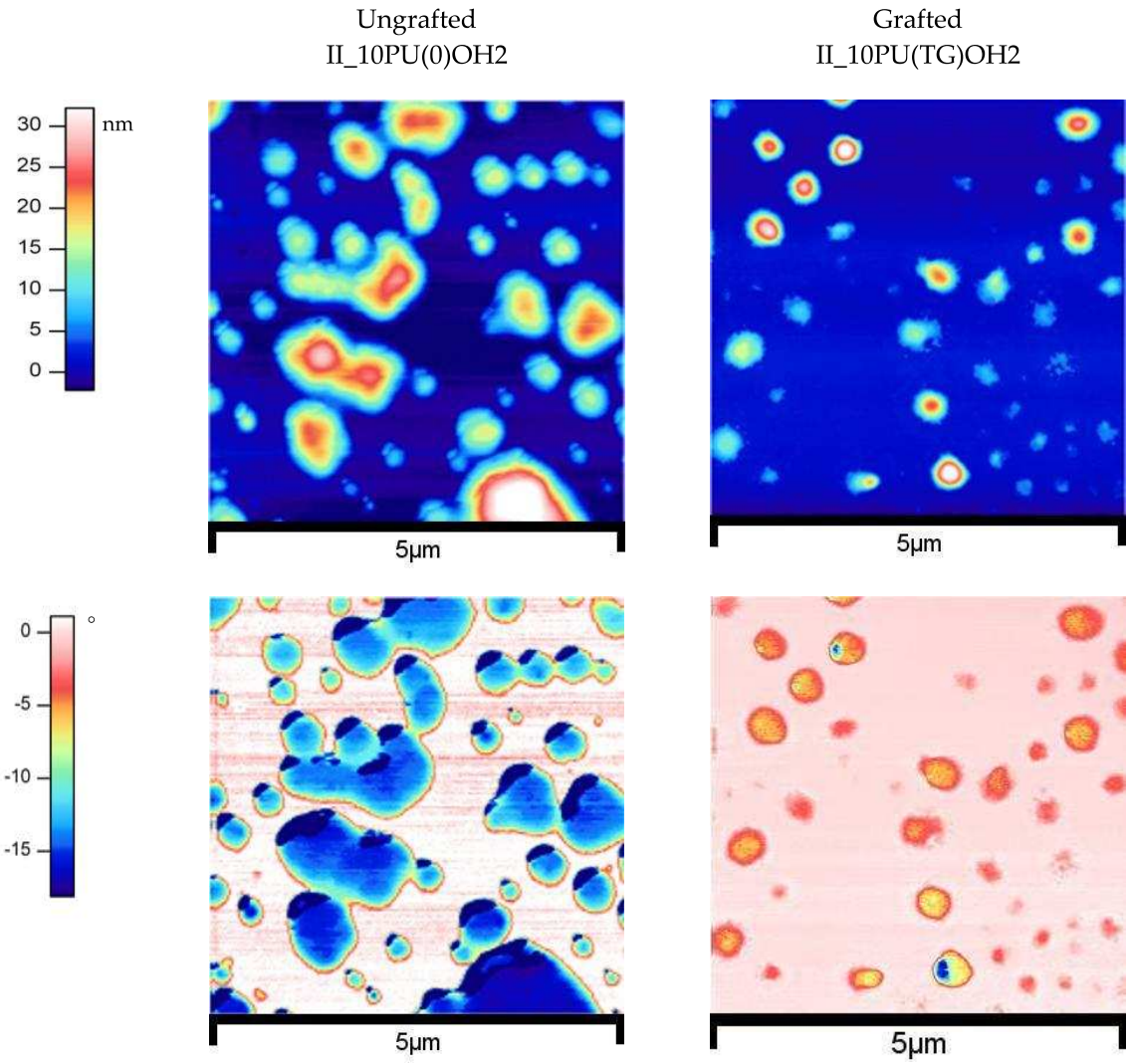

Figure 4-1 : AFM images of hybrid particles with ungrafted (II_10PU(0)OH2; on the left) and grafted (II_10PU(TG)OH2; on the right) polyurethane; top: height images; down: phase images

When PU is not grafted (Figure 4-1-left), two distinct domains can be distinguished in the interiors of the particles: one major domain surrounded by the less dissipative shell presented above and one smaller and more dissipative domain. This distinct domain represents 22 % ± 4 % of the particle projection, is invariably toward the outside from the particles and not surrounded by the hydrophilic shell. All domains observed on the particle surface are oriented in the same direction. The localization at the border of the particles could be the proof of a more hydrophilic domain which comes in contact with water, and which is even more hydrophilic than the shell described previously. The specific orientation of this domain could be due to the drying conditions of the diluted latexes. We think that a water meniscus during the drying could be the reason for the shape and localization of this domain. It could also be explained by a faster drying of the polymer present in this area which adheres to the mica sheet first. The difference in the dissipative nature of both domains is the sign of a phase separation at the particle scale. Since PU and acrylic polymers

are immiscible and taking in account the weight proportions between the two polymers, it is very probable that the major domain is acrylic whereas the minor one is mainly made of PU. The PU prepolymer chains are short (M_w ~ 3000 g.mol^{-1}) and, in this latex, extended by BPA but not crosslinked. Compared to the acrylic phase which is made of chains with M_w ~ 300 – 4000 kg.mol^{-1} (measured by SEC) and which contains a small insoluble fraction (~ 18 %), it is fully probable that the PU phase is more dissipative.
When PU is highly grafted (Figure 4-1-right), the interiors of the majority of the particles appear more uniform and less dissipative than particles with ungrafted PU. Phase contrast is present in certain particles but is not as distinct as for the ungrafted particles. These particles are smaller compared to those with ungrafted PU.
The lack of evident phase separation between PU and acrylic is consistent with the high grafting degree which results in an efficient incorporation of the PU. A high gel content was found for the particles with grafted PU (~ 82 % of insoluble chains) whereas 18% of gel is detected in the particles with ungrafted PU. The difference in the nature of the inner phase between both particles could be explained by that difference in gel content. Flattening is then favored is these less crosslinked more dissipative particles. It is possible that the phase separation between PU and acrylic hinder the chain transfer reaction during acrylic polymerization and thus limits the formation of gel content but there is no evidence of that.
Reliable and interpretable AFM images are not easy to obtain for this kind of particles. Optimized parameters have to be found to debond from tacky surfaces (energetic tapping) without indenting too much or damaging the particles. These parameters are in a tight range and are not easy to fine tune. Moreover, the interpretation of the images is complex. Only images of the surfaces can be obtained and it is not easy to know if the particles have been damaged during observation. Series of images at different tip indentations (changing amplitude A_0 and set point ratio r_{sp}) for the same surface could help to improve the analysis of these surfaces.
An alternative to AFM imaging is TEM imaging of the particles. Although it has its limitations discussed previously, experimental conditions leading to reliable observations were more easily found with this technique and it has been preferred for the rest of the paper.

TEM images

The same particles with ungrafted (II_10PU(0)OH2) and grafted PU (II_10PU(TG)OH2) but stained with PTA have then been observed by TEM. The more representative images obtained with this technique are shown on Figure 4-2 for comparison with the AFM images.

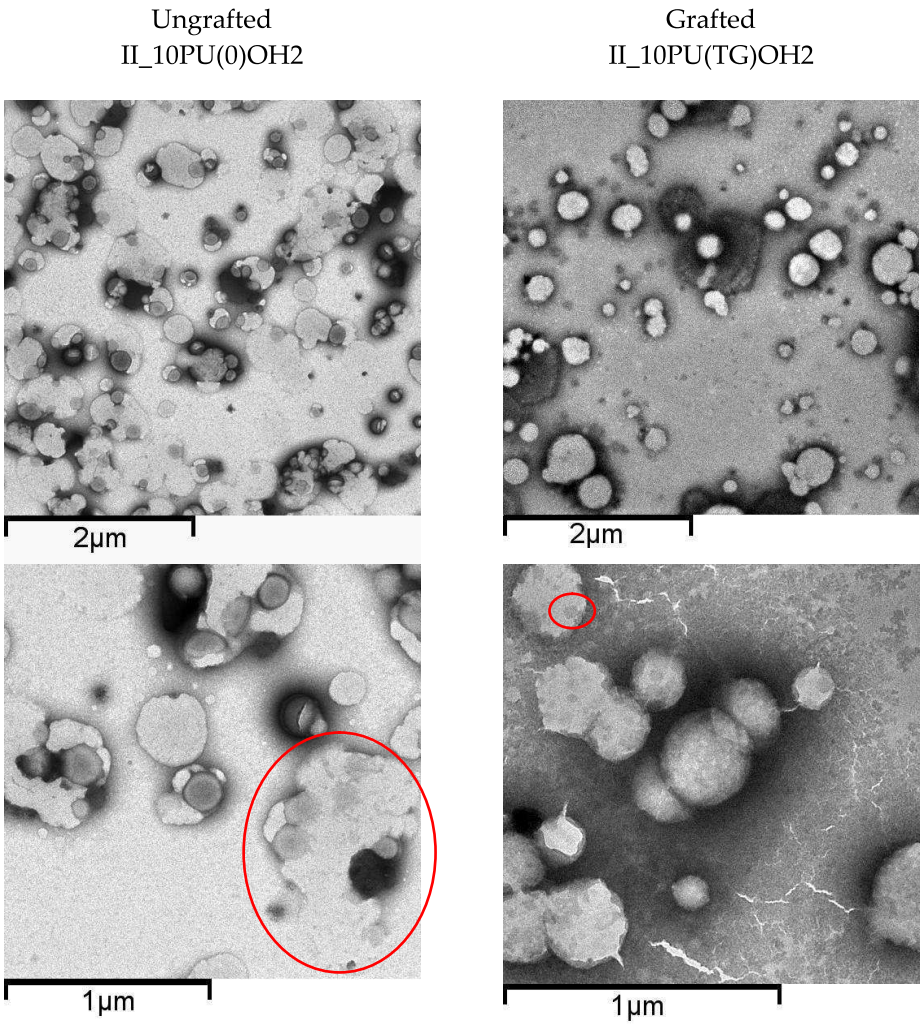

Figure 4-2 : TEM images of hybrid particles with ungrafted PU (II_10PU(0)OH2; left) and grafted PU (II_10PU(TG)OH2; right); the second row is a magnification of the first one; staining: PTA

Individual round-shaped particles are also clearly seen by TEM. In the case of ungrafted PU, particles seem to be composed of two domains: large light-grey domains touching smaller round-shaped dark-grey ones. On these images, the different shades of grey come from the different levels of PTA staining: light grey areas indicate less staining, while dark-grey zones are more stained. As the PU phase is expected to be more stained by the PTA than the acrylic phase (Li, Chiu et al. 2007), one can reasonably conclude that the small dark-grey round-shape domains are polyurethane while the large light-grey areas are made of acrylic copolymers. No core structure within the acrylic phase, such as suggested by the AFM images, is visible in the TEM images owing to lack of contrast or beam damage. These PU domains are always connected to acrylic aggregates. In some cases, the light grey domains form large areas and several dark-grey round domains are in contact with them (as shown in the red circle on Figure 4-2). They could be aggregates of particles, which is highly probable due the dissipative nature and ability to flatten of these particles. On the other hand, images of particles with highly grafted PU (II_10PU(TG)OH2) appear much more

homogeneous. This is consistent with hypothesis of an efficient incorporation of the PU chains through grafting. On the image with the bigger scale (Figure 4-2 right down), one could distinguish small darker zones (e.g. in the red circle). They may be made of PU or PU-rich nanophases. The smaller apparent diameter of particles with grafted PU indicates that they flatten less on the carbon grid compared to particles with ungrafted PU. This is also in good agreement with the higher measured gel content and with AFM images presented before.

The dark corona that can be observed around some particles regardless of the grafting of the PU could be due to PTA which is present in the water and leaves a dark ring when water evaporates.

Images from AFM and TEM (Figure 4-1 and Figure 4-2) present similar particle morphologies. When the PU is not grafted in the particles, phase separation is observed with PU domains smaller than acrylic domains. Particles are also more dissipative, due to a lower gel content. In the case of grafted PU, particles have a more homogeneous surface with PU incorporated in all the particles. However, some smaller PU rich domains could be seen in the inner part of the particle. AFM images suggest that a less dissipative shell made of more hydrophilic parts of the acrylic copolymer (MMA and MAA) surrounds a more dissipative core composed of the soft part of the copolymer (2EHA). This shell doesn't surround the PU domains. A schematic of the possible structure of the particles as obtained from the interpretation of AFM and TEM images is given below:

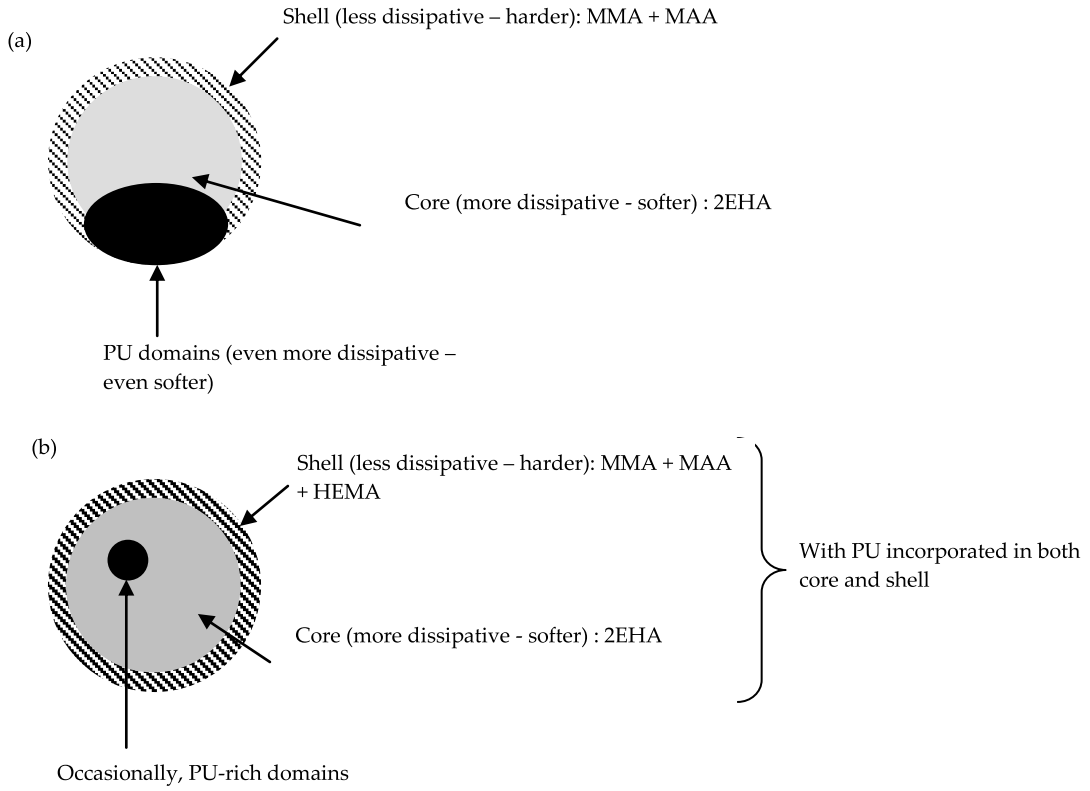

Figure 4-3: Possible structure of particles with ungrafted PU (a) and grafted PU (b)

Comments on the particle sizes

On the AFM images as well as on the TEM ones, both types of particles (with ungrafted and grafted PU) have a diameter much larger than the one measured by DLS in the latexes (measured diameters are indicated below each image). When measured by DLS, particles are in suspension in water and don't flatten nor aggregate (in the case of stable latexes). The measured diameter is the real diameter of the particles. As soon as the particles above T_g are cast on a substrate (mica sheets or carbon grids) and water starts to evaporate, they deform. The softer the particles, the more they can flatten. For this reason, the apparent diameter measured on AFM or TEM images are bigger than in suspension in the latex. Aggregation between particles is also possible due to the particle softness and is favored by a higher particle concentration in the diluted latex. Indeed, latexes are less diluted for TEM imaging than for AFM (see section 4.4.3) and aggregates are seen on TEM images whereas there are no obvious aggregates on AFM images.
The particles with ungrafted PU appear bigger than those with grafted PU and the size distribution is wider (average diameter d_{avg} = 444 nm ± 141 nm for the ungrafted and 372 nm ± 111 nm for the grafted). These particles have a lower gel content i.e. are less crosslinked in agreement with observed more dissipative particles on AFM phase images (Figure 4-1).
The fact that particles appear smaller when observed by TEM than by AFM can be due to differences in the drying process. For AFM observations, highly diluted latexes are dried at room temperature in static mode (no spin-coating process). The low particles concentration in the diluted latex doesn't favor aggregation but the static drying favors particles flattening. In the case of TEM images, latexes are less diluted so they can aggregate more easily. However, the dynamic drying by spin-coating quenches particles on the substrate and particles keep a size closer to their initial size with less flattening.

Discussion

Round-shape individual latex particles with ungrafted and grafted PU were imaged by both AFM and TEM as much larger than what is measured by DLS, due to the flattening of particles on the substrate. This has been noted also by Canetta et al. in the case of particles containing tackifying resin observed by AFM (Canetta, Marchal et al. 2009). Some differences in the apparent particle sizes obtained in AFM and TEM are presumably due to differences in the preparation of latexes on mica sheets or carbon grids.
Clear differences appear between the particles with the ungrafted PU and those with grafted PU. In the first case, a phase separation is observed. More dissipative minority domains more stained by PTA PU-rich are observed inside the particles, while the majority phase, is slightly less dissipative and less stained by PTA. The more dissipative nature of the minority domain is consistent with short uncrosslinked PU prepolymer chains. This phase separation is at the particle scale and both domains can be distinguished in the same particles. The PU phase is always present at the border of the particles indicating that it is at least as hydrophilic as the major acrylic phase. This observation is consistent with observations made by Li and El Aasser (Li, Daniel et al. 2005) or by Li and Chiu (Li, Chiu et al. 2007) who

worked with PU composed of isophorone diisocyanate (IPDI), polypropylene(glycol) (PPG) and extended with Bisphenol A. They effectively obtained PU less hydrophobic than the acrylic. Nevertheless, both research groups obtained results very different from us on particle morphology. Li and El Aasser used miniemulsion polymerization initiated by a redox system to prepare hybrid particles of PU and acrylic. They used a PU prepolymer similar to ours but the main acrylic component was butyl methacrylate (BMA, with T_g ~ 20 °C). They also extended the PU prepolymer with diols (Bisphenol A) and grafted the PU chains to the acrylic backbone with HEMA. They showed that the presence of HEMA didn't affect much the particles size and above all that grafting was not required to have homogeneous particles. Indeed, as long as the PU was extended with a hydrophobic chain extender (such as BPA), homogeneous particles could be obtained. This homogeneity of particles was also noticed by Li *et al.* (Li, Chiu et al. 2007) who calculated preferential morphologies of urethane/acrylic hybrid particles prepared by miniemulsion polymerization based on thermodynamic calculations. In particular they measured the interfacial tensions of the different systems (monomer/water, PU/water, acrylic/water and PU/acrylic) and integrated the results in their prediction. For systems based on PU (IPDI + PPG) prepolymer, hydrophobic chain extender (BPA), thermal initiator (KPS) and high T_g acrylic monomer (MMA), they showed that homogeneous particles were also expected (no grafting was added in their work) and confirmed their calculation by TEM images. The most probable explanation of the heterogeneity of our particles is the much lower miscibility of PU with a low T_g monomer (2EHA here) than with BMA or MMA. This parameter was not checked before polymerization but is very likely that PU prepolymer and 2EHA monomer phase-separate relatively fast as the degree of polymerization of the acrylic polymer increases. This phase-separation is avoided when the PU is completely grafted to the acrylic network. Thus, one can see that the transcription of methods used to prepared particles for coating to the preparation of adhesive is not trivial. This is due in particular to the more hydrophobic behavior and to the lower T_g of monomers used in adhesive recipes, which certainly decreases miscibility with polyurethane.

It is worth noting that the area occupied by the PU phase represents 22 % of the particle size in AFM and 32 % in TEM. During the latex preparation 10 wt% of polyurethane prepolymer was added in both latexes. The large area represented by the PU indicates either that PU can flatten more than acrylic or that the domains are not pure PU but made of a mix between PU and acrylic. The immiscibility between both polymers would favor the first hypothesis but no clear evidence appears and this has to be further discussed. When PU is fully grafted, homogeneous particles are observed proving that this is an efficient solution to avoid uncontrolled phase separation.

The total grafting of the PU prepolymer chains with HEMA is a way to control the homogeneity of the final latex particles morphology. Nevertheless, one can wonder if a partial grafting the PU chains could be sufficient to avoid phase separation. The next section presents images obtained from latexes where only 11 % of the PU chain ends have reacted with HEMA. Latexes with different PU weight fractions to analyze the impact of the PU weight fraction on the morphology.

4.5.1.b Impact of the weight fraction of incorporated polyurethane

With this second series of latexes, we attempted imaging with both AFM and TEM. However the AFM results were not easily interpretable and we focus here on the results obtained from TEM observations. AFM images are presented in annex 1.

TEM images

The TEM images obtained with latexes containing 5 wt% (I_5PU(0.22)OH0.55, 25 wt% (I_25PU(0.22)OH0.55) and 50 wt% (I_50PU(0.22)OH0.55), with a constant degree of grafting of 11% are presented in Figure 4-4. The particle diameters are indicated below the images.

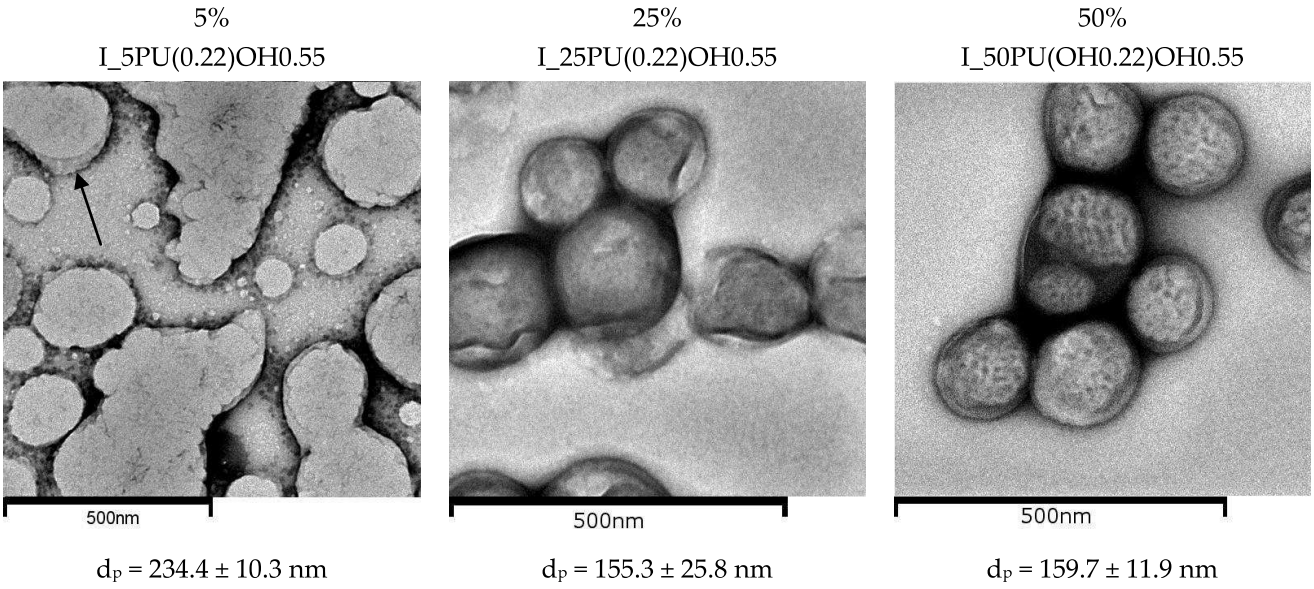

Figure 4-4: TEM images of hybrid particles with different PU amount; grafting degree= 11%; staining: PTA

For each PU weight fractions, aggregates of several particles are observed. For the lowest PU weight fraction, individual particles can also be noticed on the image but, inside the aggregate, borders of individual particles are not easy to see. For the two highest fractions (25 wt% and 50 wt%), on the contrary, individual particles are clearly observed in the clusters. Comparing the apparent diameter measured on these images with the real diameter measured by DLS, particles appear bigger on the TEM images indicating that they flatten on the carbon grid. But, the higher the PU weight fraction is, the less the difference between these two diameters. This proves that the lower the PU weight fraction is, the softer and more dissipative the particles are. The measurement of the insoluble fraction (presented in Table 4-2 for each PU proportion) indicates that the higher the PU content, the higher the gel content which must play an important role. This is consistent with an increase of the stiffness and decrease of level of dissipation.

Table 4-2: Gel fractions in samples with diferent PU weight fractions

Sample	Gel content (%)
I_5PU(0.22)OH0.55	< 20%
I_25PU(0.22)OH0.55	37%
I_50PU(0.22)OH0.55	74%

The proportion of PU also modifies the particle morphology. When 5 wt% of PU are added, the particles appears relatively homogeneous. Looking carefully, a thin shell surrounding some particles can be detected (as indicated on Figure 4-4 –left with a black arrow). For the particles with 25 wt% of PU, a shell darker than the inside can be observed on some particles. It is also possible to see some darker spots in the center of the particle image. The contrast between PU and acrylic brought by the PTA suggests that these dark-grey domains (shell and small spots) could be PU. However, on the image of the particles with 25 wt% PU, some light-grey areas are also distinguished. They are at the border of the particle, quite thin but with no specific shape. Since there should be no contrast between butylacrylate (~ 90 wt% in these formulation) and methyl-methacrylate and acrylic acid (~ 10 wt%) this is no evidence of a core-shell structure. One other possible interpretation would be that these domains are made of surfactants. However, the same amount of surfactant being used in each latex recipe, one would expect to see these domains on each picture, which is not the case. To our knowledge, no clear interpretation of the nature of these domains can be myde. If we consider the dark shell around some of the particles, those are probable made of polyurethane. They must be distinguished from the black coronas or areas seen on some part of the three TEM images and which are PTA dispersed in water, trapped during drying, as explained previously (section 4.5.1.a).

The image of particles containing 50 wt% of PU shows particles with an equivalent morphology as the particles with 25 wt% of PU. A thin dark shell around the particle may indicate that it is PU. Moreover, one can distinguish several dark spots in the apparent core of the particles. A schematic picture of the different morphologies noticed for the different PU weight fractions is presented below:

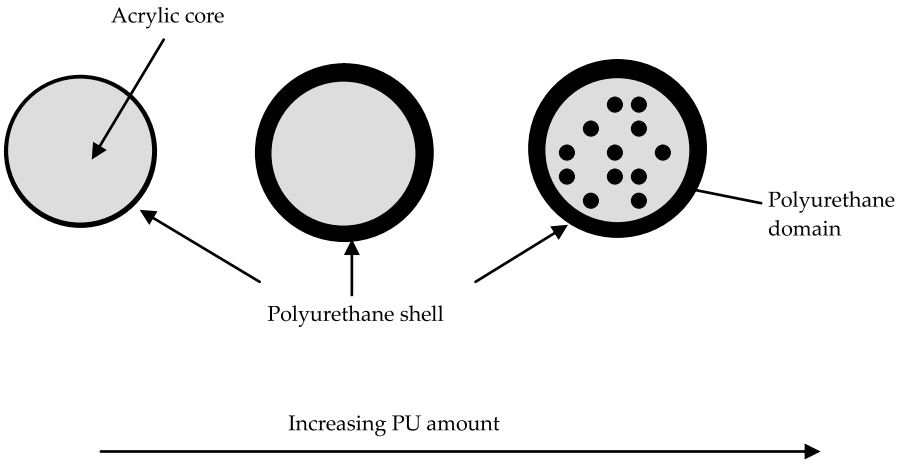

Figure 4-5: Morphology of the hybrid particles varying with the weight fraction of polyurethane

Discussion

These morphologies are consistent with the presence of an increasing proportion of PU. The more PU is effectively in the polymer, the more it can be distinguished in the TEM images. One can also say that the more PU is present and the more phase separation can be seen at the particle scale. The immiscibility between the two polymers and the tendency of PU to segregate at the particle border reinforces this hypothesis.

In conclusion, a partial grafting could not be sufficient to avoid phase separation at the particle scale above a certain PU weight fraction (at least 25 wt%). This phase separation is in contradiction with homogeneous morphologies observed by Li *et al.* ((Li, Daniel et al. 2005) when the PU is BPA-extended. One can conclude that miscibility of BA (used as main acrylic monomer here) with PU is as low as miscibility of 2EHA with PU discussed previously. Moreover, Li *et al.* noticed than an increase in the PU wt% results in a decrease of particle size and explained it by an effect of the PU on the surface properties of the particle: when there is more PU, the particle boundaries are more hydrophilic (due to less hydrophobic behavior of the PU), resulting in less consumption of surfactant per particles and then in a lower average particle size. We do observe the opposite result: the higher the PU weight fraction, the higher the particle diameter. This could be correlated with the presence of the PU on the borders when increasing the PU wt% but has to be further discussed.

Finally, one remaining question concerns the localization of the PU inside the particle. In the case of the previous system (2EHA and no grafting) asymmetric particles were obtained with a specific orientation of the PU domains inside the particle. When a higher fraction of PU is used (and BA is the main monomer) PU tends to segregate around the particle boundaries and to form symmetric particles. The hydrophobic behaviors and the miscibility of components could once again bring some elements of interpretation.

4.5.2 Film analysis

The analysis of single particles by AFM and by TEM has permitted to determine specific particle morphologies. In particular, phase separation was observed at the particle scale when the PU was not grafted at all (section 4.5.1.a) or when a high fraction of PU with low degree of grafting is added (section 4.5.1.b). The impact of such morphologies on the final film architecture appears then essential, considering that a specific phase separation could take place during the film formation process. That would result in film of poor quality that is to say non transparent and containing cracks. In this section, we present two series of images. In the first part, films obtained from particles with different levels of grafting are imaged. In the second part, we focus on the architecture of films made from particles with PU in different proportions. Only TEM images are presented. Once again, AFM images have also been performed but no clear interpretation could be made from them.

4.5.2.a Influence of the grafting

TEM images

In this series of images, films were obtained from the drying of undiluted unstained latexes and then sectioned with the help of a cryo-ultramicrotome. Conclusive images are obtained, even without staining. Stained films were also imaged by TEM but the staining was made once the films were formed by putting them for one night in a 1.5 wt% PTA solution. This procedure didn't result in a homogeneous incorporation of the PTA in the film and resulting images are a mix of stained and unstained areas. That results in less clear interpretations.
Figure 4-6 shows images of films with ungrafted PU (obtained from the drying of the latex II_10PU(0)OH2) and highly grafted PU (from latex II_10PU(2.67)OH1).

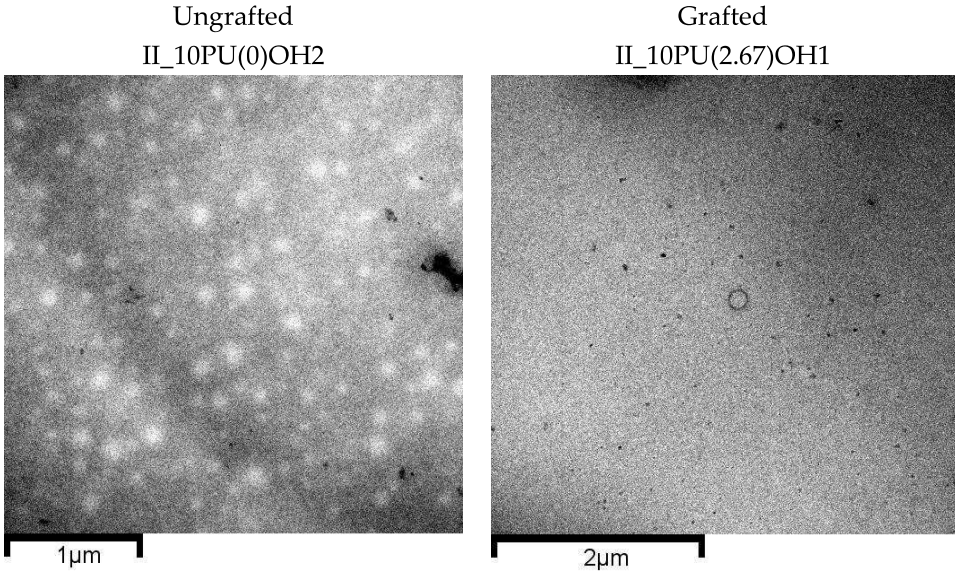

Figure 4-6: TEM images of films obtained from the drying of hybrid particles: with ungrafted PU (left) and grafted PU (right); no staining

For the ungrafted PU, some white spots are randomly dispersed in a dark-grey matrix and the film is heterogeneous. Considering the specific phase-separated morphology observed for the individual particles, these white spots could obviously be PU domains trapped in the acrylic matrix during the drying process. However given the absence of staining, one can wonder why a contrast is observed between PU and acrylic. It is worth noting that the contrast appears during the irradiation of the film by the electron beam. The contrast could then arise from beam induced mass-loss in the PU preferentially to the acrylic. No other reason could explain why unstained PU should show contrast with the acrylic. The average diameter of these white spots is 130 ± 15 nm and is slightly smaller than the domains measured for single particles (178 ± 75 nm) but individual particles tend to flatten on the substrate when dried individually. No such flattening is expected when drying highly concentrated latex (here the solid content measured gravimetrically is ~ 47 %).
When the PU is grafted to the acrylic backbone in the particle, no specific domains can be distinguished. Films are completely homogeneous. We assume that the black points randomly present in the film are due to some defects on the carbon grid trapped during cryo ultramicrotomy. Indeed, the same points can be seen also on the left image. If there is any induced beam damage in the PU it is homogeneously distributed.

Discussion

The phase separation observed in particles containing ungrafted polyurethane is retained in the final film architecture. As a consequence, the film is macroscopically cloudy and presents some cracks. Oppositely, the film with the grafted polyurethane is transparent and has dried homogeneously. Mechanically, when a debonding test is performed on a film with ungrafted PU, a cohesive debonding is noticed and the film leaves some residue on the substrate, which is not acceptable for an application as PSA. When the same test is made on homogeneous films made of pure acrylics or on films made with grafted PU, the film debonds interfacially with no residue. The PU/acrylic phase separation does therefore impacts on the macroscopic behavior of the film.
Such a phase separation was not observed on films obtained from hybrid particles based on the same ungrafted PU (but with 1,4 Butanediol as chain extender) but with an acrylic composition (BA + MMA) with a higher T_g (between 0 °C and 13 °C). Even when high PU weight fractions were used, AFM images showed smooth surfaces without viscoelastic contrast (Wang, Chu *et al.* 2005). Nevertheless, this work didn't present any picture of particles but one can suggest that they were homogeneous which resulted in homogeneous films. Clearly the phase separation observed in our particles has a strong negative effect on the film morphology.
It is worth taking into account that DSC measurements on phase-separated films give only one T_g whereas one would expect to observe the distinct T_g of each phase. Nevertheless, separate DSC measurements on pure PU polymer and pure acrylic copolymers gave very close values of T_g for each polymer (T_g(PU)= -48 °C and T_g(acrylic)= : -63 °C) with a wide distribution of the T_g of pure acrylic. It is then fully probable that a distinction between the

two T_g is masked by the vicinity of the T_g of each polymer. The use of modulated DSC measurements should be considered to refine this hypothesis.
The impact of a phase-separated morphology on the film macroscopic properties has been demonstrated. To avoid this phase separation, the grafting of a high proportion of PU appears as an efficient solution. As specific morphologies have also been observed for particles with lower grafting degree and varying fractions of PU, the question of the resulting film morphology is crucial.

4.5.2.b Impact of the weight fraction of polyurethane

TEM images

Figure 4-7 shows images of films made from particles with 5wt%, 25 wt% and 50 wt% of PU. The films with 5 wt% and 50 wt% were not PTA-stained, whereas the one with 25 wt% was. The argument for presenting images of unstained films is the same as explained in the previous section. For the film with 25 wt%, unambiguous images were obtained only with the stained film.
When a low amount of PU is added in the particles, a film without specific domain is obtained. PU has been well incorporated in the particles, giving a homogeneous film architecture at the particle scale. Increasing the amount of PU, distinct domains start to appear in the film. For the highest PU weight fraction (50 wt%, I_50PU(0.22)OH0.55), thin white circles connected to each other can be seen. They can be easily correlated to the distinct particle structure observed on the TEM images showed in Figure 4-4. Nevertheless, the PU domains observed inside the particles on the particle image cannot be seen on this image, but that may be due to an insufficient magnification.
The image of the film with 25 wt% of PU in the particle is less obvious to interpret. One can clearly observe a grey matrix in which white and dark distinct domains are randomly distributed. Since the film has beens stained, the PU should appear darker than the acrylic. However the electron beam may induce a mass loss mostly in the PU domains, argument which would identify the white domains as PU. Since the white domains are in majority and their total area is more in agreement with the PU weight fraction, this second interpretation is preferred.

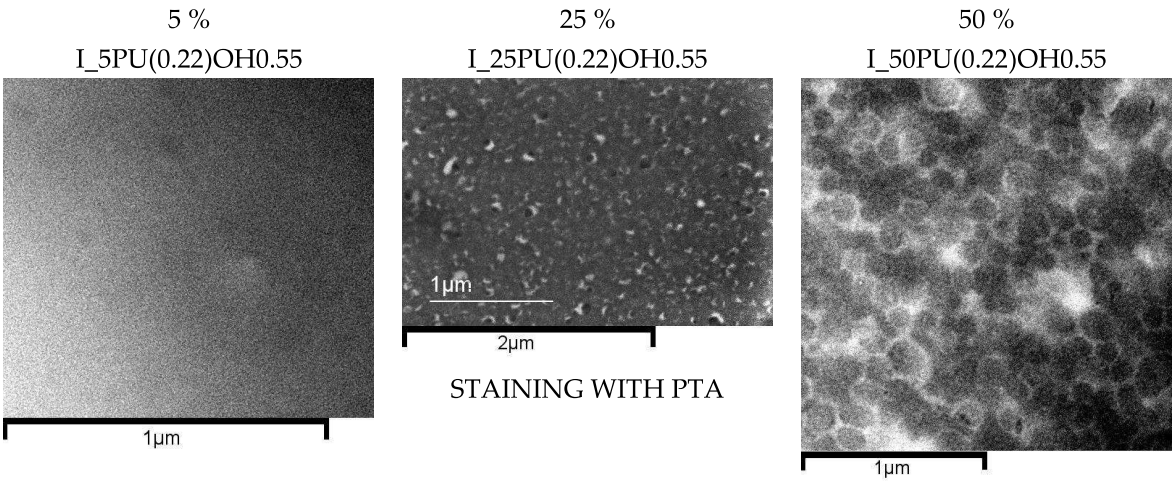

Figure 4-7: TEM images of films obtained from the drying of hybrid particles with different PU amounts; no staining

Discussion

Figure 4-7 shows that high PU weight fractions (25 wt% and 50 wt%) affect the film morphology. The image of the film with 50 wt% in particular shows that the core-shell structure obtained from the particle is still present after drying. Interpreting these white shells as surfactant trapped during the drying stage is very questionable since the white shells are observed only for the highest PU weight fraction whereas the same proportion of surfactant is present in all latex formulations.

The important question of the impact of the morphology of this film on the macroscopic properties still remains open. The dry film is typically crack-free and transparent, although for the highest PU weight fraction (50 wt%), the final film is slightly cloudy. The drying should be modified by the core-shell morphology. Hence, the PU surrounding the particles may hinder the interpenetration between particles, resulting in films with weak interfaces. The impact on the mechanical properties is discussed in the the next chapter.

4.6 Conclusion

Soft and tacky urethane/acrylic hybrid particles and films obtained upon drying of such particles have been successfully imaged by AFM and TEM. This second technique was implemented more easily and more conclusive images could be obtained in all cases. AFM and TEM, for the particles with and without grafting, and then TEM only, for the other cases, have shown that the presence of polyurethane affects the particle and the film morphology. When no PU is grafted to the acrylic network, particles are clearly asymmetric with a phase-separation between acrylic and PU domains, the PU being at one border of the particles. This heterogeneity leads to a more macroscopic phase separation in the dried film and affects the mechanical properties. The film is more dissipative and debonds cohesively when compared to a pure acrylic matrix. The grafting of the PU through the HEMA appears as an efficient solution to incorporate the PU homogeneously at the particle scale.

Similar phase-separated morphologies are obtained when the particles contain a high PU weight fraction and when only a low fraction of this PU is grafted. Indeed, with 50 wt% of PU and 11 % of the PU chains grafted to the acrylic, a core-shell morphology is observed. The PU forms a thin shell around the particles which may affect the polymer chains interpenetration during the late stages of film formation. Particle – particle interfaces are then weaker and the maximum extensibility that the films can sustain before macroscopic fracture is then reduced. This interpretation is supported by the fact that the core-shell morphology is retained in the film. For very low PU weight fractions even partial grafting is sufficient to have a continuous film and mechanical properties equivalent to those of the pure acrylic film. For a higher proportion of PU, specific PU-rich domains are observed inside the particles and remain in the films.

Such phase-separation between PU and the acrylic phase has not been observed when using an acrylic monomer composition resulting in T_g between 0 °C and 20 °C. This points out the differences in miscibility of the PU with acrylic monomers of low T_g and reveals the high challenges related to the synthesis of hybrid latex particles for adhesive applications. Furthermore PU is generic term and the exact composition of the soft block of the PU is not fully known and could be different betweent the different studies.

The characterization of the morphology of the particles and of the films provides essential information to interpret the mechanical and adhesive properties and to relate them with the synthesis and molecular structure parameters. Further analysis of the mechanical properties of the films obtained from these latexes is now the focus of chapters 5 and 6.

4.7 Reference

- Asua, J. M., *Progress in Polymer Science*, **2002,** *27*, (7), 1283-1346.
- Brandrup, J.; Immergut, E., H., *Polymer Handbook,* New York, Wiley, **1999**.
- Brown, R. A.; Coogan, R. G.; Fortier, D. G.; Reeve, M. S.; Rega, J. D., *Progress in Organic Coatings*, **2005,** *52*, 73-84.
- Canetta, E.; Marchal, J.; Lei, C. H.; Deplace, F.; Konig, A. M.; Creton, C.; Ouzineb, K.; Keddie, J. L., *Langmuir*, **2009,** *25*, (18), 11021-11031.
- Chai, S. L.; Jin, M. M.; Tan, H. M., *European Polymer Journal*, **2008,** *44*, 3306-3313.
- Chai, S. L.; Tan, H. M., *Journal of Applied Polymer Science*, **2008,** *107*, (6), 3499-3504.
- Creton, C., *MRS Bulletin*, **2003,** *28*, (6), 434-439.
- Gooch, J. W.; Dong, H.; Schork, F. J., *Journal of Applied Polymer Science*, **2000,** *76*, (1), 105-114.
- Hegedus, C. R.; Kloiber, K. A., *Journal of Coatings Technology*, **1996,** *68*, (860), 39-&.
- Hirose, M.; Kadowaki, F.; Zhou, J. H., *Progress in Organic Coatings*, **1997,** *31*, (1-2), 157-169.
- Hirose, M.; Zhou, J. H.; Nagai, K., *Progress in Organic Coatings*, **2000,** *38*, (1), 27-34.
- Jovanovic, R.; Dubé, M. A., *Journal of Macromoleculaar Science Part C: Polymer Reviews*, **2004,** *C44*, (1), 1-51.
- Kukanja D.; Golob J.; Zupancic-Vlant A.; M., K., *Journal of Applied Polymer Science*, **2000,** *78*, 67-80.
- Landfester, K., *Macromolecular Rapid Communications*, **2001,** *22*, (12), 896-936.
- Li, C.-Y.; Chiu, W.-Y.; Don, T.-M., *Journal of Polymer Science Part A: Polymer Chemistry*, **2007,** *45*, 3359-3369.
- Li, M.; Daniel, E. S.; Dimonie; Sudol, E. D.; El-Aasser, M. S., *Macromolecules*, **2005,** *38*, 4183-4192.
- Lopez, A., POLYMAT, *Universit of the Basque Country*, **2009**
- Mallegol, J.; Dupont, O.; Keddie, J. L., *Langmuir*, **2001,** *17*, (22), 7022-7031.
- Mallegol, J.; Dupont, O.; Keddie, J. L., *Journal of Adhesion Science and Technology*, **2003,** *17*, (2), 243-259.
- Routh, A.; Russel, W., *Industrial Engineering Chemistry Research*, **2001,** *40*, 4302-4308.
- Udagama, R., Laboratoire de Chimie, Catalyse, Polymères et Procédés, *University Claude Bernard -Lyon I*, **2009**
- Wang, C.; Chu, F.; Graillat, C.; Guyot, A., *Polymer Reaction Engineering*, **2003,** *11*, (3), 541-562.
- Wang, C.; Chu, F.; Graillat, C.; Guyot, A.; Gauthier, C.; Chapel, J. P., *Polymer*, **2005,** *46*, 1113-1124.
- Wang, C.; Chu, F.; Guyot, A.; C., G.; F., B., *Journal of Applied Polymer Science*, **2006,** *101*, 3927-3941.
- Wang, C. P.; Chu, F. X.; Jin, L. W.; Lin, M. T.; Xu, Y. Z.; Guyot, A., *Polymers For Advanced TEchnologies*, **2009,** *20*, (3), 319-326.

4.8 Annex 1: AFM images of particles with different PU weight fractions

We present in this annex the images obtained by AFM of particles with different PU amounts. Tapping mode was employed with the conditions described in the paper: The amplitude A_0 is equal to 74nm (set point= $0.9A_0$).

AFM observations were performed under ambient conditions of pressure, temperature and hygrometry. Latexes were diluted (1:10000) and 4 microliters of the diluted latexes were deposited on a mica sheet previously cleaved with scotch tape. The mica surfaces wet with latexes were dried at room temperature. AFM was used in stiff tapping mode. Cantilevers were performed by BudgetSensors (model Tap300) with a spring constant of 40 N/m and a resonance frequency calibrated at 300 kHz. The free oscillation amplitude A_0 varied from 48 nm to 74 nm. The set point was fixed at $0.9A_0$ and scanning speed was 1Hz. Height images are presented in Figure 4-8 while phase images are presented in then next figure.

The images are not easy to interpret, in particular the case of 25 wt% of PU.

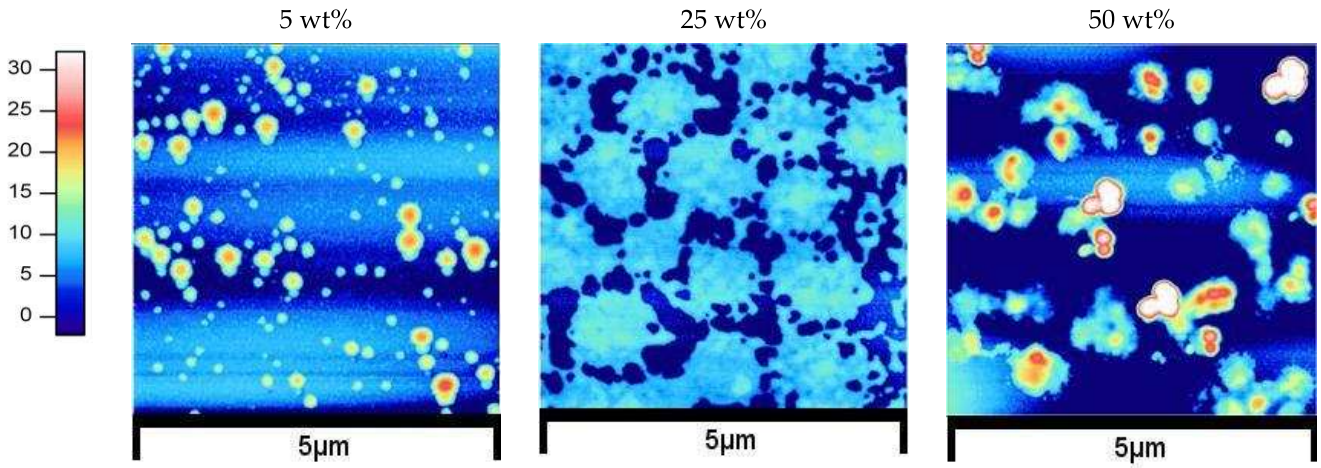

Figure 4-8: Height images of samples with PU fraction from 5 wt% to 50 wt%

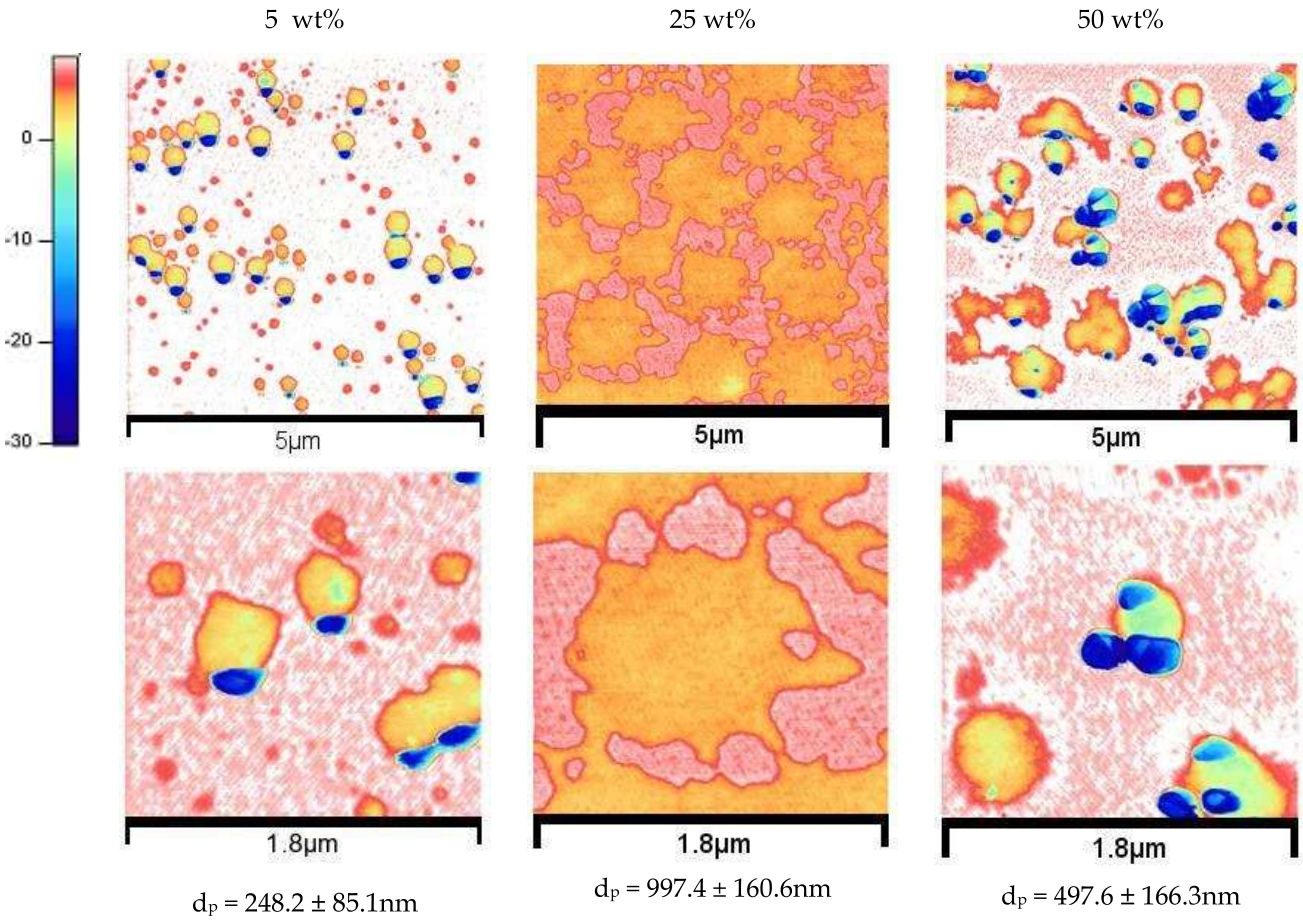

Figure 4-9: Phase images of samples with PU fraction from 5 wt% to 50 wt%; images in the second are magnification of images from the first row

5. IMPACT OF THE POLYURETHANE ON THE MECHANICAL PROPERTIES

5.1 Abstract

The small-strain linear viscoelastic properties and non-linear large-strain viscoelastic properties of urethane/acrylic adhesive films have been studied. The films were obtaine from the drying of hybrid latexes prepared by miniemulsion polymerization. After an optimization of the blank latex for application as Pressure Sensitive Adhesive (PSA), the impacts of two compositional parameters on the mechanical properties were studied: the polyurethane weight fraction and the degree of grafting of this polyurethane on the acrylic backbone. Rheological, tensile and probe-tack tests were used in parallel and some extraction and swelling experiments helped to establish relationship between the properties and the polymer architecture. We have shown that the polyurethane weight fraction is a coarse parameter modifying the small-strain elastic modulus and the insoluble fraction in the polymer. The degree of grafting is used to adjust the polyurethane chain length and thus the finite extensibility in the polymer network.

5.2 Introduction

Pressure-sensitive adhesives (PSA) are soft polymeric materials displaying an instantaneous adhesion on most surfaces upon application of a light pressure. Although the function appears relatively simple, the design of proper PSA is complex and relies heavily either on polymer chemistry (for acrylic and silicone polymers) or on formulation (for block copolymers and natural rubber) to design sparsely crosslinked polymer networks with optimized properties. An optimal balance between peel strength and shear holding power is in particular required. This balance means that the PSA must be able to dissipate energy during the peeling process (a property optimized for a highly viscous liquid) but be resistant to creep in shear (optimum for solids).

Environmental concerns stimulate the development of waterborne polymers (usually called latexes) and products obtained upon drying of these latexes. In the case of PSA for example, emulsion-based products represent an important part of the actual market (Jovanovic and Dubé 2004).

Acrylic PSA (Satas 1989; Jovanovic and Dubé 2004) are generally weakly crosslinked copolymers of a blend of monomers chosen to adjust the T_g which have insoluble (gel) and soluble (sol) fractions. A very broad molar mass dispersity combined with a highly dissipative sol fraction and a cohesive network formed by the gel is a good and relatively easy way to achieve a practical solution, but has limitations due to the impossibility to independently control sol and gel parameters during a simple synthesis. The control of the network structure of the gel becomes an essential aspect of advanced techniques to achieve a better balance of properties.

Although the emulsion polymerization process presents great advantages (low viscosity of the final latex, no limitation in molar mass, no further crosslinking step), a gap still remains between solution and emulsion-based acrylic PSA (Jovanovic and Dubé 2004). In emulsion-

based systems, the independent control of the network structure of the gel and of the gel fraction is difficult. Furthermore, the control of the interfaces between particles remaining after drying is not easy and can strongly affect the mechanical properties (Joanicot M., Wong K. *et al.*, 1996; Keddie, 1997).

To overcome these limitations, a possible design path is to incorporate another polymer (like alkyd, polyurethane…) in the network structure to form hybrid materials. The preparation of these hybrid materials could potentially bring a more favorable combination of properties compared to the initial waterborne acrylic PSA. Furthermore, the development of miniemulsion polymerization (Landfester, 2001; Asua, 2002) has helped to overcome the main issue of the homogeneous incorporation of a hydrophobic polymer in a waterborne acrylic polymer, what strongly increased the development of such bicomponent networks.

In the miniemulsion process, polymerization occurs inside each small droplet. As a consequence, homogeneous incorporation of a second phase in each particle, before radical polymerization, is easier than with standard conventional emulsion. A large range of components have been incorporated successfully and several reviews can be found, presenting the technique and the possibilities of hybridization (Landfester, 2001; Asua, 2002; El-Aasser and Sudol, 2002; Schork, Luo *et al.*, 2005).

Many studies have been carried out on the hybridization of acrylic with polyurethane (PU). Successful incorporations have been reported by the formation of interpenetrating networks (IPN) (Hegedus and Kloiber 1996), by the formation of a core-shell structure (Hirose, Kadowaki et al. 1997) or by standard emulsion with a polyurethane dispersion as a seed (Kukanja, Golob *et al.* 2000). In all cases, the physical properties of the hybrid were better than those of the physical blends. Miniemulsion polymerization appeared as a powerful method to graft polyurethane to an acrylic polymer as exposed in the work of Wang *et al.* (Wang, Chu *et al.* 2003; Wang, Chu, Graillat, Guyot and Gauthier 2005; Wang, Chu, Graillat, Guyot, Gauthier *et al.* 2005; Wang, Chu and Guyot 2006; Wang, Chu, Guyot *et al.* 2006; Wang, Chu *et al.* 2009) or Li, El-Aasser and coworkers (Li, Daniel et al. 2005). This work showed that the grafting allows avoiding phase separation at the particle scale between polyrethane and acrylic copolymer.

Despite the important number of studies on urethane/acrylic hybrids, most of systems focused on applications as coatings whereas advantages of combining acrylic with urethane for PSA applications are potentially numerous: better film-formation, better mechanical stability or temperature resistance (Hirose, Zhou *et al.* 2000; Li, Daniel *et al.* 2005; Sebenik and Krajnc 2005).

In this study and in its companion paper (Udagama, Graillat *et al.*), we selected a model acrylic copolymer typical of what is used for PSA, and investigated the incorporation of a low molar mass reactive PU in the particle. Part I (Udagama, Graillat *et al.*) focuses on the synthesis methods while part II focuses on the effect of changing synthesis parameters on the network structure, characterized by mechanical tests on dry films and by swelling experiments. Since the final application of such soft networks is adhesives we also present whenever relevant, results obtained from adhesion tests.

5.3 Materials

5.3.1 General synthesis strategy

All samples have been synthesized by miniemulsion polymerization with a batch process. The details of the polymerisation procedure are described in a companion paper (Udagama, Graillat et al. ; Udagama 2009) and we only briefly recall here the main synthesis parameters which are necessary to understand the results. The samples were based on a soft viscoelastic matrix. The main monomer was n-butylacrylate, which, as a homopolymer has a T_g of -43 °C (Brandrup and Immergut 1999) so that final samples are in the range of very soft viscoelastic materials (Mallegol, Dupont et al. 2001).
The basic acrylic monomer composition of the matrix in weight percent (wt%) is as follow:

- *Butylacrylate (BA): 89.5*
- *Methyl methacrylate (MMA): 9.5*
- *Acrylic acid (AA): 1*

Incorez 701, a NCO terminated polyurethane (PU) prepolymer provided by Industrial Copolymers Limited, was incorporated in the acrylic polymer particles. This incorporation was performed in three steps:

1) The PU prepolymer chains were dissolved in the organic monomer phase, which also contained the hydrophobe costabilizer (octadecyl acrylate ODA) and hydroxyl ethyl methacrylate (HEMA). The reaction of free isocyanate groups (NCO) of the PU with the hydroxyl moiety (OH) of the HEMA results in the grafting of the PU chains to the HEMA by polyaddition following the reaction described in Figure 5-1.

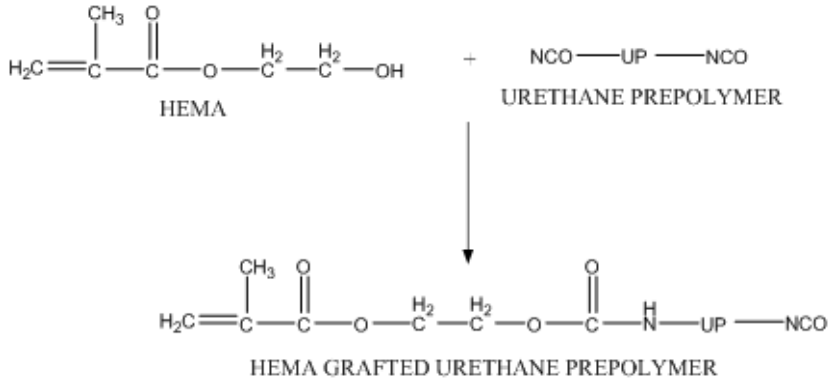

Figure 5-1: Polycondensation reaction between the end-functionalized urethane prepolymer and the hydroxyl function of the HEMA (Udagama R. 2009)

2) Bisphenol A (BPA) was added to the organic phase containing PU (including the PU that reacted with the HEMA). The Bisphenol A has a double hydroxyl moiety and can react with the remaining free NCO functions. After step 1, a large number of free NCO functions remain in the solution and BPA played the role of chain extender of the PU prepolymer.

3) The organic phase containing the monomers and the HEMA-functionalized BPA-extended PU chains were added to the aqueous solution containing surfactant (Dowfax 2AI). Nanodroplets

were formed by ultrasonication. The radical polymerization started with the addition of a redox initiator pair (Tertiary Butyl HydroPeroxide, TBHP, and Sodium Formaldehyde Sulfoxylate, SFS). Miniemulsion polymerization was carried out in batch.

5.3.2 Material parameters

To analyse the impact of the polyurethane on the hybrid systems, two parameters were varied:

- *the weight fraction of polyurethane relative to the total monomer content*
- *the molar ratio between OH groups from HEMA (grafting) and OH groups from BPA (chain extension).*

Different weight fractions of reactive PU prepolymer were incorporated in the acrylic organic phase before polymerization (step 1). The polyurethane weight ratio was calculated relative to the total monomer content to be between 5 wt% and 50 wt%.
The weight fraction of HEMA was varied to correspond to a given degree of grafting of the PU prepolymer. Between 5 % and 20 % of the NCO functions of the PU were reacted with HEMA. The extent of reaction of HEMA with the polyurethane prepolymer has been measured by inverse titration showing that a maximum of 20% of the NCO functions can react with HEMA (Udagama R. 2009). BPA was added to neutralize the remaining NCO moieties and it was possible to calculate the molar ratio of OH functions coming from HEMA over OH functions coming from BPA, the so-called HEMA/BPA ratio.
A limitation of the reaction between BPA and the free remaining NCO functions has been observed too. For these syntheses, Octadecylacrylate (ODA) was chosen as a hydrophobic component and was added to the particles to avoid Ostwald ripening (Landfester 2001). In presence of this hydrophobic costabilizer, flocculation of the particles was observed before the complete addition of the stoechiometric amount of Bisphenol A during the polymerization. The reason of this flocculation was related to the hydrophobic behavior of the particles when ODA was present in the particle core and was detailed by Udagama (Udagama, Graillat et al. ; Udagama R. 2009). Hence, only half of the calculated stoechiometric quantity of BPA could be added to the system to avoid flocculation.
The first three series of latexes have a ratio OH/NCO = 0.55. In the fourth series, ODA has been successfully taken out of the polymerization (without flocculation) and the stoechiometric amount of BPA could be added, so that OH/NCO = 1. Table 5-1 summarizes the different samples that have been prepared.

We measured the glass transition temperature of the final polymer samples (T_g) by Differential Scanning Calorimetry (DSC). No influence of the PU has been detected and only one T_g is always detected. The average value is -39 °C±3 °C. The samples are in the range of the very soft polymers at room temperature. It is worth noting that the T_g of the pure PU is estimated to be around -48 °C. Therefore, the large distribution of the T_g of the copolymer and the closeness with T_g of the PU could mask out a possible phase separation. This has been discussed in the previous chapter on the morphology of these systems.
The solid content of the latexes was measured gravimetrically and was ~ 50 wt% of polymer for all latexes.

Table 5-1 : Description of the latexes analysed in this study

Sample	CTA[a]	% PU[b]	Grafting degree (%)	OH/NCO	HEMA/BPA[c]
I_0PU(0CTA)[d]	0	0			
I_0PU(0.2CTA)	0.2		/	/	/
I_0PU(0.5CTA)	0.5				
I_25PU(0.11)OH0.55	0.2	25	5	0.55	0.11
I_25PU(0.22)OH0.55			10		0.22
I_25PU(0.36)OH0.55			15		0.36
I_25PU(0.50)OH0.55			20		0.50
I_5PU(0.22)OH0.55	0.2	5	10		0.22
I_15PU(0.22)OH0.55		15			
I_35PU(0.22)OH0.55		35			
I_50PU(0.22)OH0.55		50			
I_25PU(0.10)OH1	0.3	25	10	1	0.10
I_25PU(0.25)OH1	0.2		20		0.25

a: % rel. to monomers
b: wt% rel. to monomers
c: molar ratio of the OH groups from HEMA over the OH group from BPA
d: No PU in these latexes; only the CTA fraction is indicated in the sample name

5.3.3 Network structure of the urethane/acrylic hybrids

Several molecular analyses have shown that (Udagama 2009):

- *All NCO groups have reacted with HEMA, BPA or water.*
- *The molar mass of the PU prepolymer is ~ 3000 g.mol^{-1}*
- *Only a maximum of 20% of NCO groups can react with HEMA*

Therefore, PU chains can be incorporated in three different ways:

- *BPA-extended chains which have reacted on both side with HEMA form bonded PU chains. After acrylic polymerization, this chain will be part of the gel fraction.*
- *BPA-extended chains which have reacted on only one side with HEMA are dangling chains. They are terminated either by a BPA or by an amine (obtained after reaction with water). These chains are connected to the acrylic backbone at only one side.*

- *BPA-extended chains which did not react with any HEMA are called free chains. They are part of the soluble fraction inside the particles.*

These three types of chains coexist in the particles and their proportions and lengths obviously change according to the fraction of PU, the ratio OH/NCO and the ratio HEMA/BPA.

To have an appropriate representation of the architecture of the hybrid network inside particles, one has to take in account two other important parameters:

- *The molar mass of the acrylic copolymers (300-4000 kg.mol^{-1}) is much higher than that of the PU, even extended.*
- *Assuming that the soft chain is mostly polyether(polypropylene glycol PPG) , the PU chains are probably much more entangled than the acrylic ones. Molar mass between entanglements (M_e) for this type of PU has been found to be around 5000 g.mol^{-1} (Florez, Munoz et al. 2006) when it is ~ 20 - 30000 g.mol^{-1} for the main monomer, butyl acrylate (Tong and Jerome, 2000; Moghbeli, Zamir et al., 2008).*

The final PU chains are thus much smaller and much more entangled compared to the acrylic network. Taking in account the different connections of the PU chains, a schematic representation of the network is presented in Figure 5-2 (except that no reaction of NCO with water is shown).

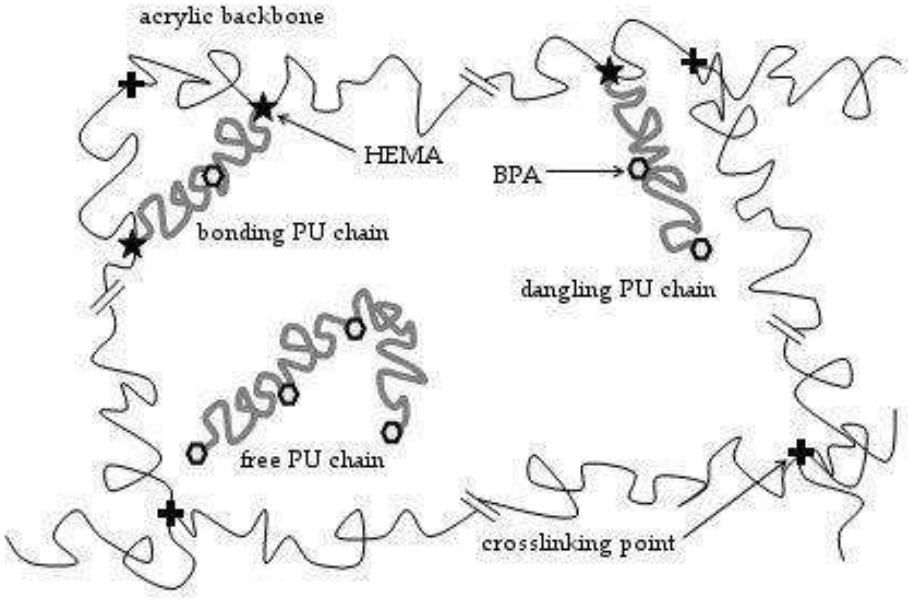

Figure 5-2: Theoretical urethane/acrylic hybrid network

5.4 Experimental techniques

5.4.1 Gel and swelling measurements

We measured the gel content and the swelling ratio Q by static measurements. A small piece of solid film was cut and weighed (W_1). Then, it was immersed in THF for a week. After a week, the sample completely swollen by the solvent was taken out and weighed again (W_2). It was then dried at 60 °C during 30 minutes to extract all the solvent and the dried part was weighed (W_3).

The gel content was given by: $$\%\text{gel} = \frac{W_3}{W_1} \times 100$$ **Eq. 5-1**

And the swelling ratio by: $$Q = \frac{W_2}{W_3}$$ **Eq. 5-2**

5.4.2 Adhesive properties

For all samples, we performed analysis of the adhesive properties with the probe-tack test. In this well-known experiment (Zosel 1989; Lakrout, Sergot et al. 1999), a stainless steel probe comes in contact with the adhesive layer dried on a glass slide. After a controlled contact (time and pressure), the probe is debonded at a controlled velocity. A mirror is installed upon the glass slide and allows the visualisation of the debonding mechanism and the measurement of the real contact area for each sample.

In this section, we used standard parameters for the approach velocity (V_{app}), contact time (t_c), contact force (F_c) and debonding velocities (V_{deb}). The tests were made at room temperature. The Table 5-2 gives the values of the different parameters.

Table 5-2 : Experimental parameters for the probe-tack tests

V_{app}	30 µm.s^{-1}
t_c	1 s
F_c	-70 N
V_{deb}	10-100 µm.s^{-1}

Force is measured by a load cell (250N, resolution 0.5N). The displacement of the probe is measured with an LVDT extensometer (range 5mm, resolution 0.5µm). After data analysis, nominal stress versus strain curves $\sigma_N = f(\varepsilon)$ are obtained. Three parameters from these curves are mainly used to compare materials (Lakrout, Sergot et al. 1999; Roos and Creton 2005):

- *σ_f: nominal stress (MPa) at the beginning of fibrillation. It is correlated to the density of crosslinks in the network.*
- *ε_{max}: strain for which adhesive completely detaches from the probe. Characterizing the maximum deformability or the distance between crosslink points.*

- W_{adh}: adhesion energy ($J.m^{-2}$), corresponding to the area under the curve multiplied by the initial thickness of the film, h_0.

Furthermore, the overall shape of the curve can be analyzed (Crosby, Shull et al. 2000; Creton, Hooker et al. 2001; Shull and Creton 2004). The absence of fibrillation plateau with a ε_{max} lower than 1 is characteristic of an interfacial debonding with crack propagation at the probe-adhesive interface. This debonding mode corresponds to a highly crosslinked sample. On the contrary, a plateau stabilized around 0.1 MPa with a drop in the stress at intermediate strain appears in the case of a cohesive debonding, where residues of the adhesive remain on the probe. Liquid-like samples with low degree of crosslinking behaves that way.

5.4.3 Linear viscoelastic properties

The linear viscoelastic properties of the adhesives were characterized by a rheometer RDAII with parallel plate geometry. Frequency sweeps ($5.10^{-2} < F < 20$ Hz) with a torsion deformation between 5% and 10% were made on free-standing samples with a thickness around 500 µm. Tests were performed at room temperature. The storage modulus G', the loss modulus G'' and the phase angle tanδ were reported in function of frequency for each test.

5.4.4 Large strain properties

We used a standard tensile INSTRON machine (model 5565) equipped with a videoextensometer (model SVE). The machine uses a 10 N load cell with a resolution of 0.5% from 1% to 100% of the full scale.
Rectangular strips were cut within self-standing films with a die-cutter. All of them are 5 mm wide (w_0) and the average thickness (e_0) is 500µm. These values were controlled before each test.
The initial velocity of the crosshead was chosen to obtain an initial strain rate of 0.1 s^{-1} and 1 s^{-1} which are equivalent to the ones of the probe-tack tests. To avoid slippage of the samples, jaws are closed with a dynamometric key with a controlled torque (from 15 $cN.m^{-1}$ to 25 $cN.m^{-1}$). All tests were performed at room temperature.

Data Analysis

The post-treatment of the data gives the nominal stress σ_N and the strain λ. The classical curve of the nominal stress σ_N versus strain λ can be analyzed. In particular, the Young modulus E_y is measured for the very small strains. It is defined as the slope of a line fitting the curve between λ=1 and λ=1.02. It has to be note that the strong decrease of the curve after its maximum corresponds to the fracture of the sample. Due to spurious effect such as slippage or striction in this very large strain domain, the end of the curve after its maximum was not taken into account.
Typical stress-strain curves for PSA show a softening at intermediate strains and hardening at large strains relative to a Gaussian rubber. The detailed shape of the stress-strain curve is very sensitive to even small changes in network architecture. They provide complementary information to the small strain Young's modulus E_y.
Softening and hardening relative to Gaussian rubber elasticity can be more easily viewed in the Mooney representation. The reduced strain σ_R, also named Mooney stress, is defined as:

$$\sigma_R = \frac{\sigma_N}{\left(\lambda - \frac{1}{\lambda^2}\right)} \qquad \text{Eq. 5-3}$$

It corresponds to the normalization of the reduced stress by the predicted behaviour of a standard (or Neo-Hookean) rubber. In the Mooney representation, this reduced stress is typically represented versus the inverse of strain 1/λ.Obviously, the curve has to be read from right to left. As explained for the nominal stress representation, the decrease of the curve in the very large strain domain was not considered because of the slippage or striction sometimes occuring at the end of the test.
From this representation, two characteristic parameters of the non-linear behaviour can be determined: the C_{soft} for the softening at intermediate strain and the C_{hard} at large strain. These parameters have been first defined by Deplace (Deplace, Carelli et al. 2009).
The C_{soft} characterizes the relaxation and orientation of the entanglements present in the materials. It is defined as the slope of a line drawn between ($\sigma_R(0.8)$; $1/\lambda = 0.8$) and (σ_{Rmin}; $1/\lambda_{min}$). The C_{soft} characterizes the non-permanent crosslinking in the network and the relaxation phase. After this softening phase, the minimum in reduced stress is characteristic of the beginning of the hardening, that is to say the moment where the finite extensibility of the network chains can be felt. C_{hard} is defined as the reduced stress corresponding to this minimum.
Figure 5-3 illustrates the determination of these two parameters which have the physical meaning of relaxing and non relaxing part of the initial modulus.

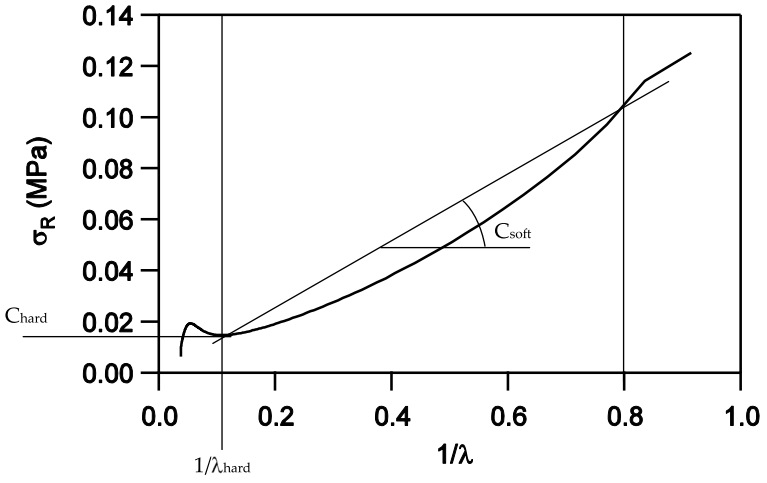

Figure 5-3: Determination of C_{soft}, C_{hard} and $1/\lambda_{hard}$

Two other values have to be taken in account to interpret large strain data:

- *The strain level corresponding to the minimum in reduced stress, called λ_{hard}. It is correlated to the finite extensibility of the chains and thus to the network architecture.*
- *The ratio C_{soft}/C_{hard} which characterizes the viscoelastic relaxation of the sample relative to its permanent crosslink structure and is the ratio.*

When polymer networks are very lightly crosslinked, chains flow instead of harden when finite extensibility is reached. No macroscopic hardening can be observed on the Mooney representation but

a decrease of the nominal stress is observed at failure. This point is used then to define the slope for the determination of C_{soft} but C_{hard} is then undefined.

Relaxation processes

Tensile experiments have been performed at two different nominal strain rates, $d\varepsilon/dt=0.1\ s^{-1}$ and $d\varepsilon/dt=1\ s^{-1}$ and we calculated the ratio $R(\lambda)$ between the stresses obtained for each λ at the two different nominal strain rates.The objective was to separate the two components of the softening at intermediate strain: the reversible strain-dependent non-linear elasticity and the time-dependent relaxation process.The representation of the ratio $R(\lambda)$ as a function of λ shows only the time-dependent relaxation. A constant ratio $R(\lambda)$ (see Figure 5-4(a)) indicates that the two processes are fully independent whereas any variation of this ratio with λ (see Figure 5-4(b)) reveals non-linear viscoelastic processes, i.e. the extent of relaxation depends on the strain. Moreover, the absolute value of $R(\lambda)$) is an indication of the level of viscoelasticiy in the sample.

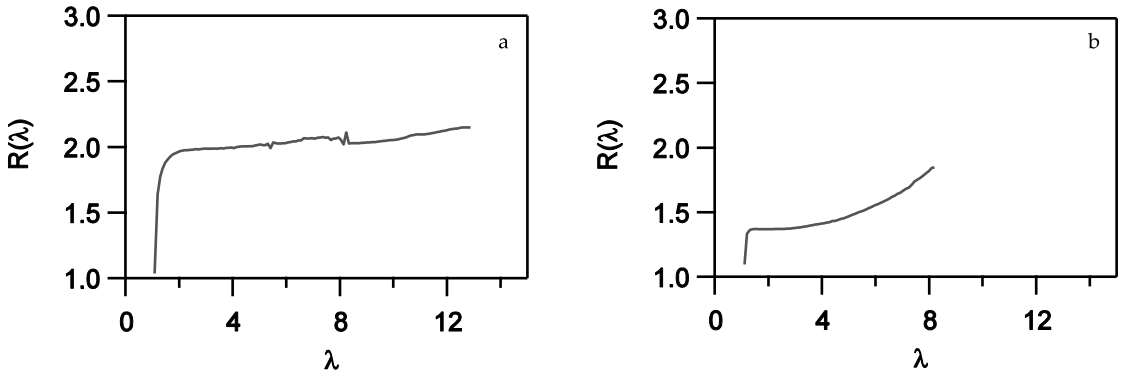

Figure 5-4: Example of the evolution of R(λ) with λ; (a): constant ratio R(λ) whatever λ due to independent softening processes; (b): R(λ) increases with λ because of non-linear viscoelastic processes

5.5 Results and discussion

5.5.1 Optimization of the blank latex

When crosslinked or of high molar mass, the polyurethane added is generally stiffer than the acrylic matrix due to its more densely entangled structure. It is then necessary to choose carefully the base acrylic matrix in order to maintain a reasonably low modulus and a certain level of adhesion, after addition of the PU chains. A very soft matrix, with a low fibrillation stress σ_f and a high deformation ε_{max} is required. Keeping the monomer composition constant (see 5.3), Chain Transfer Agent (CTA) was added during polymerization. The CTA is well known to help reducing the number of crosslinking points and hence decreasing the elastic modulus while increasing the dissipation.
Several amounts of CTA have been tested to optimize the matrix. Adhesive properties of the three different films are presented below. The Figure 5-5(a) shows the result of the probe-tack test at a debonding velocity V_{deb} = 10 µm.s^{-1} (i.e. nominal strain rate dε/dt = 0.1 s^{-1}) for three adhesive films with different CTA fractions: 0%, 0.2% and 0.5%. They correspond to the samples I_0PU(0CTA), I_0PU(0.2CTA) and I_0PU(0.5CTA). On Figure 5-5(b), the adhesion energy measured from the tack curve at dε/dt = 0.1 s^{-1} is represented for each CTA fraction.

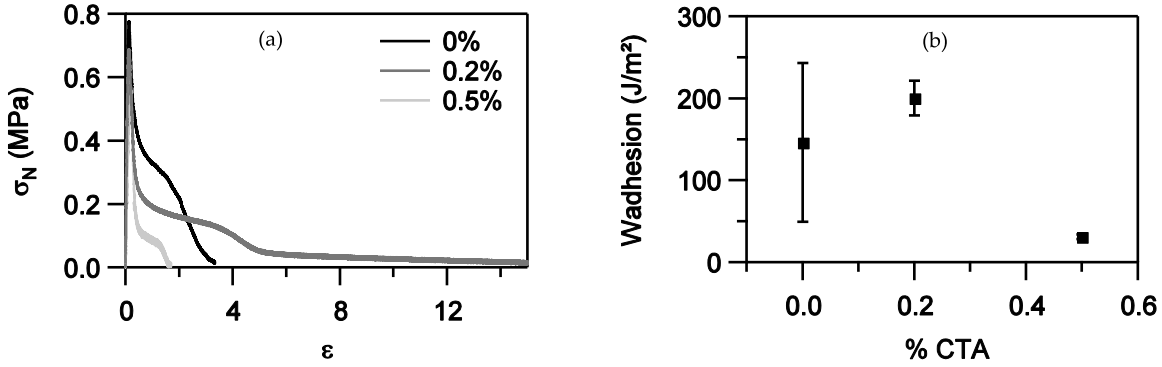

Figure 5-5: (a) Tack curves for the matrices with different amounts of Chain Transfer Agent for Vdeb=100µm/s; (b) Evolution of the adhesion energy with the amount of CTA

On Figure 5-5 (a), a plateau, even very short, appears in all cases indicating the beginning of fibrillation. When increasing the amount of CTA, the stress corresponding to the beginning of this plateau σ_f decreases, due to a lower level of elasticity.
The film with 0.2 % of CTA has a maximum deformation ε_{max} much higher, also indicating a high dissipation in the material. However, for this sample one can observe on the tack curve a relatively sharp decrease in stress at intermediate strain (ε~5). This feature in the stress-strain curve characterizes air penetration in the bubbles formed at the interface (Poivet, Nallet et al. 2004). Then, stress decreases continuously back to zero. A cohesive failure of the fibrils is observed and some adhesive remains on the probe. This is a liquid-like debonding due to a low level of crosslinking (Shull and Creton 2004).

For the sample containing 0.5 % of CTA, the air penetration is observed with the in-situ visualisation and the residus on the probe also indicates the liquid-like debonding mode. However, the decrease in the plateau stress cannot be detected because the debonding occurs at a very low deformation and very low stress: this sample is even more liquid-like.
This type of debonding observed when CTA is added characterizes low densely polymer networks. This is consistent with the effect of CTA which reduces the kinetic chain length and thus the chain transfer reactions, limiting the branching and crosslinking in the network.
On the other side, when no CTA is added, one can observe a very small deformation of the layer at failure. In-situ visualisation shows that debonding occurs by propagation of cracks at the probe-adhesive interface (Creton, Hooker *et al.* 2001; Shull and Creton 2004). This is the typical debonding mode of highly crosslinked materials, with high elastic modulus. The adhesion energy shows an important dispersion and this is explained by consequent differences in the relative value of the maximum deformation. Nevertheless, the level of adhesion is acceptable for a standard PSA, because of the debonding by propagation of cracks. The blank latex, with neither PU nor CTA is then highly crosslinked, probably due to the presence of a high amount of butyl acrylate (89.5 wt%) which favors the chain transfer reaction during radical polymerisation. Because of this high crosslinking level, the blank without CTA cannot be used as matrix for the incorporation of PU, for the reason explained before.
Finally, the value of 0.2 % of CTA has been used during polymerization of hybrid samples. Although cohesive debonding occurs for this amount, the adhesion energy is maximized, as confirmed by Figure 5-5(b). One can expect that addition of polyurethane will introduce some visible changes in adhesion energy and debonding mode.

5.5.2 Impact of the PU weight fraction

5.5.2.a Modification of the mechanical properties

The behavior of samples with PU weight fractions from 5 wt% to 50 wt% has been investigated. The acrylic monomer composition was kept constant (see section 5.3.1) and 0.2 % of CTA was added during the polymerization. In all cases, 10 % of the NCO functions were grafted to the acrylic backbone with hydroxyl ethyl methacrylate (HEMA). Octadecylacrylate (ODA) was used as costabilizer, which implies that only half of the stoechiometric amount of BPA was added during polymerization, so that OH/NCO=0.55. There was an excess of NCO which could eventually react with water. The ratio between OH functions coming from HEMA and OH functions coming from BPA was 0.22. These values were kept constant for all samples.

Linear small-strain viscoelastic properties

Characterization of the linear viscoelastic properties have been undertaken for three different samples with different PU weight fractions (samples I_5PU(0.22)OH0.55, I_25PU(0.22)OH0.55 and I_50PU(0.22)OH0.55). Figure 5-6 represents the evolutions of the storage modulus and tanδ with frequency, for an deformation ε~8%. As can be seen on Figure 5-6 (a), the more polyurethane is added to the hybrid, the higher is the elastic modulus and the more elastic is the material. It is clear that the dissipation becomes much lower and frequency independent in the presence of high fractions of polyurethane.

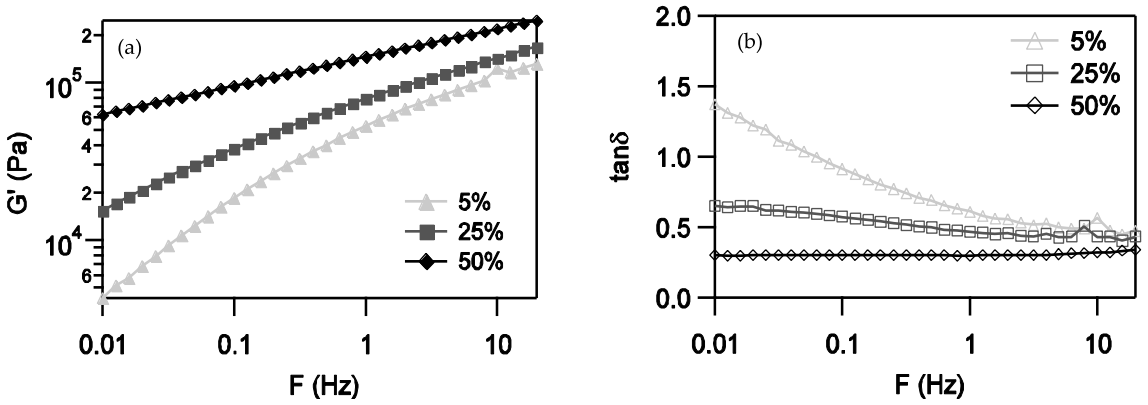

Figure 5-6: Evolution of G' (a) and tanδ (b) as a function of frequency for different PU weight fractions: 5 wt% (I_5PU(0.22)OH0.55), 25 wt% (I_25PU(0.22)OH0.55) and 50 wt% (I_50PU(0.22)OH0.55)

The linear viscoelastic properties can be used to predict the suitability of the soft network for PSA applications. The value of the storage modulus at 1 Hz is interesting: the Dalhquist criterion for a PSA says that G'(1 Hz) should be below 1-200 kPa to allow an easy contact with a rough surface (Dahlquist 1969). The value of tan δ/G' at the relevant debonding

frequency is also used to predict whether fibrillation will occur or not upon debonding (Carelli C., Déplace F. et al. 2007; Nase, Lindner et al. 2008; Deplace, Carelli et al. 2009).
For the sample with 50% of PU, the value of G' is $1.45.10^5$ Pa, i.e. in the upper limit for the Dahlquist criterion. At the tack test frequencies (0.1 Hz and 1 Hz), the values of tanδ/G' are respectively $0.31.10^{-5}$ Pa^{-1} and $0.21.10^{-5}$ Pa^{-1}. On stainless steel, tanδ/G' ~ $0.5.10^{-5}$ is a lower limit for the fibrillation debonding mode to occur (Deplace 2008; Deplace, Carelli et al. 2009). The fact that tanδ/G' is too low indicates a lack of dissipation coupled to a high value of the elastic modulus. An interfacial debonding with crack propagation at the probe interface can be expected.
In the opposite case, for 5% of PU, the storage modulus is low enough ($0.53.10^5$ Pa) but dissipation is very important ((tanδ ~ 0.9 at 0.1 Hz and ~ 0.6 at 1 Hz) and the debonding criteria is very thus very high (tanδ/G' ~$4.93.10^{-5}$ Pa^{-1} at 0.1 Hz and $1.15.10^{-5}$ Pa^{-1} at 1 Hz). Dissipation dominates and we are in presence of a viscoelastic liquid. A cohesive failure of the adhesive layer may be observed, with some residus retained on the probe surface.

Non-linear large-strain properties

Rheology experiments can help to roughly predict the debonding mode of an adhesive layer, but large strain properties are required to finely characterize the fibril formation and the detachment of these fibrils, by the analysis of the strain softening and hardening (Deplace, Carelli et al. 2009). Figure 5-7 and Figure 5-8 show the results of tensile experiments for the 5 samples with different amounts of PU (see Table 5-1) in standard and Mooney representations. For each representation, a magnification in the domain of the lower stresses is given after the global curve.

Very significant differences due to the presence of PU are immediately apparent. On the nominal stress *vs* strain curve, the softening stress σ_S increases, the softening is less pronounced and a more pronounced hardening occurs at a lower srtain while increasing the PU weight fraction (at equal grafting proportion). The observations from the $\sigma_N=f(\lambda)$ can be seen on the Mooney representation also: the slope of the reduced stress in the intermediate strain increases and the minimum of the curve moves to the higer stress and $1/\lambda$ (i.e. lower λ). It is also important to note that the two samples with the lowest PU weight fractions (I_5PU(0.22)OH0.55 and I_15PU(0.22)OH0.55) do not present hardening. No brutal increase of the stress is observed on the nominal stress curve, and no minimum can be detected from the Mooney representation. This characterizes samples with an important dissipative component and a low level of elasticity.

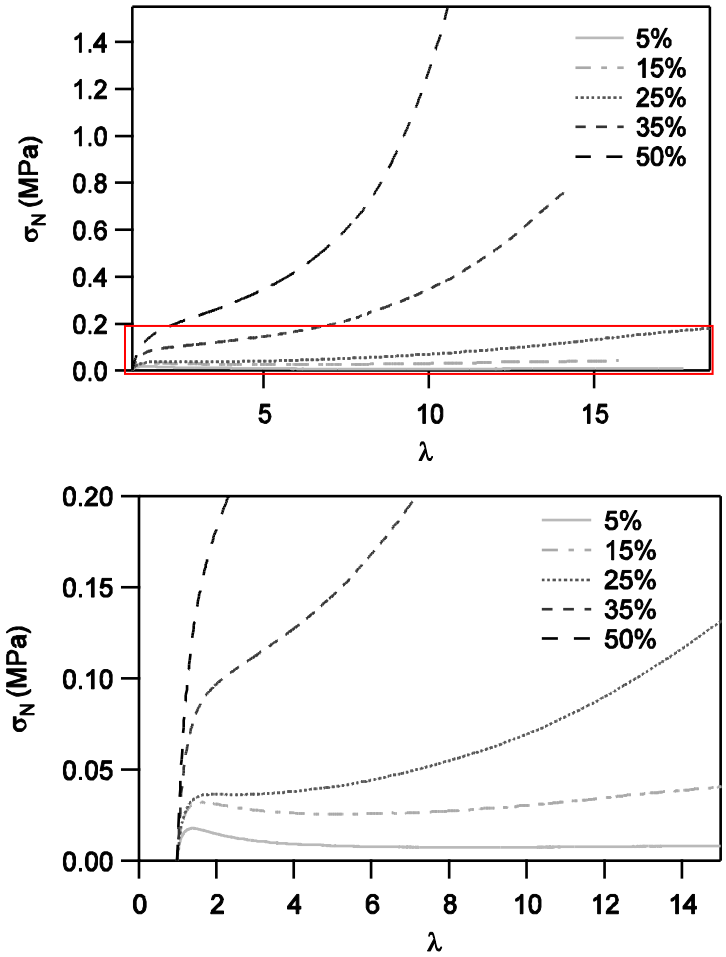

Figure 5-7: Nominal stress versus lambda for the 5 different PU weight fractions; $d\varepsilon/dt=0.1s^{-1}$; the bottom figure is a magnification of the red square

The combination of these observations indicates as a first hypothesis that, starting from very low crosslinked sample, the relaxation in the sample decreases and network becomes more tightly crosslinked when the PU weight fraction increases. The PU chains are 10 to 100 times shorter than the acrylic copolymers (M_w(PU) ~ 3 kg.mol^{-1} wherase M_w(acrylic) 300 - 4000 kg.mol^{-1}) and are mostly attached at both ends to the acrylic network. This implies that the PU chains reach their finite extensiblity before the acrylic ones. When more PU is added, more small chains are present in the polymer network. Thus, the probability to fully extend a short PU chain before a long acrylic chain increases with the PU fraction and hardening occurs for lower strains. Furthermore, PU chains are also more densely entangled than the acrylic ones due to the PPG constituing the soft segment (M_e ~ 3 – 5 kg.mol^{-1} for the PU while M_e ~ 20 – 30 kg.mol^{-1} for the acrylics (Tong and Jerome 2000)) That affects the stress level at which the chains can be deformed. This is consistent with the increase of the softening stress with the PU fraction.

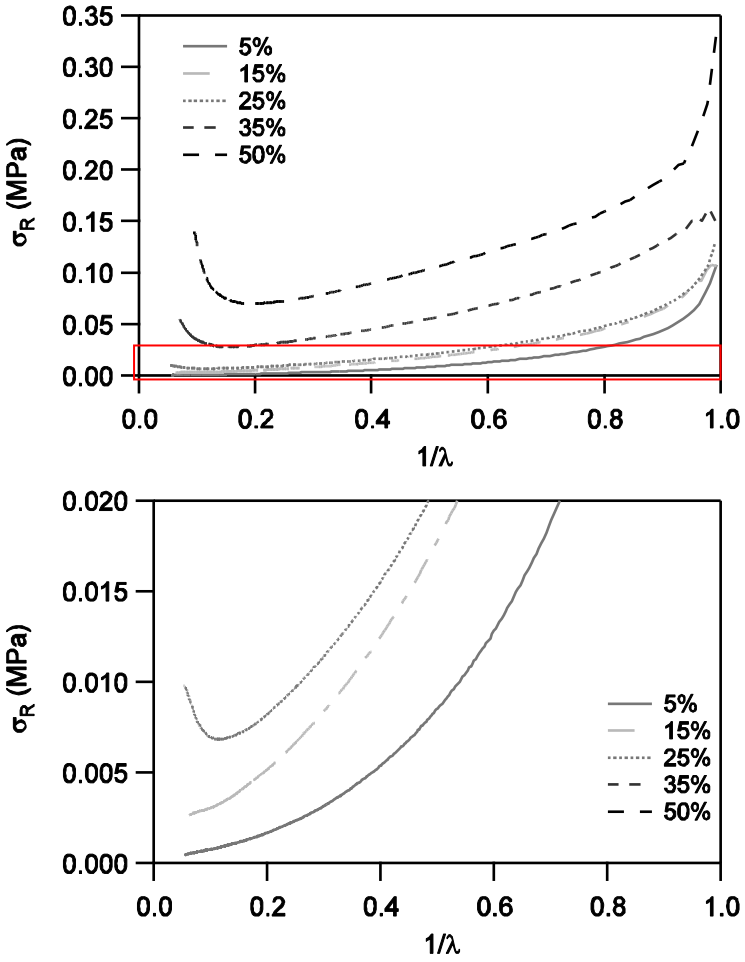

Figure 5-8: Reduced stress versus 1/λ for the 5 different PU weight fractions; $d\varepsilon/dt=0.1s^{-1}$; the bottom figure is a magnification of the red square

To quantify the softening and hardening stages, the viscoelastic parameters C_{soft} and C_{hard} obtained from the Mooney representation are shown in Table 5-3. The Young's modulus was also calculated, based on the nominal stress *vs* strain curve. The slope of the line fitting the curve between λ=1 and λ=1.02 is considered as a good evaluation of the linear elastic modulus. Evolutions of the ratio C_{soft}/C_{hard} and of the Young modulus with the PU fraction are represented inFigure5-9.

Table 5-3: Values of the Mooney-Rivlin viscoelastic parameters for different PU amounts; $d\varepsilon/dt=0.1s^{-1}$

Sample	% PU	C_{soft} (kPa)	C_{hard} (kPa)	C_{soft}/C_{hard}	E_y (kPa)
I_5PU(0.22)OH0.55	5%	36.8	ND	∞	261.2 ± 26.5
I_15PU(0.22)OH0.55	15%	57.9	ND	∞	317.5 ± 0.12
I_25PU(0.22)OH0.55	25%	59.2	6.8	8.7	320.4 ± 34.8
I_35PU(0.22)OH0.55	35%	113.9	27.9	4.1	479.8 ± 16.9
I_50PU(0.22)OH0.55	50%	146.4	69.9	2.1	757.3 ± 75.8

As the samples with a low PU fraction (5 wt% and 15 wt%) do not harden at large strain, C_{hard}, and by definition C_{soft}/C_{hard}, are not defined for these materials. However, one can comment on the evolution of C_{soft} and E_y. Both quantities increase with the PU content due to an overall increase in the modulus of the materials with increasing PU content. However the ratio C_{soft}/C_{hard} decreases significantly, reflecting the less and less viscoelastic character of the films (see Figure5-9).

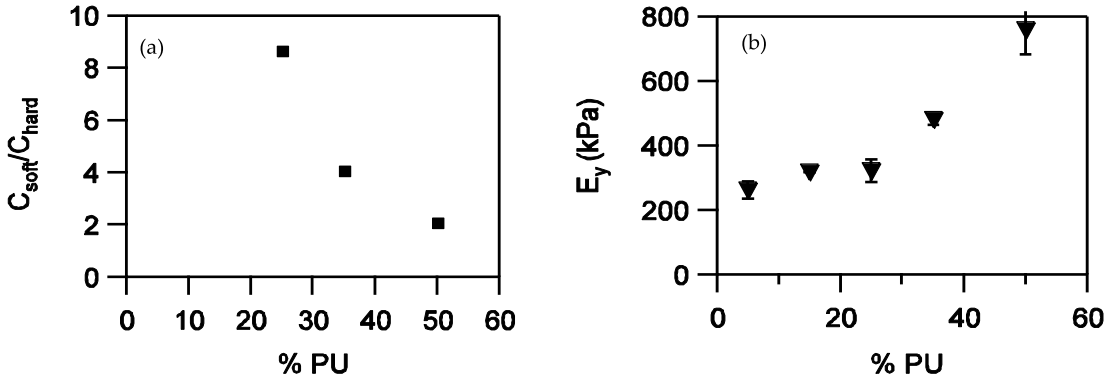

Figure5-9: Evolution of the ratio C_{sotf}/C_{hard} (a) and of the Young modulus E_y (b) measured at $d\varepsilon/dt = 0.1\ s^{-1}$ with the PU weight fraction

The strong increase of $C_{soft} + C_{hard}$ is in good agreement with the increase of E_y. The Young modulus is a small-strain high frequency modulus. It is affected by the crosslink points and by the entanglements (that are all trapped at high frequencies). Its increase indicates that the network has more crosslink points and also more entanglements. The increase of C_{hard} only reflects the increase in crosslink points. The low density of crosslinking points, on the other hand, is responsible of the lack of hardening for 5 wt% and 15 wt% of PU.
Hence, the analysis of the Mooney parameters confirms the hypothesis of low crosslinking when a small PU fraction is added, and of the increase of the crosslinking density with the PU weight fraction.

Even if the fracture mode can be different from a sample to another, one can comment on the average maximum strain obtained when performing tensile experiment at two different initial strain rates. These values are reported in Table 5-4 for three different PU weight fractions.

Table 5-4: Values of strain at failure for different PU weight fractions

PU weight fraction (wt%)	Strain at failure λ_{max} (with initial $d\varepsilon/dt = 0.1\ s^{-1}$)	Strain at failure λ_{max} (with initial $d\varepsilon/dt = 1\ s^{-1}$)
5	17.7	25.1
25	18.5	25.9
50	10.6	8.2

It clearly appears that the deformability is strongly influenced by the highest PU weight fraction (50 wt%). This can be explained by the increase of the crosslinking in the sample but also has to be connected to the results on particle morphology from chapter 4.
In this chapter, it has been observed that for the highest PU weight fraction, the PU appears to form a shell around the particle. The consequence of this specific morphlogy could be a lower interpenetration of the chains during the drying process, resulting in weak particle-particle interfaces. Indeed, the PU chains are more entangled than the acrylic ones. Thus, interpenetration between particles surrounded by PU is less easy than if the borders are made of acrylics. Moreover, the PU prepolymer chains are short (M_w(PU) ~ 3 kg.mol^{-1}) and remains of a lower size than the acrylics even after extension with BPA. For example, with a grafting degree of 11%, the theoretical PU molar mass should be ~ 30 kg.mol^{-1}. It has to be compared to the molar masses of the acrylic chains, which is between 300 and 4000 kg.mol^{-1} depending on the sample. Small PU chains interpenetrate on a short range. Less interpenetration on a shorter range results in weaker interfaces between particles compared to homogeneous particles (e.g. as it is the case for 5 wt%). Due to the immiscibility between PU and acrylics there is no reason for acrylic chains to diffuse across the PU shell and interpenetrate on large range. The interfaces are made of PU only and they are weaker. It results that they break at lower strains compared to more homogeneous interfaces obtained with less PU wt%.

Strain rate dependence: Analysis of the relaxation

The Figure 5-10 shows a comparison of tensile experiments performed at two different nominal strain rates, $d\varepsilon/dt = 0.1\ s^{-1}$ and $d\varepsilon/dt = 1\ s^{-1}$. For each λ, the ratio $R(\lambda)$ between the value of the stress at $1s^{-1}$ and the value at $0.1s^{-1}$ has been calculated. This ratio is represented in function of λ for different PU weight fractions.

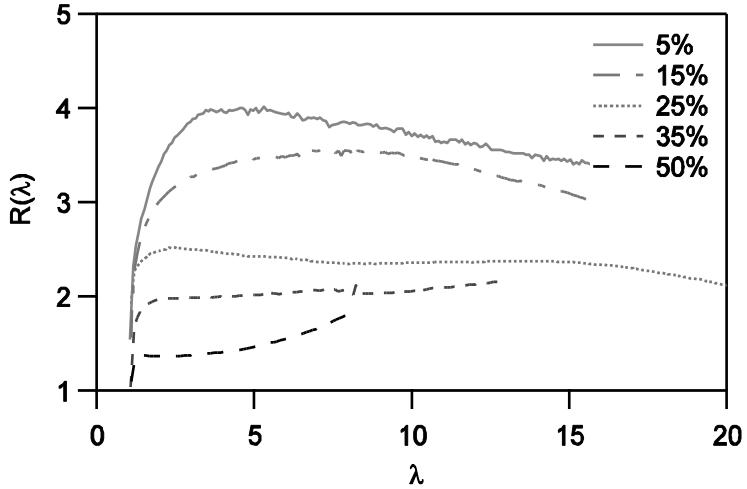

Figure 5-10: Evolution of the ratio $R(\lambda)$ with the deformation λ for the five PU weight fractions

For almost all the PU fractions, this ratio is quite constant with λ implying that the strain and the strain rate dependent components of the relaxation are not strongly coupled.

The value of the stress ratio clearly decreases to get closer to 1 when the PU fraction increases. The effect of strain rate on the relaxation decreases when the PU weight fraction increases and viscoelasticity tends to disappear. The ratio even slightly increases with λ when PU = 50 wt%. The effect of strain rate at high λ becomes more important for this high PU content, indicating weaker interfaces between particles. Samples less and less strain rate dependent with λ are in good agreement with increasing elastic character with increasing λ. It is also consistent with the observed particle morphology from chapter 4 and the comments on the interfaces between particles made right before.

As a conclusion, two families of adhesives can be distinguished depending on the amount of polyurethane. When the PU fraction is low (5% and 15%), samples present an important relaxation at intermediate strain and no hardening. This relaxation is mostly due to viscoelasticity. This important level of dissipation is an advantage for the adhesive properties because samples can then deform a lot during debonding. However, the lack of hardening during the tensile test will result in a cohesive failure of the fibrils (characteristic of a liquid-like debonding) which is not desirable for PSA's (Creton 2003).
On the other end of the spectrum appear samples with an important hardening and low level of relaxation. A strongly and tightly crosslinked network is expected. That would favor the adhesive failure of the PSA layer and enhance the resistance to shear. Nevertheless, the low relaxation and the decreased viscoelasticity are critical for the formation of fibrils during debonding and the increase of the adhesion energy.
Only one fraction of polyurethane (25 wt%) presents an optimum balance between relaxation and hardening. This sample should debond adhesively in a fibrillation mode, with important adhesion energy.

Adhesive properties

The probe-tack measurements have been performed on the five samples with different PU weight fractions and results are presented in Figure 5-11 for a debonding velocity V_{deb} = 10 $\mu m.s^{-1}$, which corresponds to nominal strain rate $d\varepsilon/dt = 0.1\ s^{-1}$.
Results obtained with the probe-tack tests are consistent with the small and large strain analysis of properties. Indeed, samples with a low amount of polyurethane (less than 25%) are characterized by a low fibrillation stress (σ_f) and a high maximum strain $\varepsilon_{max.}$ [a]. At intermediate strain (ε ~2 for 5 wt% of PU and ε ~4 for 15 wt%), the drop of the stress is characteristic of air penetration in the vacuum cavities as described previously (5.5). The residus remaining on the probe after the debonding also indicates a cohesive debonding inside the fibrils. These tack curves are characteristic of samples with a low level of elasticity, due to a low level of crosslinking.

[a] : For 15% of PU, the stress does not go back to zero for technical reasons. The maximum scale of the extensometer measuring the probe displacement is 5 mm. For the 15% sample, when the probe reaches 5 mm, fibrils joining the probe and the adhesive layer remain. These fibrils neither fail for a high deformation nor after waiting a long time. They break adhesively when the test is stopped and the probe is removed manually.

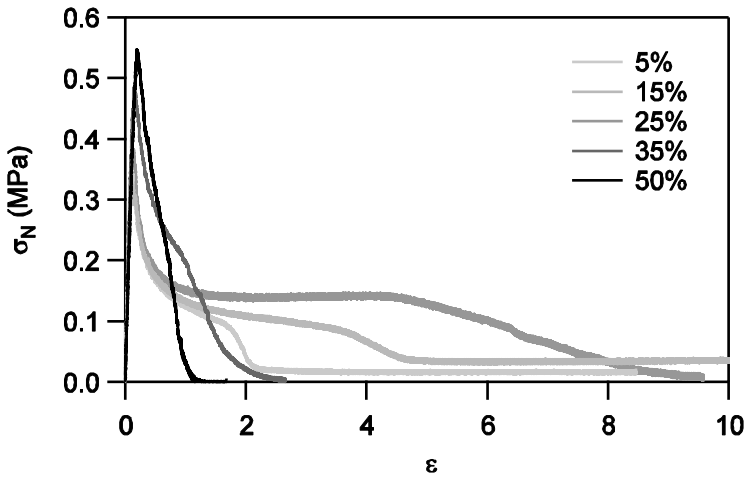

Figure 5-11: Stress-strain tack curves for the 5 PU weight fractions; V_{deb}=10µm.s^{-1} (i.e. dε/dt=0.1 s^{-1})

On the contrary, for samples with 35 wt% or 50 wt% of PU, the tack curves present almost no fibrillation plateau and the ε_{max} is low. Despite nucleation of cavities at the beginning of debonding, these cavities coalesce and interfacial propagation of cracks leads to an adhesive debonding. As can be seen on Figure 5-12, the adhesion energy is strongly decrease by this lack of long fibrillation plateau.

Finally, the sample with 25% of PU forms a fibrillar structure upon debonding, with a long plateau and a high maximum strain ε_{max}.. The final drop of the stress characterizes an adhesive debonding, resulting in the absence of residus on the probe. The adhesion energy is maximized for this percentage (Figure 5-12) which is the best equilibrium between maximum deformability and still clean detachment from the substrate. Adhesive properties are optimized for this fraction of PU.

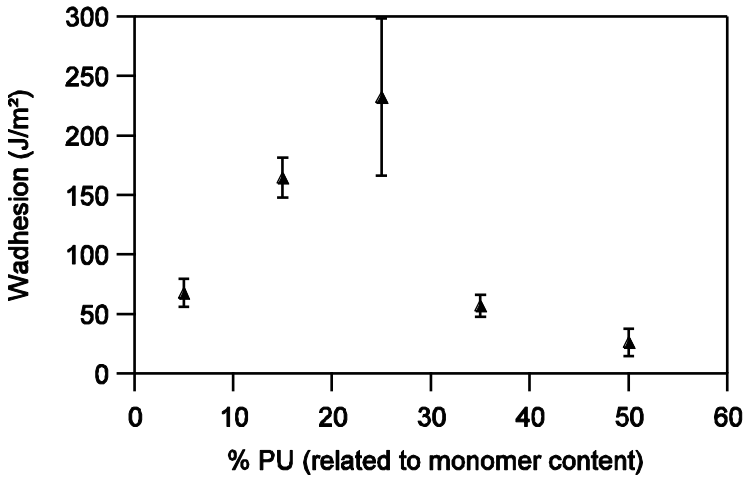

Figure 5-12: Evolution of the adhesion energy with the 5 PU weight fractions; V_{deb}=10µm.s^{-1} (i.e. dε/dt = 0.1 s^{-1})

In summary the increase in polyurethane content at a fixed degree of graftiong leads to a more elastic and less dissipative adhesive layer. On the molecular level, this means that the

polymer network in each particle is more crosslinked. The nature of this crosslinking (physical entanglements and covalent bonds) can be partially determined with swelling experiments.

5.5.2.b Influence of the polyurethane on the polymer network architecture

We have seen that the PU fraction affects both elastic and dissipation moduli, and that adhesive properties are directly affected by these changes. However, it is interesting to correlate these modifications of macroscopic properties with a molecular analysis of the polymer network. To do so, measurements of the gel content and of the swelling capability of the gel fraction have been performed. It is worth noting that the gel content for 5 wt% is so low that it cannot be measured by static extraction because there is not enough precision in the measurement.

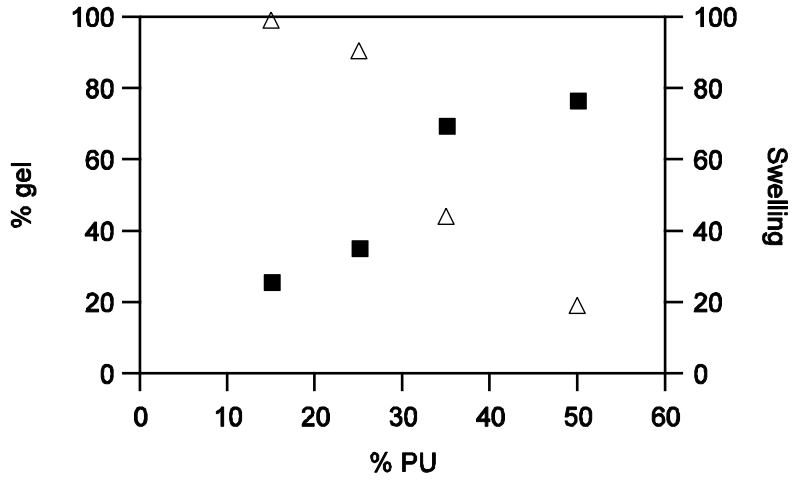

Figure 5-13: Evolution of the gel content (■) and of the swelling ratio (△) with the polyurethane content

According to Figure 5-13, the fraction of polyurethane affects both the gel content (i.e. the fraction of crosslinked chains) and the degree of swelling, (i.e. the size of the average mesh in the crosslinked polymer network). If we consider that this mesh size depends on the length of the shortest chain, the swelling results are consistent with the mechanical results. The PU chains are the smallest compared to the acrylic ones and define the mesh size. More over, increasing the PU fraction for a constant degree of grafting enhances the number of crosslinking points. Hence, the higher the fraction of PU chain, the higher the gel fraction is, the smaller the mesh is and the less the network can swell. Smaller meshes imply that the chains (and mostly PU chains) relax on shorter lengths. Dissipation does decrease for the same reason that the elastic modulus increases.

The decrease of the mesh size of the network in each particle is compared in Figure 5-14 with the hardening strain λ_{hard} obtained from tensile experiments of the films. One can see that, when the swelling decreases, so does the λ_{hard}. The small chains defining the finite extensibility also define the mesh size.

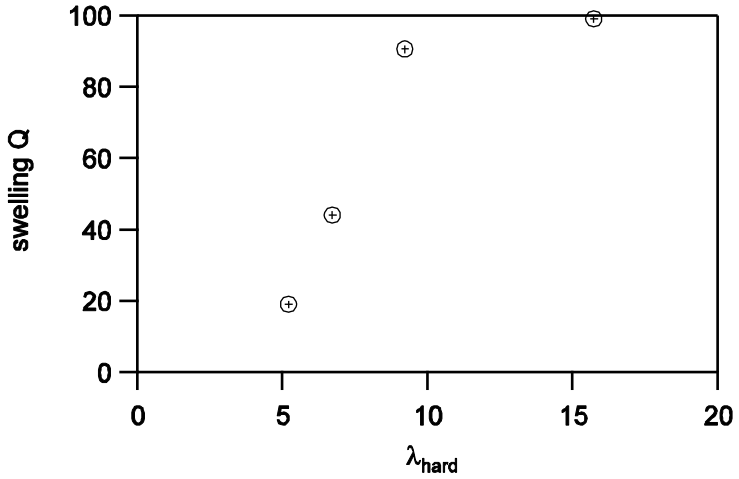

Figure 5-14: Evolution of the swelling with the hardening strain λ_{hard}

5.5.2.c Comparison with the matrix and with industrial adhesives

The effect of polyurethane on mechanical properties was characterized by the combination of rheology, tensile and probe-tack, experiments. However, to confirm that hybridization of polyurethane with acrylic copolymer can have a positive effect, a comparison with the pure matrix containing no PU (I_0PU(0.2CTA)) is presented in Figure 5-15.

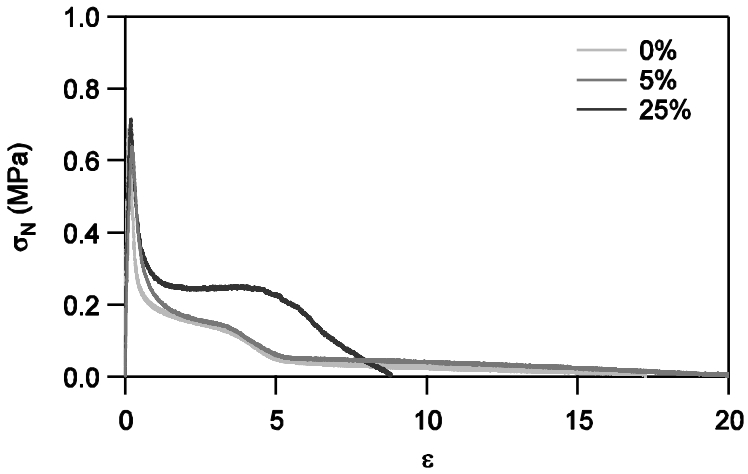

Figure 5-15: Tack results for the pure matrix (I_0PU(0.2CTA) and the samples containing 5 wt% of PU (I_5PU(0.22)OH0.55) and 25 wt% of PU (I_25PU(0.22)OH0.55); V_{deb}=100µm.s^{-1} (i.e. dε/dt = 1 s^{-1})

When a low fraction of PU is added (5 %) to the matrix composition, the behavior of the hybrid is equivalent to the one of the blank. In particular, air penetration at intermediate strain (ε~4) and cohesive debonding are observed in both cases. The low elastic modulus in the matrix, obtained with 0.2 % of chain transfer agent (CTA) in the recipe is not increased by the 5 wt % of polyurethane. With 25 wt % PU, the fibrillation mode is reached and adhesive properties are optimized, as explained in

5.5.2.a. The addition of polyurethane strongly improves the adhesive properties of the matrix because of an increase of the crosslinking brought by the PU[b].

Lab results on adhesive and mechanical properties can also be compared to results of peel and shear resistance (performed at CYTEC Surfaces Specialties following the FINAT test method) which are presented in Table 5-5. To fully understand these results, some comments on the experiments have to be made:

- The adhesion energy (in $J.m^{-2}$) was calculated from the tack test performed at $d\varepsilon/dt = 0.1\ s^{-1}$.
- The latexes were dried on a polyester (PE) layer 23µm thick during 3 minutes at 110 °C. These adhesive + PE layers were then deposited on a stainless steel (SS) substrate.
- The shear resistance measured the holding time (in min) before failure of an adhesive layer to which a mass of 1inch/kg² was applied. The maximum time measured was 10000 min. After this limiting time, the test was stopped. If a cohesive failure occured, CF was noted with the value.
- The peel was a 180° peeling test on stainless steel performed after a 20 min contact time between the adhesive and the SS substrate. CT is for Cohesive Transfer between the adhesive layer and the stainless steel substrate, which is not desirable for good PSA properties.

Table 5-5: Adhesion energy measured for $V_{deb}=10\mu m.s^{-1}$ and industrial shear and peel results

Sample	% PU	W_{adh} ($J.m^{-2}$)[a]	Shear resistance (min)	Peel (N/m)[b]
I_0PU(0.2CTA)	0%	200.4 ± 21.2[c]	181 ± 15 CF	436 ± 47
I_5PU(0.22)OH0.55	5%	67.5 ± 11.6	46 ± 15 CF	532 ± 47 CT
I_15PU(0.22)OH0.55	15%	164.3 ± 17.2	222 ± 15 CF	340 ± 47
I_25PU(0.22)OH0.55	25%	232.1 ± 65.9	9463 ± 15 CF	276 ± 47
I_50PU(0.22)OH0.55	50%	26.2 ± 11.5	> 10000	172 ± 47

a: for $V_{deb}=10\mu m.s^{-1}$
b: at 300mm.min-1
c: for $V_{deb}=100\mu m.s^{-1}$ in that particular case

The industrial results are consistent with the mechanical experiments. The addition of polyurethane strongly decreases the peel force. With a low fraction of PU, a cohesive transfer to the SS substrate indicates a very viscous sample, with high dissipation. The peel strength then decreases to unacceptable industrial values. The difference between the probe tack results and the peel test results is due to the different strain rates (the peel tests are more equivalent to 1000 µm/s in tack experiments) and contact times.
On the other side, the shear resistance is improved by the addition of PU. This can be explained by the increase of the elastic modulus previously observed. As the number of

[b] : These complementary results will not be included in the paper but are still presented in the thesis

crosslinks and entanglements is higher, the cohesion inside the material is higher and shear resistance increases.
Furthermore, there is a strong gap between shear resistance for 15 % and 25 % whereas adhesion does not decrease that much. Although there still is a cohesive failure for 25 %, we are in the range of interesting mechanical properties.
However, the industrial experiments indicate that it is not possible to have an increase of both peel and shear with this polymer architecture. Although PU offers a new way to organize the network, both properties are still strongly correlated.

5.5.2.d Discussion

Mechanical experiments at small and large strains have shown that increasing the PU weight fraction enhances the sample stiffness while decreasing its viscous component. Two explanations correlated with the PU weight fraction can be given:

- The polyurethane is partially grafted to the network (here, 10 % of the chain ends are grafted to the acrylic). As a consequence, crosslinks due to the PUgrafting are added to the crosslinks of the acrylic network. Hence, the more polyurethane, the more crosslinks are added to the network and the gel content increases.
- The polyurethane used here has a lower molar mass between entanglements M_e than the acrylics (Tong and Jerome 2000; Florez, Munoz et al. 2006). Thus, the polyurethane adds entanglements to the network. These entanglements play a crucial role on the elastic modulus at small strain.

Compared to the blank sample, an optimum value of the PU weight fraction exist around 25 wt% to optimized PSA properties. Below this value, there is not enough crosslinking points and entanglements brought by the PU and the samples remain too soft with a liquid-like behavior. Above this value, the elastic component is too important and an interfacial propagation of cracks is observed, due to a too high gel content.
It is interesting to note that equivalent optimum in the PU weight fraction has been observed by Wang *et al.* (Wang, Chu, Graillat, Guyot, Gauthier *et al.* 2005) on the same type of PU/acrylic hybrid but for coating applications.

The analysis of the gel and swelling ratio has brought interesting information on the impact of the PU on the polymer architecture at the molecular scale. For practical reason, we considered a homogeneous incorporation of the PU when making this analysis. Nevertheless, the results on morphology from chapter 4 clearly showed that the PU is not homogeneously located in the particle. For 50 wt%, a distinct shell is even detected, whom influence on the elongation at failure has been noticed. Despite the homogeneity of the final dried film, the morphology should be taken into account to analyse more precisely the gel and swelling ratio.
The polyurethane affects mostly the elastic modulus due to an increase of physical (entanglements) and chemical (gel part) crosslinking. It is a coarse parameter having a very strong effect even for relatively modest differences. However, according to the industrial

results, this parameter alone is not able to displace the balance between peel strength and shear resistance. The other parameter that can be modified is the degree of grafting of the polyurethane. This is developed in the next part of the chapter.

5.5.3 Impact of the degree of grafting of the PU

5.5.3.a Analysis of the mechanical and adhesive properties

The reaction between PU and HEMA, the OH-functionalized acrylic monomer allowing grafting to the acrylic backbone (see Figure 5-11) can be well controlled during the synthesis (Udagama 2009). In this series, the grafting of polyurethane is varied from 5% to 20% of the PU chain ends, taking into account that 20% is the maximum level of grafting allowed by the reaction between HEMA and PU. The grafting degree is directly connected to the HEMA/BPA ratio: the higher the HEMA/BPA ratio, the more grafted is the PU.
In this section, we compared samples with a constant weight fraction of PU (25%) but HEMA/BPA ratios changing from 0.1 to 0.5. In the first part of the section, the ratio between OH and NCO moieties is 0.55, whereas a stoechiometric ratio (i.e. OH/NCO = 1) is used in the second part.

Small-strain linear viscoelastic properties

G' and tanδ as a function of frequency for different HEMA/BPA ratios with 25 wt% of PU show interesting differences (Figure 5-16). The values of the storage modulus at 1 Hz present no significant differences and are in the acceptable range for PSA application.
The tanδ does change more significantly but mostly at low frequencies, a regime which is more sensitive to crosslinking architecture than entanglements. The resulting values of tanδ/G' are all predicting a fibrillation debonding (from $0.44.10^5$ Pas^{-1} for the lower HEMA/BPA (I_25PU(0.11)OH0.55) to $0.40.10^5$ $Pa.s^{-1}$ for the higher ratio (I_25PU(0.50)OH0.55)). In all cases, it is important to note however, that changes of the grafting ratio do not affect much the linear viscoelastic properties.

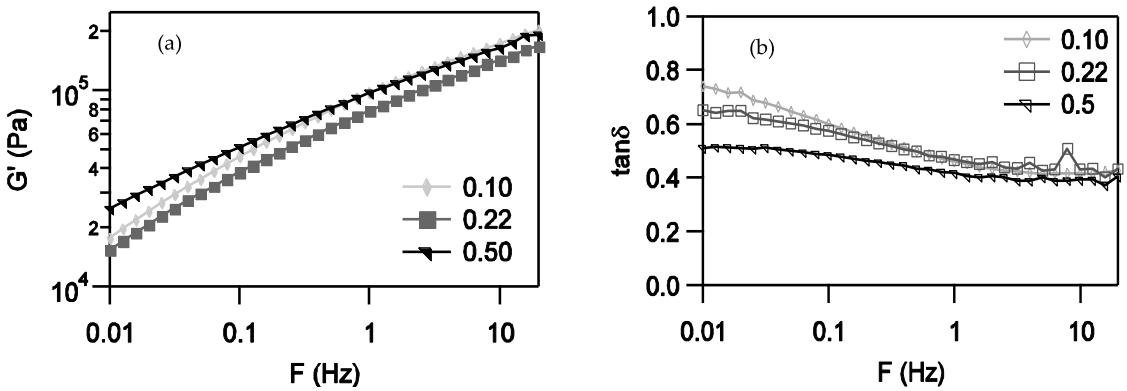

Figure 5-16: Evolution of the G' (a) and of the ratio tanδ/G' (b) as a function of frequency for HEMA/BPA=0.10 (I_25PU(0.11)OH0.55), for HEMA/BPA=0.22 (I_25PU(0.22)OH0.55) and HEMA/BPA=0.50 (I_25PU(0.50)OH0.55); ε ~ 8 %

Non-linear large-strain properties

The tensile experiments are more sensitive to the subtil changes in polymer architecture and they have been performed on the same samples, at a nominal strain rate dε/dt=0.1s-1. The results are presented in the Figure 5-17.
The different curves present an identical shape for all the HEMA/BPA ratios. A pronounced softening occurs at σ_N ~ 40 kPa for the three first ratios. When HEMA/BPA is equal to 0.5, the softening stress σ_S slightly increases to reach 50 kPa.

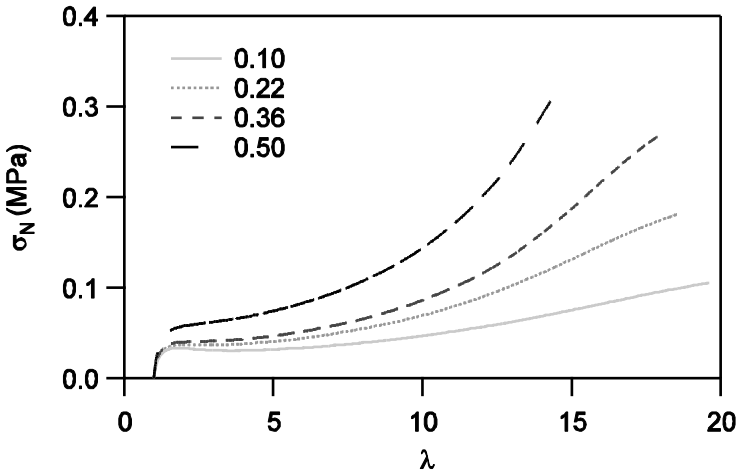

Figure 5-17: Nominal stress versus lambda for the 4 different HEMA/BPA ratios; dε/dt=0.1s^{-1}

The Mooney representation (Figure 5-18) shows that the softening has an equivalent λ dependence for all ratios. The main change that can be noted is on the hardening stress and strain. From the Mooney graph, one can observe that the position of the minimum in reduced stress corresponding to the onset of the hardening changes from λ~11 with a σ_R ~ 5 kPa for the smallest HEMA/BPA ratio (0.10) to λ ~ 8 with a σ_R ~ 13 kPa for the largest one (0.50).

The viscoelastic parameters C_{soft} and C_{hard} confirm the observations. The C_{soft} does not change much for the three first ratios (i.e. equivalent shape of the nominal stress curve) but C_{hard} does (i.e. increase of the hardening stress with HEMA/BPA). The increase of Chard and above all the decrese of the hardening strain λhard characterize the decrease of the finite extensibility of the PU chains. Consistent with the rheological measurements, the elastic modulus is quite constant.
Based on these measurements, one can think that mesh size decreases (i.e. the density of crosslinks increases) when the HEMA/BPA ratio increases.

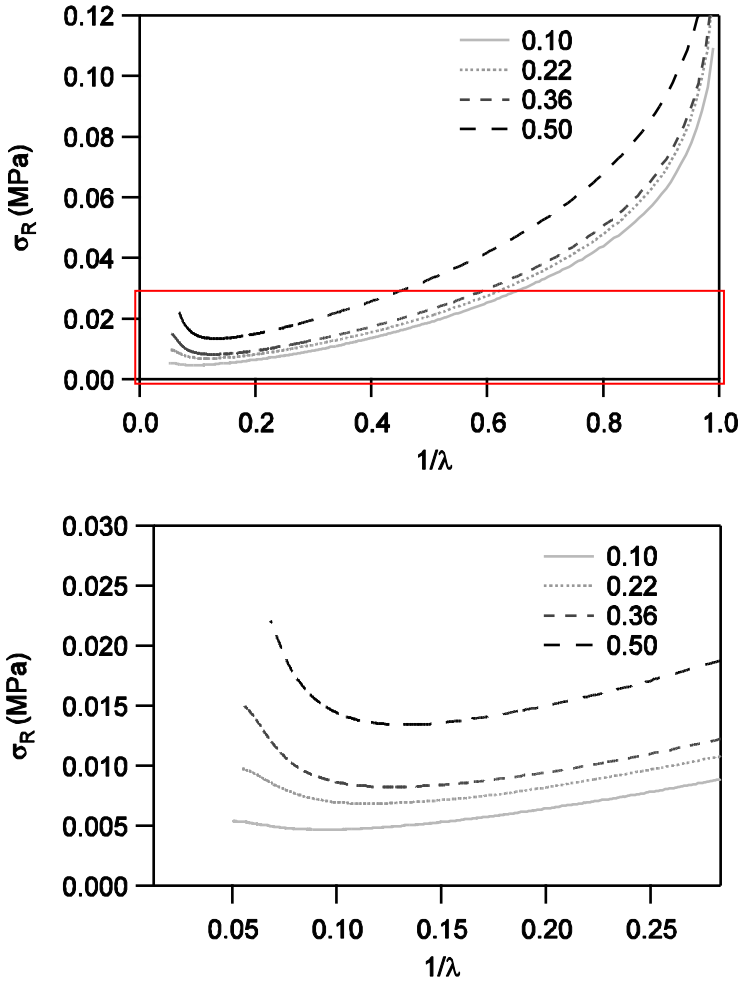

Figure 5-18: Reduced stress versus 1/λ for the 4 different HEMA/BPA ratios; dε/dt=0.1s^{-1}; the bottom figure is a magnification of the red square

Table 5-6: Values of the Mooney-Rivlin viscoelastic parameters for the 4 different HEMA/BPA ratios; dε/dt=1s^{-1}

Sample	HEMA/BPA	C_{soft} (kPa)	C_{hard} (kPa)	C_{soft}/C_{hard}	E_y (kPa)
I_25PU(0.11)OH0.55	0.11	55.5	4.7	11.9	221.8 ± 18.9
I_25PU(0.22)OH0.55	0.22	59.2	6.8	8.7	250.6 ± 27.3
I_25PU(0.36)OH0.55	0.36	62.4	8.2	7.6	203.1 ± 8.9
I_25PU(0.50)OH0.55	0.50	81.5	13.4	6.1	306.9± 21.5

Strain rate dependence

The ratio R(λ) of tensile experiments at several strain rates are analyzed here again (see Figure 5-19). Results are very different from those obtained with a varying PU fraction. For the lowest and the highest HEMA/BPA ratios, R(λ) with λ which means that viscoelasticity increases with strain. This λ-dependence of the relaxation could indicate weak interfaces between particles that do not relax at too high strain rate but harden and break.

The interesting point is that at intermediate HEMA/BPA, the opposite influence of the strain rate is observed. Viscoelasticity is very pronounced at intermediate strain (the absolute value of R(λ) is high), but the higher λ is, the less viscoelastic the sample is. This is usually preferred since it gives a more pronounced softening (favoring fibril formation) but hardening (favoring fibril detachment) still occurs at low strain rate.
The changes between the curves indicate that the network architecture is strongly modified by the HEMA/BPA ratio. Depending on the level of grafting, interdiffusion between particles can be hindered, forming weak (HEMA/BPA= 0.1 or 0.5) or acceptable interfaces.
The differences in the network architecture can be explained by changes in the PU chain length. For low grafting, more extension by BPA is expected and PU chains are longer while their length decreases for higher grafting. It also probable that there is a change in the PU organization and that more dangling or free chains can be present for low grafting whereas a large part of bonded chains appeared for high grafting.
However, the reason why this evolution is not constant with the grafting degree is not yet completely clear.

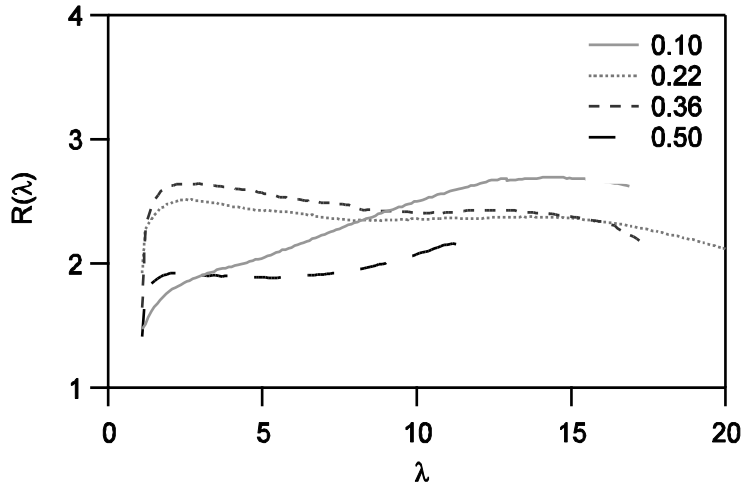

Figure 5-19: Evolution of the ratio R(λ) with the deformation λ for 4 different HEMA/BPA ratios

If analysis of samples with different grafting gives interesting results very different from the previous ones on the impact of the PU fraction, we have to take into account that the ratio HEMA/BPA has a more subtle effect on the mechanical properties. The main effects are observed on the hardening (indicating a finite extensibility decreasing with increasing grafting ratio) and on the λ-dependence of the relaxation (that could indicate strong changes in the network architecture).
From the rheological and tensile measurements (i.e. from the small and large strains domains), one can expect acceptable adhesion with a fibrillation debonding mode whatever the HEMA/BPA ratio. Indeed, the rheological properties all fulfil criteria on G' and tanδ/G' so that neither interfacial crack propagation nor flow should occur. Moreover, softening and hardening at large strains indicates that fibrils can deform enough and break adhesively from the substrate.

Adhesive properties

Tack results are fully consistent with the prediction from the rheology and tensile experiments. Indeed, one can notice on Figure 5-20 that a fibrillation plateau is always observed. The maximum deformation ε_{max} decreases when the ratio HEMA/BPA increases. A lower ε_{max} means that fibrils are less stretched, due to a lower finite extensibility of the chains. On the other side, the increasing fibrillation stresses σ_f of the tack curves indicates that the large strain stiffness increases consistently with the increase in C_{hard} which dominates the large strain behavior.

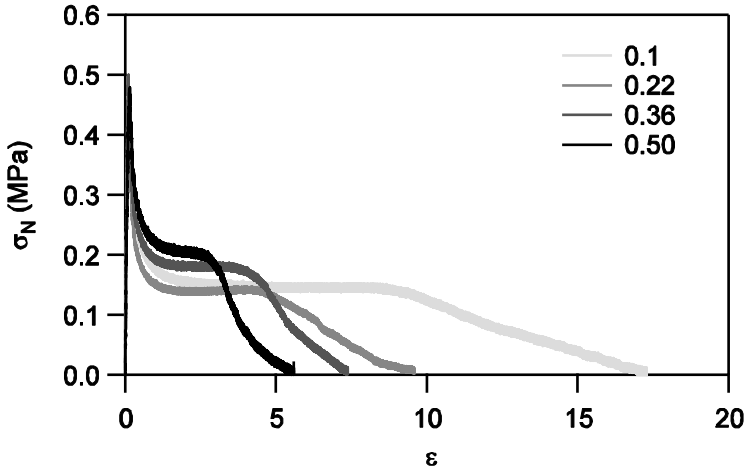

Figure 5-20: Stress-strain tack curves for 4 different HEMA/BPA ratios; V_{deb}=10µm.s^{-1} (i.e. dε/dt = 0.1 s^{-1})

5.5.3.b Influence of the grafting on the polymer network architecture

Mechanical experiments have shown that the HEMA/BPA affects the finite extensibility and the large strain elastic modulus. Figure 5-21 showing the evolution of the gel content and the swlling ratio with the HEMA/BPA ratio confirms this hypothesis: the gel content increases slightly and the swelling ratio decreases more consequently when HEMA/BPA increases.
These interesting results prove that the additional grafting of the PU takes place both in the gel fraction and in the high molar mass fraction of the polymer in the particles.
The change in the grafting affects above all the extension by BPA, PU chains are thus shorter and the network can be less swollen. The swelling measurements and strain hardening are well correlated (see Figure 5-22) and reflect this change in the PU chain length.

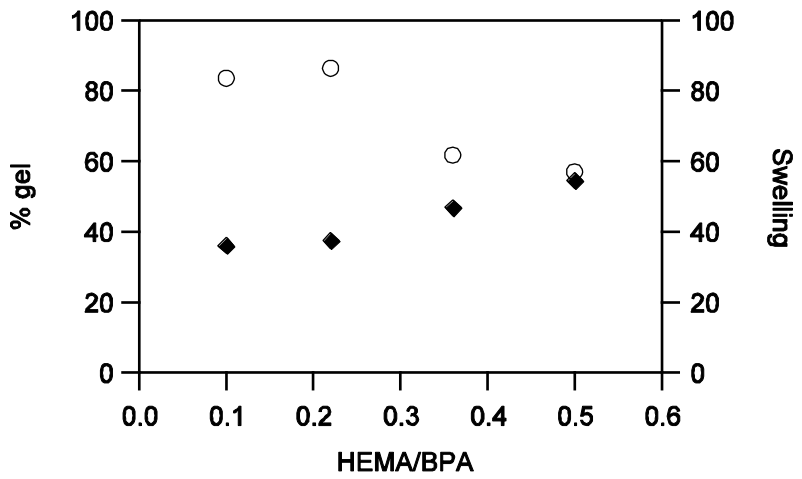

Figure 5-21: Evolution of the gel content (◆) and of the swelling (○) in function of the HEMA/BPA ratio

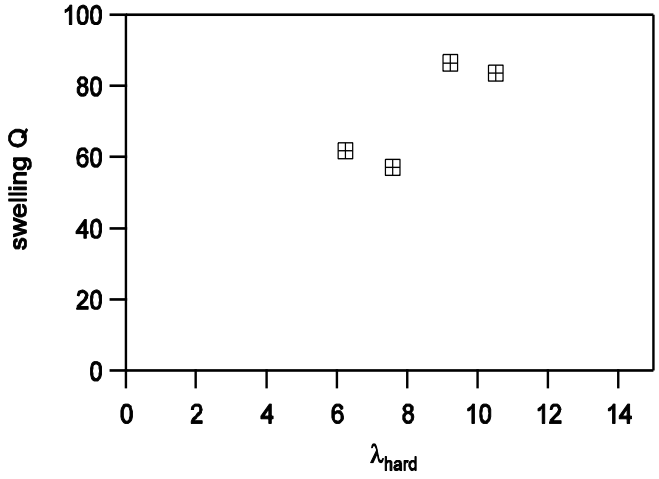

Figure 5-22: Correlation between swelling Q and strain hardenning λ_{har}

5.5.3.c Comparison with industrial results

Table 5-7 compares the adhesion energy obtained with probe-tack test at V_{deb} = 100µm.s^{-1} to the industrial experiments performed at CYTEC Surface Specialties for different HEMA/BPA ratios.

These results are very interesting. Although the energy of adhesion measured in probe tack decreases with the HEMA/BPA ratio, it never goes below that of the matrix with no PU. A certain level of adhesion is maintained regardless the degree of grafting. In parallel, the industrial values of peel remain high in the range of ratios we have tested. Finally, and this is the interesting conclusion, the shear resistance increases dramatically with the ratio HEMA/BPA.

Table 5-7: Adhesion energy measured at V_{deb} = 100 µm.s^{-1} and industrial shear and peel results for the blank sample and the 4 HEMA/BPA ratios; in all cases OH/NCO=0.55

Sample	HEMA/BPA	Wadh (J.m^{-2})	Shear resistance (min)	Peel (N/m)
I_0PU(0.2CTA)	0.0	200.4 ± 21.2	181 ± 15 CF	436 ± 47
I_25PU(0.11)OH0.55	0.11	548.4 ± 128.2	1680 ± 15 CF	284 ± 47
I_25PU(0.22)OH0.55	0.22	284.9 ± 93.3	9463 ± 15CF	276 ± 47
I_25PU(0.36)OH0.55	0.36	228.8 ± 46.5	> 10000	252 ± 47

These results confirm the molecular interpretation made previously where we argued that the HEMA/BPA ratio affects the maximum deformation but has a low impact on the small strain elasticity.
The maximum deformation is the key parameter to improve the energy of adhesion once the fibrillation starts. The more fibrils can be stretched before detachment (so the higher the finite extensibility), the higher the adhesion energy is.
The storage modulus and Chard, on the other hand, have to be related to the cohesion inside the polymer network. Indeed, the higher the cohesion is, the better the shear resistance (as can be observed in Table 5-7).
The HEMA/BPA parameter is as important as the amount of PU. Its effect on the polymer architecture is to modify the chain length of the weak chains. It affects both the organisation of the insoluble or gel part of the network and the ratio between soluble and insoluble parts. This directly affects the low frequency dissipation in the polymer network, improving the resistance to flow, and not the small strain and high frequency elasticity. It is then possible to get separate tools to adjust the storage modulus (PU fraction as explained in section 5.5.2) and the finite extensibility (PU grafting).

5.5.3.d Effect of the OH/NCO ratio

During the miniemulsion synthesis, it is necessary to add a hydrophobic monomer to avoid Ostwald ripening of particles (Asua 2002). Here 5.15 % in weight (relative to the monomer content) of octadecylacrylate (ODA) was incorporated in the recipe. In presence of this hydrophobic component, it was not possible to incorporate the total amount of Bisphenol A required to have a stoechiometric ratio OH/NCO = 1. For amounts higher than 50% of the theoretical amount, flocculation of the particles was observed during the synthesis (Udagama 2009).
The consequence on the polymer architecture and mechanical properties is that the PU chains, extended by the Bisphenol A, are shorter. Furthermore, as no isocyanate can be observed by ^{13}C NMR, it is reasonable to say that reaction with water occurs. In other words, the reaction of polyurethane prepolymer chains is not completely controlled.
To allow a total reaction of the remaining isocyanate with BPA, some samples have been prepared without costabilizer ODA and with OH/NCO=1. No flocculation was observed and some solid films have been prepared from these new latexes to evaluate the impact of the

OH/NCO ratio on the mechanical properties and the polymer architecture. In these samples, 25 wt% of PU is incorporated and two grafting ratios of the PU were chosen: 20% (high grafting) and 10% (low grafting). CTA content also varied from 0.2% for the high grafting to 0.1% for the low grafting. Main parameters of these four samples are detailed in the Table 5-8.

Table 5-8: Major characteristics of the samples with and without costabilizer ODA

Sample	Monomer composition	wt% of PU	% of grafting	ODA	HEMA/BPA	OH/NCO	% CTA
I_25PU(0.50)OH0.55	BA: 89.5%	25	20	Yes	0.5	0.55	0.2
I_25PU(0.25)OH1	MMA: 9.5% AA: 1%	↓	↓	No	0.25	1	↓
I_25PU(0.22)OH0.55	↓	↓	10	Yes	0.22	0.55	↓
I_25PU(0.10)OH1	↓	↓	↓	No	0.1	1	0.3

Probe-tack and tensile results of four samples are presented in Figure 5-23. For this series, mechanical tests have been performed at a higher strain rate of 1 s^{-1} (i.e. V_{deb}=100µm.s^{-1} for the probe-tack and V=15mm.s^{-1} for the tensile test).

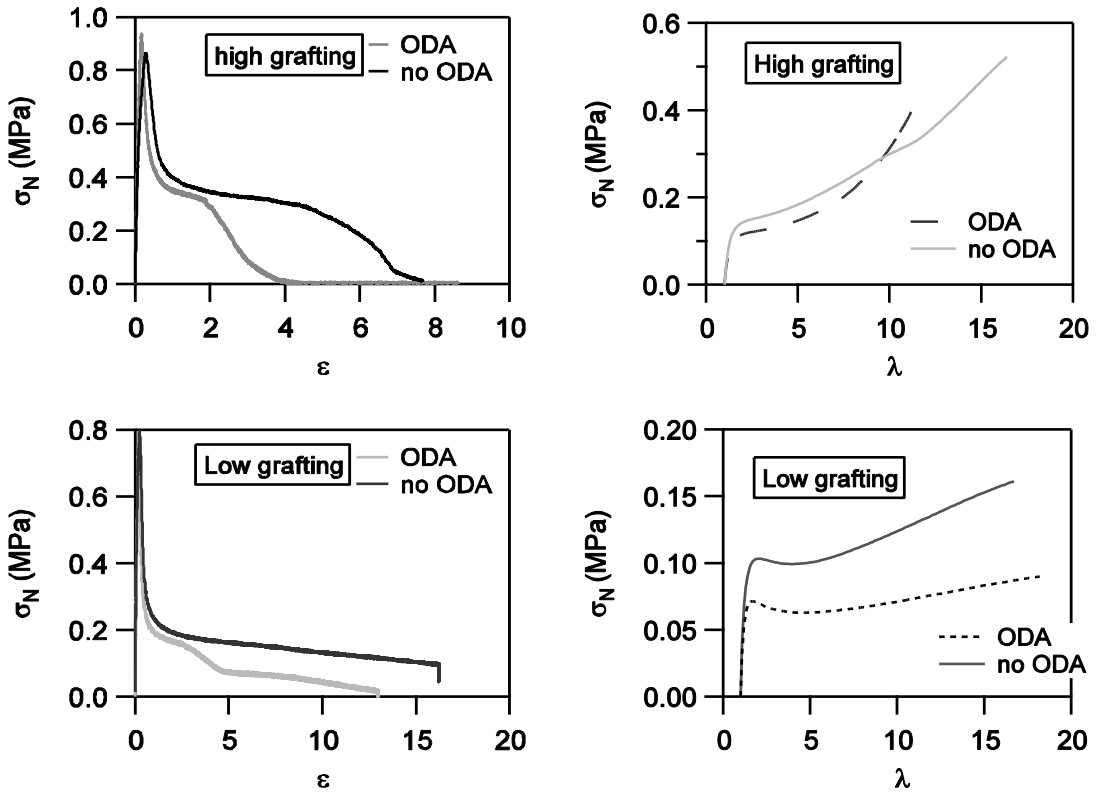

Figure 5-23: Probe tack (left) and tensil results (right) of samples with and without ODA for high grafting of PU (high; samples I_25PU(0.22)OH0.55 and I_25PU(0.22)OH1) and low one (down; samples I_25PU(0.11)OH0.55 and I_25PU(0.11)OH1); for probe-tack tests V_{deb}=100µm.s^{-1} (i.e. dε/dt = 1s^{-1}); for tensile tests dε/dt=1s^{-1}

As seen on Figure 5-23, the effect of the change in process is different in the case of high grafting and low grafting. When a high degree of grafting of PU is used, the material synthesized without ODA (and more BPA) has a higher ε_{max} while keeping the same level of large strain modulus σ_f. This is consistent with constant grafting and PU fraction. The tensile curves show a less pronounced softening for the sample with high BPA and a more progressive hardening at very large strains.
On the contrary, for a lower level of grafting, the material without ODA (and more BPA) is more cohesive. The tack curve of the sample without ODA does not present air penetration at intermediate strain (ε~5) and the pronounced softening and then hardening seen on the tensile curve both occur for a higher stress (even if both tensile curves, with and without ODA have values typical of a very soft PSA).
In both cases, the lack of ODA has a positive effect. For low grafting, the material becomes more elastic, stabilizing the fibril extension while for high grafting, the deformability of the sample is really improved. Of course athe absence of ODA for a constant degree of grating is accompanied by a more important addition of Bisphenol A. To clarify the impact of more BPA, it is necessary to recall the different types of PU chains that can be present in the hybrid particle at the end of the polymerization:

- free extended PU chain terminated by BPA or amine on both sides
- dangling PU chain connected on one side through HEMA
- PU chains connected on both side to HEMA

When the grafting is low (10% of the chain ends), the elasticity increases when extension is higher (in absence of ODA). Since many PU chains are free, Bisphenol A will mainly transform free chains into dangling chain or two dangling chains into a bonded chain.
For a higher grafting (20% of chain ends), one can think that reactions between Bisphenol A and PU will mainly promote extension of the bonded chains. Thus, more reactions of BPA will increase the average PU chain length of these bonded chains and the finite extension, determined by the length of shortest PU chains, will increase.
The gel and swelling measurements partially confirm this interpretation. The gel content decreases from 54.5 % when there is ODA (less reaction of BPA) to 44.3 % when there is no ODA (more reaction of BPA). On the other side, the swelling increases from 57.0 (ODA) to 74.6 (no ODA). This is the indication that the meshes of the network are bigger, but with only a small effect of the decrease of the gel on the elasticity.

If the effect of the extension on the mechanical properties (see Figure 5-23) is quite clear in both cases, it is not easy to determine when is the transition from the first mechanism (formation of dangling or bonded chains) to the second one (extension of the bonded chains) and the effect of reaction with water is not clear.

5.5.3.e Discussion

Mechanical and molecular analyses of samples with different HEMA/BPA ratios have demonstrated that this parameter is directly connected to the PU chains molar mass. This molar mass is crucial to determine the deformability of materials with a constant amount of polyurethane, i.e. a constant small strain elastic modulus. The higher the HEMA/BPA ratio, the more favored is the grafting in comparison with the chain extension. The more grafting there is and the shorter the PU chains are. The finite extensibility then decreases and samples are less deformable but harder to deform. As a result the adhesion energy remains rather constant but the material can be made a bit less crosslinked (favorable for adhesion on low energy surfaces) or more crosslinked (favorable for high shear resistance)
This is observed on the mechanical measurements (Figure 5-20 and Figure 5-18, where we can see a decrease of maximum deformation in all cases) as well as on the gel and swelling measurements (Figure 5-21, where the swelling decreases when the HEMA/BPA ratio increases whereas the gel content slightly increases). One can conclude that this parameter affects the architecture and size of the meshes of the insoluble part, more than the balance between soluble and insoluble parts. The effect on the quantity of insoluble is masked by the quantity of gel formed by the acrylic.
Nevertheless, it is worth noting that no reaction with water is considered in this description. Moreover, due to a lack of data concerning the particle morphology in this case, a homogeneous incorporation of the PU was considered. We know from chapter 4 that a phase separation occurs at particle scale 25 wt% of PU and a degree of grafting of 10 %.

On a macroscopic point of view, the consequence is that it is possible to adjust this parameter to maintain a certain level of tack and peel and in the same time improve the shear experiments (see Table 5-7). A HEMA/BPA ratio between 0.2 and 0.4 can give the best equilibrium between these properties.

However, this HEMA/BPA ratio depends also on the OH/NCO ratio that is to say on the possibility to have a stoechiometric fraction of BPA or not related to the free NCO moieties. Results obtained for samples without ODA allow us to better understand the mechanisms of chain extension. One has seen that there is a transition from improvement of elasticity (with the formation of dangling and bonded chains) in the case of very low grafting of PU to an increase of the deformability (with the extension of already bonded chains). Although this transition can be qualitatively observed on the mechanical measurements, it is necessary to make more systematic measurements to point out the mechanisms responsible for this transition.
With this second optimization, the best properties are obtained for a polymerization with 25% of polyurethane compared to the acrylic monomer, without ODA, with HEMA/BPA ~ 0.25 and 0.2% CTA.

5.6 Conclusion

This chapter analyzed the polymer architecture of hybrid latex particles. These particles, produced by miniemulsion polymerization, are based on a very low T_g acrylic matrix to result in PSA films upon drying. A second phase made of reactive polyurethane is incorporated as a prepolymer during the first step of polymerization.

The objective was to find synthesis parameters which can improve the shear resistance of the latex films without changing the adhesive properties and to understand the effect of these parameters. In this paper, the weight fraction of PU and the way it is connected to the acrylic backbone were varied separately. The two parameters play different roles in controlling the polymer architecture inside each particle.

The amount of polyurethane affects strongly the ratio between soluble and insoluble parts. Indeed, as the polyurethane is grafted, the incorporation of this resin adds crosslinks to the acrylic matrix. In addition, since the polyurethane is more entangled than the acrylic, it also affects the small strain elastic modulus with the incorporation of many entanglements, which behave like permanent crosslinks at high frequency. Being trapped in the important gel part of the particles, these entanglements do not behave as non permanent relaxing crosslink points.

The degree of grafting and the PU chain length (controlled by the ratio between the grafting agent HEMA and the chain extender BPA) play a role in the architecture of the insoluble part. Although, the variation of this ratio changes slightly the number of permanent crosslinks (for a fixed fraction of PU) its main effect is on the PU average chain length. Thus, the swelling of the soluble part directly depends on this degree of extension, i.e. on the HEMA/BPA ratio.

Results obtained with industrial standard tests have shown a clear improvement in shear resistance while the peel force remained reasonable, when this parameter was modified. One can conclude that the structure of the insoluble part is as important as the fraction of gel, a point which has been often neglected so far.

To optimize the materials for a specific industrial application, it is necessary to first adjust the amount of polyurethane to a given matrix (coarse parameter), and then to adjust the ratio between grafting and extension (fine parameter).

Two independent parameters can be used to adjust a polyurethane/polyacrylic polymer network. One optimized set of parameters has been determined (25% of polyurethane and HEMA/BPA ~ 0.25 with 0.2% CTA). However, it could be interesting to test other combinations of parameters for different applications.

5.7 References

- Asua, J. M., *Progress in Polymer Science*, **2002,** *27*, (7), 1283-1346.
- Brandrup, J.; Immergut, E., H., *Polymer Handbook,* New York, Wiley, **1999**.
- Carelli C.; Déplace F.; Boissonnet L.; C., C., *Journal of Adhesion*, **2007**.
- Creton, C., *MRS Bulletin*, **2003,** *28*, (6), 434-439.
- Creton, C.; Hooker, J.; Shull, K., *Langmuir*, **2001,** *17*, 4948-4954.
- Crosby, A. J.; Shull, K. R.; Lakrout, H.; Creton, C., *Journal of Applied Physics*, **2000,** *88*, (5), 2956-2966.
- Dahlquist, C. A., *Treatise on Adhesion and Adhesives*, Patrick, R. L., Dekker, ***2:*** 219-260,**1969**.
- Deplace, F., PPMD, *University Paris VI*, **2008**
- Deplace, F.; Carelli, C.; Mariot, S.; Retsos, H.; Chateauminois, A.; Ouzineb, K.; Creton, C., *Journal of Adhesion*, **2009,** *85*, 18-54.
- Florez, S.; Munoz, M. E.; Santamaria, A., *Macromolecules Materials Engineering*, **2006,** *291*, 1194-1200.
- Hegedus, C. R.; Kloiber, K. A., *Journal of Coatings Technology*, **1996,** *68*, (860), 39-&.
- Hirose, M.; Kadowaki, F.; Zhou, J. H., *Progress in Organic Coatings*, **1997,** *31*, (1-2), 157-169.
- Hirose, M.; Zhou, J. H.; Nagai, K., *Progress in Organic Coatings*, **2000,** *38*, (1), 27-34.
- Jovanovic, R.; Dubé, M. A., *Journal of Macromoleculaar Science Part C: Polymer Reviews*, **2004,** *C44*, (1), 1-51.
- Kukanja, D.; Golob, J.; Zupancic-Vlant, A.; Kranjc, M., *Journal of Applied Polymer Science*, **2000,** *78*, 67-80.
- Lakrout, H.; Sergot, P.; Creton, C., *Journal of Adhesion*, **1999,** *69*, (3/4), 307-359.
- Landfester, K., *Macromolecular Rapid Communications*, **2001,** *22*, (12), 896-936.
- Li, M.; Daniel, E. S.; Dimonie; Sudol, E. D.; El-Aasser, M. S., *Macromolecules*, **2005,** *38*, 4183-4192.
- Mallegol, J.; Dupont, O.; Keddie, J. L., *Langmuir*, **2001,** *17*, (22), 7022-7031.
- Nase, J.; Lindner, A.; Creton, C., *Physical Review Letters*, **2008,** *101*, 074503.
- Poivet, S.; Nallet, F.; Gay, C.; Teisseire, J.; Fabre, P., *European Physical Journal E*, **2004,** *15*, 97-116.
- Roos, A.; Creton, C., *Macromolecules*, **2005,** *38*, (18), 7807-7818.
- Satas, D., *Handbook of pressure-sensitive-adhesives*, Satas, D., New York, Van Nostrand Reinhold, ***1:*** 396-456,**1989**.
- Sebenik, U.; Krajnc, M., *Journal of Polymer Science Part A: Polymer Chemistry*, **2005,** *43*, 4050-4069.
- Shull, K. R.; Creton, C., *Journal of Polymer Science Part B-Polymer Physics*, **2004,** *42*, (22), 4023-4043.
- Tong, J. D.; Jerome, R., *Polymer*, **2000,** *41*, (7), 2499-2510.
- Udagama, R., Laboratoire de Chimie, Catalyse, Polymères et Procédés, *University Claude Bernard -Lyon I*, **2009**
- Udagama, R.; Graillat, C.; Degrandi, E.; Creton, C.; Bourgeat-Lami, E.; McKenna, T., *To be published*.
- Udagama R., Laboratoire de Chimie, Catalyse, Polymères et Procédés, *University Claude Bernard -Lyon I*, **2009**
- Wang, C.; Chu, F.; Graillat, C.; Guyot, A., *Polymer Reaction Engineering*, **2003,** *11*, (3), 541-562.

- Wang, C.; Chu, F.; Graillat, C.; Guyot, A.; Gauthier, C., *Polymers For Advanced TEchnologies*, **2005,** *16*, 139-145.
- Wang, C.; Chu, F.; Graillat, C.; Guyot, A.; Gauthier, C.; Chapel, J. P., *Polymer*, **2005,** *46*, 1113-1124.
- Wang, C.; Chu, F.; Guyot, A., *Journal of Dispersion Science and Technology*, **2006,** *27*, (3), 325-330.
- Wang, C.; Chu, F.; Guyot, A.; C., G.; F., B., *Journal of Applied Polymer Science*, **2006,** *101*, 3927-3941.
- Wang, C. P.; Chu, F. X.; Jin, L. W.; Lin, M. T.; Xu, Y. Z.; Guyot, A., *Polymers For Advanced TEchnologies*, **2009,** *20*, (3), 319-326.
- Zosel, A., *Journal of Adhesion*, **1989,** *30*, (1-4), 135-149.

6. From Laboratory to Industrial Systems

6.1 Abstract

Urethane/hybrid latex particles have been prepared by miniemulsion polymerization for application as pressure sensitive adhesive (PSA). Urethane prepolymer was incorporated in a one-step process in the monomer phase and a semi-continuous process was employed for polymerization. Full incorporation of the PU was ensured by the grafting of the reactive PU prepolymer on the acrylic backbone. A constant PU weight fraction was added while different ratios of grafting agent over PU chain extender were used. Rheology and tensile tests on self-standing films and probe-tack tests on adhesive layer were performed. They showed that the materials are over-crosslinked for adhesive applications, what reduces the tack and peel properties of PSA, while a high shear resistance is observed due to this high level of crosslinking. More precisely, it has been seen that increasing the HEMA/BPA ratio favors the grafting of the PU instead of its extension and decreases the deformability of the samples. The addition of an excess of hydroxyl functions results in an even higher gel content and a loss of cohesion in the bulk film because of weak particle-particle interfaces in the final structure.

6.2 Introduction

Recent legislations concerning Volatile Organic Compounds (VOC) have led to important developments in waterborne coatings and adhesives as replacements of their solvent-borne counterparts. Conventional emulsion polymerization is a classic way to prepare latexes. Even if widely used in the industry, emulsion polymerization has two main limitations: the monomers must have some water solubility and the control of the copolymer composition is not easy and the latex particles are quite heterogeneous. Overcoming these limitations has led to the recent development of miniemulsion polymerization (Landfester, 2001; Asua, 2002) One of the advantages of miniemulsion polymerization is the possibility to easily produce hybrid particles. These hybrid particles generate in turn new types of products with synergetic properties.

Polymers usually produced in the field of Pressure Sensitive Adhesive (PSA) (Satas, 1989; Creton, 2003) by emulsion polymerization are acrylic copolymers (Satas, 1989). One good candidate to improve solvent resistance and temperature resistance of acrylic PSA is the polyurethane. Previous chemistry papers have shown that it is possible to produce hybrid network combining an acrylic backbone with a polyurethane graft. However, existing studies have focused on polymerization in solution of soft acrylics (Baron, Rodriguez-Hernandez *et al.*, 2005) or on polymerization in emulsion or miniemulsion of hard acrylics suitable for coatings (Gooch, Dong *et al.*, 2000; Wang, Chu *et al.*, 2003; Li, Daniel *et al.*, 2005).

In the previous chapter, we have studied systematically the mechanical and adhesive properties of soft urethane/acrylic hybrid films. In particular, we have highlighted that two main parameters affect the mechanical and adhesive properties. First, the weight fraction of polyurethane related to the acrylic content is a coarse parameter acting mainly on the small

strain elastic modulus of the material. Secondly, the PU chain length (in direct correlation with the way the PU is grafted to the acrylic) is a finer parameter that impacts the large strain behavior of the polymer network and in particular the strain hardening. With the help of these two parameters it is possible to control the two important aspects of a PSA: the elastic behavior which helps to resist shear, defined by the Dahlquist criterion (Dahlquist, 1969), and the dissipative behavior which results in large viscoelastic deformation during a debonding test such as peel or tack test.

This first study was based on a complex step by step preparation developed by Udagama *et al.* (Udagama, 2009) and based on the work of El-Aaser *et al* (Li, Daniel *et al.*, 2005). If this preparation leads to the production of a well characterized product, it is not easy to reproduce in the industry.

The same type of urethane/acrylic latexes with urethane chains grafted to the acrylic backbone can be produced in conditions closer to the industrial ones and it is the goal of this chapter to analyze mechanical properties of films obtained with this method. In particular, a semi-continuous process was used instead of batch polymerization (Lopez, 2009). The question is then whether the fine parameter determined in the previous chapter (i.e. the chain length of the PU) has the same effect when the latexes are produced in these conditions. Analysis of the properties of the latexes is presented. This analysis is based on the combination of three macroscopic tests. The adhesive properties are analyzed with a design probe-tack test, while standard tests are performed to analyze rheology and tensile properties. The correlation of swelling experiments with these mechanical results is quite new and brings additional information on the polymer microstructure.

If the chain length and thus the maximum extensibility of the polymer chains is affected by the ratio between the grafting agent (here, hydroxyl ethyl methacrylate HEMA) and the chain extender (here, Bisphenol A BPA), some differences with the results from chapter 5 are yet observed. Indeed, HEMA and BPA are mixed at the same time with the polyurethane prepolymer and their reactivity with the urethane functions, which is different from one to the other, cannot be neglected in the polyurethane organization. The correlation between the HEMA/BPA ratio and the chain length estimated in the previous chapter is not here as simple to establish.

The other parameter studied here is the overall ratio between the isocyanate functions (NCO) coming from urethane chains and the hydroxyl functions OH. Latexes with OH/NCO = 1 and OH/NCO = 2 were prepared. Thus, the impact of an excess of OH is analyzed relative to samples with the same HEMA/BPA ratios. Two different situations are observed depending whether the level of grafting of urethane is high or not.

6.3 Experimental section

6.3.1 Preparation of the latex

Miniemulsion polymerization has been used to produce all the latexes presented here. Conditions close to the ones used in the industry have been chosen. In particular, the polymerization was performed by a semi-continuous process. All the details concerning the synthesis can be found in a specific thesis manuscript (Lopez, 2009). We remind here only the required elements to understand the structure of the latexes.

The monomer composition of the acrylic matrix was a follow:

- *2 ethyl hexyl acrylate (2EHA): 97 %*
- *methyl methacrylate + hydroxy ethyl methacrylate (MMA + HEMA): 2 %*
- *methacrylic acid (MAA): 1 %*

A hydrophobic compound, octadecyl acrylate (ODA, 4 % wbm) was added in the particles as costabilizer against Oswald ripening.
Industrial reactive polyurethane prepolymer (Incorez 701, provided by Industrial Copolymers Limited) was incorporated in the organic phase. A total amount of 10 wt% related to the total organic phase (wbo) was added in all the latexes.

All organic components (monomers, PU, grafting agent HEMA, chain extender BPA, costabilizer ODA) were first mixed together. The organic phase was then mixed to the aqueous phase, miniemulsified in a high pressure homogenizer and transferred in the reactor. Droplets formed during miniemulsification were stabilized by two surfactants: Dowfax 2A1 (2 % in weight by monomer, wbm) and SDS (1 % wbm). Polymerization occurred directly inside the particles by the addition of a thermal initiator, the potassium persulfate (KPS, 0.5% in weight by monomer, wbm).

The reactive PU prepolymer added in the formulation was terminated on both sides by an isocyanate (NCO) which could react with OH function of the hydroxyl ethyl methacrylate (HEMA) or of the Bisphenol A (BPA) present in the organic phase. HEMA reacted on one side with the PU prepolymer and could polymerize with the acrylic monomer effectively grafting the PU on the acrylic backbone. As seen in chapter 4, the grafting is necessary to avoid phase separation inside the particles (Li, Daniel et al., 2005). The BPA acted as a chain extender to couple two PU chains together.

Contrary to the method described in chapter 5, acrylic monomers (including HEMA), PU prepolymer and BPA were mixed all together to form the organic phase and then miniemulsified. There was therefore no specific preparation of the PU prepolymer prior to miniemulsification (Udagama, 2009).

6.3.2 Physical and chemical parameters of the latexes

The solid content was measured gravimetrically. A value of 47 % ± 1.5 % of solid particles in water was found. It was maintained constant for all latexes presented here.

The glass transition temperature was measured by Differential Scanning Calorimetry (DSC) on several samples and it was constant for all latexes. The average T_g is: -63.08 °C ± 0.73 °C. No impact of the PU on the global T_g of the hybrid could be noticed. This is due to the closeness of the T_g of the pure acrylic (-65 °C) and T_g of the pure PU (-48 °C).

Three different quantities can be varied to modify the polymer architecture:

- *OH/NCO is the molar ratio between OH functions from HEMA and BPA and NCO functions coming from PU*
- *HEMA/BPA is defined as the molar ratio between OH functions coming from the grafting agent HEMA and OH functions coming from the chain extender BPA*
- *The degree of grating φ is the ratio between OH functions coming from HEMA and isocyanate functions coming from the PU*

Based on OH/NCO and on the weight fractions of HEMA and PU, one can calculate HEMA/BPA and φ as detailed in annex.

The weight fraction of PU is fixed at 10 % wbo (weight based on organic) in all the latexes. In the first series, the OH/NCO ratio was kept equal to 1 and the HEMA/BPA ratio was varied from 0.5 to 2.5. In a second series, the ratio between the hydroxyl and isocyanate functions was varied (OH/NCO = 1 and OH/NCO = 2) for three HEMA/BPA ratios (~ 0.2, ~ 0.5. and ~ 2.5). The main characteristic of each sample are summarized in Table 6-1.

Table 6-1 : Samples prepared in Route II

Sample	PU content	HEMA/BPA	Theoretical grafting degree [a] (%)	OH/NCO
II_10PU(0.5)OH1	10 %	0.5	35 %	1
II_10PU(1)OH1		1	48 %	
II_10PU(1.5)OH1		1.5	57 %	
II_10PU(2.67)OH1		2.67	70 %	
II_10PU(0)OH2	10 %	No grafting	0 %	2
II_10PU(0.21)OH2		0.21	35 %	
II_10PU(0.54)OH2		0.54	70 %	
II_10PU(2.32)OH2		2.32	140 %	

a: Based on the hypothesis that all HEMA reacts with PU

6.3.3 Characterization Techniques

Bulk films were obtained from the drying of the latex particles under well-controlled conditions of time and temperature. A combination of mechanical tests has been used to characterize the properties of these films.

Rheological measurements were performed with a RDAII on circular samples of ~ 500 μm in thickness and 8 mm in diameter. Circular parallel plates were used and frequency sweep were made from $F = 0.01\ s^{-1}$ to $F = 20\ s^{-1}$.

The large strain viscoelastic properties have been analyzed with tensile tests using an INSTRON machine (model 5565) equipped with a 10 N load cell (resolution 0.5 %) and a videoextensometer (model SVE) measuring the displacement. Thick stripes of ~ 500 nm are used for the tests. Two initial strain rates were used: $d\varepsilon/dt = 0.1\ s^{-1}$ and $d\varepsilon/dt = 1\ s^{-1}$.

Probe-tack tests (Lakrout, Sergot et al., 1999) have been performed to determine adhesive properties of the latex films. A 10 mm stainless steel probe was put in contact with the film dried on microscope glass slide and then debonded at the initial strain rate of $d\varepsilon/dt = 0.1\ s^{-1}$ or $d\varepsilon/dt = 1\ s^{-1}$. Force was measured by a load cell (250 N, resolution 0.5 N) and the displacement of the probe by a LVDT extensometer (range 5 mm, resolution 0.5 μm). In-situ visualization was used to determine the contact area between the probe and the adhesive layer as well as the debonding mode.

Standard industrial peel and shear tests have been performed at CYTEC Surface Specialties following the FINAT methodology (FINAT Technical Handbook, 2005).

Gravimetric measurements of the gel content and the swelling of samples were made in THF to complete the analysis by bringing information on the polymer architecture.

6.4 Results and discussion

6.4.1 Effect of the HEMA/BPA ratio

In the chapter 5, we showed that the polyurethane chains drive the maximum extensibility of the global network due to the fact that these chains are much smaller than the acrylic ones. In the case of laboratory systems, the polyurethane chain length is controlled by the balance between the grafting to the acrylic backbone with the HEMA and the extension of the PU prepolymer with the BPA. Thus, the HEMA/BPA ratio has been determined as a key parameter for the mechanical properties and in particular for the deformability of the network.
This HEMA/BPA ratio has been varied for the semi-continuous systems. Values equal to 0.5, 1, 1.5 and 2.5 were used. Mechanical properties and adhesion of such films are presented below.

6.4.1.a Experimental results

Small strain viscoelastic properties

The results obtained with rheological tests are given in the Figure 6-1. We represented the evolution of G' (left) and tanδ (right) with the frequency for different HEMA/BPA ratios.

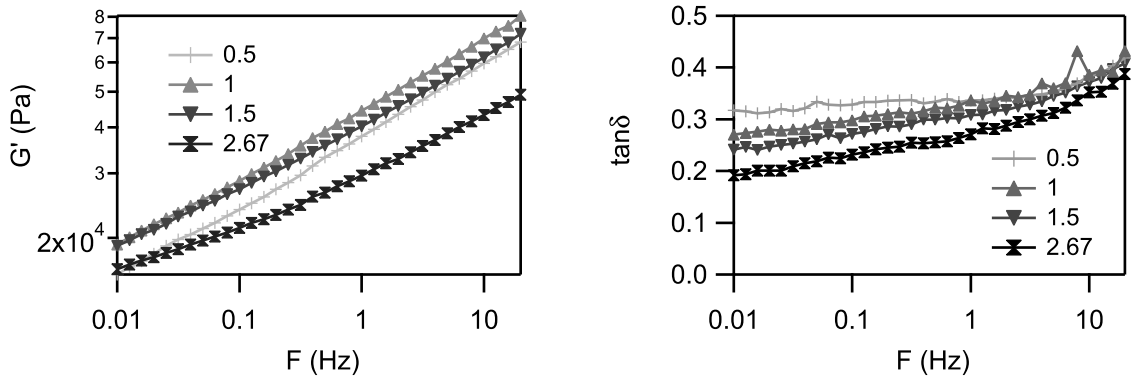

Figure 6-1 : Evolution of the elastic modulus G' (left) and of the phase angle tanδ (right) with frequency for different HEMA/BPA ratios; Strain ~ 8 %

It can be noticed that the HEMA/BPA ratio has a low impact on the elastic modulus but affects mostly the phase angle tanδ, in particular at low frequencies. Equivalent results were obtained in the previous chapter for the laboratory systems (see Figure 5-16). This low-frequencies regime is more sensitive to crosslinking than entanglements, and the results indicate that the HEMA/BPA ratio does deeply affect the crosslinking density. The quantity

of PU being the same in the sample, no change in the number of entanglements is indeed expected.
For the three lower ratios, the elastic modulus is almost the same. Interestingly, the values of G' for the highest HEMA/BPA ratio are always under values measured for the lower ratios. As a high HEMA/BPA ratio is supposed to increase the number of crosslinks, higher values of elastic modulus are expected for this sample. One possible explanation is a slippage of the sample between the plates during the rheology test

It can be note that the values of G' are below the Dahlquist limit imposed for adhesives (G' at 1 Hz lower than 100 – 200 kPa (Dahlquist, 1969)). Nevertheless, the values of tanδ are low for adhesive application (a minimum of ~ 0.5 is expected for optimized properties). This indicates that the samples have a high loss modulus and do not dissipate much energy under a mechanical solicitation. We calculated the tanδ/G' ratio at 1 Hz for the different values of HEMA/BPA. This ratio is a good criterion to determine the debonding mode. On stainless steel values of tanδ/G' above $0.5.10^{-5}$ Pa^{-1} are required to observe fibrillation debonding (Deplace, Carelli *et al.*, 2009). The high values of tanδ observed for this series of samples result in low values of tanδ/G' (from $9.16\ 10^{-6}$ Pa^{-1} for the higher HEMA/BPA ratio to $7.58\ 10^{-6}$ Pa^{-1} for the HEMA/BPA = 1 ratio) and no fibrillation debonding should be expected.

Large strain properties

Figure 6-2 represents standard tensile curves, at a nominal strain rate $d\varepsilon/dt = 0.1\ s^{-1}$, of the nominal stress σ_N versus the strain λ for the four different HEMA/BPA ratios. The $\sigma_N=f(\lambda)$ curves have been limited to homogeneous deformation: the end of the curves have been cut after apparition of slippage or striction. Thus, no comment can be made on the maximum λ observed on Figure 6-2 but only on the softening and hardening.

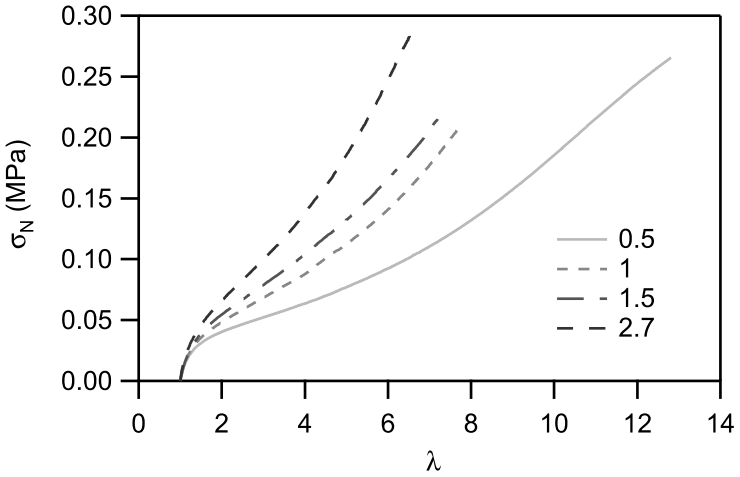

Figure 6-2: Nominal stress versus lambda for different HEMA/BPA ratios; OH/NCO=1; $d\varepsilon/dt=0.1s^{-1}$

For the four ratios, the curves show a low softening and an important hardening initiated at small strain. This type of curve with a less pronounced softening and a pronounced

hardening starting at low strain indicates that the samples are stiffer and less deformable than a typical PSA. This is the signature of a well crosslinked network with a substantial gel fraction compared to its soluble fraction. This is confirmed by the elevated values of the static elastic Young's modulus measured on the stress-strain curves in the domain of linear elasticity and given in Figure 6-2. As observed with the rheology measurements, the values for the first three ratios are close but a consequent difference can be note for the highest HEMA/BPA. It is worth noting that the elastic modulus is higher in this case, whereas it was smaller with the rheology measurements. In all cases, values of the elastic modulus reached the upper limit for adhesive applications (Dahlquist, 1969) what confirms the overcroslinking.

Figure 6-3 shows the Mooney representation of the reduced stress σ_R vs $1/\lambda$ for the different HEMA/BPA ratios. This representation is easier to interpret in terms of structure because it helps to quantify the softening (characterize by C_{soft}, the slope of the curve between $1/\lambda = 0.8$ and $1/\lambda$ of the minimum of the curve) and the hardening (C_{hard}, minimum stress of the curve) (Deplace, Carelli *et al.*, 2009).

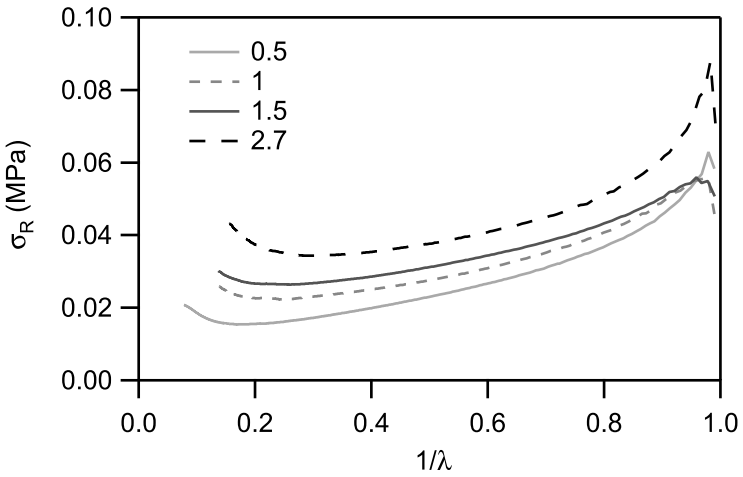

Figure 6-3: Reduced stress vs $1/\lambda$ for different HEMA/BPA ratios; OH/NCO=1; dε/dt=0.1s-1

The softening is mostly equivalent for all samples (the slope at intermediate λ is equivalent) whereas the hardening strongly increases with the HEMA/BPA ratio while the strain λ_{hard} at which hardening starts decreases. These observations are confirmed by the calculated values of C_{soft} , C_{hard} and λ_{hard} presented in Table 6-2 The evolutions of the C_{soft}/C_{hard} ratio and the Young elastic modulus E_y with the HEMA/BPA ratio are also shown in Figure 6-4.

Table 6-2: Viscoelastic parameters for different HEMA/BPA ratios; dε/dt=0.1s^{-1}

Sample	HEMA/BPA	C_{soft} (kPa)	C_{hard} (kPa)	C_{soft}/C_{hard}	λ_{hard}	E_y(kPa)
II_10PU(0.5)OH1	0.5	34.9	15.4	2.3	5.5	164.6 ± 5.8
II_10PU(1)OH1	1	33.5	22.3	1.5	4.0	147.6 ± 13.5
II_10PU(1.5)OH1	1.5	30.9	26.4	1.2	3.8	143.8 ± 4.8
II_10PU(2.67)OH1	2.7	34.3	34.3	0.9	3.3	230.4 ± 25.4

As C_{soft} is related to the non permanent crosslinking points of the network (in other words, the entanglements), a constant value of C_{soft} indicates an equivalent relaxation of these non permanent topological obstacles. The polyurethane used in the hybrids is made of polypropylene glycol PPG and isophorone diisocyanate IPDI. Due to the presence of PPG in the PU prepolymer, the PU is highly entangled compared to the acrylic backbone. The consequence is that the entanglements present in the polymer microstructure come mostly from the polyurethane. Thus the orientation and alignment of the entanglements occurring during the relaxation process is mainly due to the PU. As a constant level of PU amount is present in these samples, a constant level of softening is consistent with this hypothesis.

With this series, the C_{hard} increases from 15.4 kPa to 34.3 kPa (see Table 6-2). Between HEMA/BPA = 0.5 and HEMA/BPA = 2.5, one can also observed a decreasing value (from 5.5 to 3.3) of the λ_{hard}. The C_{hard} is more directly related to the permanent crosslinks of the network which have an important effect at large strain, whereas λ_{hard} depends on the finite extensibility in the polymer network. Referring to Table 6-1, one can note that the grafting degree increases with the HEMA/BPA ratio. Indeed, when HEMA/BPA increases, it directly means that a higher fraction of HEMA is added to the recipe, what increases the probability of grafting. Moreover, if more PU chains are grafted on one side to acrylic, the probability to form bonded PU chains between acrylic is higher. Thus the number of permanent crosslinks present in the network then increases what is consistent with increasing values of C_{hard}. In parallel, when HEMA/BPA increases, the fraction of BPA decreases and less extension of the PU chains is possible. The final chains are shorter, and this is reflected by the decreasing values of λ_{hard}. Finally, when increasing HEMA/BPA, the polymer network is not only more crosslinked but also tighter.

The large strain behavior and in particular the shape of the stress train curve, is mostly affected by the C_{soft}/C_{hard} ratio. Since C_{soft} does not change much with the HEMA/BPA ratio while C_{hard} increases, the ratio decreases significantly with increasing degree of grafting reaching values which are too low to be acceptable for commercial PSA (2 to 5 is typical (Deplace, 2008)). These very low values of C_{soft}/C_{hard} point to an over crosslinked network.

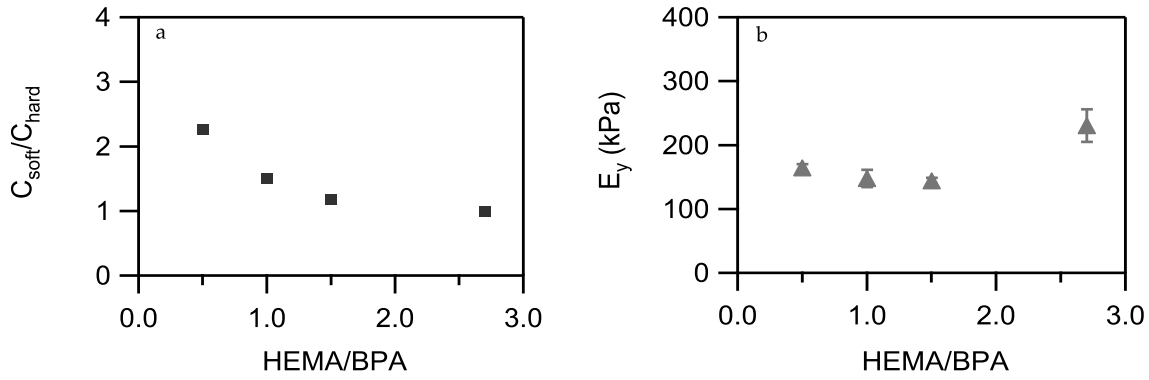

Figure 6-4: Evolution of Csoft/Chard (a) and of the elastic modulus Ey (b) with the HEMA/BPA ratio

The case of the sample with the highest value of HEMA/BPA is interesting. Indeed, the relaxation seems to stabilize when the Young elastic modulus increases strongly compared to the other HEMA/BPA ratios. This is due to a consequent increase of the crosslinking and could indicate that the formation of PU chains bonding two acrylics is favored above a certain value of HEMA/BPA whereas dangling chains (PU chains connected only on one end to the acrylic backbone) are mostly formed for lower HEMA/BPA ratios. The bonding chains would affect more the crosslinking density than the dangling chains, explaining the brutal increase of the elastic modulus. Figure 6-5 summarizes the expected effect of the HEMA/BPA ratio.

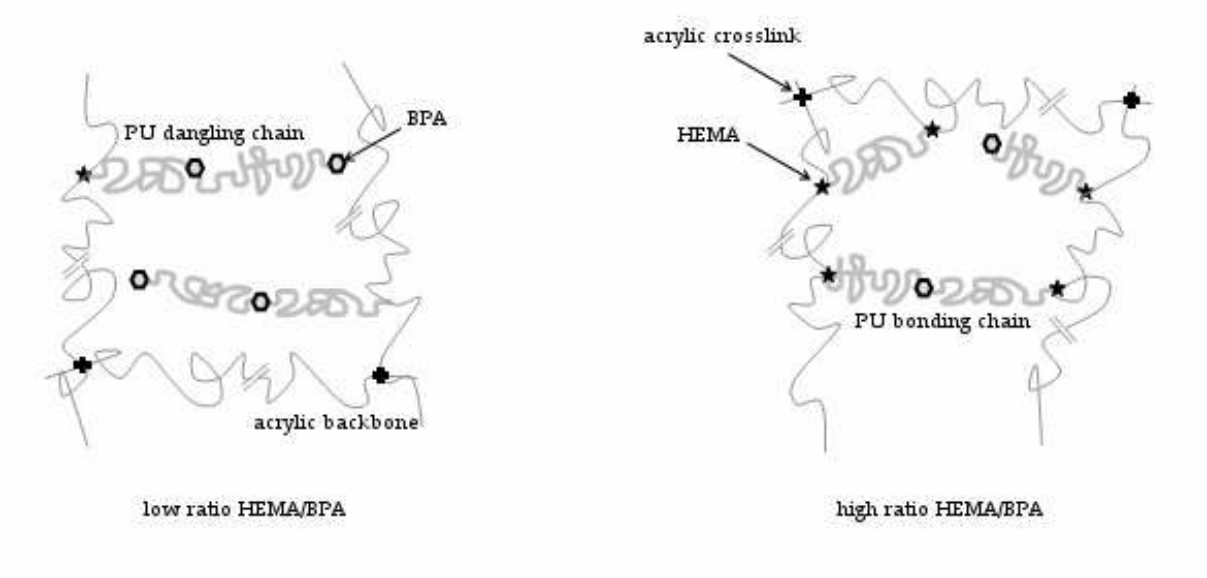

Figure 6-5 : Possible organization of the PU according to the HEMA/BPA ratio

Strain rate dependence in the domain non-linear viscoelasticity

A more refined analysis of the large strain viscoelastic behavior of the system can be carried out by comparing the large strain behavior of the adhesive at different nominal strain rates.
The observed nonlinear behavior in the adhesives in a tensile test is due to a reversible strain-dependent non-linear elasticity and to a time-dependent relaxation process. One way to decorrelate both effects is to compare two tests performed at different nominal strain rates. In this case the non-linear elastic contribution should be the same but the extent of relaxation varies. A simple but instructive representation of the data is the ratio (for each λ) between the stress obtained for test carried out at a high strain rate ($d\varepsilon/dt=1s^{-1}$) and the stress obtained for a test carried out at a low strain rate ($d\varepsilon/dt=0.1s^{-1}$, presented before). The calculation of this ratio $R(\lambda)$ decorrelates time-dependent relaxation and λ-dependent non-linear elasticity. Only the time-dependent relaxation between the two strain rates is represented as a function of λ. The results for different HEMA/BPA ratios are presented in Figure 6-6.

If the two processes are fully separated the ratio is constant whatever the λ. On the other hand any variation of this ratio with λ reveals non-linear viscoelastic processes, i.e. the extent of relaxation depends on the strain.

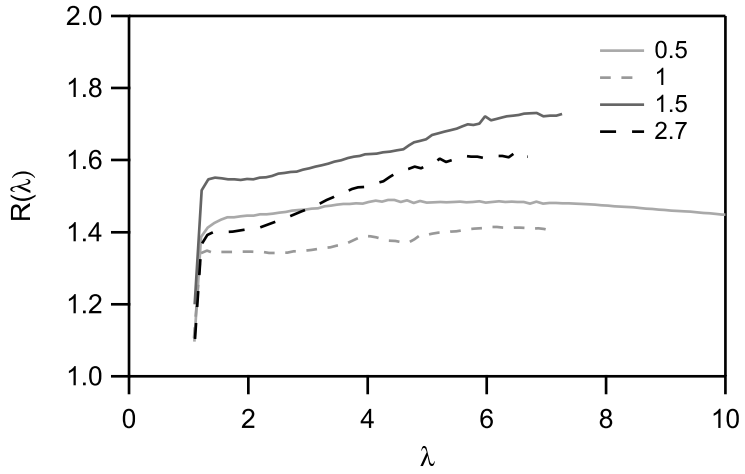

Figure 6-6: Stress ratio R(λ) between two strain rates (high speed over low speed) versus the deformation λ for different HEMA/BPA ratios

It is worth noting that the values of R(λ) are included between 1.3 and 1.8 for all the range of λ. These values are quite close to 1 what indicates a low dependence in nominal strain rates. The different samples are not much viscoelastic and the HEMA/BPA ratio hardly affects this viscoelasticity.
However, some differences in the shape of the curves can be observed for the different ratios. Indeed the higher HEMA/BPA is, the more pronounced is the increase of R(λ) at large strains. Since the particles at high HEMA/BPA are more crosslinked, the reason could be the signature of over crosslinked particles with relatively weak interfaces between particles (where polymer chains cannot interpenetrate easily during film formation).
On the other hand, when HEMA/BPA is low, more dangling chains are present in the network of the particle. A consequence is that dangling PU chains and acrylic chains can interpenetrate easier between particles during film formation. The resulting film structure is more homogeneous and lead to a full decorrelation between the non-linear elastic softening and the linear viscoelastic one.

Gel and swelling measurements

Although the rheological and large strain experiments are essential to characterize the mechanical behavior of the adhesive films they do not provide direct information on the molecular architecture of the polymer network. The characterization of the gel fraction (in other words, the insoluble part permanently crosslinked) and of its swelling ratio in THF as a function of the HEMA/BPA ratio completes the mechanical characterization by a structural analysis.

The evolutions of these two quantities with HEMA/BPA are presented on Figure 6-7 and indicate that gel fraction and swelling ratio evolve in opposite directions: the gel content increases with HEMA/BPA while the swelling ratio decreases. The decrease in swelling ratio is consistent with the increase in C_{hard} and the decrease in λ_{hard}. The higher HEMA/BPA is and the tighter the network is. Its swelling ratio decreases as well as its maximum extensibility. The increase of the gel fraction is less obvious to relate to the mechanical properties, but reflects an increased density of crosslinks as well.

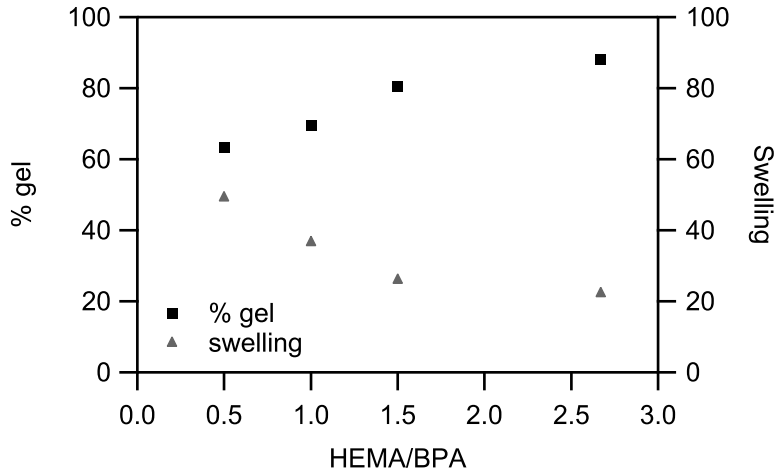

Figure 6-7: Evolution of the gel and the swelling capability versus the HEMA/BPA ratio; OH/NCO=1

More generally, all gel values are very high for PSA applications (from 63% until 88% when the required value for a PSA is around 50-60% (Creton, 2003). On the contrary, the swelling of the polymer network is quite low (from 49% to 22%). This confirms over crosslinked systems.

Adhesive and industrial results

Generally speaking, the samples obtained here from industrial-like latexes are more crosslinked than the one prepared in the lab conditions and analyzed in the previous chapter. Indeed, the higher gel content of the latexes in semi-continuous process is 88 % with strong variations with the HEMA/BPA ratio, when it is 54 % for the batch system. These over crosslinked samples present low adhesive properties, as seen in Figure 6-8 which shows tack curves for different HEMA/BPA ratios at a debonding velocity V_{deb} = 10 μm.s^{-1} (i.e. dε/dt = 0.1 s^{-1}). Indeed, even if the three first samples debond by a fibrillation mode, the plateau is very short (almost no plateau for HEMA/BPA=1 and 1.5) and not very high compared to a standard PSA tested at the same debonding velocity. For the highest value of HEMA/BPA, there is no fibrillation but interfacial propagation of cracks, confirming the important crosslinking in the system. The lack of fibrillation and the very short fibrillation plateau are also consistent with the values of tanδ/G' evaluated with the rheology tests.

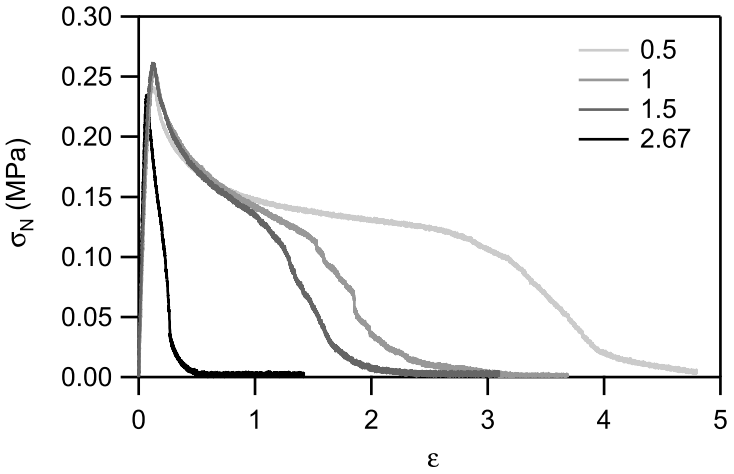

Figure 6-8 : Tack curves for samples with different HEMA/BPA ratios; Vdeb=10µm/s; OH/NCO=1

Industrial tests to characterize properties as PSA have also been performed and results are sum up in the Table 6-3, as well as the adhesion energy measured from the tack curves at V_{deb} = 10 µm.s^{-1} (i.e. dε/dt = 0.1 s^{-1}).

As a consequence of the overcrosslinking in the materials of this series, low values of adhesion energy and peel are observed. On the contrary, the highly crosslinked samples have a good cohesion and high resistance to shear are then measured. The relatively low resistance to shear of the sample with HEMA/BPA = 1 could be attributed to slippage during the test. For practical reason, this test could not be made another time and the value has to be considered carefully.

Table 6-3 : Adhesion energy for V_{deb}=10µm.s^{-1} and industrial shear and peel results

Sample	HEMA/BPA	W_{adh} (J.m^{-2})[a]	Shear resistance (min)	Peel (N/m)[b]
II_10PU(0.5)OH1	0.5	73.8	10000 ± 15 CF[c]	136 ± 47 CT[d]
II_10PU(1)OH1	1	54.7	645 ± 15 CF	164 ± 47
II_10PU(1.5)OH1	1.5	43.9	4477 - 1978 CF 1 x > 10000	132 ± 47
II_10PU(2.67)OH1	2.67	7.3	1 x 4860 CF 2 x > 10000	160 ± 47

a: for Vdeb=10µm.s-1
b: at 300mm.min-1
c: CF is for cohesive failure
d: CT is for cohesive transfer

A direct consequence of the synthesis with a semi-continuous process is the formation of an important gel fraction in the particles. This high gel fraction results in a satisfying shear resistance but peel and tack properties are lost and no optimized PSA formulation can be obtained.

6.4.1.b Comparison with a less crosslinked system

To better understand the impact of the high gel content present in this series of materials, the samples with the highest adhesion energy from this series and from the series of samples prepared in Route I (presented in the previous chapter) are compared (samples II_10PU(0.5)OH1 and I_25PU(0.11)OH0.55). Gel and swelling of both samples are reminded in Table 6-4.

Table 6-4: Gel content and swelling of two different samples

Sample	Gel content (%)	Swelling
II_10PU(0.5)OH1 Route II	63.2 ± 4	49.1 ± 7.8
I_25PU(0.11)OH0.55 Route I	36.0 ± 4.5	83.5 ± 5.9

Their probe-tack curves at V_{deb} = 10 µm.s^{-1} (Figure 6-9) indicates that both samples debond with a fibrillation mode although the more crosslinked one presents a lower maximum deformation ε_{max}. It is worth noting that the fibrillation strain σ_f (the strain for which a plateau starts to get form) is almost equivalent for both samples whereas the maximum deformation is much higher in the case of the low crosslinked system.

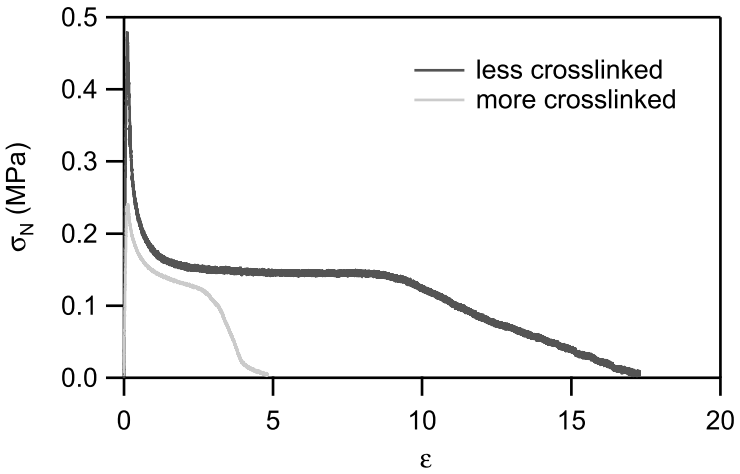

Figure 6-9: Tack curves of samples with different crosslinking; V_{deb} = 10 µm.s^{-1}

It is also interesting to note that the less crosslinked sample has a Young elastic modulus E_y of 221.8 kPa when the modulus of the more crosslinked system is 164.6 kPa. In principle, one would expect a higher elastic modulus in the case of the sample having the highest gel fraction, which is not the case.

The system with the lower gel fraction has a higher weight fraction of the highly entangled PU (25 wt% instead of 10 wt%) and a different monomer composition giving a higher T_g (-43 °C instead of -63 °C). Both reasons could explain a higher elastic modulus in spite of a lower gel fraction. The higher maximum deformation ε_{max} of the sample with the lower gel

fraction is explained by the swelling ratio which is much higher for this sample, resulting in a more deformable adhesive film.

However, if a low level of crosslinking and a high swelling ratio increase the adhesion energy of the sample, the shear resistance is, on the contrary, strongly reduced. Figure 6-10 shows the values of resistance to shear in function of the adhesion energy measured on the tack curve at Vdeb = 10 µm.s-1. The reference of a standard PSA is also indicated.

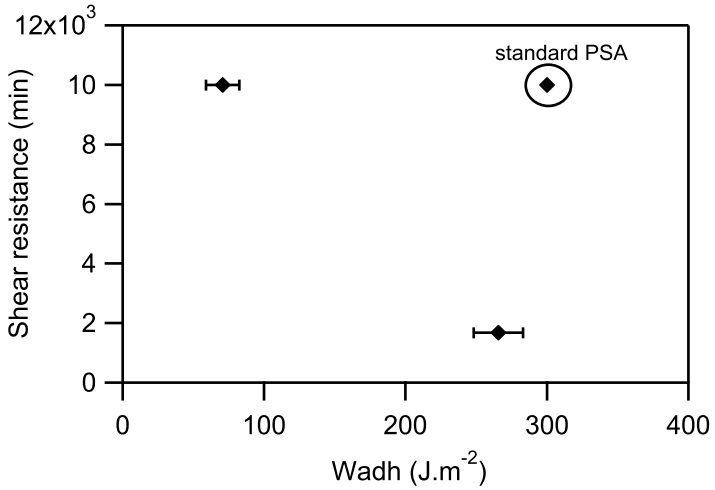

Figure 6-10: Evolution of adhesion energy with the shear resistance for samples with different crosslinking

Indeed, the shear resistance strongly decreases when the gel content decreases and swelling increases. A much better shear resistance is obtained for a sample with a gel > 60% and a swelling < 50% because of a higher C_{hard}. For small deformations as sustained during a shear resistance test, a high network density is preferable to limit disentanglement and softening. This is the case for the samples prepared in Route II and the different mechanical analyses confirm that.
However both routes result in properties inferior to those of a standard PSA.

6.4.1.c Discussion

The latexes prepared by Route II are made of particles with a high gel fraction. The resulting films have an overcrosslinked microstructure and the mechanical properties are inferior to those of a standard PSA. In particular, the samples are neither much viscoelastic nor much deformable. Several synthesis elements can explain the presence of this high gel fraction.

At first, no chain transfer agent (CTA) has been used in the formulation. The formulation of the blank latex has been optimized without CTA (the results of this latex are not presented here). Satisfying adhesive properties are obtained but the blank already has a consequent gel fraction (~ 68 %). As expected from the analysis of chapter 5, the addition of PU increases the

number of permanent and non permanent crosslinks. The hybrid latexes are thus more crosslinked than the blank.
Furthermore, the main monomer used here in the recipe is 2-ethyl hexyl acrylate (2EHA) and no butyl acrylate (BA). 2EHA was chosen to decrease the global T_g of the samples but the radical polymerization of that monomer also generates more chain transfer reactions which increases the crosslinking in the acrylic polymer network (Kohut-Svelko, Pirri *et al.*, 2009).
The values of HEMA/BPA must also be taken into account to explain the overcrosslinking. Indeed, the corresponding degrees of grafting are very high in this series. A minimum of 35 % of the PU chain ends is expected to react with HEMA what is high referring to samples prepared by Route I. Moreover, all the ingredients are mixed together with this route and the reactivity of HEMA and BPA with the isocyanate functions have to be taken in to account. HEMA is a primary alcohol and its reactivity with the isocyanate is higher compared to the one of Bisphenol A. This results in preferential reactions of PU with the grafting agent. As no limitation of the reaction of HEMA with PU could be detected with this synthesis (on the contrary to what has been discussed by Udagama (Udagama, 2009) on samples prepared by Route I), and considering that hydroxyl and isocyanate functions are in a stoechiometric ratio (OH/NCO = 1), all the HEMA is expected to react with the available PU functions. The real values of the degree of grafting should be close from the theoretical ones increasing the gel fraction.
A complementary comment can be made on the reactivity of isocyanate with water in the particles. To simplify the analysis of the polymer microstructure, we consider neither reaction between isocyanate water nor between isocyanate and amine formed by the reaction with water. It is yet known that these reactions can occur (Udagama, Graillat *et al.*), what surely modifies the polyurethane and the global polymer microstructures.

Due to the synthesis process, the role of the HEMA/BPA parameter on the PU chain length is less obvious than in the previous chapter. Nevertheless, the same effect of this parameter on the mechanical properties is observed. Indeed, the maximum deformation decreases when the ratio increases, whereas the softening remains quite constant. However, the case of the sample with the highest degree of grafting (HEMA/BPA = 2.67) has to be commented. A strong increase of the elastic modulus is noticed for this sample relatively to the three other ones. This evolution could be explained by changes in the polymer microstructure. One can indeed think that below a certain value of HEMA/BPA, there is not enough reaction of the PU with the grafting agent and the probability to form bonding chain is low. Dangling chains are preferred in the network. This polymer microstructure is inversed above a given degree of grafting and PU is bonded on both sides to the acrylic backbone. For the same degree of grafting, the presence of dangling or bonding chains in the microstructure does not change the gel fraction but increases the elastic modulus. This hypothesis could explain the strong increase of the elastic modulus after HEMA/BPA = 2.67.
The analysis of the strain rate dependence shows that for very high degree of grafting, some strain-dependent viscoelasticity appears when the degree of grafting increases. This indicates that particle-particle interfaces become weak and break at moderate strains, because of low

interpenetration between particles. This is consistent with the observation of particle morphology made in chapter 4. TEM and AFM showed homogeneous low dissipative particles when the degree of grafting is high. The high gel content affects the polymer chain interpenetration. Although the final film is homogeneous, it is probable that the interpenetration occurs on a short range. A direct consequence of low or short-range interpenetration is the weakness of the interfaces and the low deformability of the resulting film.

6.4.2 Effect of the OH/NCO ratio

Another parameter affecting the reaction of isocyanate during polymerization, and thus the polymer architecture, is the ratio between hydroxyl and isocyanate functions OH/NCO. Previously, samples were synthesized with a stoechiometric OH/NCO ratio. In this second part we compared these samples to some prepared with an excess of OH (OH/NCO = 2) for equivalent HEMA/BPA ratios. Two situations were considered: in one case, HEMA/BPA was low (0.5) and chain extension should be emphasized, in the other case, HEMA/BPA was high (around 2.5) and more grafting was expected.

6.4.2.a Experimental results

An excess of OH compared to the isocyanate in the initial formulation strongly affects the properties when a low HEMA/BPA ratio is used. Figure 6-11 and Figure 6-12 present mechanical results for HEMA/BPA = 0.5, respectively the tack curve and representations standard and Mooney of the tensile experiments, for a nominal strain rate $d\varepsilon/dt = 0.1\ s^{-1}$. The sample with stoechiometric OH/NCO is II_10PU(0.5)OH1 and the sample with an excess of OH is II_10PU(0.54)OH2.

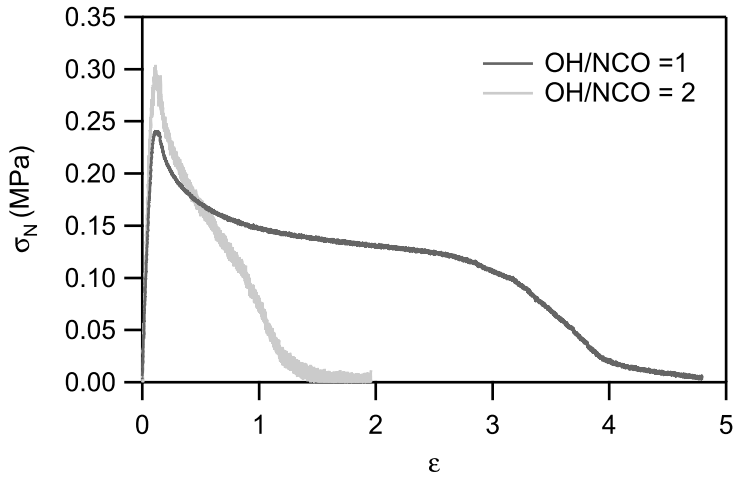

Figure 6-11 : Probe-tack curves of samples with HEMA/BPA=0.5 and different OH/NCO; $V_{deb} = 10\mu m.s^{-1}$

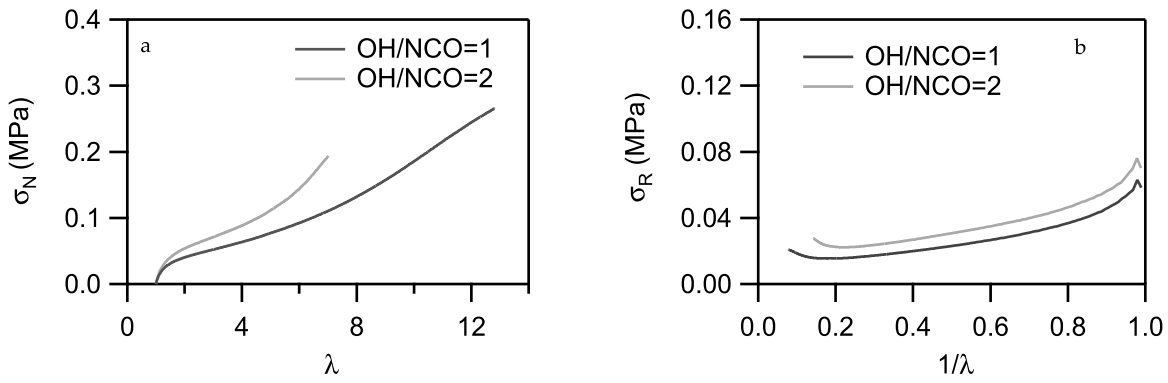

Figure 6-12: Large strains properties of samples with HEMA/BPA=0.5 and different OH/NCO: (a) nominal strain σ_N vs λ; (b) reduced stress σ_R vs 1/λ; $d\varepsilon/dt=0.1s^{-1}$

In this situation, an excess of hydroxyl functions reduces the adhesion energy and modifies the large strain tensile behavior. Concerning the debonding mechanism, a transition from fibrillation for OH/NCO = 1 to interfacial debonding for OH/NCO = 2 is observed. For an excess of OH, the hardening is more pronounced and takes place for a smaller λ_{hard} but the softening is hardly affected, as confirmed from values of Table 6-5.

Table 6-5: Viscoelastic parameters for different OH/NCO for two different HEMA/BPA; $d\varepsilon/dt=0.1s^{-1}$

Sample	OH/NCO	HEMA/BPA	C_{soft} (kPa)	C_{hard} (kPa)	C_{soft}/C_{hard}	λ_{hard}	E_y (kPa)
II_10PU(0.5)OH1	1	0.5	34.9	15.4	2.3	5.5	164.6 ± 5.8
II_10PU(0.54)OH2	2		41.8	22.2	1.9	4.5	223.3 ± 8.7
II_10PU(2.67)OH1	1	2.5	34.3	34.3	1.0	3.3	230.4 ± 25.4
II_10PU(2.32)OH2	2		63.4	18.0	3.5	4.7	287.6 ± 19.8

Although changes in large strain deformation are not that dramatic, the transition from fibrillation to interfacial debonding reflects a significant evolution in the microstructure. Indeed, the gel content is 20% higher and the swelling divided by a factor two (see Table 6-6). Increasing the cohesion this way decreases slightly the viscoelastic behavior but strongly changes the deformability of the network. The increase in the elastic modulus (see Table 6-5) is in good agreement with the transition from fibrillation to interfacial crack propagation in the probe tests.

To better understand these microstructural changes, it is worth noting that changing the OH/NCO ratio also affects the degree of grafting. Indeed, to maintain equivalent HEMA/BPA, it is necessary to increase both the HEMA and BPA quantities. Increasing the HEMA is intrinsically equivalent to an increase of the degree of grafting. If one refers to Table 6-1, 35% of the PU chain ends are supposed to be grafted for HEMA/BPA=0.5 and OH/NCO=1, and it is twice higher for OH/NCO=2. The direct consequence is the increasing of the level of crosslinking in the sample with OH/NCO=2. As the sample with

stoechiometric OH/NCO is not much viscoelastic and is in the low range of adhesive, an increase of the gel content induces the brutal change of debonding mode.

Table 6-6: Gel content and swelling values for samples with different OH/NCO ratios for two different HEMA/BPA ratios

Sample	OH/NCO	HEMA/BPA	Gel content (%)	Swelling
II_10PU(0.5)OH1	1	0.5	63.2	49.1
II_10PU(0.54)OH2	2		75.8	25.0
II_10PU(2.67)OH1	1	2.5	88.2	22.2
II_10PU(2.32)OH2	2		81.6	13.2

The results obtained for samples with a high HEMA/BPA and stoechiometric (II_10PU(2.67)OH1) or excessive (II_10PU(2.32)OH2) OH fraction are given in Figure 6-13 (tack curve at $d\varepsilon/dt = 0.1\ s^{-1}$) and Figure 6-14 (standard and Mooney curves at $d\varepsilon/dt = 0.1\ s^{-1}$). They show interesting behavior.

It is clear that both samples are much over crosslinked to present satisfying adhesive properties (see Table 6-6). However, the maximum deformation before debonding obtained from probe-tack tests varies in an opposite way relative to what was observed for the series at HEMA/BPA = 0.5. In other words, the maximum deformation is higher in the case of an excess of OH. Although in absolute values the evolution is small, relatively speaking it is significant. Furthermore, the tensile tests show that the sample softens more in situation of an excess of OH and almost no hardening is observed.

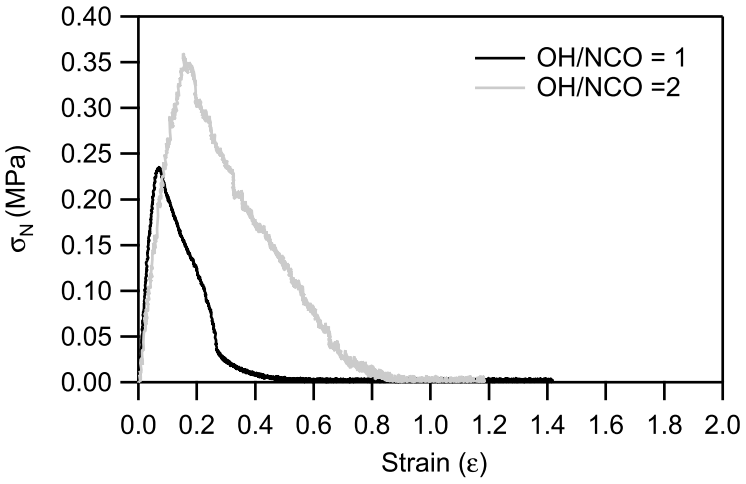

Figure 6-13: Tack curves of samples with different OH/NCO ratios and HEMA/BPA=2.5; V_{deb}=10µm.s^{-1}

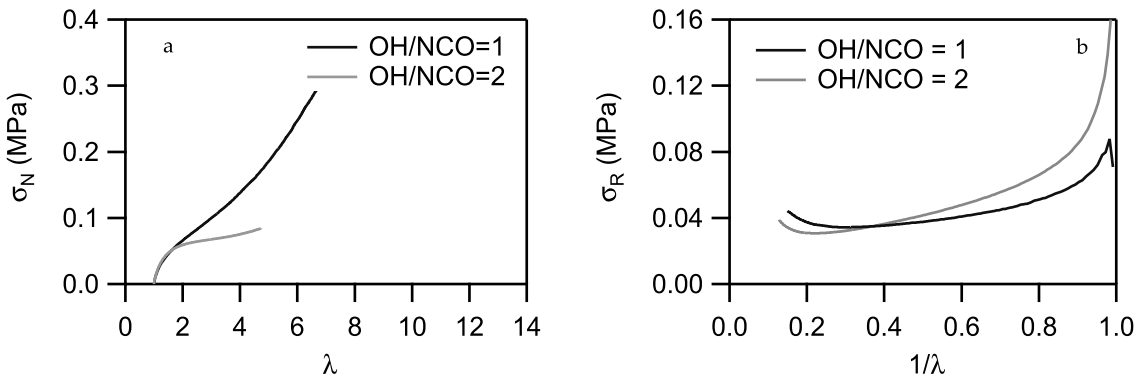

Figure 6-14: Large strains properties of samples with HEMA/BPA=2.5 and different OH/NCO: (a) nominal strain σ_N vs λ; (b) reduced stress σ_R vs $1/\lambda$; $d\varepsilon/dt=0.1s^{-1}$

As it has been explained in the previous section, the drying of the latex particles is a crucial point in the final film architecture. In the case of OH/NCO = 1, we have shown that the high gel content in the particle affects the interpenetration between particles. The tensile curve presented here for OH/NCO = 2 clearly indicates a fragile failure of the film due to weak interfaces. The swelling ratio is much lower in this case, what emphasizes the hypothesis of worse interpenetration compared to the sample with OH/NCO = 1. These weak interfaces fail under a lower stress at lower strain. Nevertheless, in the range of small strain where debonding takes place, sample II_10PU(2.32)OH2 (excess of OH) requires higher adhesion energy to debond due to the higher elastic modulus.
This is an excellent example where the combined microstructural and mechanical characterizations are necessary. If we only had the mechanics, it would have been logical to explain this softening of the OH/NCO = 2 samples at high HEMA/BPA ratio by a limit in the effective number of HEMA reacting with the PU. In the previous chapter a maximum of 20 % of HEMA hydroxyl functions reacted with isocyanate. For the series where all ingredients are mixed together, such a limitation would have favored chain extension, softening the particles. The swelling ratio of the gel fraction however invalidates this hypothesis.

6.4.2.b Discussion

The ratio between isocyanate and alcohol is as much important as the ratio between extension and grafting. Even if HEMA/BPA ratios are kept constant, changes in the degree of grafting modifies the polymer architecture.
An excess of OH (OH/NCO = 2) doubles the grafting ratio with logical consequence of a more cohesive sample. In the case of low HEMA/BPA, the increased grafting leads to a transition from fibrillation to interfacial crack propagation decreasing the adhesion energy. In the case of very high HEMA/BPA, the increase in the crosslinking leads to weaker interfaces between particles and to an apparent softening of the adhesive film. The low cohesion is however apparent from the tensile tests results and adhesive properties remain very poor.

6.5 Conclusion

With the objective to scale up the production of urethane/acrylic hybrid particles for adhesive applications, latexes have been produced with synthesis conditions close to the ones used in the industry. Mechanical properties of the films obtained from these latexes have been studied by combination of rheology, tensile and probe-tack tests. Tensile experiments have been performed at two different nominal strain rates to analyze the large-strain relaxation through the decorrelation of strain and strain-rate dependent processes. We also measured the gel content and the swelling of the polymer network to establish correlation between the properties and the polymer microstructure.

All films studied in this chapter show overcrosslinked polymer network compared to standard PSAs. This high gel fraction can be explained by several synthesis parameters. First, the choices of 2EHA instead of BPA and the lack of chain transfer agent result in an increase of the crosslinking of the acrylic network during radical polymerization.

Secondly, no limitation of the reaction between PU and HEMA was detected and high HEMA weight fractions are used in the particles. The resulting degree of grafting of PU can increase the crosslinking of the PU fraction.

A consequence of the one-step process is that the reactivity of the grafting agent HEMA and chain extender BPA with the isocyanate NCO impact on the polyurethane organization. The relationship between HEMA/BPA and the PU chain length is less simple to establish than when the PU is reacted with HEMA and then BPA before radical polymerization. Nevertheless, when a stoechiometric OH/NCO ratio (i.e. OH/NCO = 1) is used, the effect of HEMA/BPA is similar as in the previous chapter, i.e. an increase of HEMA/BPA decreases the maximum extension of the global network. The particular values of elastic modulus obtained for the highest value of HEMA/BPA make us think that the formation of bonding chains is favored in this situation, whereas dangling chains are preferred for lower values of HEMA/BPA.

The comparison of samples with OH/NCO = 1 and with OH/NCO =2 gives interesting results. The excess of OH results in a higher HEMA weight fraction in the latex recipe and the crosslinking does increase. However, with high values of HEMA/BPA, a softening of the sample is observed with an excess of OH. The complex results obtained for these latexes show the real help brought by the analysis of the polymer microstructure to understand the mechanical properties.

On an industrial point of view, the samples present very satisfying resistance to shear but the balance with the adhesive properties is not optimized yet.

6.6 References

- Asua, J. M.; *Progress in Polymer Science*; **2002**; *27*; (7); 1283-1346.
- Baron, A., Rodriguez-Hernandez, J.,Papon, E.; *Macromolecular Chemistry and Physics*; **2005**; *206*; (23); 2381-2389.
- Creton, C.; *MRS Bulletin*; **2003**; *28*; (6); 434-439.
- Dahlquist, C. A.; *Treatise on Adhesion and Adhesives*; Patrick, R. L., Dekker; **1969**; *2;* 219-260.
- Deplace, F.; *Adhésifs Nanostructurés en Voie Emulsion*; PPMD: Paris; **2008.**
- Deplace, F., Carelli, C., Mariot, S., Retsos, H., Chateauminois, A., Ouzineb, K.,Creton, C.; *Journal of Adhesion*; **2009**; *85*; 18-54.
- *FINAT Technical Handbook*; **2005**.
- Gooch, J. W., Dong, H.,Schork, F. J.; *Journal of Applied Polymer Science*; **2000**; *76*; (1); 105-114.
- Kohut-Svelko, N., Pirri, R., Asua, J. M.,Leiza, J. R.; *Macromolecular Reaction Engineering*; **2009**; *3*; (1); 11-15.
- Lakrout, H., Sergot, P.,Creton, C.; *Journal of Adhesion*; **1999**; *69*; (3/4); 307-359.
- Landfester, K.; *Macromolecular Rapid Communications*; **2001**; *22*; (12); 896-936.
- Li, M., Daniel, E. S., Dimonie, Sudol, E. D.,El-Aasser, M. S.; *Macromolecules*; **2005**; *38*; 4183-4192.
- Lopez, A.; POLYMAT: San Sebastian; **2009.**
- Satas, D.; *Handbook of pressure-sensitive-adhesives*; Satas, D.: New York, Van Nostrand Reinhold; **1989**; *1;* 396-456.
- Udagama, R.; *Synthesis of polymer-polymer hybrids by miniemulsion polymerization and characterization of hybrid latex*; Laboratoire de Chimie, Catalyse, Polymères et Procédés: Lyon; **2009.**
- Udagama, R., Graillat, C., Degrandi, E., Creton, C., Bourgeat-Lami, E.,McKenna, T.; *To be published*.
- Wang, C., Chu, F., Graillat, C.,Guyot, A.; *Polymer Reaction Engineering*; **2003**; *11*; (3); 541-562.

7. ANALYSIS OF THE CREEP RESISTANCE OF PSA

7.1 Introduction

Pressure sensitive adhesives (PSA) are based on soft viscoelastic polymers with well balanced properties of peel, tack and shear resistance. Indeed, an optimized PSA must have a high energy of adhesion during debonding by a tack test, a high peel force when the adhesive is peeled from a substrate and a high resistance to shear when a static load is applied (Creton, 2003).

Over the recent years, efforts have been made to establish correlations between the peel force and the linear viscoelastic properties of the adhesives (Derail, Allal *et al.*, 1997; Derail, Allal *et al.*, 1999). Along the same lines, the role played by rheological properties on tackiness has been studied and discussed (Verdier and Piau, 2003; Nase, Lindner *et al.*, 2008). In chapters 5 and 6, we presented an effective criteria based on the rheological phase angle tanδ and storage modulus G' to predict the debonding mode during a tack test (Carelli, Deplace *et al.*, 2007; Nase, Lindner *et al.*, 2008; Deplace, Carelli *et al.*, 2009). Moreover, relationship can be established between the mechanisms involved in peel and tack tests (Kaelble, 1965; Creton and Fabre, 2002). Both tests involve large deformations of the adhesive at relatively high strain rates and these short-times, high strain rate failure mechanisms are now reasonably well understood for viscoelastic layers.

The long-time low strain-rate behavior has been less studied for this type of materials whereas we know that not only tack and peel but also resistance to shear must be optimized in a pressure-sensitive adhesive. In particular, the holding time (the time before an adhesive fails from a substrate when a constant weight is applied) must be as high as possible. But the shear tests can be long (for example FINAT test method recommends a holding time of 10000 min to validate the shear resistance of a PSA) and this is a major motivation to try to find a criteria for shear resistance based on the viscoelastic properties of the materials.

Typical tests to measure shear resistance are very simple (a weight is fixed to the adhesive layer and the holding time is measured) but do not allow any precise measurement of the deformation and failure mechanisms in the adhesive layer. Some studies have been performed on PSA to overcome these limitations. Zosel, for example, developed in 1994 (Zosel, 1994) a specific static shear test with the goal to correlate the results with rheological properties of the adhesive layer. He established that for low-viscosity samples (with zero shear viscosity η_0 in the range of $2.5\ 10^5$ Pa.s), satisfying predictions of the holding time are obtained from the dynamic viscosity of the polymer. When PSA are highly-branched or slightly crosslinked, a further study by Vaynberg (Vaynberg, Berta *et al.*, 2001) showed that a power law constitutive equation for the viscosity is more accurate to predict shear resistance of highly viscous PSA.

More recently, Lindner and coworkers (Lindner, Maevis *et al.*, 2004) focused on failure mechanisms in the long time range. They studied the behavior of confined adhesive layers placed in a probe-tack test geometry. The adhesive was pulled and then kept under load for a given time thanks to a spring. Deformation was measured as a function of time and a video set-up allowed the observation of the failure mechanism. They noticed that two specific mechanisms are in competition during this long term loading: additional cavities nucleation

(creation of additional high strain zones) and growth of existing cavities along the polymer/probe interface, but no homogeneous creep was observed. In their geometry, they could also study the creep in the fibrils formed during the tack test which are a under tensile load.

With the objective to better understand the behavior of the materials at very low strain-rate, we developed here the most appropriate parameters for a creep experiment designed for PSA films. The tensile geometry was preferred to single or double lap-shear to compare the mechanisms to those observed in typical high strain-rate tensile tests.

Specific studies focused on the long-time creep behavior of an adhesive under constant load but these studies applied to structural adhesives such as epoxy (Dean, 2007) or fiber reinforced composites (Ashcroft, Hughes *et al.*, 2001) in single or double lap-shear geometries. Few reports could be found on creep in tensile geometries. Wang and Thompson (Wang, Thompson *et al.*, 2001) used a DMA apparatus to study the creep behavior in a tensile geometry and they used the Burgers model to describe their data. Their work focused on elastomers, i.e. materials more crosslinked than materials used as PSA. The same type of work has been carried out by a German team (Gleiss and Brockmann, 1997) on pressure-sensitive tapes and they obtained a satisfying description of the creep behavior with this model.

The implementation of the test is presented in a first part of the chapter. We detailed the influence of the different experimental parameters and we explained the final choices for the set-up. The creep experiments have been performed on both PSA systems described in chapters 5 and 6. We detailed the possible interpretation of the creep data and explained the use of the Burgers model. In the end we focus in particular on the differences between urethane/acrylic hybrid and pure acrylic samples. Indeed, if a satisfying correlation is observed between the holding time and the creep for most of the samples, this specific case proves that rheological properties must also be taken in account to predict the long-time low-strain rate behavior of samples.

7.2 Materials

The tensile creep experiment we developed was used on two series of samples. The first series, described in

Table 7-1, was synthesized by Route I. Three samples had varying weight fractions of PU with a constant degree of grafting and the three others had a fixed weight fraction of PU with different degrees of grafting. More data concerning synthesis can be found in chapter 2 and the mechanical characterization of these samples was presented in chapter 5.

Table 7-1: Main parameters of samples synthesized in Route I

Sample	% PU	HEMA/BPA	OH/NCO
I_5PU(0.22)OH0.55	5	0.22	0.55
I_25PU(0.22)OH0.55	25	↓	↓
I_50PU(0.22)OH0.55	50	↓	↓
I_25PU(0.11)OH0.55	25	0.11	↓
I_25PU(0.36)OH0.55	↓	0.36	↓
I_25PU(0.50)OH0.55	↓	0.50	↓

The second series consisted of samples prepared by Route II. It has been shown in chapter 6 that the synthesis process used in route II produces higher gel content than for samples prepared by route I. The influence of such gel content on the creep behavior was studied. The main mechanical properties of these samples are recalled in Table 7-2 :

Table 7-2 Main parameters of samples prepared in Route II

Sample	% PU	HEMA/BPA	OH/NCO
II_0PU(0)OH0	0	/	/
II_10PU(0.5)OH1	10	0.5	1
II_10PU(1)OH1	↓	1	↓
II_10PU(1.5)OH1	↓	1.5	↓
II_10PU(2.67)OH1	↓	2.67	↓

7.3 Development of a creep test for soft viscoelastic solids

7.3.1 Set-up of the creep experiments

The creep experiments have been performed on the same INSTRON machine (model 5565 equipped with a videoextensometer SVE) than the tensile tests presented before and the same self-supported adhesive strips were used. A given stress is applied to the sample in a tensile geometry at a defined loading rate for a given time (Figure 7-1 (a)). For practical reasons, the duration of the tests has been limited to 1800s, but for selected samples a constant stress has been applied until failure of the sample. The choices of the stress level and initial loading rate are detailed in the next section.
The raw data of the force and the displacement during the tests can be processed to obtain a strain ε *vs* time *t* curve. The logarithmic representation is generally preferred as in Figure 7-1 (b).

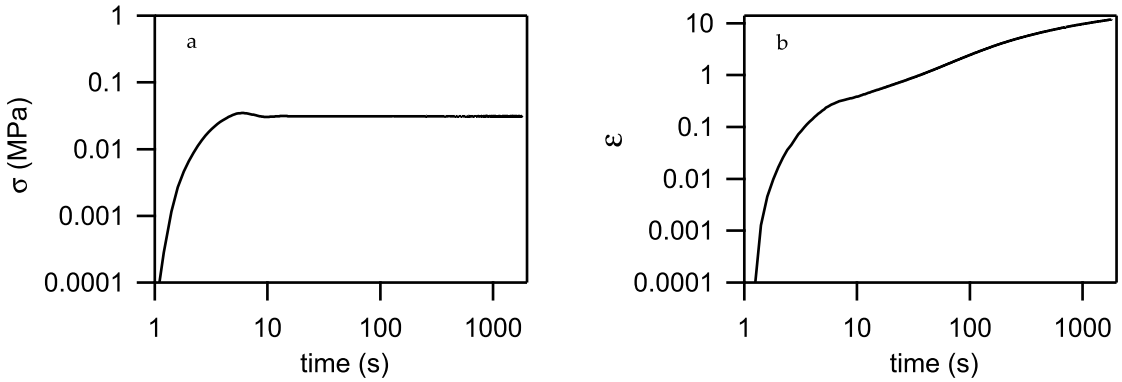

Figure 7-1: Examples of curves obtained with a creep experiment; (a) stress vs time; (b) strain vs time

7.3.2 Choice of the experimental parameters

Although ideally a creep test should consist of an instantaneous loading to a given stress which is then maintained constant for a preset time, in reality the initial loading rate cannot be infinite and has to be carefully chosen.
Figure 7-2 represents the evolution of ε *vs* time for the same sample with different loading rate but with the same final stress (left) or loaded at different level of stress at a fixed initial loading rate (right).

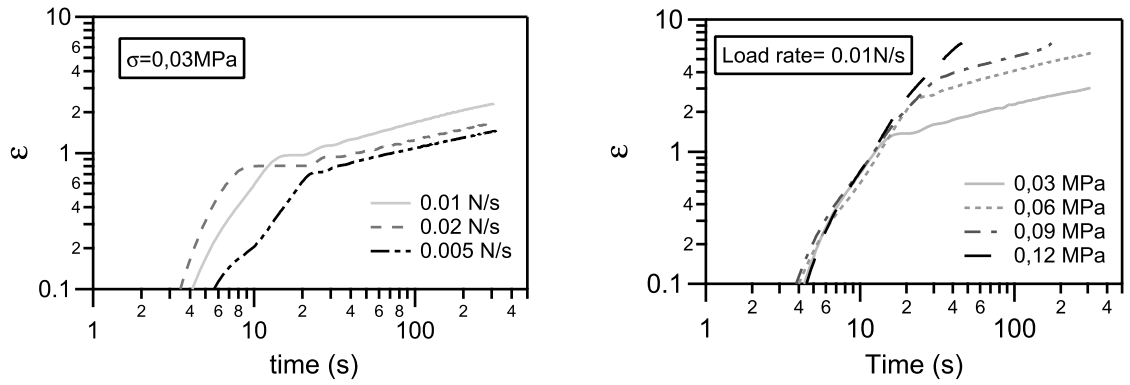

Figure 7-2: Effect of the loading (left) and of the loading rate (right) on the creep behavior

It can be seen on these curves that a certain time (around 50 s) is required to reach the preset load and to stabilize the stress so that the load is not instantaneously applied to the sample. Nevertheless, curves on the left show that the loading rate has little influence on the strain at the beginning of the stabilization. The time required for the stabilization of the strain is not influenced by the loading rate either. When a high loading rate is employed (0.02 N/s) it takes less time to reach the creep stress but the applied load (and the strain) requires a longer time to stabilize. When the loading rate is lower (0.005 N/s), it takes a longer time to reach the preset load but the stabilization of the load (and then of the strain) happens faster. Finally, the highest loading rate (0.02 N/s) was chosen for the test to be as close as possible to instantaneous loading and to limit relaxation before the beginning of the creep process.

If the initial loading rate is kept constant but the preset stress is varied (Figure 7-2-right), ε at the beginning of the creep test varies. For the highest stress value tested here, one can even detect the failure of the sample before stabilization occurs.

To understand this, one has to refer to the standard tensile curve shown in Figure 7-3 where the corresponding stresses applied in the tests of Figure 7-2-right) are represented. If the preset load is higher than the softening point, the sample starts to deform more and may even fail rapidly.

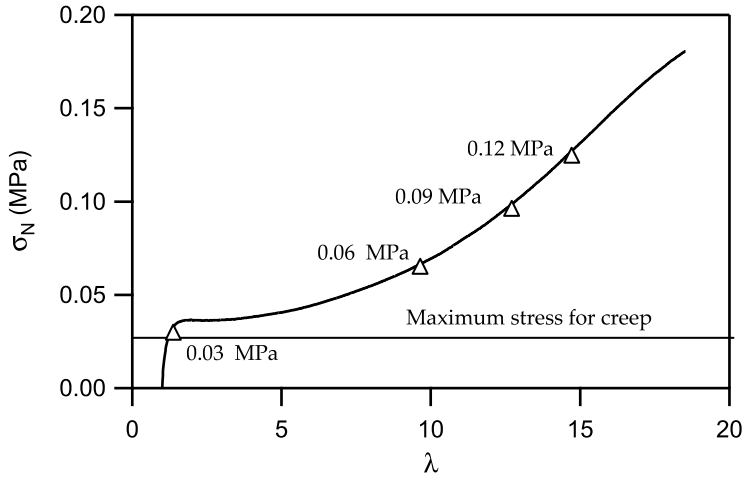

Figure 7-3: Upper limit for the stress level: the creep stress mustn't be higher than the softening stress

Our goal is not of course to cause rapid failure which would be akin to perform a simple tensile test but to analyze the creep process. For this, it is important to be below the softening point. Considering the initial strain rate which we used during the loading phase of the creep test, the tensile experiment at $d\varepsilon/dt = 0.1\ s^{-1}$ must used to determine the softening point. Finally, a stress lower than the softening stress σ_S was chosen.
However, due to limitation on the load cell which cannot maintain a fixed force low below 0.1 N and considering the geometry of our samples, a stress of 0.03 MPa was chosen for all the tests, checking that this corresponds to a stress inferior to the softening point. The experimental parameters chosen for the tests are listed in table below:

Table 7-3: Experimental parameters for the creep tests

Load rate	0.02 N/s
Creep stress	0.03 MPa
Creep time[a]	1800 s

a: with exception for selected samples where load were maintained until failure

7.3.3 Interpretation of the results

Creep tests are typically represented as $\varepsilon(t)$ for a fixed applied stress. One model has been found in the literature that describes well the behavior of viscoelastic materials under creep, known as the Burger's model (Gleiss and Brockmann, 1997; Wang, Thompson et al., 2001). As all linear viscoelastic models, the Burgers model is based on the addition in series and in parallel of Hookean springs and Newtonian dashpots. It is based on a Kelvin-Voigt model which is constituted of a spring and a dashpot in parallel and which is known to describe well the creep in viscoelastic materials (Ferry, 1980). A Hookean spring and a Newtonian dashpot are added in series to the Kelvin-Voigt model to improve the simple Voigt model (Figure 7-4 -right).
The three elements can be associated to the different phases of the creep test. At the beginning of the loading, the sample is in the regime of the small strains and the elastic behavior dominates. The Hookean spring corresponds to that regime. In the domain of intermediate strains the viscoelastic behavior, described by the Kelvin-Voigt model, dominates. It corresponds to the appearance of the relaxation process in the sample. Finally, when the load has stabilized, a constant creep stress is imposed to the sample and the viscoelastic element reaches its equilibrium and its maximum deformation. In the last stage, the material deformation is pure creep that can be associated to the Newtonian dashpot at large strains.

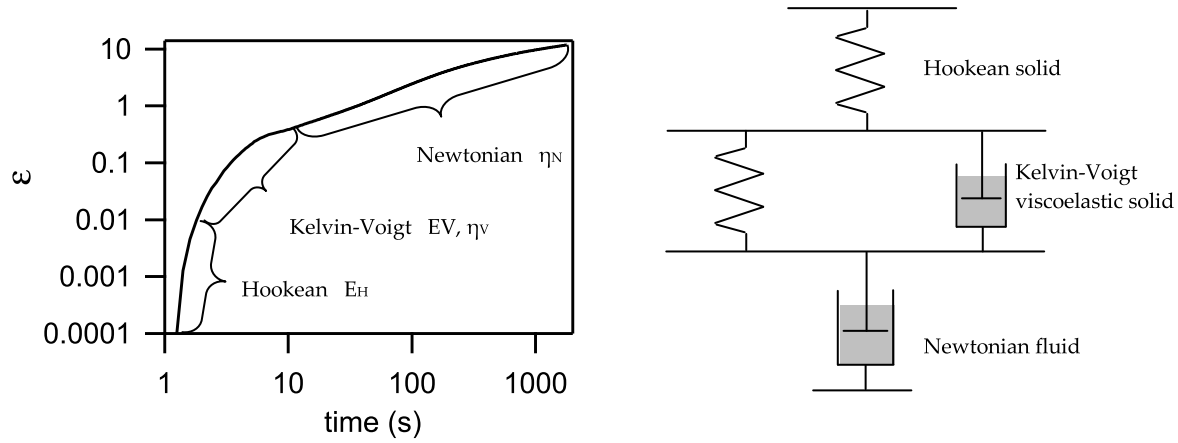

Figure 7-4: Analysis of the creep curve with the Burger's model and schematic of this model

Based on this representation, it is possible to establish a relationship between the strain ε and the time t. The stress-strain response of an ideal spring follows Hooke's law: the magnitude of the stress is directly proportional to the strain.

$$\sigma_H = E\ \varepsilon_H \qquad \textbf{Eq. 7-1}$$

The coefficient E is the spring constant and represents its elasticity. On the other side, the response of an ideal dashpot can be written according to the Newtonian law:

$$\sigma_N = \eta \frac{d\varepsilon_N}{dt} \qquad \textbf{Eq. 7-2}$$

where η is the dynamic viscosity and $d\varepsilon_N/dt$ the strain rate. One can make the assumption that a constant load results in a constant strain rate in the case of an ideal dashpot. Equation 7-2 then becomes:

$$\varepsilon_N = \frac{\sigma_N t}{\eta} \qquad \textbf{Eq. 7-3}$$

The viscoelastic model of Kelvin-Voigt, the central element of the Burger's model, combines a spring and a dashpot in parallel. This means that strain is the same in both elements whereas the stress is the sum of Newtonian stress σ_N and the Hookean stress σ_H, as seen below.

$$\varepsilon_V = \varepsilon_H = \varepsilon_N \qquad \textbf{Eq. 7-4}$$

$$\sigma_V = \sigma_H + \sigma_N \qquad \textbf{Eq. 7-5}$$

The differential equation of the Kelvin-Voigt model is obtained from equations 7-1 and 7-2:

$$\sigma_V = E\varepsilon_H + \eta \frac{d\varepsilon_N}{dt} \qquad \textbf{Eq. 7-6}$$

It gives the final expression of the strain as a function of time:

$$\varepsilon_V = \frac{\sigma_V}{E}\left(1 - \exp\left(-\frac{Et}{\eta}\right)\right) \qquad \textbf{Eq. 7-7}$$

The Burgers model is a combination of a Hookean spring, a Newtonian dashpot and a Kelvin-Voigt model in series. The final strain is the sum of the strains of the three elements:

$$\varepsilon_B = \varepsilon_H + \varepsilon_N + \varepsilon_V \qquad \textbf{Eq. 7-8}$$

The final expression of the strain according to the time in the Burgers model is:

$$\varepsilon_B = \frac{\sigma}{E_H} + \frac{\sigma}{E_V}\left[1 - \exp\left(-\frac{E_V t}{\eta_V}\right)\right] + \frac{\sigma t}{\eta_N} \qquad \textbf{Eq. 7-9}$$

The stress is kept constant in all elements. The model has four adjustable parameters and corresponds to a constant stress applied at the beginning of the creep test. Before analyzing the creep results and the consistency with the model, it is useful to make some comments on the physical interpretation of these four parameters.

Physical interpretation of the Burgers parameters:

- E_H corresponds to the elastic modulus at small strains. No relaxation has started at this point and the permanent and non-permanent crosslinks affect this parameter. The higher E_H is, the smaller the deformation at the end of the elastic stage. It is worth noting that in the theoretical Burgers model, the stress is applied instantaneously and is constant in the whole creep test. In our case, it is not possible, for technical reasons, to apply an instantaneous stress. During the first elastic part σ increases continuously with time. Nevertheless, E_H determines the strain level at the end of the pure elastic regime.

- E_V and η_V are viscoelastic parameters and they correspond to the viscoelastic creep in the polymer. They are connected by the definition of the retardation time by $\tau_V=\eta_V/E_V$. The longer the relaxation time is, the longer is the viscoelastic stage of the creep. This viscoelastic stage is correlated with the non-permanent crosslinks (or entanglements) that reorganize themselves and with the viscoelastic behavior of the soluble free chains that flow under stress.

- η_N is a classical viscosity characterizing the long-time relaxation in the sample. It corresponds to the pure creep phase of the test.

The raw data of the deformation *vs* time are fitted with the model with the Igor software and the four Burger's parameters are the ones that better adjust the fit to the data. It is worth noting that the evolution of the stress with time during the first loading stage is taken into account for the fitting.

7.4 Creep behavior of model systems

To facilitate the interpretation, the creep results obtained on samples prepared by Route I are first presented. The polymer architecture of these samples is well controlled and the effects of the composition parameters are clear. The density of the permanent and non permanent crosslinks increases markedly when the PU increases and the HEMA/BPA ratio affects mostly the gel part with a network tighter and tighter when the ratio increases. The creep behavior according to these two parameters is studied first.

7.4.1 Impact of the fraction of PU weight fraction on the creep behavior

The main results for the samples with varying PU weight fraction are recalled in Figure 7-5 and Table 7-4. One can see that the higher the PU fraction, the stiffer and less deformable is the sample. This has been explained in chapter 5 by an increase of the number of both permanent and non-permanent crosslinks when the PU weight fraction increases.

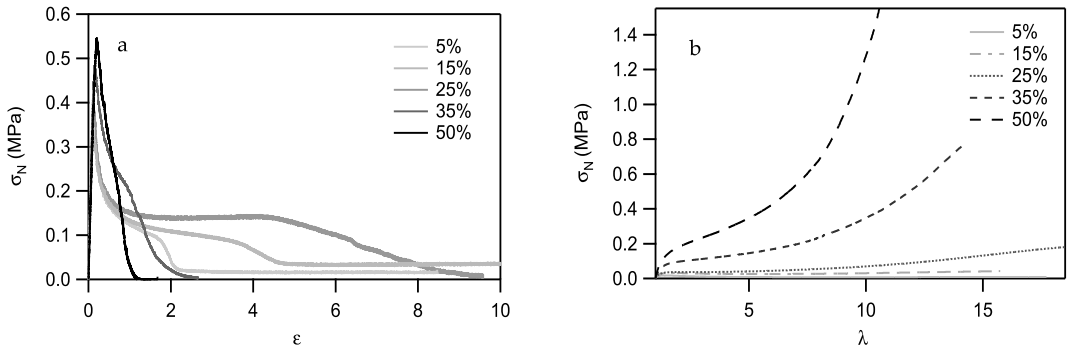

Figure 7-5: Results for different PU fractions; (a) tack with V_{deb}=10µm.s^{-1}; (b) tensile with dε/dt=0.1s^{-1}

Table 7-4 : Values of the main mechanical parameters measured for different PU weight fraction

Sample	wt% PU	E_y (kPa)[a]	C_{soft} (kPa)[a]	λ_{hard}[a]	Resistance to shear (min)[b]
I_5PU(0.22)OH0.55	5	261.2 ± 26.5	36.8	17.8	46 ± 15 CF[c]
I_25PU(0.22)OH0.55	25	320.4 ± 34.8	59.2	9.2	9463 ± 15 CF
I_50PU(0.22)OH0.55	50	757.3 ± 75.8	146.4	5.2	> 10000

a: for an initial strain rate dε/dt = 0.1 s^{-1}
b: measured by CYTEC Surface Specialties according to the FINAT methodology
c: CF is for Cohesive Failure of the adhesive layer

Creep results (Figure 7-6) are consistent with these high strain rate mechanical properties. For the same applied stress, when the weight fraction of PU increases, the maximum deformation reached during the test is divided by a factor close to 1000 (at t = 50 s). For the sample with 5 wt% PU, the creep test is aborted very early due to sample failure. When 5

wt% of PU are added to the acrylic matrix, the sample flows instead of hardening at large strain, due to low level of crosslinking. The stress σ = 0.03 MPa is much higher than the softening stress, and the sample cannot sustain such a high stress. Other tests have been carried out at σ = 0.015 MPa (lower than the softening stress) and results are presented below. Even if the creep is lower with this stress, there is still an early catastrophic failure of the sample compared to samples with higher PU wt%.

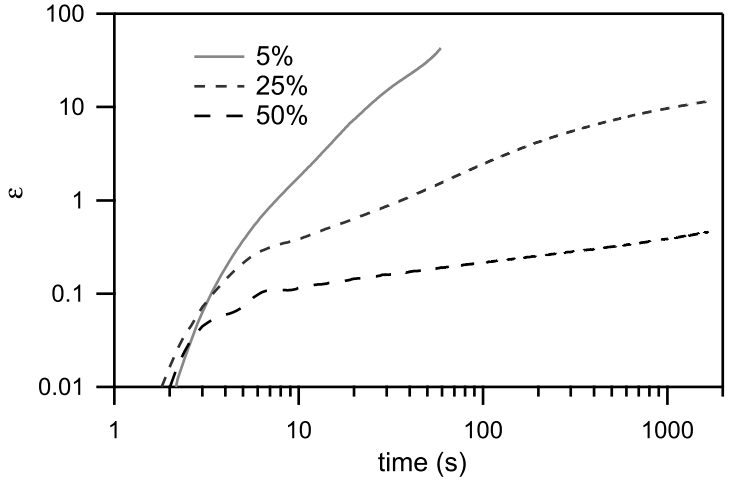

Figure 7-6: Creep behavior of samples with different PU fraction; σ=0.03 MPa; V=0.02 N.s-1

The Burger's model has been applied to the data. Examples of the quality of the fit are given for two PU weight fractions in Figure 7-7. For the sample with 5 wt% of PU, results are shown for σ = 0.03 MPa (Figure 7-7 (b)) and σ = 0.015 MPa (Figure 7-7 (c)). The Burgers model fits well the data from t > 10 s until the end of the test in the case of 50 wt% of PU and 5 wt% of PU when σ = 0.015 MPa.

For σ = 0.03 MPa and 5 wt%, there is almost no coincidence between the curve and the fit. This is because this sample is very lightly crosslinked and starts to flow for a level of stress lower than the one applied, which is higher than the softening stress (see Figure 7-5 (b)).

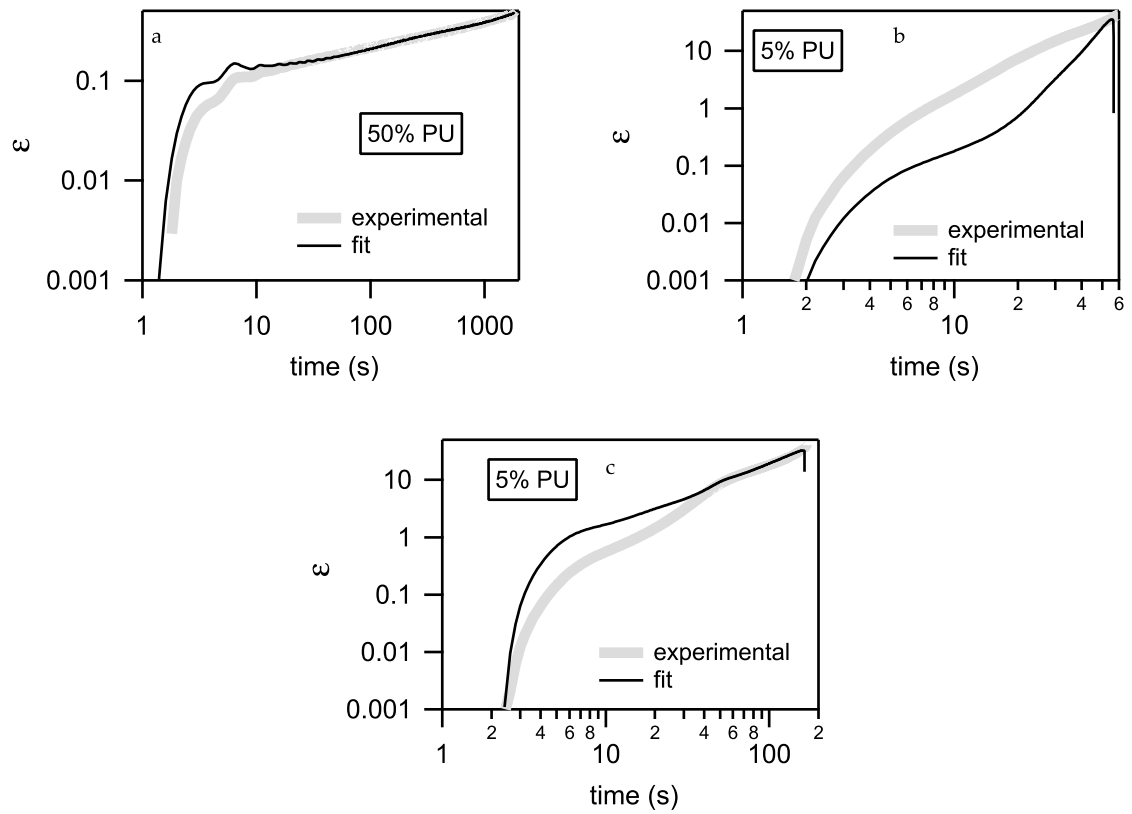

Figure 7-7: Comparison between experimental results and fit with the Burger's model for different PU weight fractions and different stress level; (a) sample I_50PU(0.22)OH0.55 with 50 wt% PU and σ=0.03 MPa; (b) sample I_5PU(0.22)OH0.55 with 5 wt% PU and σ=0.03 MPa; (c) sample I_5PU(0.22)OH0.55 with 5 wt% PU and σ= 0.015 MPa

The Burgers parameters obtained from the fits are given in Table 7-5. The increasing elastic moduli and viscosities reflect well the decreasing ε as PU increases. For 50 wt% and 25 wt%, numerical values of the viscosities are in the range of those expected for soft polymers and the moduli are in the range of values obtained with rheology and tensile experiments (see chapter 5, Table 5-3). For 5 wt% of PU, low values of viscosities are consistent with the liquid behavior. Nevertheless, the unphysical value of E_H and E_V are questionable given the gap between the data and the fit.

Table 7-5: Burger's parameters obtained for different PU wt% for σ = 0.03 MPa (except sample with 5 wt% where σ = 0.015 MPa)

Sample	% PU	E_H (kPa)	E_V (kPa)	η_V (Mpa.s)	η_N (MPa.s)
I_5PU(0.22)OH0.55	5 % (for σ=0.015 MPa)	20 746 (± 2560)	-6.36 (± 21.9)	0.57 (± 1.3)	0.18 (± 0.15)
I_25PU(0.22)OH0.55	25 %	159.91 (± 0.303)	4.27 (± 0.038)	1.33 (± 0.0019)	12.55 (± 0.024)
I_50PU(0.22)OH0.55	50 %	245.22 (± 0.677)	222.622 (± 0.538)	33.76 (± 0.21)	276.79 (± 0.38)

We also calculate the retardation time τ_V, defined as η_V/E_V. This decrease opposite to the increase of the PU weight fraction is in agreement with the mechanical results. The higher the PU weight fraction is, the less viscoelastic is the sample and the faster are the molecular relaxation processes affecting the retardation time. Again, the negative value obtained for the lowest PU weight fraction does not have physical meaning if we consider that the sample starts to flow before the stabilization of the preset load.

Table 7-6 : Values of the retardation time for different PU weight fractions

Sample	% PU	τ_V (s)
I_5PU(0.22)OH0.55	5 % (for σ=0.015 MPa)	-89.52
I_25PU(0.22)OH0.55	25 %	312.41
I_50PU(0.22)OH0.55	50 %	151.66

7.4.2 Impact of the grafting of the PU chains

In the chapter 5, we observed that the degree of grafting of the polyurethane on the acrylic backbone affects above all the large strain properties compared to the small strain elastic modulus. This parameter can be used to improve the resistance to shear while keeping a satisfying level of adhesion (Figure 7-8 and Table 7-7).

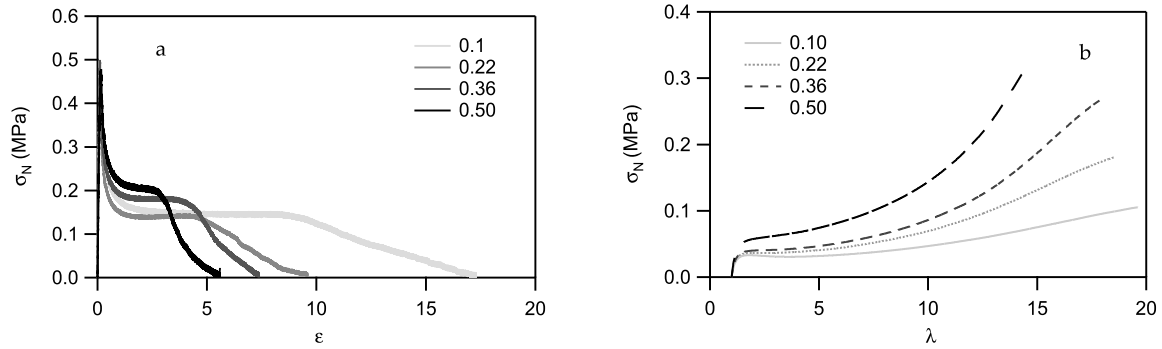

Figure 7-8: Samples prepared in Route I; Results for different HEMA/BPA ratios: (a) tack with V_{deb}=10µm.s^{-1} and (b) tensile with dε/dt=0.1s^{-1}

Table 7-7 : Values of the main mechanical parameters for different HEMA/BPA ratios

Sample	HEMA/BPA	E_y (kPa)[a]	C_{soft} (kPa)[a]	λ_{hard}[a]	Resistance to shear (min)[b]
I_25PU(0.10)OH0.55	0.10	283.5 ± 24.1	55.5	10.5	181 ± 15 CF[c]
I_25PU(0.22)OH0.55	0.22	320.4 ± 34.8	59.2	9.22	9463 ± 15 CF
I_25PU(0.36)OH0.55	0.36	338.4 ± 32.7	62.4	8.4	> 1000
I_25PU(0.50)OH0.55	0.50	392.4 ± 27.5	81.5	7.6	ND[d]

a: for nominal strain rate dε/dt = 0.1 s^{-1}
b: measured by CYTEC Surface Specialties according to the FINAT methodology
c: CF is for Cohesive Failure of the adhesive layer
d: No value for this sample

Creep experiments have been made in the same conditions as for the previous series (σ = 0.03 MPa, t = 1800 s) and are presented in Figure 7-9. For all samples, we are below the softening stress. When the HEMA/BPA ratio increases, which is equivalent to an increase of the degree of grafting, the sample is less deformable and hardens at a lower strain in the uniaxial tensile tests. Consistent with this result, the time dependent strain in the creep experiment decreases when the HEMA/BPA ratio increases.
The tensile experiments on this series showed that the change in the degree of grafting of the PU impacted above all the strain hardening part of the curve. The comparison between high and low strain rates tensile tests (figure 5-19) did not show very consistent differences. At low grafting there was less strain rate dependence than at high grafting. The strain rates were however quite high (between 10^{0} s^{-1} and 10^{-1} s^{-1}). In the creep experiments the typical strain rates are of the order 10^{-2} s^{-1} or below and in this range, it is clear that a higher grafting degree slows down the strain rate significantly. The time to reach 200 % strain at an applied stress of 30 kPa varies from 30 seconds to 500 seconds when HEMA/BPA increases from 0.1 to 0.5.

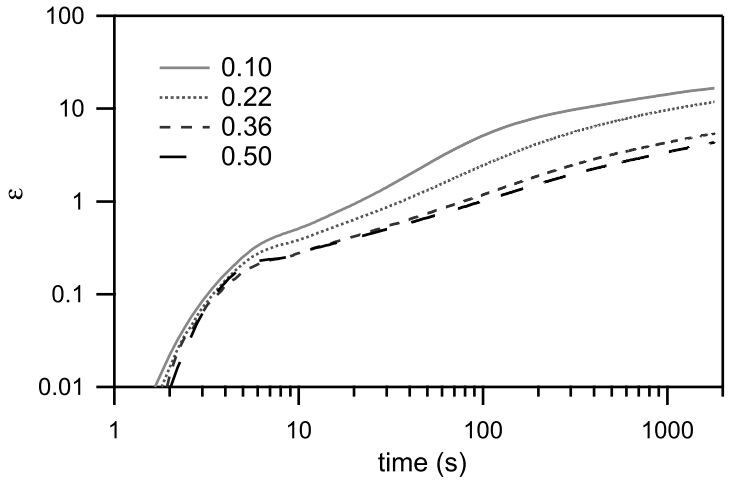

Figure 7-9: Creep behavior for samples with different ratios HEMA/BPA; σ = 0.03MPa; V = 0.02N.s^{-1}

The Burger's model also fits properly the data mainly after the ten first seconds and the relevant values obtained from the Burger's fit are presented in Table 7-8.
A quick analysis of Figure 7-10 shows qualitatively equivalent results to those presented previously for the effect of the PU weight fraction: the stiffer the material is and the better the model can fit the data. Nevertheless, the interpretation of the results from this series of samples is more complex. The effect of the degree of grafting is more subtle relative to the effect of the PU fraction and impacts above all the large strain properties and finite extensibility of the network.

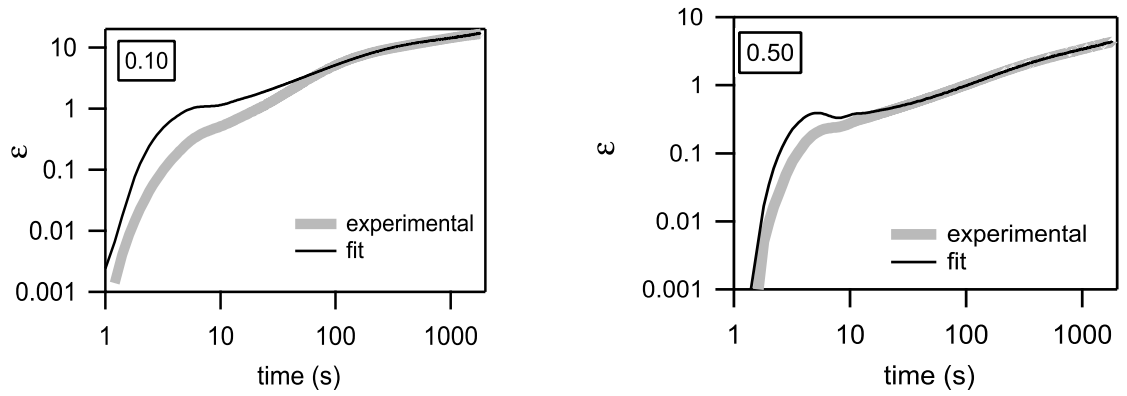

Figure 7-10: Experimental results and fit with the Burger's model for HEMA/BPA = 0.10 (sample I_25PU(0.11)OH0.55 on the left) and HEMA/BPA = 0.50 (sample I_25PU(0.5)OH0.55 on the right); $\sigma = 0.03$ MPa

The analysis of the Burgers fit shows that the most important parameters controlling the time dependence are the parameters of the Kelvin-Voigt element E_v and η_v which fit the central part of the creep curve. What is clear is that the elastic stiffness of the Voigt element increases significantly with grafting whereas the retardation time does not change much between the different samples. That means that the material becomes stiffer without greatly changing its retardation time. The retardation time indicates at which strain rate (or time) one expects maximum dissipation while the modulus controls the extent of deformation.
In essence the creep results show that the grafting does not change much the dissipative properties of the adhesive at a strain rate of the order of 10^{-3} -10^{-2} s^{-1} but does change its stiffness, consistent with the high strain rate tensile test results.

Table 7-8: Values of the Burgers parameters for different HEMA/BPA ratios; σ=0.03 MPa

Sample	HEMA/BPA	E_H (kPa)	E_V (kPa)	η_V (MPa.s)	η_N (MPa.s)	τ_V (s)
I_10PU(0.11)0H0.55	0.11	362.57 (± 68.4)	2.75 (± 0.004)	0.49 (± 0.002)	8.234 (± 0.020)	181.45
I_10PU(0.22)0H0.55	0.22	159.91 (± 0.303)	4.27 (± 0.038)	1.33 (± 0.002	12.55 (± 0.024)	312.42
I_10PU(0.36)0H0.55	0.36	123.04 (± 0.909)	10.33 (± 0.012)	3.26 (± 0.0562)	24.09 (± 0.046)	315.59
I_10PU(0.50)0H0.55	0.50	104.41 (± 0.545)	14.50 (± 0.017)	4.26 (± 0.0085)	26.24 (± 0.040)	293.79

7.4.3 Discussion

We have shown that creep experiments can be performed with this type of materials and that results are consistent with the previous results of tack and tensile tests. However, some improvements of the experimental conditions can be made. In particular, we have seen that within a series of samples, the softening stress σ_S can change drastically. Then it would be more interesting to define a creep stress σ_C relative to the softening stress determined at a low initial strain-rate. For example, $\sigma_C = 0.7\sigma_S$ could be relevant to be just below the softening

stress and have the opportunity to include relaxation processes, as long as the load cell can maintained the corresponding stress. However in this case it would be best to compare the compliance rather than the strain between different materials.
The creep results on the two series of samples (varying PU wt% and varying HEMA/BPA) are consistent with the resistance to shear measured by CYTEC Surfaces Specialties (see tables 5-4 and 5-6) and one can conclude that a minimized creep does result in a high resistance to shear.
The data can be fitted appropriately by the Burger's model but some remarks have to be made. First of all, it is clear that the more elastic the sample is and the better the Burger's model fits the data. The case of the sample with 5 wt% of PU (sample I_5PU(0.11)OH0.55) proves that. Then, the loading stress is not applied instantaneously as described by the model and it cannot match well the 10 first seconds of the test. The first part of the model (the Hookean part) is thus questionable in the case of such viscoelastic samples. The last part describing the pure creep must also be reconsidered. Indeed, it is based on a Newtonian dashpot, which implies that the sample should flow. But the samples presented are crosslinked and cannot flow at large strains. Then refinements to the Burger's model should be made to better describe lightly crosslinked PSA's at low strain rates.
Finally, it appears that the viscoelastic element, and therefore the parameters E_v and τ_v are the most relevant to interpret the data. From the creep results in tensile and in shear geometries (that can be found in chapter 5), one can conclude that a maximized E_v and a minimized τ_v are required to get a maximum holding time. Nevertheless, the use of this model on PSA is pretty new and physical interpretations of the results are not completely understood for the moment. It seems in particular that a specific equilibrium between E_v (related to the stiffness of the material) and τ_v (related to the viscoelastic processes) must be found to optimize the PSA properties at long times and low strain rates.

7.5 Impact of the level of crosslinking on the creep behavior

Targeting a scale-up at industrial levels, urethane/acrylic hybrid latexes have been also prepared in one-step in a semi-continuous process (Route II). We have seen in chapter 6 that the main effect of this Route II is to strongly increase the gel content in the particles. Dry films obtained from this process are much more crosslinked and thus less deformable. The impact of this crosslinking has been studied in chapter 6 and the effect on the creep behavior is analyzed here.

7.5.1 Influence of the degree of grafting of the polyurethane

In this route II samples, the HEMA/BPA ratio is also an important and relevant parameter to evaluate the degree of grafting of the PU to the acrylic. As demonstrated in chapter 2, the higher the HEMA/BPA ratio, the higher is the theoretical degree of grafting. Figure 7-11 recalls the mechanical results analyzed in chapter 6. The effect of the HEMA/BPA ratio on the deformability and the stiffness of the samples is close to what is observed with samples prepared by Route I: when the grafting increases, the material is stiffer but the relaxation does not change much.

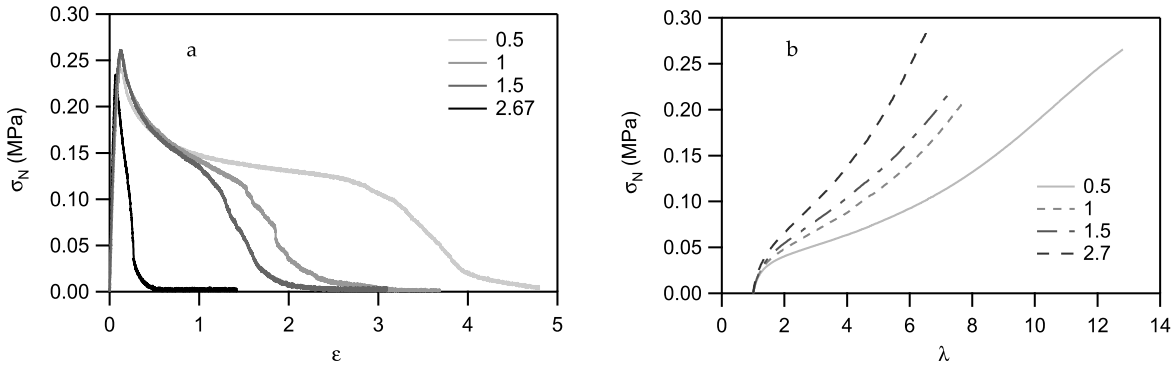

Figure 7-11: Samples prepared by Route II ; results for different HEMA/BPA ratios: (a) tack tests with Vdeb = 10μm.s^{-1}; (b) tensile tests with dε/dt = 0.1 s^{-1}

Consistently, the creep results obtained for the samples prepared by Route II with different HEMA/BPA ratios show equivalent results to the samples prepared by Route I when varying the same parameter HEMA/BPA (see Figure 7-12). The three samples with the lowest HEMA/BPA ratios deforms faster at a fixed stress than the one with HEMA/BPA=2.67.

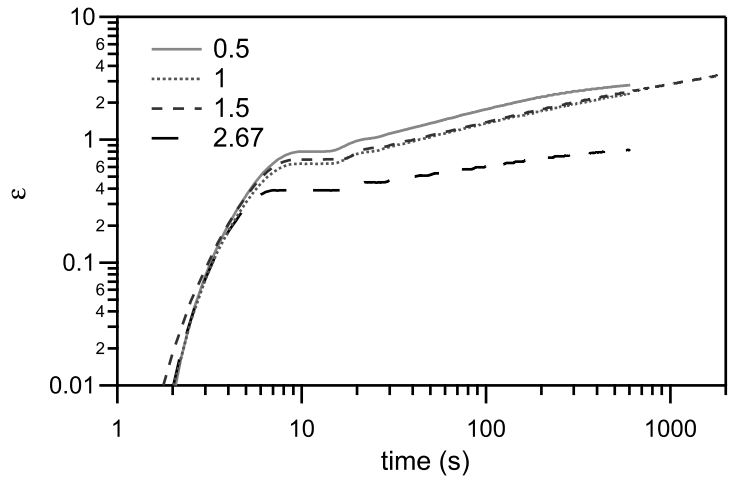

Figure 7-12 : Creep results for samples prepared by Route II with different ratios HEMA/BPA; σ = 0.03 MPa; V=0.02 N.s^{-1}

The Burger's model can be used to fit the ε(t) curves and some examples are presented in Figure 7-13. We have seen before that when the polymer is stiffer, the model fits better. Here again, the same conclusion can be drawn. Furthermore, after stabilization of the loading stress, the fit is also better.

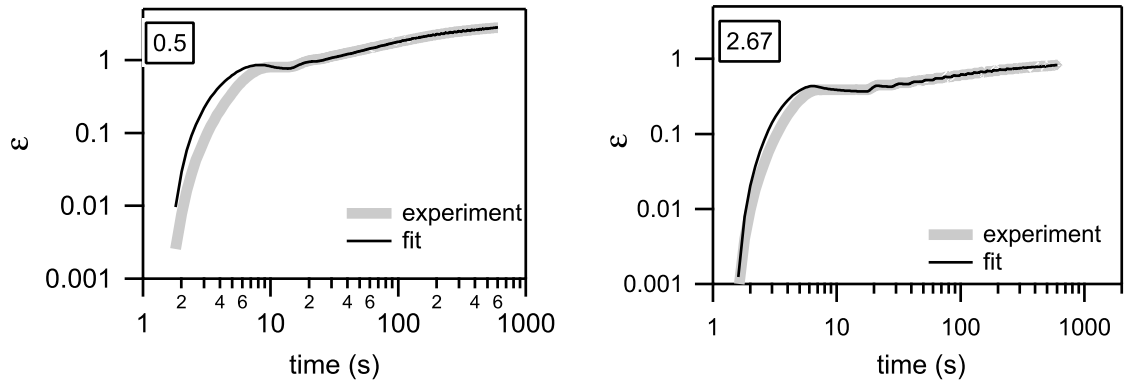

Figure 7-13: Experimental results and fit with the Burger's model for HEMA/BPA = 0.5 (sample II_10PU(0.5)OH1, on the left) and HEMA/BPA = 2.67 (sample II_10PU(2.67)OH1 on the right); σ = 0.03 MPa

Interesting comments can be made from the values of the Burger's parameters (Table 7-9). Compared to values from route I (reminded at the end of Table 7-9), the values of E_v are significantly higher (more crosslinking) and the values of the retardation times (defined as η_v/E_v) are much lower (for the less adhesive samples of each series, τ(Route I) = 151.7 s and τ(Route II) = 79.4 s). This is consistent with the lower softening and the bigger gel fraction in samples from route II.

Table 7-9: Values of the Burgers parameters (E_v and τ_v) for different HEMA/BPA ratios; σ = 0.03 MPa

Sample	HEMA/BPA	E_v (kPa)	τ_v (MPa.s)
II_10PU(0.5)OH1	0.5	18.645 (± 0.049)	91.65
II_10PU(1)OH1	1	30.299 (± 0.147)	81.39
II_10PU(1.5)OH1	1.5	22.93 (± 0.0575)	196.25
II_10PU(2.67)OH1	2.67	92.865 (± 0.335)	79.40
I_10PU(0.11)0H0.55	0.11	2.75 (± 0.004)	181.45
I_10PU(0.22)0H0.55	0.22	4.27 (± 0.038)	312.42
I_10PU(0.36)0H0.55	0.36	10.33 (± 0.012)	315.59
I_10PU(0.50)0H0.55	0.50	14.50 (± 0.017)	293.79

As a conclusion, the elastic mechanisms dominate the behavior of samples prepared with this synthesis route. The relaxation mechanisms are less important and viscoelasticity is clearly decreased. Similar to the route I samples, the increase in degree of grafting does increase the modulus. However the trend is less obvious. At these very low strain rates, the more crosslinked system really detaches itself from the others, while at higher strain rates, presumably weak interfaces between latex particles (as explained in chapter 6) reduce this difference. Conversely in the intermediate grafting regime the creep test does not distinguish the materials while the tensile tests and the adhesive tests are more discriminating. This may reflect viscoelastic dissipation mechanisms active at different strain rates.
Finally, if one compares results of the route II samples in tensile creep and in resistance to shear (see Table 6-3), one can conclude that the resistance to shear is in good agreement with the creep results and that a minimized creep results in a high resistance to shear.

7.5.2 Comparison of samples from Route I and Route II

The impact of the synthesis route on the adhesive properties has been shown in the previous chapter and is confirmed by the creep results: more crosslinking points results in higher gel content. It is now interesting to compare creep results for samples from each series. I_25PU(0.10)OH0.5 from Route I and II_10PU(0.5)OH1 from Route II have been chosen. Although several compositional parameters are different (PU weight fraction, degree of grafting, HEMA/BPA), these samples have in common to be the most deformable of each series. Results are compared in Figure 7-14.

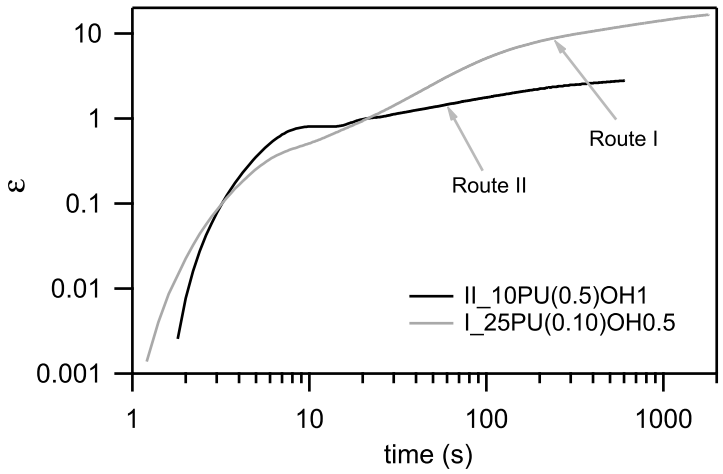

Figure 7-14: Creep behavior of samples prepared in Route I and Route II; σ = 0.03 MPa; V= 0.02 N .s^{-1}

If the sample from Route I clearly appear to be more deformable, one can also note that the viscoelastic contribution to the strain (as defined by the Burger's model and active for the intermediate times) is also larger for the sample in route I. Moreover the sample prepared by Route II presents a higher slope for the initial stage of deformation but a lower one for the "late stage" of the test implying quite different viscoelastic properties.
The values of the E_v and τ_v measured from the Burger's model fit (see Table 7-8 and Table 7-9) also confirm that the route II samples have a much more elastic behavior.

If the results in tensile creep and resistance to shear are consistent for the different series of samples presented until now, distinct interpretations have to be made if one compares the urethane/acrylic behavior with the pure acrylate sample.

7.5.3 Impact of the polyurethane on the creep behavior

The power-law dependence of the creep strain for the sample with the highest HEMA/BPA ratio is close to that of the blank latex containing no PU at all, as can be seen in Figure 7-15 (a). The prefactor is however divided by a factor 2. The tensile tests at high strain rate are even more similar (Figure 7-15 (c)). However the tack results (Figure 7-15 (b)) and the resistance to shear (performed at CYTEC Surface Specialties) are very different between the two samples. In particular the sample with PU has a very good resistance to shear (more than 10 000 min according to the standard tests) whereas the sample without PU has a poor one (332 min).

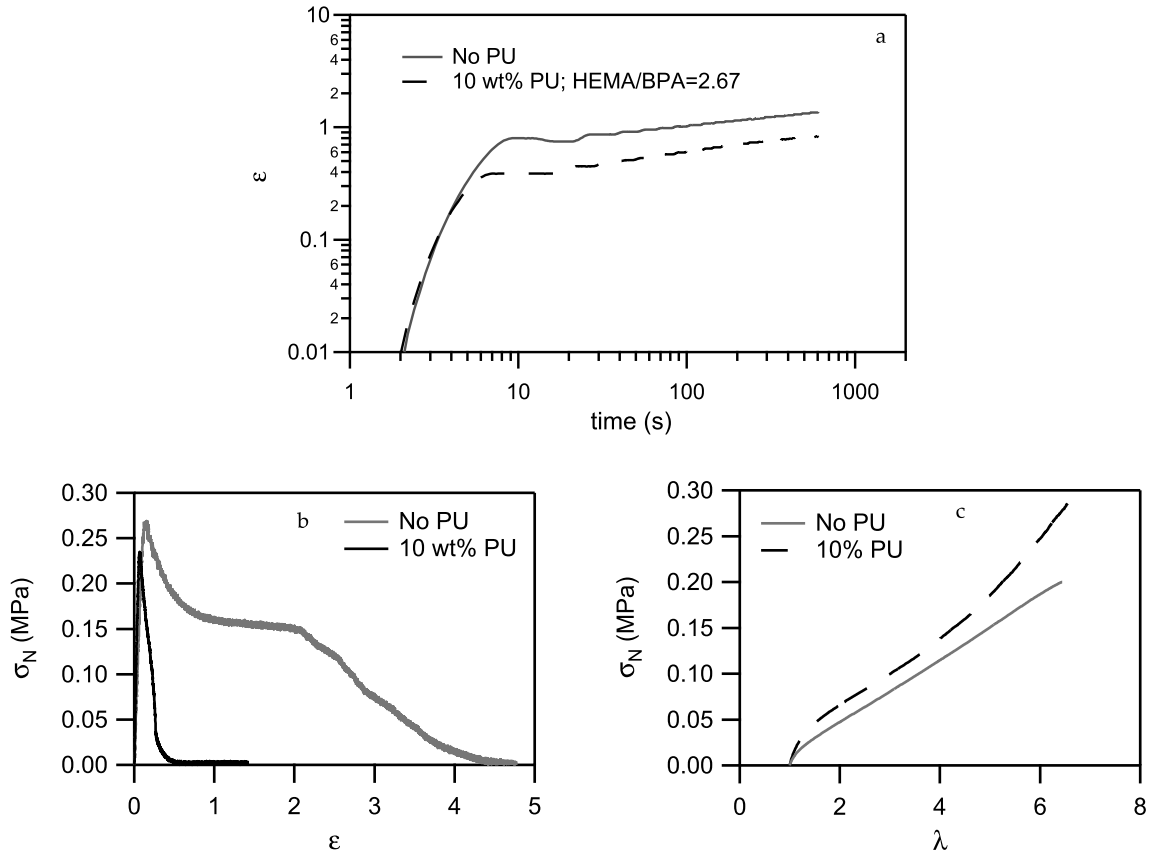

Figure 7-15: Samples prepared in Route II ; results for samples with PU (sample II_10PU(2.67)OH1 with 10 wt% and HEMA/BPA= 2.67) and without (sample II_0PU(0)OH0): (a) creep tests with σ = 0.03 MPa and V = 0.02 N.s^{-1} (b) tack tests with V_{deb} = 10µm.s^{-1} and (c) tensile tests with dε/dt = 0.1 s^{-1}

Contrary to the previous results, there is no direct relation between resistance to shear and resistance to creep. One way to understand this discrepancy is to analyze the small strain viscoelastic properties. The evolution of the storage and loss modules and of the ratio tanδ/G′ with frequency is presented in Figure 7-16 for the hybrid sample (red triangles) and the blank one (black squares). The elastic moduli are almost equivalent for both samples but the frequency dependence of the ratio tanδ/G′ is quite different from a sample to another. For the blank sample, tanδ/G′ presents a maximum around 0.5 s^{-1}, whereas it decreases constantly with frequency for the hybrid sample. At low strain rates, the hybrid is more viscoelastic and it is hard to propagate cracks at the adhesive/probe interface (Carelli, Deplace *et al.*, 2007; Nase, Lindner *et al.*, 2008; Deplace, Carelli *et al.*, 2009). This improves the holding time of the adhesive. On the contrary, at short contact times and high strain rates, it is much less viscoelastic and resists poorly interfacial crack propagation. As a result it does not deform much and tack values are low. On the other hand, the blank (which is less viscoelastic at low frequencies) does not resist well to crack propagation at the low frequencies corresponding to the resistance to shear. At higher frequency yet, we are close to the maximum of tanδ/G′ and the sample can deform more: the tack values are higher. Moreover the higher swelling ratio (see Table 7-10) of the blank confirms that it can deform

more if cracks cannot propagate at the interface, which improves the adhesion energy at high strain rate.

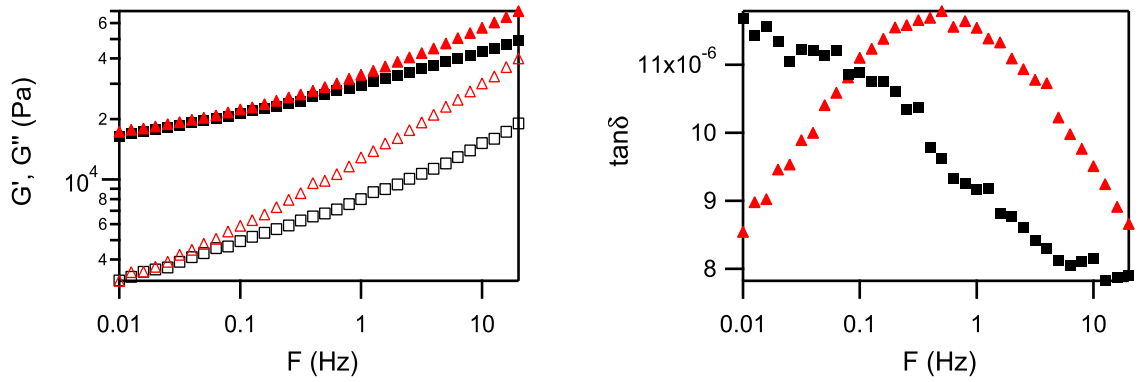

Figure 7-16 : Evolution of the elastic and loss modulus (left) (▲ G', sample without PU (II_0PU(0)OH0); △ G'', sample without PU; ■ G' sample with 10% PU (II_10PU(2.67)OH1); □ G'', sample with 10% PU) and of the ratio tanδ/G' (right) (▲, sample without PU; ■, sample with 10 % PU) with frequency for a deformation of 8%

Table 7-10: Gel content (%) and swelling ratios of the blank and the hybrid with 10% PU and the highest HEMA/BPA ratio

Sample	Gel content (%)	Swelling ratio
II_0PU(0)OH0	68.05	31.50
II_10PU(2.67)OH1	88.20	22.20

The values obtained from the Burger's fit of the creep data confirms that the blank is less viscoelastic at low strain-rates. Indeed, the elastic modules of the hybrid and the blank are quite close (E_v(blank) = 88.35 kPa and E_v(hybrid) = 92.87 kPa) which explains why the creep strains are close. However, the retardation time of the hybrid is almost twice higher than the that of the blank (τ_v(hybrid) = 79.4 s and τ_v(blank) = 47.4 s) which is the signature of a more viscoelastic sample that can better resist interfacial crack propagation.

The comparison of the urethane/acrylic hybrid and the blank points to very different rheological behaviors. It is clear that the polyurethane added even in small quantities (10 wt% here) strongly modifies the global polymer architecture and may affect also the acrylic architecture.

Nevertheless, the differences in linear viscoelastic behavior can explain the samples behavior in tack and resistance to shear but this does not explain why creep measurements are not sensitive to this difference. The Burger's parameters indicate that the deformation should be equivalent, which is the case but different resistance to shear are expected from the different retardation times. Our hypothesis is that the creep tests were too short to distinguish some differences. The same creep experiments have then been performed until the failure of the sample.

7.5.4 Correlation with resistance to shear

With the objective to explain the difference of creep in shear and tensile geometries between the hybrid and the blank, we performed tensile creep experiments until failure and compared the results to the measurements of shear resistance performed at CYTEC Surface Specialties. Times at failure are given in Table 7-11 for the sample with no PU (II_0PU(0)OH0) and for the sample with 10 w% of PU and high degree of grafting(II_10PU(2.67)OH1).

Table 7-11 : Resistance to shear and resistance to creep for samples without PU and with 10% PU and the highest grafting ratio

Sample	wt% PU	Shear test (min)	Creep test (min)
II_0PU(0)	No PU	332 ± 15 CF[a]	32.5
II_10PU(2.67)OH1	10	1 x 4860 ± 15 CF 2 x > 10000	176.4

a: CF is for cohesive failure

Two observations can be made: the sample containing PU fails after a longer time than the one without PU for the two tests and the time to failure in shear is ten times higher than the time to failure in the creep experiment for the pure acrylic and at least 60 times higher for the PU hybrid. Two arguments can explain this difference:

- The average stress applied to the sample in the creep geometry is higher than in the shear resistance geometry. Indeed, in creep, we applied a stress of 30 kPa when it is only 15 kPa in the shear tests.
- In the creep measurements, a homogeneous tensile stress is imposed to a self-standing thick film (~ 500 μm), while in shear a heterogeneous shear field is applied to a much thinner layer (~ 20 μm).

This clearly points out that the failure mechanisms are different between tensile creep and shear creep. In a shear test, adhesive failure occurs most of time by crack propagation at the interface between the adhesive layer and the substrate for an optimized adhesive. In creep on the contrary, the failure occurs by failure in the bulk when the finite extensibility of the chains is reached. The failure mechanisms are thus very different from a geometry to another. Then one can understand that it would have been difficult to predict the observed differences in shear resistance between the hybrid and the blank from the resistance to creep alone. The fact that the failure occurs adhesively points to differences in resistance to crack propagation rather than differences in creep resistance. This shows the limits of the creep experiment to predict the shear behavior.

A high shear resistance requires a high resistance to creep (i.e. to avoid cohesive failure) while maintaining a certain level of viscoelasticity at low frequency (i.e. to avoid crack propagation). It is this particular balance which is improved by the addition of PU.

7.6 Conclusion

Considering that an improved shear resistance requires a minimized creep, we developed a creep experiment based on a tensile geometry to study the failure mechanisms occurring at long times. The tensile geometry has been chosen to get an effective uniaxial and uniform loading in the sample.

The feasibility of such tensile creep tests has been demonstrated, although some improvements of the experimental conditions can be made. Hence, we defined a creep stress σ_C to apply to the sample and suggest that this creep stress should be chosen below the softening stress measured from a standard tensile experiment at low strain rate. Applying the preset load during ~ 2000 s is already satisfying to bring information on the material behavior in most cases.

For a majority of samples, a satisfying correlation between the creep and the shear resistance could be determined. Hence, the smaller the creep strain is when the preset load stabilizes, the higher is the resistance to shear. In other words, a minimized creep results in a high resistance to shear.

We determined that the Burger's model describes well the creep behavior of our hybrid samples, in particular after the stabilization of the preset load. Nevertheless, some improvements of the model could be made by taking into account that our materials are very soft and viscoelastic. In particular, we do not apply an instantaneous load and the viscoelastic behavior must be taken into account in the loading part.

The parameters obtained from the viscoelastic element of the model (the Kelvin-Voigt element) are the most relevant in our case. To minimize the creep and thus to maximize the shear resistance, a high elastic modulus E_V (to minimize the strain) and a retardation time τ_V (to decrease the relaxation processes) are required.

Nevertheless, the use of tensile creep experiments shows its limitation in the case of samples with very different rheological behaviors. The difference observed between the hybrid and the blank latexes prepared in route II is a good example. In this case, the results obtained from creep experiments are neither consistent with the mechanical results nor with the shear resistance. The linear viscoelastic properties cannot be neglected to explain the different behaviors in this case.

Creep tests performed until failure on these samples point to a crucial difference between creep in the tensile and shear geometries. Although the load applied during the tensile creep test is higher than in the shear test, the main difference comes from the failure mechanisms in both tests. In the shear geometry, interfacial debonding can take place between the adhesive layer and the substrate by crack propagation at the interface. Shear is then optimized with a less deformable viscoelastic adhesive. On the contrary, in creep, the propagation of crack in the bulk provokes the failure. These results also demonstrate that the creep test we developed may be too short to fully analyze the sample behavior. Both type of failure requires different rheological profiles.

Finally, one has to note that this type of experiment and analysis are still new on such viscoelastic materials. The systems studied here are very complex and they are not model

systems. Hence, it could be interesting to perform the same experiments on PSA with a polymer architecture better controlled in order to establish relationship between molecular architecture, creep behavior and resistance to shear. Then, the fine analysis of the creep behavior and of the Burger's parameters could result in a predictive tool of the shear resistance. Acrylic or styrene-isoprene block copolymers appear as good candidate for a systematic study of the long-term low strain-rate behavior in tensile geometry.

7.7 References

- Ashcroft, I. A., Hughes, D. J., Shaw, S. J., Wahab, M. A.,Crocombe, A.; *Journal of Adhesion*; **2001**; *75*; (1); 61-+.
- Carelli, C., Deplace, F., Boissonnet, L.,Creton, C.; *Journal of Adhesion*; **2007**.
- Creton, C.; *MRS Bulletin*; **2003**; *28*; (6); 434-439.
- Creton, C.,Fabre, P.; *The mechanics of adhesion*; Dillard, D. A. and Pocius, A. V.: Amsterdam, Elsevier; **2002**; *1;* 535-576.
- Dean, G.; *International journal of adhesion and adhesives*; **2007**; *27*; (8); 636-646.
- Deplace, F., Carelli, C., Mariot, S., Retsos, H., Chateauminois, A., Ouzineb, K.,Creton, C.; *Journal of Adhesion*; **2009**; *85*; 18-54.
- Ferry, J. D.; *Viscoelastic Properties of Polymers*; **1980**.
- Gleiss, P. L.,Brockmann, W.; *Journal of Adhesion*; **1997**; *63*; (4); 253-263.
- Kaelble, D. H.; *Transactions of the Society of Rheology*; **1965**; *9;* (2); 135-163.
- Lindner, A., Maevis, T., Brummer, R., Luhmann, B.,Creton, C.; *Langmuir*; **2004**; *20*; (21); 9156-9169.
- Nase, J., Lindner, A.,Creton, C.; *Physical Review Letters*; **2008**; *101*; 074503.
- Vaynberg, K. A., Berta, A. T.,Dunckley, P. M.; *Journal of Adhesion*; **2001**; *77*; (4); 275-284.
- Wang, H. C., Thompson, D. G., Schoonover, J. R., Aubuchon, S. R.,Palmer, R. A.; *Macromolecules*; **2001**; *34*; (20); 7084-7090.
- Zosel, A.; *Journal of Adhesion*; **1994**; *44*; (1-2); 1-16.

CONCLUSION GENERALE

Nous avons étudié des films adhésifs produits à partir de latex hybrides uréthane/acrylique. En combinant les propriétés de deux polymères différents, les latex hybrides offrent de nouvelles propriétés alliant les avantages des deux composants. Dans ce cas particulier, l'ajout du polyuréthane dans les particules adhésives d'acrylique doit permettre d'augmenter notamment la résistance aux solvants et de maintenir l'adhérence à plus haute température que pour un adhésif acrylique classique.

La miniémulsion s'est révélée être une méthode de synthèse efficace pour préparer des latex hybrides uréthane/acrylique avec des taux de solide importants et dans lesquels le polyuréthane est réparti de façon homogène dans les particules. Cependant, il a été nécessaire d'utiliser un agent de greffage (le HEMA) pour connecter les chaînes de polyuréthane au réseau acrylique. En effet, nous avons montré par des observations en AFM et TEM qu'en l'absence de cet agent de greffage, une séparation de phase a lieu dans la particule entre les chaînes courtes de polyuréthane et le copolymère acrylique. Cette séparation de phase se produit également quand un faible taux de greffage des chaînes est combiné à un fort taux de polyuréthane. De plus, des observations en TEM ont confirmé que cette séparation de phase dans la particule se répercute dans le film issu du séchage de ces particules, avec des conséquences négatives sur les propriétés macroscopiques du film, par exemple sa transparence.

Pour procéder au greffage du PU, deux solutions peuvent être envisagées, correspondant à deux stratégies de synthèse différentes utilisées dans cette étude. La première méthode consiste à faire réagir d'abord le prépolymère de PU avec l'agent de greffage, ainsi qu'avec un extenseur de chaîne permettant d'augmenter sa masse, avant d'être mélangé aux monomères acryliques. La polymérisation en miniémulsion de la phase acrylique a lieu dans un deuxième temps. Cette méthode, appelée route I, offre la possibilité de bien contrôler le degré de greffage et la longueur finale des chaînes de PU. Par contre, le procédé de batch utilisé limite la portabilité d'une telle synthèse à plus grande échelle. Dans la deuxième méthode, ou route II, le prépolymère de PU est mélangé à la phase acrylique directement avec l'agent de greffage et l'extenseur de chaînes, et la polymérisation radicalaire de

l'acrylique a lieu en même temps que le greffage et l'extension du PU. Cette route II ayant lieu en une seule étape et avec un procédé semi-continu, elle peut en principe être reproduite plus facilement à échelle industrielle. En revanche, il est moins évident de bien contrôler les différentes réactions de greffage et d'extension.

Ces deux voies de synthèse conduisent après une certaine optimisation, à des latex aux propriétés intéressantes mais relativement différents. Ainsi les latex produits par la route II ont un taux de gel nettement plus important que ceux produits par la route I. De manière générale, les films obtenus par les latex de la route II présentent donc des propriétés de pelage et de tack moindres, mais une résistance au cisaillement nettement supérieure.

Malgré les différences entre ces produits, nous avons pu déterminer deux paramètres moléculaires communs permettant de modifier l'architecture du réseau polymère à l'intérieur de chaque particule et les propriétés mécaniques macroscopiques finales. Le taux de polyuréthane, dont l'effet a été étudié sur les latex produits en route I, est un paramètre de premier ordre permettant d'ajuster l'élasticité aux petites déformations. En effet, augmenter le taux de polyuréthane en gardant un taux de greffage constant a pour conséquence d'augmenter la fraction de gel dans les particules en ajoutant des points de réticulation chimiques par le greffage du PU et des points de réticulation physiques dus aux enchevêtrements apportés par le PU. Des images de TEM indiquent également qu'une quantité importante de polyuréthane peut entraîner une séparation de phase dans la particule, malgré le greffage partiel. Cette structure core-shell n'influe pas sur la qualité du film à l'échelle macroscopique mais peut avoir un effet sur sa déformabilité en grandes déformations.

L'effet du taux de greffage du PU sur les propriétés macroscopiques est plus subtil et a été étudié sur les latex préparés en route I comme en route II. Nous avons montré qu'en jouant sur le taux de greffage pour une quantité de PU fixe, la masse molaire moyenne des chaînes les plus courtes du réseau que sont les chaînes de PU est modifiée. Dès lors, seule la déformabilité du réseau change et un niveau de cohésion satisfaisant est maintenu. Ainsi, en augmentant le taux de greffage, on peut améliorer nettement la résistance au cisaillement tout en assurant un niveau d'adhérence satisfaisant. Cette double amélioration ne pourrait être obtenue uniquement avec un réseau acrylique dont le niveau de réticulation serait modifié (via un agent de transfert ou un agent réticulant par exemple), et cela révèle donc tout l'intérêt d'avoir des matériaux hybrides uréthane/acrylique.

Il faut noter que ces résultats ont été obtenus grâce à une forte collaboration avec les deux équipes de chimie qui ont pris en charge la synthèse de ces latex. Les échanges scientifiques et techniques que nous avons eus tout au long de cette thèse ont permis de comprendre au mieux ces systèmes, de dégager les paramètres ayant des effets importants sur les propriétés macroscopiques, notamment les deux que nous venons de citer, et enfin de déterminer les conditions exactes permettant d'optimiser les produits finaux, en particulier pour les latex produits par la route I.

Ce travail de thèse a aussi permis de dégager des résultats novateurs concernant la méthodologie utilisée pour l'étude d'adhésifs PSA. Dans un premier temps, nous avons confirmé que la combinaison des propriétés viscoélastiques linéaires aux petites

déformations et des propriétés élastiques non-linéaires aux grandes déformations aboutit à une prédiction satisfaisante des propriétés d'adhérence mesurée par le test de probe-tack. Nous avons par ailleurs amélioré la compréhension des processus de relaxation dans le matériau par des tests de traction à plusieurs vitesses initiales de déformation. Cela nous a permis de découpler la dépendance de la vitesse de déformation et l'adoucissement aux déformations intermédiaires qui dépend essentiellement de la déformation. Nous avons montré qu'une analyse fine de ces dépendances apporte des informations utiles sur l'architecture du film, notamment la qualité des interfaces entre particules formant ce film.
Au cours de cette thèse, nous avons également beaucoup utilisé les mesures d'extraction et de gonflement de la fraction insoluble de polymère pour établir des relations entre la structure du réseau faiblement réticulé et les résultats mécaniques. Cela n'avait été que peu fait auparavant, et nous avons ainsi pu mieux comprendre la structure du réseau polymère dans les films étudiés. Il est en effet confirmé que la fraction de gel présente dans les particules n'est pas la seule à modifier les propriétés mécaniques mais que le taux de gonflement est aussi fortement révélateur de l'architecture du réseau. Ce taux de gonflement peut par exemple être directement relié à l'extensibilité limite des chaînes lors des tests de traction et au niveau de cohésion mesuré par un test de résistance eau cisaillement.
Enfin, nous avons mis en place un test de fluage en traction avec pour objectif le développement d'un outil de prédiction de la résistance au cisaillement. Réalisé sur plusieurs séries d'adhésifs, ce test a montré une bonne corrélation avec les résultats en cisaillement au sein d'une même série de produits. En revanche, des différences importantes entre les propriétés rhéologiques de deux matériaux montrent que ce test ne peut être utilisé seul pour prédire le comportement en cisaillement aux temps longs. Il semble donc qu'une bonne prédiction de la résistance au cisaillement passe par une étude combinée des résultats de fluage en traction et de rhéologie. Cela est expliqué notamment par les modes de rupture différents pouvant avoir lieu entre le fluage en cisaillement et en traction.

Ces différents résultats permettent d'envisager plusieurs perspectives à ce travail. Tout d'abord, maintenant que les conditions de synthèse pour produire ces latex hybrides uréthane/acrylique sont bien maîtrisées et que les paramètres de synthèse sont optimisées, il convient de tester ces adhésifs à plus hautes températures. Quelques résultats intéressants ont été observés par CYTEC Surface Specialties mais des mesures systématiques doivent être réalisées pour confirmer l'intérêt du polyuréthane dans les formulations hybrides.
La production à échelle industrielle de ces latex a également commencé à être étudiée par CYTEC Surface Specialties, mais elle doit être développée plus avant
Enfin, il pourrait être intéressant d'utiliser plus finement le test de fluage en traction pour comprendre les mécanismes de déformation et de rupture aux temps longs. Afin de comprendre l'impact des paramètres du réseau sur ces mécanismes, il conviendrait de mener une étude sur des matériaux modèles bien contrôlés et compris, par exemple sur des adhésifs préparés à partir de copolymères à bloc (acrylique ou styrène-isoprène) en solution. D'autre part, une optimisation du modèle de Burger utilisé pour décrire les données de fluage peut être envisagée afin de mieux prendre en compte les comportements aux temps très longs.

EXTENDED ABSTRACT IN FRENCH

Les adhésifs sensibles à la pression (PSA pour pressure sensitive adhesive en anglais) sont des films minces présentant dans le même temps les caractéristiques d'un liquide pour créer rapidement un bon contact avec tout type de surface et les caractéristiques d'un solide pour résister au cisaillement et se décoller sans laisser de résidu sur la surface. Des polymères viscoélastiques mous dont l'architecture de réseau est finement contrôlée sont généralement utilisés. Grâce au développement des techniques de polymérisation en voie aqueuse, de nouveaux types de PSA ont vu le jour. Il s'agit de films obtenus par le séchage de suspensions aqueuses de particules (autrement appelées latex). Dans ce travail, nous nous intéressons particulièrement à des films adhésifs obtenus par le séchage de particules de latex hybrides uréthane/acrylique.

La polymérisation en miniémulsion a été choisie pour la synthèse de ces latex afin d'assurer une incorporation homogène du polyuréthane dans chaque particule d'acrylique. Nous avons travaillé en étroite collaboration avec les équipes chargées de la préparation de ces latex pour mettre en évidence des conditions de synthèse permettant d'optimiser les propriétés adhésives. Par la suite, l'analyse de la morphologie de ces systèmes optimisés (tant à l'échelle de la particule qu'à celle du film) et la compréhension des propriétés macroscopiques en fonction de l'architecture du réseau polymère uréthane/acrylique ont été au centre du travail.

Après avoir présenté les matériaux et les méthodes de synthèse, nous expliquerons quelles techniques expérimentales ont été utilisées. Les résultats expérimentaux et les conclusions principales sont délivrés en dernière partie de ce résumé.

Matériaux

Tous les latex uréthane/acrylique de ce travail on été préparé par polymérisation en miniémulsion (Landfester 2001; Asua 2002). Cette technique de synthèse élargit le champ des possibilités offertes par la polymérisation en émulsion conventionnelle. Lors de la

miniémulsion, de petites gouttelettes de monomères (80 – 300 nm) généralement composées de monomères acryliques, sont stabilisées par des tensioactifs. Lorsque l'amorceur est ajouté, l'aire importante couverte par la surface des gouttelettes favorise sa pénétration dans les gouttelettes. La polymérisation radicalaire de l'acrylique a donc lieu directement dans les gouttelettes, sans diffusion de monomères dans la phase aqueuse comme c'est le cas dans la polymérisation conventionnelle. Un des avantages de la miniémulsion est qu'il est possible d'incorporer des composants hydrophobes dans les gouttelettes au moment de leur formation. Ces composants sont alors répartis de façon homogène dans les gouttelettes et donc dans les particules obtenues après polymérisation. De plus, à l'intérieur même de la particule peuvent avoir lieu d'autres types de réactions comme la polymérisation par addition.

La miniémulsion est donc une technique particulièrement puissante pour incorporer du polyuréthane dans des particules d'acrylique. Ici, un prépolymère d'uréthane réactif, c'est à dire terminé par des fonctions isocyanate à chaque extrémité, est introduit dans les particules. Ce prépolymère peut réagir par polymérisation par addition avec des groupements hydroxyles. Deux situations sont possibles :

- la réaction avec un monomère acrylique terminé par un alcool (ici hydroxy ethyl methacrylate, HEMA) assure le greffage de l'uréthane dans le réseau acrylique. On parle alors d'agent de greffage.
- La réaction avec un diol (ici Bisphenol A, BPA) permet l'extension du prépolymère. Ce diol est qualifié d'extenseur de chaînes.

Deux voies de synthèse différentes sont utilisées. Elles ont en commun d'utiliser le même prépolymère uréthane qui réagit avec le même agent de greffage et le même extenseur de chaînes. D'autre part, la composition en acrylique est faite de manière à avoir une T_g globale du copolymère très basse (entre -40 °C et -65 °C) comme le requiert la préparation de PSA.

Dans le procédé appelé Route I, le monomère principal est l'acrylate de butyl (ABu) qui représente 89.5 wt% de la partie monomère. Du méthyl méthacrylate (MMA) est ajouté pour ajuster la T_g et de l'acide acrylique (AA) complète la formulation. Celui-ci permet d'améliorer les performances adhésives des films obtenus suite au séchage des latex en générant notamment des liaisons hydrogène à l'interface adhésif-substrat.

Le prépolymère uréthane est ajouté à la phase de monomères acryliques qui contient également le HEMA. L'uréthane réagit donc d'abord avec l'agent de greffage. Un maximum de 20% des terminaisons isocyanate peut réagir avec le HEMA. Le BPA est ensuite ajouté à la phase uréthane + monomères acrylique. La réaction entre uréthane et BPA permet d'augmenter la masse molaire finale du polyuréthane. La phase organique contenant le polyuréthane modifié, les monomères acryliques et un costabilisant permettant d'éviter la dégradation des particules est alors mélangée à la phase aqueuse contenant le tensioactif afin de former les gouttelettes. Le mélange est soumis aux ultrasons pour réduire la taille des gouttelettes. L'ajout d'un amorceur redox permet d'entamer la polymérisation radicalaire de la phase acrylique dans un procédé batch. Un agent de transfert (CTA pour Chain Transfer

Agent) est introduit dans la phase organique afin de réduire la fraction de polymère réticulé dans le réseau final.
La seconde méthode, nommée Route II, consiste à mixer les différents éléments de la phase organique (prépolymère uréthane, monomères et costabilisant, agent de greffage et extenseur de chaîne) dans la phase aqueuse (contenant eau et tensioactif) avant toute réaction du prépolymère uréthane. Après formation des gouttelettes grâce à un homogénéiseur à haute pression (type Manton-Gaulin), la polymérisation commence avec l'ajout d'un initiateur thermique. Un procédé semi-continu est utilisé.
Les latex obtenus en route I comme en route II sont déposés en couches minces sur des substrats de différentes natures (lames de verre ou moules en silicone). Le séchage à température ambiante permet d'obtenir des films solides grâce à la simple évaporation de l'eau et à la coalescence des particules. Un passage rapide des films secs à haute température (110 °C) finalise le séchage. Dans les latex préparés en route I, des films sont préparés à partir de quatre séries de latex différentes faisant varier :

- soit la fraction molaire d'agent de transfert (CTA) dans des latex purement acrylique
- soit la fraction massique de PU par rapport à la masse d'acrylique
- soit le rapport HEMA/BPA
- soit le rapport OH/NCO.

Dans les latex de la route II, les paramètres dont les effets sont analysés sont :

- le rapport HEMA/BPA
- le rapport OH/NCO

La morphologie des particules et des films est analysée pour certains latex. Puis l'analyse des tests mécaniques permet de comprendre comment le PU modifie le réseau polymère des films adhésifs. Enfin, la résistance au fluage aux temps longs est étudiée pour certains échantillons.

Techniques Expérimentales

Morphologie des particules et des films

Les particules et les films ont été observés par microscopie à force atomique (AFM) et par microscopie électronique en transmission (TEM).
Les conditions d'observation en AFM doivent être optimisées pour des particules et films mous mais adhésifs : la pointe AFM scannant la surface ne doit pas endommager celle-ci, mais doit pouvoir malgré tout s'en détacher. Un cantilever rigide fonctionnant en contact intermittent léger est choisi.
Afin d'augmenter le contraste entre les phases acrylique et uréthane lors des observations par TEM, on choisit de marquer le PU avec de l'acide phosphotungstique (PTA). Ce

marquage est réalisé pour l'observation des particules. Dans le cas des films, des images convaincantes sont obtenues avec des échantillons non marqués. Cela peut s'expliquer par une dégradation (et donc une perte de masse) du PU préférentiellement à l'acrylique lors de l'exposition au champ d'électron.

Propriétés viscoélastiques linéaires

Un rhéomètre solide RDAII en géométrie plan-plan a été utilisé pour déterminer les propriétés viscoélastiques linéaires dans le domaine des petites déformations.
Un échantillon circulaire d'environ 500 µm d'épaisseur et de diamètre 8 mm est placé entre les plateaux du rhéomètre. L'obtention des échantillons se fait par le séchage d'une quantité donnée de latex dans des moules en silicone à température ambiante pendant une semaine puis à 110 °C pendant 5 minutes. Les films sont ensuite détachés des moules en silicone et placés entre deux feuilles de papier siliconé pour les protéger avant utilisation. Les échantillons circulaires sont découpés avec un emporte-pièce.
Une sollicitation sinusoïdale en torsion d'environ 8 % est appliquée. Les modules élastique et dissipatif et l'angle de déphasage sont obtenus lors de balayages en fréquence de 0.01 Hz à 20 Hz, à température ambiante.

Propriétés élastiques non-linéaires

Les tests de traction sont réalisés sur des éprouvettes rectangulaires d'environ 500 µm d'épaisseur et 5 mm de largeur, préparées dans les mêmes conditions que les échantillons de rhéologie. Ils sont placés entre les mors d'une machine de traction INSTRON 5565 espacés de 15 mm. Des marques blanches permettent de mesurer la longueur initiale et la déformation via un extensomètre vidéo (modèle SVE). Les tests de traction sont effectués à différentes vitesses de déformation initiales (0.1 s^{-1} et 1 s^{-1}), à température ambiante.
Deux représentations des résultats sont analysées : la représentation standard de la contrainte nominale σ_N en fonction de la déformation λ, et la représentation de Mooney qui trace la contrainte réduite σ_R en fonction de $1/\lambda$. La contrainte réduite est définie par :

$$\sigma_R = \frac{\sigma_N}{\left(\lambda - \frac{1}{\lambda^2}\right)}$$

Elle correspond à la normalisation de la contrainte nominale par le comportement gaussien d'un élastomère standard. A partir de cette représentation il est possible de déterminer deux paramètres quantifiant le caractère viscoélastique du matériau, les paramètres C_{soft} et C_{hard} (Deplace, Carelli *et al.* 2009). Le module d'Young E_y est déterminé sur la courbe $\sigma_N=f(\lambda)$, comme la pente d'une droite lissant les points entre $\lambda=1$ et $\lambda=1.02$.

Propriétés adhésives

Les propriétés adhésives des films de latex sont évaluées à travers un test de probe-tack (Zosel 1985; Lakrout, Sergot *et al.* 1999). Dans ce test, un poinçon de diamètre 10 mm, dont la surface est en acier inoxydable, est fixé sur le vérin mobile d'une machine de traction MTS810 (Lakrout, Sergot *et al.* 1999). Ce poinçon est approché à vitesse constante, V_{app}, d'une lame de verre placée sur le vérin fixe sur laquelle est séché le film adhésif. Le poinçon est approché jusqu'à entrer en contact avec le film adhésif, avec une force F_c et pour un temps t_c contrôlés. Le parallélisme entre le poinçon et la lame de verre est réglé par un système de trois vis micrométrique monté sur le vérin fixe.
Le poinçon est ensuite décollé à vitesse constante, V_{deb}. La force nécessaire au décollement du poinçon et le déplacement de celui-ci sont enregistrés. Comme le film adhésif est séché sur un substrat transparent (lame de verre), la visualisation du contact et du décollement est possible grâce à une installation développée au laboratoire (Lakrout, Sergot *et al.* 1999).
Les valeurs des différents paramètres sont indiquées dans le tableau suivant :

V_{app}	30 $\mu m.s^{-1}$
t_c	1 s
F_c	-70 N
V_{deb}	10 - 100 $\mu m.s^{-1}$

Les courbes contrainte-déformation $\sigma_N=f(\varepsilon)$ sont ensuite analysées. La forme de la courbe et la vidéo de l'aire de contact enregistrée pendant le décollement permettent de déterminer le mode de décollement.
Un adhésif standard est caractérisé par la formation de cavités micrométriques aux petites déformations. Ces cavités croissent jusqu'à atteindre un diamètre d'environ l'épaisseur du film. Ensuite, les parois entre ces cavités sont étirées et forment des fibrilles. Le décollement se termine par le détachement des fibrilles de la surface du poinçon. On parle alors de décollement par fibrillation. Ce mode de décollement est obtenu pour un réseau polymère dont les propriétés élastique et dissipative sont parfaitement équilibrées.
Pour un adhésif dont le module élastique est trop élevé, le décollement du poinçon se fait par propagation interfaciale de fissure. La courbe $\sigma_N=f(\varepsilon)$ présente un unique pic mais pas de plateau et la déformation maximale est très faible. Ce comportement caractérise une sur-réticulation du réseau polymère.
A l'inverse, un film mince très dissipatif présente un plateau de contrainte de faible niveau (~0.1 MPa, ce qui correspond à la simple pression atmosphérique sur les parois des fibrilles) et une déformation maximale importante. Un phénomène de digitation sur les bords du contact aboutit à la pénétration d'air dans les cavités et donc à la rupture cohésive des fibrilles. Il y a alors décollement cohésif.

Nature et organisation du réseau polymère

Finalement, nous avons réalisé de manière systématique des mesures d'extraction de gel et de gonflement à l'équilibre de la partie réticulée du polymère. Un morceau de film solide est découpé et pesé, puis placé en bon solvant (ici le THF) pendant une semaine. Des mesures gravimétriques permettent d'obtenir la fraction massique de gel et le gonflement à l'équilibrée de cette fraction de gel.

Résultats

Morphologie des particules et des films

Les techniques d'AFM et de TEM ont permis d'obtenir avec succès des images de particules hybrides uréthane/acryliques molles mais adhésives. Les films issus du séchage de ces particules ont également pu être imagés. Cependant, la technique du TEM est plus facile à mettre en place et des images plus concluantes peuvent être enregistrées. L'AFM et le TEM ont été utilisés pour les particules avec différentes conditions de greffage mais seul le TEM a été utilisé dans les autres cas.
Nous avons montré que le PU modifie fortement la morphologie des particules comme des films. Si le PU n'est pas greffé au réseau acrylique via le HEMA, les particules présentent une nette asymétrie correspondant à une séparation entre les deux phases, le PU étant localisé sur les bords des particules. Cette hétérogénéité conduit à une séparation de phase à plus grande échelle dans le film solide, comme cela peut être vu sur les images ci-dessous.

Non greffé

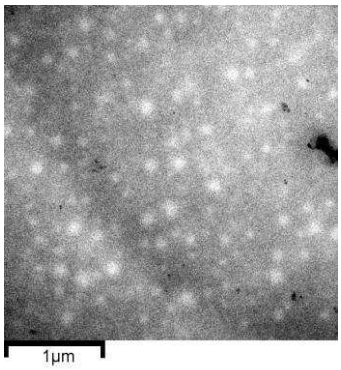

Greffé

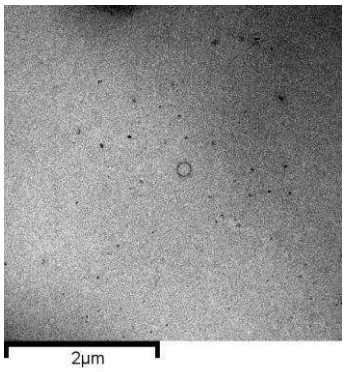

Macroscopiquement, le film présentant une séparation de phase est de plus mauvaise qualité : des fissures apparaissent à l'issue du séchage et le film est légèrement opaque. De plus, le décollement d'un tel film est cohésif, indiquant une sous-réticulation par rapport à la matrice acrylique seule. En revanche quand le PU est greffé au réseau acrylique grâce au HEMA, il n'y a pas de séparation de phase dans la particule ni dans le film.
Il est important de noter que cette séparation de phase à l'échelle du film n'est pas observée dans les mesures de transition vitreuse par DSC ou DMA. En effet, tous les latex présentent

une seule T_g, peu influencée par la quantité ou le greffage du PU mais dépendant uniquement de la composition en monomères (T_g(Route I) ~ -39 °C et T_g(Route II) ~ -63 °C). Cette T_g unique dans les systèmes hybrides, même présentant une séparation de phase macroscopique, semble s'expliquer par la proximité des T_g des composants (T_g(PU) = - 48°C).

Dans les particules contenant une fraction massique de PU importante et où le PU n'est greffé que partiellement, une séparation de phase est également observée. En effet, dans les systèmes préparés en route I avec 50 wt% de PU dont 11 % des bouts de chaîne sont greffés, une morphologie cœur-écorce a pu être relevée. Le PU forme une écore mince autour des particules dont le cœur est constitué principalement d'acrylique. Cette écorce semble gêner l'interpénétration des chaînes d'acrylique lors du séchage des particules et cette morphologie se retrouve dans les films secs (voir figure ci-dessous).
Les particules contenant 25 wt% de PU avec le même taux de greffage présentent également une séparation de phase que l'on retrouve dans le film, mais la structure cœur-écorce est moins nette.
En revanche, dans le cas de faibles quantités de polyuréthane (5 wt%), le greffage partiel semble être suffisant pour éviter la séparation de phase puisque les particules comme les films présentent un aspect relativement homogène.

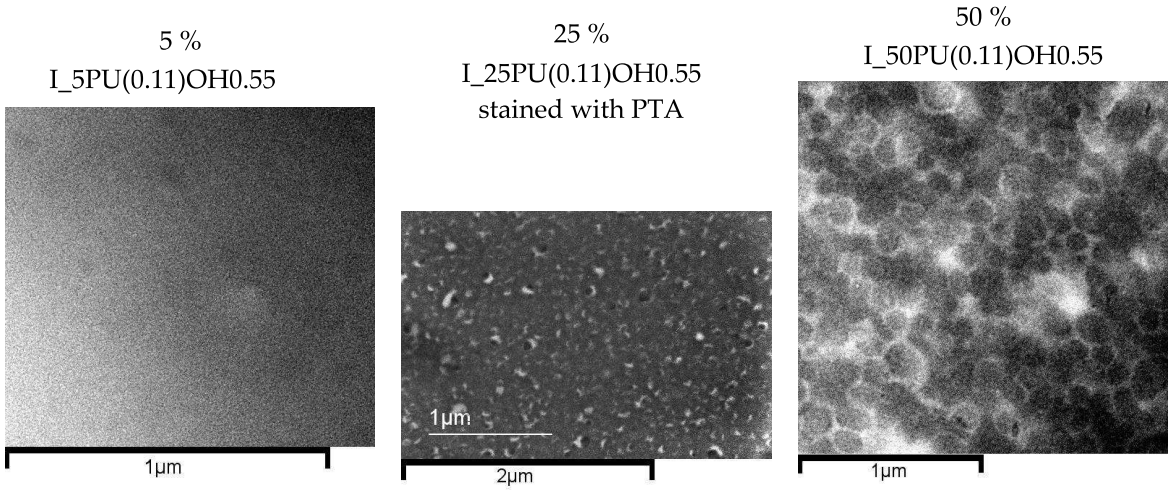

Rôle du polyuréthane sur les propriétés mécaniques

Cette partie analyse le rôle joué par le PU sur l'architecture des réseaux polymères des particules hybrides préparés en route I. L'objectif est d'une part de déterminer des conditions de synthèse permettant d'optimiser les propriétés adhésives des films PSA, et d'autre part de comprendre le rôle de ces paramètres de synthèse sur l'architecture du réseau. Nous avons montré que les propriétés mécaniques de ces films hybrides uréthane/acrylique sont contrôlées par deux paramètres indépendants. La fraction massique de polyuréthane affecte la viscoélasticité linéaire de ces films adhésifs alors que le taux de greffage du

polyuréthane modifie le comportement en grandes déformations en modifiant la maille du réseau réticulé.
Ainsi, des mesures de rhéologie montrent que le module élastique en petites déformations augmente fortement avec la fraction massique de PU, alors que la dissipation diminue. Les tests de traction révèlent une diminution brutale de la déformabilité des échantillons et un adoucissement beaucoup moins prononcé quand la quantité de PU augmente. Ces observations sont en bon accord avec les tests de tack qui montrent qu'on a une transition d'un matériau fortement dissipatif présentant un décollement cohésif vers un matériau sur-réticulé avec un décollement interfacial au fur et à mesure que la quantité de PU croît. La fraction massique de polyuréthane a donc un effet conséquent sur les propriétés adhésives et mécaniques des films. Cela est expliqué par deux éléments moléculaires. Le taux de greffage du PU étant constant, augmenter la fraction massique de PU revient à augmenter le nombre de points de réticulation. Cela augmente la fraction de gel et le matériau est donc plus élastique. De plus, le PU étant partiellement constitué de polypropylène-glycol, il est fortement enchevêtré. Plus de PU correspond à plus d'enchevêtrements qui, aux petites déformations, jouent le rôle de points de réticulation physique. Ces deux arguments se combinent pour expliquer l'augmentation du module élastique.
Nous avons montré que les meilleurs résultats pour un PSA sont obtenus avec 25 wt% de PU.

Le rôle du rapport HEMA/BPA, et donc du greffage du PU dans le réseau acrylique, est plus subtil. Un taux de PU fixe de 25 wt% est incorporé dans les particules et le rapport HEMA/BPA est modifié. Nous avons vu que, en petites déformations, ce rapport modifie de façon plus important la dissipation dans le système, alors que le module élastique reste constant. Les tests de traction montrent également que l'adoucissement aux moyennes déformations est relativement constant alors que le durcissement a lieu pour une contrainte plus importante et une déformation plus faible. Il est intéressant de noter que tous les échantillons testés se décollent par fibrillation avec un plateau qui augmente légèrement et une déformation maximale qui diminue quand HEMA/BPA augmente. Ainsi, ce paramètre semble affecter plus la déformation maximale et donc l'extensibilité limite des chaînes du réseau que son élasticité. D'un point de vue moléculaire, on comprend que l'augmentation de HEMA/BPA revient à diminuer l'extension de la chaîne de PU. Le degré de greffage est également modifié mais à moindre échelle et HEMA/BPA influe donc particulièrement sur la masse molaire des chaînes de PU. Comme ces chaînes sont les plus courtes que les chaînes acryliques, elles atteignent leur extensibilité limite d'abord. Augmenter leur taille revient à augmenter l'extensibilité limite, ce qui est observé mécaniquement et confirmé par les mesures d'extraction et de gonflement de gel.
Les résultats optimaux sont obtenus pour 25 wt% de PU et un taux de greffage de 11% (ce qui équivaut à HEMA/BPA = 0.22).

Une amélioration possible du système consiste à augmenter le rapport OH/NCO. Ce paramètre affecte fortement l'organisation des chaînes de PU. Ainsi, le même échantillon

avec 25 wt% de PU et 11 % de greffage mais OH/NCO passant de 0.55 à 1 se caractérise par une meilleure adhésion et une plus grande déformabilité. Cela s'explique par le fait que plus de BPA est incorporé dans le système pour augmenter la quantité de OH, permettant un allongement plus important des chaînes de PU.

L'impact de la longueur des chaînes de PU sur les propriétés industrielles est intéressant. En effet, quand HEMA/BPA augmente, l'adhésion dans le système (mesurée industriellement par des tests de pelage à 180 °) est maintenue mais la résistance au cisaillement est fortement améliorée. Le rapport HEMA/BPA permet donc de découpler énergie de pelage et résistance au cisaillement, ce qui est particulièrement intéressant et nouveau.

Vers des systèmes industriels

Les systèmes préparés par la route II sont analysés dans le chapitre suivant. Cette méthode de synthèse vise à se rapprocher des méthodes utilisées dans l'industrie, en vue d'une production à grande échelle de ces latex. Nous avons cherché à savoir si les paramètres déterminés dans le chapitre précédent ont les mêmes effets sur les propriétés mécaniques et adhésives des films. Notre étude s'est limitée ici au rôle du rapport HEMA/BPA et du rapport OH/NCO.

Le premier élément à retenir est que la route II augmente de façon importante la fraction de gel dans le film par rapport à la route I. Les films sont donc sur-réticulés et présentent une adhésion plus faible. Plusieurs raisons expliquent cette sur-réticulation. D'abord, dans la formulation en monomères, le 2EHA a été préféré au ABu. Cela favorise les réactions de transfert de chaînes et donc la formation de points de réticulation. De plus, il n'y a pas d'agent de transfert dans les différentes compositions. Ces deux éléments ont pour conséquence une augmentation forte du taux de gel de la phase acrylique seule.

Cependant, les rapports HEMA/BPA et OH/NCO semblent avoir les mêmes conséquences que pour la route I. Il faut noter que les rapports HEMA/BPA sont globalement plus élevés, favorisant le greffage par rapport à l'extension de chaîne. De plus, il n'a pas été déterminé de limitation de la réaction entre le PU et le HEMA. Cela entraîne un degré de greffage plus important du PU dans le réseau acrylique, et donc une fraction de gel plus grande. Cela tend à diminuer les propriétés d'adhésion en limitant la dissipation dans le matériau.

De plus, en raison de la synthèse en une seule étape, il est moins facile d'établir une relation entre le rapport HEMA/BPA et la longueur des chaînes de PU. En effet, il serait d'abord nécessaire de déterminer précisément dans quel ordre interviennent les réactions de greffage et d'extension et avec quelles cinétiques. Ainsi, il semble que dans le cas des très grands rapports HEMA/BPA, la formation de chaînes de PU pontant deux chaînes acryliques soit majoritaire, alors que les chaînes pendantes sont préférées pour les rapports plus faibles.

D'un point de vue industriel, la sur-réticulation présente dans tous les échantillons tend à réduire les propriétés de pelage. En revanche, la résistance au cisaillement de ces matériaux est très satisfaisante et prédomine pour tous les échantillons.

Analyse de la résistance au fluage des PSA

Un adhésif PSA optimisé doit avoir une résistance au pelage importante pour augmenter son énergie d'adhésion et présenter un caractère collant instantané pour adhérer à une surface de rugosité donnée dans un temps court. Cependant, il doit aussi présenter une résistance au cisaillement importante pour améliorer sa tenue aux temps longs et assurer un décollement sans résidu de la surface.

Le rôle joué par les propriétés viscoélastiques linéaires sur la résistance au pelage (Derail, Allal *et al.* 1997; Derail, Allal *et al.* 1999) et sur le pouvoir collant (Verdier and Piau 2003; Nase, Lindner *et al.* 2008) a été largement étudié depuis une décennie. L'impact du comportement élastique en grandes déformations a également été étudié (Creton, Hooker *et al.* 2001; Deplace, Carelli *et al.* 2009). Les mécanismes permettant l'adhésion et la résistance à la propagation de fracture aux temps courts et taux de déformation élevés sont aujourd'hui bien compris.

En revanche, le comportement aux temps longs et basses vitesses de sollicitation a été moins étudié pour ces matériaux fortement viscoélastiques. Les tests industriels mesurant cette résistance au cisaillement sont relativement simple à mettre en place mais ne permettent pas une compréhension précise des mécanismes intervenant dans ce type de sollicitation et sont de plus assez longs. Avec l'objectif de comprendre le comportement des matériaux viscoélastiques dans un domaine de faible fréquence de sollicitation, nous avons développé un test de fluage du matériau en traction à partir d'une machine INSTRON 5565.

Dans un premier temps, nous avons étudié le rôle joué par les paramètres de test afin de fixer les conditions d'étude. Nous avons choisi d'imposer une contrainte de 0.3 MPa à une vitesse de 0.02N/s pendant un temps donné. Ces paramètres représentent un bon compromis entre les conditions requises pour l'observation des phénomènes dissipatifs et les performances de la machine de traction.

Les résultats de ces tests, montrant l'évolution de la déformation dans le temps, ont été modélisées avec le modèle mécanique de Burgers, qui place en série un ressort hookéen, un élément de Kelvin-Voigt et un amortisseur newtonien. De prime abord, ce modèle semble bien décrire le comportement aux temps longs et vitesses lentes.

Les résultats obtenus pour les matériaux hybrides préparés en route I et en route II montrent une bonne corrélation entre la résistance au cisaillement et la résistance en traction. Ainsi, plus la déformation en traction est faible, plus la résistance au cisaillement est importante. En effet, résister à une sollicitation de fluage en traction ou en cisaillement requiert une cohésion important dans le matériau.

En revanche, la comparaison d'un échantillon hybride et d'un échantillon contenant de l'acrylique uniquement montre qu'un même niveau de déformation en traction peut exister même si la résistance au cisaillement et les propriétés aux temps plus courts sont complètement différents. Les mécanismes d'initiation et de propagation de fissure sont très différents entre une sollicitation en traction ou en cisaillement. Cela explique que les résistances soient différentes. De plus, il apparaît que les comportements rhéologiques aux petites déformations de ces deux matériaux sont radicalement différents. Finalement, si les tests de fluage en traction donnent une bonne prédiction du comportement aux temps longs,

ils ne peuvent être découplés d'une étude rhéologique. Celle-ci permet alors de connaître le comportement du matériau sur une large gamme de fréquence.
Cette étude préliminaire a permis de mettre en place les conditions expérimentales de tels tests et ouvre des pistes d'interprétation des résultats. Cependant, plusieurs améliorations possibles ont été relevées et l'analyse des résultats peut être encore développée.

Références

- Asua, J. M., *Progress in Polymer Science*, **2002,** *27*, (7), 1283-1346.
- Creton, C.; Hooker, J.; Shull, K., *Langmuir*, **2001,** *17*, 4948-4954.
- Deplace, F.; Carelli, C.; Mariot, S.; Retsos, H.; Chateauminois, A.; Ouzineb, K.; Creton, C., *Journal of Adhesion*, **2009,** *85*, 18-54.
- Derail, C.; Allal, A.; Marin, G.; Tordjeman, P., *Journal of Adhesion*, **1997,** *61*, (1-4), 123-157.
- Derail, C.; Allal, A.; Marin, G.; Tordjeman, P., *Journal of Adhesion*, **1999,** *68*, (3-4), 203-228.
- Lakrout, H.; Sergot, P.; Creton, C., *Journal of Adhesion*, **1999,** *69*, (3/4), 307-359.
- Landfester, K., *Macromolecular Rapid Communications*, **2001,** *22*, (12), 896-936.
- Nase, J.; Lindner, A.; Creton, C., *Physical Review Letters*, **2008,** *101*, 074503.
- Verdier, C.; Piau, J. M., *Journal of Polymer Science Part B-Polymer Physics*, **2003,** *41*, (23), 3139-3149.
- Zosel, A., *Colloid and Polymer Science*, **1985,** *263*, (7), 541-553.

Résumé : Cette thèse a pour objet l'étude de films adhésifs obtenus par le séchage de particules de latex hybrides uréthane/acrylique. Ces latex ont été préparés par polymérisation en miniémulsion pour assurer une incorporation homogène du polyuréthane dans chaque particule. L'étude de la morphologie des particules et des films a montré que le greffage du polyuréthane sur le réseau acrylique est essentiel pour éviter une séparation de phase à l'échelle du film, néfaste pour les propriétés macroscopiques. Les propriétés mécaniques de ces films hybrides sont contrôlés par deux paramètres indépendants : La fraction massique de polyuréthane affecte la viscoélasticité linéaire de ces films adhésifs alors que le taux de greffage du polyuréthane modifie le comportement en grandes déformations en modifiant la maille du réseau réticulé. En modifiant le taux de greffage, il est possible de maintenir un niveau d'adhérence satisfaisant par rapport à un film d'acrylique pur tout en augmentant la cohésion dans le matériau et donc la résistance au cisaillement. Cette méthode de synthèse par miniémulsion peut être transposée vers un processus plus industriel et l'effet des paramètres moléculaires reste globalement le même. L'effet du greffage apparaît toujours comme essentiel sur la déformabilité maximale des films adhésifs mais les conditions de synthèse augmentent fortement la densité de points de réticulation dans le matériau, ce qui diminue leur adhérence mais augmente leur résistance au cisaillement. Nous avons enfin mis au point un test de fluage en traction, permettant d'appréhender la résistance mécanique des adhésifs dans le temps.
Mots clés : PSA en voie aqueuse, miniémulsion, latex hybride, polyuréthane, acrylique, morphologie, propriétés mécaniques, fluage

Abstract: This work focuses on adhesive films obtained upon film formation of urethane/acrylic hybrid latex particles. These latexes were prepared by a miniemulsion polymerization to ensure a homogeneous incorporation of the PU inside the particles. Studying the morphology of particles and films showed that the grafting of polyurethane is essential to avoid phase separation at the film scale which is harmful for the macroscopic properties. Two parameters affect the mechanical properties of the films: the polyurethane weight fraction controls the linear viscoelastic properties while the degree of grafting of the PU modifies the maximum deformability of the film by modifying the mesh size of the network. The primary interest of the hybridization is to maintain a satisfying adhesion compared to pure acrylic films while increasing the cohesion in the polymer network and thus the shear resistance both at ambient and at high temperature. The preparation of similar hybrid latexes by methods closer to the industrial ones generates adhesive films with qualitatively similar properties. The degree of grafting still affects the maximum deformability of the adhesive but the synthesis conditions strongly increase the level of crosslinking inside each particle resulting in a decreased adhesion level. We finally developed a tensile creep test for this soft material targeted at better evaluating the long term properties of the adhesive films.
Keywords: Waterborne PSA, miniemulsion, hybrid latexes, urethane, acrylic, morphology, mechanical properties, creep